

MODELLING OF STEAM GENERATOR PERFORMANCE
BY FREON WITH SPECIAL REFERENCE
TO THE ANNULAR FLOW REGIME

By

Ahmed Hassan Mariy

Thesis submitted for the degree of
Doctor of Philosophy in the University
of London

Imperial College, November, 1975
Mechanical Engineering
Department,
Thermal Power Section.

ABSTRACT

The present work is concerned with an investigation into methods of simulation of different burn-out and boiling phenomena in high pressure steam generators using Freon to simulate water. The conception of this simulation and modelling and a review of relevant modelling techniques has been presented in Chapter 1. In the process of simulation several sets consisting of dimensionless groups are derived for an annular flow model, in addition to other dimensionless groups obtained by previous researchers (Chapter 2). As these sets comprise a large number of dimensionless groups, it is difficult to fulfil the condition of equality between specific dimensionless groups for the model and the prototype. Also in Chapter 2, a theoretical model based on the compensating distortion technique is introduced. According to this model, the simulation errors that occur due to the inequality of the dimensionless groups between the model and prototype can be compensated. Experimental burn-out data for water and Freon were used to determine the distortion factors so as both the Freon and water-steam burn-out experimental results can be represented on the same graph.

As a further test to the application of the introduced compensating distortion technique for simulation and modelling, the rewetting of dry patches formed in motivated thin films

flowing on heated surfaces was investigated. The interfacial surface waves on the film were considered and their effect on the motion of the triple-phase front was found. The characteristics of the surface waves of heated liquid film are studied in Chapter 3, while in Chapter 4 the effect of interfacial waves on rewetting speed is found and the compensating distortion technique is used to simulate the triple-phase front motion of water-steam and Freon. The results were encouraging and a further step was taken in Chapter 5, where the interfacial shear force between the vapour and the free liquid surface was introduced.

A Arcton-113 closed loop has been designed, manufactured and constructed with the objective of observing and measuring burn-out conditions and the rewetting speed of a motivated thin film flowing over a vertical heated rod. A complete description of the test facility is given in Appendix 4.

Unfortunately, because of long delays in ordering, delivery, construction and changing economic circumstances no tests have been carried out.

ACKNOWLEDGEMENTS

I wish to express my sincere gratitude to my supervisor, Professor W. Murgatroyd, for his encouragement, guidance, advice and interest in the work, and also to Dr. A.A. El-Shirbini, who gave so generously of his time, assistance and advice at all stages of the work.

Thanks are also due to Messrs. J. Knight, W. Wood and J. Martin of the steam laboratory for their efforts in installing the test facility.

Acknowledgements are also made to the Imperial Chemical Industry Ltd. (I.C.I.) for supplying the Imperial College Mechanical Department with 1.5 tons of ARKONEX free of charge.

My thanks are extended to Miss. D. Day and Miss. E. Archer of the Mechanical Engineering Department.

I am also grateful to Mrs. S. Murdock who helped with the typing of this thesis.

I am very much indebted to my employer, the National Electric Power Authority of Egypt, who granted me a study leave for Doctorate studies in Imperial College, and to the

British Council for awarding me the O.S.F.A.S. grant.

I wish to express my gratitude and my respect to my parents, who supported me financially and encouraged me in all aspects during the period of my study. Thanks are also due to my wife, Faiza, whose patience and encouragement helped me in devoting all my time to my work and my colleague B.M. Al Chalabi for always finding a humourous side of every difficult situation.

SUMMARY

The overall objective of the work described in this thesis was to improve our ability to model complex two-phase flow phenomena which occur in high pressure water-steam boiling by the use of refrigerant fluids at a lower pressure. Because it is not always possible, for practical reasons, to model accurately all the parameters, it is important to find procedures for reducing (and if possible quantifying) the effects of incomplete modelling. This requires a careful search for the most important parameters and for the best ways of interpolating and extrapolating those parameters which cannot be properly modelled.

After reviewing previous work on modelling in this field the author proposes a new extension of a technique previously reported by Ahmad (1971), the so-called "distortion technique". As a demonstration, new correlations are produced by this technique from existing data and are shown to be an improvement on previous correlations based on the same data.

Next, in order to provide guidance for the experimental modelling of the annular flow regime and especially of the effect of waves on the triple-phase front of a dry patch, the

author develops two new mathematical models. Although these form part of the overall objectives, they are self-contained. With these models as a guide and using the extended distortion technique mentioned above, modelling parameters and functions were developed and validated using existing data.

Originally it had been planned to provide additional validation by an independent experiment using Freon-113. The author spent considerable time designing this and supervising its construction and commissioning. Unfortunately, because of long delays in ordering and construction occasioned by changing economic circumstances, it was not possible to carry out any experiments before the writer had to return to Egypt. The details of the equipment designed by the author are given in Appendix 4.

CONTENTS

| | <u>Page</u> |
|---|-------------|
| Abstract | 2 |
| Acknowledgement | 4 |
| Summary | 6 |
| List of Symbols | 11 |
| | |
| Chapter 1: Preamble and a Review of Existing Simulation Techniques | 15 |
| 1.1 Boiling Phenomena | 15 |
| 1.1.1 The idea of simulation and modelling | 19 |
| 1.2 Review of Different Modelling Techniques | 20 |
| | |
| Chapter 2: Simulation of Critical Heat Flux | 44 |
| 2.1 Introduction and Definitions | 44 |
| 2.2 Mathematical Model for simulating Critical Heat Flux | 44 |
| 2.2.1 Results and Discussion | |
| 2.3 Formulation of Dimensionless Groups for an Annular Flow Model | 53 |
| 2.3.1 The Model | 53 |
| 2.3.2 Governing Equations | 54 |
| 2.3.3 Boundary Conditions | 55 |
| 2.3.4 The Dimensionless Groups | 56 |
| 2.3.5 Results and Discussion | 58 |
| 2.4 Conclusion | 61 |
| | |
| Chapter 3: Falling Liquid Film with Heat Transfer and Surface Waves | 87 |
| 3.1 Introduction | 87 |
| 3.2 Mathematical Formulation | 89 |
| 3.3 Discussion | 96 |

| | <u>Page</u> |
|--|-------------|
| Chapter 4: Simulation of the Effect of Waves on the Motion of the Triple-Phase Front of a Dry Patch in a Wavy Film by the use of Freon | 104 |
| 4.1 Introduction | 104 |
| 4.2 The Model | 105 |
| 4.3 Analytical Solution | 107 |
| 4.4 Numerical Solution | 114 |
| 4.5 Results and Discussion | 120 |
| 4.5.1 Triple-phase Front Motion for Water and Freon | 120 |
| 4.5.2 Errors in the Simulation of the Triple-Phase Front Speed | 126 |
| Chapter 5: A Modified Method to Simulate the Effect of Waves on the Motion of the Triple-Phase Front of a Dry Patch formed in a Thin Motivated Liquid Film | 155 |
| 5.1 Introduction | 155 |
| 5.2 The Model | 155 |
| 5.3 Governing Equations | 156 |
| 5.4 Solution | 159 |
| 5.5 Results and Discussion | 160 |
| 5.5.1 Triple-Phase Front Motion | 160 |
| 5.5.2 Simulation of the Triple-Phase Front Speed | 164 |
| 5.6 Simulation of the Triple-Phase Front Speed using the Dimensionless Groups derived in Chapter 2. | 169 |
| Chapter 6: General Conclusions and Recommendations. | 191 |
| References | 196 |

| | <u>Page</u> |
|---|-------------|
| Appendix 1: Mathematical procedure in derivation of the equations in Chapter 3. | 210 |
| Appendix 2: Periodic solution for the wavy film flow. | 225 |
| Appendix 3: Newton's method of iteration. | 228 |
| Appendix 4: Description of the experimental facilities. | 229 |
| A4.1 Introduction | 229 |
| A4.1.1 The idea of using refrigerants as a simulating substance. | 230 |
| A4.2 General description of test facility. | 232 |
| A4.3 Components, control and safety devices in the rig. | 233 |
| A4.3.1 Heating tank. | 233 |
| A4.3.2 Condenser. | 235 |
| A4.3.3 Holding tank. | 236 |
| A4.3.4 Circulating Pump. | 238 |
| A4.4 The test section. | 239 |

Note: All programmes are available at Imperial College, London University, Thermal Power Section.

LIST OF SYMBOLS

| | | |
|-------------------------------|---|---|
| A | Cross-sectional area | ft ² . |
| C _p | Specific heat | Btu/lb. °F |
| Cl | Dimensionless wave amplitude | |
| C _T | Multiplying factor | |
| C | Wave celerity | ft/sec. |
| D | Tube diameter | ft. |
| D _e | Equivalent diameter (= 4A/P _p) | ft. |
| E | Stevens et al Empirical function | |
| F _{qa} | Surface heat flux (at burn-out) | Btu/h.ft ² . |
| f _{qa} | Surface heat flux | Btu/h.ft ² . |
| F _G | Mass velocity scaling factor | |
| F _{ΔH} | Subcooled liquid scaling factor | |
| F _D | Diameter scaling factor | |
| f | Friction factor | |
| F _{qa} [*] | Dimensionless heat group [F _{qa} · δ _o / T _{sat} · K _l] | |
| F _{qa} ^{**} | Dimensionless heat quantity [β · F _{qa} [*] · T _{sat}] | |
| F _Q | Surface heat flux scaling factor | |
| G _a | Mass velocity | lb/h.ft ² . |
| Gr | Grashof number [gβδ _o ³ (T _w - T _∞) / ν ²] | |
| g | Acceleration due to gravity | ft/sec ² . |
| g _o | Gravitational constant [= 32.16] | lb _m .ft/lb _f .sec ² . |
| ΔH | Degree of subcooling | Btu/lb. |
| H _{fg} | Latent heat of evaporation | Btu/lb. |
| H | Enthalpy | Btu/lb. |
| K | Thermal conductivity | Btu/h.ft. °F. |
| L | Tube length | ft. |
| L _b | Boiling length | ft. |
| m | Rate of mass flow | lb/h. |
| n | Wave number (2π/λ) | 1/ft |
| N _{Re} | Reynolds number [4W _o δ _o / ν] | |
| N _{We} | Weber number [δ _o W _o ² / γ] | |
| N _W | Wave Number [2πδ / λ] | |

| | | |
|-----------------|--|-------------------------|
| N_{Fr} | Froude number $\left[W_o / \sqrt{g \delta_o} \right]$ | |
| P | Pressure | lb/in ² . |
| P_o | Ambient pressure | lb/in ² . |
| P_o | Capillary pressure | lb/in ² . |
| P^* | Dimensionless pressure $\left[P / \rho W_o^2 \right]$ | |
| Pr | Prandtl number $\left[\mu C_{pl} / K_l \right]$ | |
| P_c | Critical pressure | lb/in ² . |
| P_p | Perimeter | ft. |
| P_{rr} | Pressure ratio $\left[P / P_c \right]$ | |
| q | Surface heat flux | Btu/h.ft ² . |
| R.M.S. | Root Mean Square Error | |
| | $\left[\frac{\sum \left[100 \left\{ \left(\pi_{1_{actual}} - \pi_{1_{predicted}} \right) / \pi_{1_{actual}} \right\}^2 \right]}{\text{Number of points}} \right]$ | |
| SP | Dimensionless triple front speed | |
| S.T. | Standard deviation | |
| | $\left[\frac{\sum \left(\pi_{1_{actual}} - \pi_{1_{predicted}} \right)^2}{\text{Number of points} - 2} \right]$ | |
| T | Temperature | °F. |
| t | Time | Sec. |
| ΔT_{SC} | Subcooling at liquid core | °F |
| T_c | Critical temperature | °F. |
| T^* | Dimensionless time group $\left[t W_o \xi / \delta_o \right]$ | |
| v | Specific volume | ft ³ /lb. |
| V | Dimensionless velocity in Y-direction | |
| W_z | Velocity component in the Z-direction | ft/sec. |
| W_y | Velocity component in the Y-direction | ft/sec. |
| W_o | Velocity of mean stream section at δ_o | ft/sec. |
| W_m | Mean film velocity | ft/sec. |
| W^* | Dimensionless velocity $\left[W_z / W_o \right]$ | |
| W_1^* | Dimensionless mean velocity in Z-direction | |
| X | Fluid quality | |
| X_{CRT} | Fluid quality at boiling crisis | |

| | | |
|----------|--|-----|
| X_{TT} | Lockhart and Martinelli parameter | |
| Y^* | Dimensionless distance $[Y/\delta_o]$ | |
| Z_o | Distance at $Z = 0$ | ft. |
| Z^* | Dimensionless distance $[(Z-Z_o)/\lambda]$ | |

Subscripts

| | |
|------------------|----------------|
| w | Wall condition |
| ∞ | Upstream |
| l | Liquid |
| v | Vapour |
| sat | Saturation |
| TP | Two-phase |
| F | Freon |
| H ₂ O | Water |
| p | Period |
| i | Inlet |
| n | Normal |
| t | Tangential |

Greek Symbols

| | | |
|------------|---|---------------------------------------|
| α | Dimensionless wave celerity (C/W_o) | |
| β_s | Coefficient of thermal expansion | 1/ ^o F. |
| β | Temperature to pressure ratio $[dT/dP]$ | ^o F/(lb/in ²). |
| γ_s | Kinematic surface tension (σ/ρ) | ft ³ /h ² . |
| γ | Density to pressure ratio $[d(\rho_l/\rho_v)/dP]_{sat}$ | in ² /lb. |
| δ | Film thickness | ft. |
| δ_o | Mean film thickness | ft. |
| δ^* | Dimensionless film thickness $[\delta/\delta_o]$ | |
| δ_c | Critical film thickness | ft. |
| ξ | Thin film parameter $[\delta_o/\lambda]$ | |
| θ | Contact angle | |
| λ | Wave length | ft. |

| | | |
|--------------|--|-----------------------|
| μ | Viscosity | lb/h.ft. |
| ν | Kinematic viscosity $[\mu/\rho]$ | ft ² /h. |
| ρ | Density | lb/ft ³ . |
| σ | Surface tension | lb/sec ² . |
| ϕ | Dimensionless free surface deformation function $[\phi = f(z,t) = (\delta - \delta_o)/\delta_o]$ | |
| ψ_{CHF} | Critical heat flux parameter. | |

PREAMBLE AND A REVIEW OF EXISTING
SIMULATION TECHNIQUES

1.1 BOILING PHENOMENA

The majority of fossil fuel steam generators and all the commercial nuclear steam supply systems operate at sub-critical pressures. A comprehension of the boiling process is essential in the design of these units.

In order to obtain information on the nature of boiling, investigators have either to experiment with electrically heated wires in a pool of water or to perform their experiments on heated tubes or other types of flow channels cooled by a flow of water at pressures below critical.

When subcooled water is introduced into a vertical, uniformly heated channel, the flow being upwards, it attains several patterns ranging from subcooled liquid to superheated steam. There are no specific agreed notations for the different regimes of flow. Vohr (1960, 1963) in his review of the work on flow regimes in both horizontal and vertical heated straight tubes noticed the confusion which existed in the description of the regimes and the transition regions between such flow regimes. However, if we follow Collier's (1972) analysis, the flow regimes are, as shown in Figure (1.1):

single-phase flow (liquid), bubbly flow, slug flow, churn flow, wispy-annular flow, annular flow, droplet region and single-phase flow (vapour).

In all cases it is important to keep the heat flux below a certain critical value at which a phenomenon termed "boiling crisis" occurs, which is characterised by a sudden drop in the heat transfer coefficient as a vapour film is formed which insulates the heating surface from the coolant.

The reduction in the rate of heat transfer below that supplied, causes an extreme and rapid temperature excursion of the heated surface. The extent of the excursion varies from very slight temperature increases to increases so large that the melting of the heating surface results. For temperature controlled systems, the boiling crisis is not usually a problem, but heat transfer coefficients could be markedly reduced.

According to Tong (1965), the boiling crises can be divided into two types:-

- 1) Burn-out (i.e. boiling crisis) in a subcooled or low quality flow: this occurs only at a relatively high heat flux, which causes extensive boiling so that the vapour bubbles are crowded near the heated surface;

thus local voids impair the surface cooling. This type of boiling crisis usually occurs at high flow rates, and the fluid near the surface may not be in thermodynamic equilibrium with the bulk stream. The core may remain subcooled even though the bulk enthalpy indicates a saturated fluid. Thus, the magnitude of the critical heat flux depends strongly upon the surface proximity parameters, which include the surface condition, local void fraction, local mass velocity, and boundary layer superheat. When burn-out occurs, the high heat flux may cause the surface temperature to rise rapidly to the extent of physical burn-out; this is sometimes called fast burn-out.

- 2) Burn-out in high quality flow; this type occurs at a lower heat flux than the case of fast burn-out. The total mass flow rate could be small, but the vapour velocity may still be high and the flow pattern is generally annular. If there is excessive evaporation due to boiling, this annular film layer breaks down, and a boiling crisis occurs. The magnitude of the critical heat flux in the high-quality region depends strongly upon the flow regime parameters, which include the average void fraction, slip ratio, vapour velocity and annular liquid film thickness. The surface

parameters are not as dominating as the fluid parameters. When the burn-out occurs, the surface temperature rises, but because of the fairly good heat transfer coefficient of a fast-moving vapour core in a high void fraction flow, the transient wall temperature rise is usually lower than in the subcooled case. This type of boiling crisis is sometimes called slow burn-out.

Lee and Obertelli (1963) distinguished experimentally between fast and slow burn-out, using a uniformly heated tube fitted with two different temperature indicators, thermocouples and bridge detector. They found that the burn-out occurred when the temperature rise was very rapid, for example, less than one second elapsed between the initiation of burn-out and the time at which the metal temperature became dangerously high. The channel power was quickly interrupted, otherwise a fast burn-out would have resulted in physical burn-out. Lee and Obertelli (1963) reported that in the case of water, fast burn-out is nearly always associated with subcooled or low quality conditions. They also noticed that slow burn-out corresponded loosely with a temperature excursion which took several seconds. The temperature rise was found to be smooth. Slow burn-out tended to be associated with high quality burn-out conditions and did not produce excessive wall-temperature rise.

Several attempts have been made to study the phenomena of burn-out based on either correlation of the parameters related to the critical heat flux or by describing the hydrodynamics of heat transfer processes which lead to the critical conditions.

Firman et al (1966) presented a map of the heat flux to the different regimes of the flow (Figure 1.2), from which they conclude that while there is some correspondence between heat transfer and the two-phase flow regimes, they are by no means synonymous. This distinction is evident in the middle ranges of the steam quality where, with an annular form of flow, the boiling process may be either convective, nucleate or film.

1.1.1 The Idea of Simulation and Modelling

Simulation and modelling is a valuable technique in almost any sphere of engineering, as it allows the prototypes and novel systems to be studied at lower cost, in less time, and with the opportunity of exploring the effect of modifications easily. In large complex boiling systems, there is need for simulation and modelling and considerable progress has recently been made in establishing successful techniques for dealing with the problem of forced convection burn-out.

Fluids such as Freons allow testing to be done at lower pressures and temperatures and require relatively smaller powers. Thus, wider ranges of all variables influencing the critical heat flux can be studied with lighter and more accessible hardware. Also, because of the decreased operating pressure, visual test sections can be easily constructed.

1.2 REVIEW OF DIFFERENT MODELLING TECHNIQUES

The Société Nationale d'Etude et de Construction de Moteurs d'Aviation (1961) used Freon to simulate both the hydrodynamics and thermal behaviour of boiling water reactor systems. This effort was directed towards the determination of the critical heat flux and the pressure drop in forced-convection systems. No comparison with water systems or correlations were reported.

Barnett (1963, 1964) developed scaling techniques to relate model and water data for round tubes. Using dimensional analysis of system parameters, he was able to link Freon-12 and Freon-21 data with water data at 1000 psia within $\pm 7\%$ by applying sets of fourteen parametric combinations of scaling laws.

Experimental investigations by Barnett (1964, 1965) showed that the most consistent set was:

$$\frac{F_{qa} \cdot \gamma^{\frac{1}{2}}}{H_{fg} \cdot \rho_l^{\frac{1}{2}}} = F\left(\frac{L}{D}, \frac{D \cdot C_{pl} \cdot \rho_l^{\frac{1}{2}}}{K_l \cdot \gamma^{\frac{1}{2}}}, \frac{G_a \cdot \gamma^{\frac{1}{2}}}{\rho_l^{\frac{1}{2}}}, \frac{\rho_l}{\rho_v}, \frac{\Delta H}{H_{fg}}\right) \quad (1.1)$$

Plots obtained from testing this set are shown in Figures 1.3 and 1.4.

Figure 1.3 shows that at mass velocity of 1.5×10^6 lb/hr.ft², an error of $\pm 7\%$ can occur when data for water and water equivalent are compared. However, the errors occurring at the longer tube length (Figure 1.4) are smaller ($\pm 5\%$).

Barnett's work laid the foundations for the more direct empirical techniques that followed.

Stevens and Kirby (1964) suggested a graphical correlation which they developed by considering the flow inside a uniformly heated tube. They noticed that the same shape of curve was obtained when Freon-12 and water data were plotted as X_{CRT} versus E, where

X_{CRT} = fluid quality at boiling crisis

$$= \frac{4L \cdot F_{qa}}{D \cdot H_{fg} \cdot G_a} - \frac{\Delta H}{H_{fg}}$$

E = Empirical function for graphical scaling

$$= G_a \cdot D^{\frac{1}{4}} \cdot (D/L)^{0.59} \times 10^{-4} \quad \left(\frac{\text{lb} \cdot \text{in}^{\frac{1}{4}}}{\text{hr} \cdot \text{ft}^2}\right)$$

Also, they found that all water and Freon data could be superimposed on the same curve by changing the abscissa from E to K.E, where $K = 0.658$. Accordingly, they were able

to obtain scaling factors which related the two fluids. Predictions obtained from this latter graphical technique have proven to be more accurate when compared with experimental data than that conducted by Barnett (1963, 1964).

Later, Stevens and Macbeth (1970) showed that the mass flux scaling factor technique yielded also accurate modelling results for a range of annular and rod bundle geometries and axial power profiles. Later, Hauptmann and Lee (1971) presented an experimental study on burn-out using carbon dioxide as a working fluid to simulate burn-out in water systems. Applying the parameter grouping suggested by Stevens and Kirby (1964) they managed to show that different sets of curves for different fluids could empirically coincide on a single curve by using a scaling factor K . Their results are shown in Figures 1.5a and 1.5b. The value of K (i.e. = 0.74) was required to fit the CO_2 data to Freon-12 data. This procedure of Stevens and Kirby (1964) has created widespread interest and confidence in the Freon/water, Freon/ CO_2 and CO_2 /water modelling of burn-out. Nevertheless, it does not provide any physical basis for the calculated scaling factor, and it has also the disadvantage of lacking generality as it is only valid for a considered particular fluid at a specified pressure only. It was suggested by Behar (1967) that the

factor (K) should be considered as a function of pressure, and that its value could be calculated in terms of fluid properties, i.e.,

$$K = \left(\frac{\rho_{lF}}{\rho_{lH_2O}} \cdot \frac{\gamma_{H_2O}}{\gamma_F} \right)^{\frac{3}{8}} \cdot \left(\frac{K_{lF}}{K_{lH_2O}} \cdot \frac{C_{PlH_2O}}{C_{PlF}} \right)^{\frac{1}{4}}$$

This could be a convenient way of modifying the Stevens et al (1964) (K) factor to account for different pressures and fluids. There is agreement between the predicted and the experimental results for Freon-12 for simulation of water at high pressures (2000 lbf/in²) but the formula fails to simulate water at 1000 lbf/in² or below. It appears that, due to the large number of parameters which affect burn-out, a more complex formula is required.

Staub (1969) proposed a modification to the Stevens and Kirby graphical correlation. He replaced the test length (L) by the boiling length (L_b), defined as the equilibrium boiling length, starting from zero equilibrium quality. Applying this modification, a single curve (Figure 1.6) showed the data over a large range of values of inlet subcooling. In Figure 1.6 the solid square symbols are used to denote the method of plotting the correlation of X_{CRT} versus G_a · D^{1/4} (D/L)^{0.59} as recommended by Stevens et al. The open square symbols denote Staub's modified correlation, i.e.

calculated with the same Freon-12 data, but plotted with (L_b) . There is good agreement between Freon-22, Freon-12 and water when the modified correlation is applied (Figure 1.7 and Table I). In Figures 1.7a and 1.7b Staub showed that the scaling factor did not appreciably vary with pressure in the range tested.

Coffield (1969) extended the application of critical heat flux modelling to subcooled liquid conditions. He used two methods to show that the scaling factor technique was successful for subcooled critical heat flux. The first method for dynamic similitude was obtained by using dimensional analysis of a hydrodynamic behaviour as suggested by Barnett (1963) (i.e. equation 1.1). Surface heat flux was plotted versus mass velocity for the actual water data and the equivalent water data from scaling on the same diagram, one set of parameters being at $\frac{\Delta H}{H_{fg}}$ equal to 0.612 and 0.410 and pipe diameter 0.425" for $\rho_l/\rho_v = 7.2$, and the other set of parameters (water pressure 2000 lb/in²) at $\frac{\Delta H}{H_{fg}}$ equal to 0.254, 0.443 and pipe diameter 0.44" for $\rho_l/\rho_v = 20.6$ (water pressure 1000 lb/in²). The maximum discrepancy between the actual data and the scaled data was found (Coffield, 1969) to be about +15%.

The second method is based on Stevens et al (1964)

multiplicative factor (K) which leads to the scaling factors. The values necessary to produce good superpositioning of the Freon-113 and water data were:-

$$K = 0.684 \text{ for } \rho_l/\rho_v = 20.6$$

$$K = 0.690 \text{ for } \rho_l/\rho_v = 11.8$$

$$K = 0.715 \text{ for } \rho_l/\rho_v = 7.2$$

It seems that the inlet subcooling has no effect on the value of K. However, the curve is displaced to the left by increased inlet subcooling. As in the first method, the second method simulates the subcooled Freon-113 boiling crisis data to the equivalent subcooled water data to within ±15%.

Groenveld (1969, 1970) developed a new optimisation technique for the determination of accurate scaling factors from experimental data. He suggested that the critical heat flux could be correlated against two groups of parameters frequently used in critical heat flux correlations:

$$F_{qa} = f(D, L/D, G_a^{\cdot}, \Delta H), \quad (1.2a)$$

or,

$$F_{qa} = f(D, L/D, G_a^{\cdot}, X), \quad (1.2b)$$

which could be correlated by an optimisation technique to obtain the following correlations:

$$i) \quad F_{qa} = D^{b_1} \cdot f_1(L/D) \cdot f_1(G_a^{\cdot}) \cdot f(\Delta H) \quad (1.3a)$$

where:

$$b_1 = -0.201936$$

$$f_1(L/D) = 2.39038 \times 10^3 - 12.533(L/D) + 2.71225 \times 10^{-2}(L/D)^2$$

$$f_1(G'_a) = 12.2933 + 23.8733(G'_a/10^6) - 13.7705(G'_a/10^6)^2 + 2.986(G'_a/10^6)^3$$

$$F(\Delta H) = 0.983585 + 3.31376 \times 10^{-3}(\Delta H) - 1.56024 \times 10^3(\Delta H)^2 + 9.67859 \times 10^{-5}(\Delta H)^3$$

$$\text{ii) } F_{qa} = D^{b_2} \cdot f_2(L/D) \cdot f_2(G'_a) \cdot f(x) \quad (1.3b)$$

where:

$$b_2 = -0.362713$$

$$f_2(L/D) = 9.71043 \times 10^6 - 2.1714 \times 10^4(L/D) + 42.2492(L/D)^2$$

$$f_2(G'_a) = 1.16244 \times 10^{-2} - 1.15061 \times 10^{-2}(G'_a/10^6) + 6.28448 \times 10^{-3}(G'_a/10^6)^2 - 1.17288 \times 10^{-3}(G'_a/10^6)^3$$

$$f(x) = 1.36368 - 2.88422x + 3.5288x^2 - 2.23072x^2$$

In the Groenveld analysis, the inlet subcooling scale factor was kept fixed at 11.72, the ratio of the latent heat of vaporisation in water and Freon-12 at $\rho_l/\rho_v = 20$ and length to diameter scaling factors were both fixed at 1.0. Assuming Freon-12 correlations are valid for the water data, if the proper scaling factors are used, then equation (1.3a) can be re-written for water as follows:

$$\frac{(F_{qa})_{H_2O}}{F_Q} = D^{b_1} \cdot f_1(L/D) \cdot f_1\left(\frac{G'_a}{F_G}\right) \cdot f\left(\frac{\Delta H_{H_2O}}{11.72}\right)$$

$$\text{i.e. } F_Q = \frac{(F_{qa})_{H_2O}}{D^{b_1} \cdot f_1(L/D) \cdot f_1\left(\frac{G}{F_G}\right) \cdot f\left(\frac{\Delta H_{H_2O}}{11.72}\right)} \quad (1.4a)$$

Equation (1.3b) can be manipulated in the same way.

Groenveld managed to calculate the mass flux and the critical heat flux scaling factors at the minimum error points. It was found that $F_G = 1.42$ and $F_Q = 17.8$ for the first group of parameters (i.e. equation 1.2a), a minimum R.M.S. error of 7.8% and $F_G = 1.75$ and $F_Q = 17.0$ for the second group of parameters with a minimum R.M.S. error of 9.2%. This method of correlation yields scaling factors fairly similar to those found by Stevens et al (1964), except for the mass flux scaling factors, which is 1.42 instead of being 1.54.

Dix (1970) suggested that scaling factors exhibit effects of mass flux, length to diameter ratio, and pressure. In his work he used the thermal equilibrium energy balance equation.,

$$\frac{F_{qa}}{G_a \cdot H_{fg}} = \left(\frac{A_F}{A_H}\right) \left(X + \frac{\Delta H}{H_{fg}}\right) \quad (1.5)$$

where $A_F = \text{flow area (ft}^2\text{)}$
 $A_H = \text{total heated area (ft}^2\text{)}$

to define his dimensionless scaling factor. It is apparent from equation (1.5) that comparison of data from identical

geometries with equal quality and dimensionless subcooling values must have equal values for the dimensionless heat flux grouping on the left hand side of equation (1.5). Since equation (1.5) is independent of the fluid type, then a required Freon/water modelling relation for these conditions becomes

$$\left(\frac{F_{qa}}{G'_a \cdot H_{fg}}\right)_{\text{Freon}} = \left(\frac{F_{qa}}{G'_a \cdot H_{fg}}\right)_{\text{Water}} \quad (1.6)$$

which can be written in the form

$$(G'_a)_{\text{Freon}} = K(G'_a)_{\text{Water}} \quad (1.7)$$

where K is the flow scaling factor (F_G) and is not necessarily constant. He managed to obtain an equation for the modelling factor (K) by using the correlation given by Basi (1967), i.e.

$$K = F_G = \frac{(G'_a)_{\text{Freon}}}{(G'_a)_{\text{H}_2\text{O}}} = C_T (1.0 - 0.09(G'_a)_{\text{H}_2\text{O}} \times 10^{-6}) (1.04 - 0.05L/D \times 10^{-2}) (1.41 - 0.02\left(\frac{\rho_l}{\rho_v}\right)) \quad (1.8)$$

which he showed to be dependent on the pressure (density ratio), the length to diameter ratio and mass velocity. Then the modelling relations presented in equations (1.6), (1.7) and (1.8) were used together with Basi water correlation to predict a critical heat flux value. The resultant R.M.S. error in the heat flux predicted was 4.2%. He also mentioned

that the pressure effect needs to be studied more and compared with future data. As the range of parameters tested was not large, no definite conclusions can be drawn.

Bouré (1970) obtained dimensionless groups from arbitrarily selected parameters by the dimensionless analysis method. These groups were then amended by correction factors. The correction factors given were only applicable to Freon-12/water modelling at a liquid/vapour density ratio of 7.0. No explanation was given of the method by which the correction factors were determined. Bouré claims a correlating accuracy of within $\pm 10\%$ for his method, but this shows no improvement over Barnett's scaling technique.

Tong et al (1970) have formulated a simulating model for subcooled boiling crisis. They mentioned that flow-boiling crisis simulation required geometric and dynamic similitudes. The geometric similitude implied a similar channel size, length and shape, while the dynamic similitude implied both hydrodynamic and thermodynamic similitudes. The hydrodynamic similitude required a similar flow pattern, similar velocity and shear distribution. The thermodynamic similitude required a similar heat transfer mechanism and equivalent thermodynamic properties of the coolant, such as the system pressure, temperature and specific volume which were mostly a function of the reduced pressure $P_{rr} = P/P_c$.

In their approach they suggested the existence of a bubble layer sliding between the subcooled core and the heating surface. The thermodynamic similitude is expressed in terms of a boiling number (B_o):

$$B_{o\text{crit}} = \frac{F_{qa}}{H_{fg} \rho_l W_z}$$

while the hydrodynamic similitude was expressed by the two-phase friction factor (f_{TP}) which is a function of a two-phase Reynolds number:

$$f_{TP} \propto Re_{TP}^{-0.6}$$

Then the scaling factor was given as:

$$B_{o\text{crit}} = C_o f_{TP}$$

where C_o is a function of P_{rr} (or $\rho_l \rho_v$) and the properties of liquid core. From the experimental data given by Coffield (1969) for subcooled Freon-113 the numerical constants in the scaling law were evaluated for water and Freon-113 as follows:

Water:

$$F_{qa} = (1.5 + 0.032\Delta T_{SC}) H_{fg} (\rho_l W_z)^{0.4} (\mu_l / D_e)^{0.6} \quad (1.9a)$$

Freon-113:

$$F_{qa} = 0.4e^{0.783P_{rr}} \left(\frac{v_{c_{F-113}}}{v_{c_{H_2O}}} \right) (1.5 + 0.032\Delta T_{SC}) H_{fg} \cdot (\rho_l W_z)^{0.4} (\mu_l / D_e)^{0.6} \quad (1.9b)$$

where ΔT_{SC} is the subcooling of the liquid core,
 $\frac{v_{c_{F-113}}}{v_{c_{H_2O}}}$ is the critical specific volume ratio = 0.55,
 $0.4e^{0.783P_{rr} \cdot (\frac{v_{c_{F-113}}}{v_{c_{H_2O}}})}$ is the scaling factor.

However, it was reported by Tong et al (1970) that applying the above equations for the simulation of water by Freon-113 and then by comparison with Coffield's (1969) experimental data an error of +25% was encountered. Tong et al (1970) also suggested that the scaling factor K (i.e. $K = 0.4e^{0.783P_{rr} \cdot (v_{c_{F-113}}/v_{c_{H_2O}})}$) is a function of the critical pressure and the ratio of the properties of the model and prototype fluid, which usually can be expressed by $v_{c_{model}}/v_{c_{prototype}}$.

Ahmad (1971) found that the selection of equal density ratios to scale the operating pressures of model and prototype fluids produced inequalities in the ratios of other physical properties. The problem of multiple errors was treated by Ahmad by introducing a modelling parameter which is a function of Weber number and liquid and vapour superficial Reynolds numbers.

Ahmad described the flow boiling heat transfer by the equation

$$f(F_{qa}, G'_a, \Delta H, L, D, g, H_{fg}, \rho_l, \rho_v, \mu_l, \mu_v, C_{pl}, C_{pv}, K_l, K_v, \sigma, \gamma, \beta) = 0 \quad (1.10)$$

With the aid of a dimensional analysis method given by Langhaar (1967) and applying Buckingham's Pi theorem (1914) he derived the following equation from equation (1.10):

$$\pi_1 = F(\pi_2, \pi_3, \pi_4, \dots, \pi_{13}) \quad (1.11)$$

where:

| | |
|---|--|
| $\pi_1 = F_{qa}/G'_a \cdot H_{fg}$ | (Boiling number) |
| $\pi_2 = G'_a \cdot D/\mu_l$ | (Reynolds number) |
| $\pi_3 = \mu_l^2/\sigma \cdot D \cdot \rho_l$ | (Weber-Reynolds number) |
| $\pi_4 = \mu_l/\mu_v$ | (Liquid/vapour viscosity ratio) |
| $\pi_5 = \Delta H/H_{fg}$ | (Subcooling number) |
| $\pi_6 = \rho_l/\rho_v$ | (Liquid/vapour density ratio) |
| $\pi_7 = L/D$ | (specific geometric similarity) |
| $\pi_8 = gD^3\rho_l/\mu_l^2$ | (Froude-Reynolds number) |
| $\pi_9 = C_{pl} \cdot \mu_l/K_l$ | (Liquid Prandtl number) |
| $\pi_{10} = C_{pv} \cdot \mu_v/K_v$ | (Vapour Prandtl number) |
| $\pi_{11} = K_l/K_v$ | (Liquid/vapour thermal conductivity ratio) |
| $\pi_{12} = \gamma^{1/2} \mu_l/D\rho_l^{1/2}$ | (Barnett number) Barnett et al (1963, 1964) |
| $\pi_{13} = \beta C_{pl}/\gamma H_{fg}$ | (Saturation temperature number) |

Equation (1.11) is a general equation for flow boiling heat transfer; it applies to any system which is

a function of the same variables. For complete similitude $(\pi_1)_{\text{prototype}}$ must equal $(\pi_1)_{\text{model}}$, and this implies that $(\pi_2)_{\text{prototype}}$ equals $(\pi_2)_{\text{model}}$, $(\pi_3)_{\text{prototype}}$ equals $(\pi_3)_{\text{model}}$, etc. But obviously it is impracticable to satisfy all twelve Pi terms on the right hand side of equation (1.11). So he discarded the Pi terms which do not play a significant role in critical heat flux (burn-out) problems and equation (1.11) was reduced to

$$\pi_1 = f(\pi_2, \pi_3, \pi_4, \pi_5, \pi_6, \pi_7) \quad (1.12)$$

For complete similitude π_r for prototype must equal π_r for model for all values of r from 1 to 7. π_5 , π_6 and π_7 can be equalised independently for the model and the prototype, which leaves us with π_2 , π_3 and π_4 , which can be equalised for model and prototype. Therefore he grouped these Pi's as follows:

$$\psi_{\text{CHF}} = \pi_2 \times \pi_3^{n_1} \times \pi_4^{n_2} \quad (1.13)$$

where n_1 and n_2 are empirical constants. The values of n_1 and n_2 are determined from experimental data to be $\frac{2}{3}$ and $\frac{1}{8}$ respectively.

Examination of the proposed modelling method (Figure 1.8) for different fluids (i.e. CO₂, water, Freon-12, Freon-113, etc.) at a constant ρ_l/ρ_v , $\Delta H/H_{fg}$, L/D shows the relation between π_1 ($= F_{qa}/G'_a \cdot H_{fg}$) versus ψ_{CHF} .

In spite of the generality of Ahmad's (1971) modelling method, its range of validity has inherent limitations because of the nature of the two empirical constants, n_1 and n_2 . Consequently the range of validity can be established only by testing the modelling parameter with available experimental observations. Furthermore, it is stated that the Prandtl number, specific heat, and thermal conductivity are unimportant in boiling crisis prediction. This implies that since Prandtl number equals $C_{p\ell} \cdot \mu_{\ell} / K_{\ell}$, the viscosity must also be unimportant. But due to the assumption that the viscosity is important, one of the above parameters might also be important and need to be included.

CONCLUSIONS

Among different suggested sets of dimensionless groups, Barnett et al (1964) found that the most consistent set was the one described by equation (1.1) by which errors in simulation were not likely to be reduced below +7%. Nevertheless, to reduce such error Barnett et al attempted the inclusion of the group $(H_{fg} \gamma / \beta C_{pl})$. This entails that the two property groups ρ_l / ρ_v and $H_{fg} \gamma / \beta C_{pl}$ should be equal in the two systems. But this is not possible in Freon/water modelling. However, Freon-12 and Freon-21 exhibit almost identical values of $H_{fg} \gamma / \beta C_{pl}$ and Prandtl number. The addition of the second property group in equation (1.1) gave a slight improvement in the correlating accuracy, which could be due to the addition of either β or μ_l or both to the set described by equation (1.1). To enable these effects to be separated and other properties to be analysed, Andersen and Pejtersen (1969) suggested the use of azeotropic mixtures as modelling fluids.

Barnett's (1964) scaling laws have reached an impasse in their present form, unless the effect of other parameters is included. This would impose too restrictive conditions on the model fluid.

It appears that the method used by Ahmad (1971) has proven to be promising in the development of the modelling procedure.

Part of the present thesis includes a combination between the compensated distortion technique developed in Chapter 2, and the use of the dimensionless simulating parameters suggested by Barnett (1964, 1965). This allows the group of parameters $H_{fg} \cdot \gamma / \beta \cdot C_{p1}$ or $C_{p1} \cdot \sigma \cdot \gamma^{1/2} \cdot \rho_l^{1/2} / K_l$ or $\mu_l \cdot C_{p1} / K_l$ to be added to equation (1.1) and their effect on the simulation errors can be investigated.

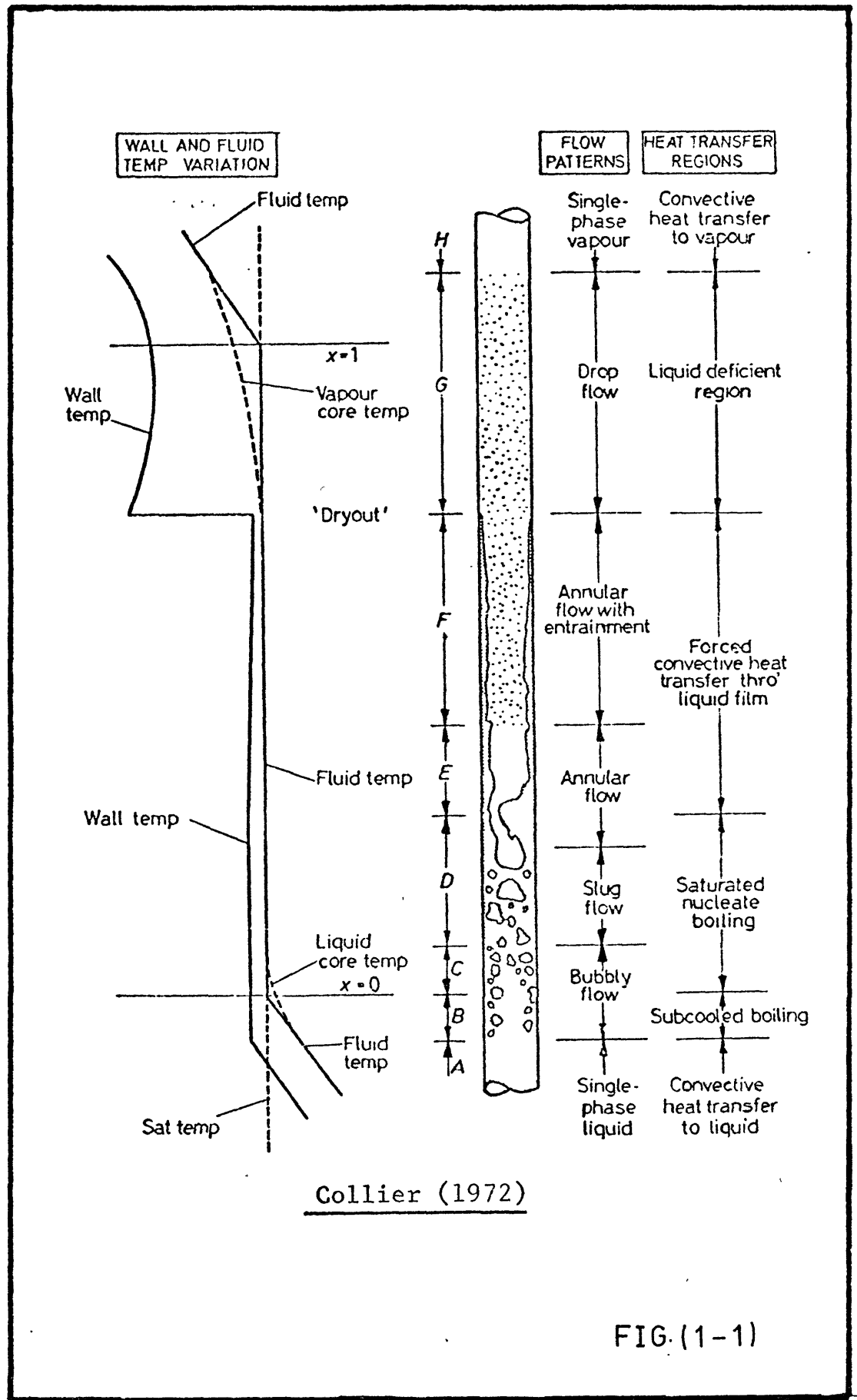


FIG. (1-1)

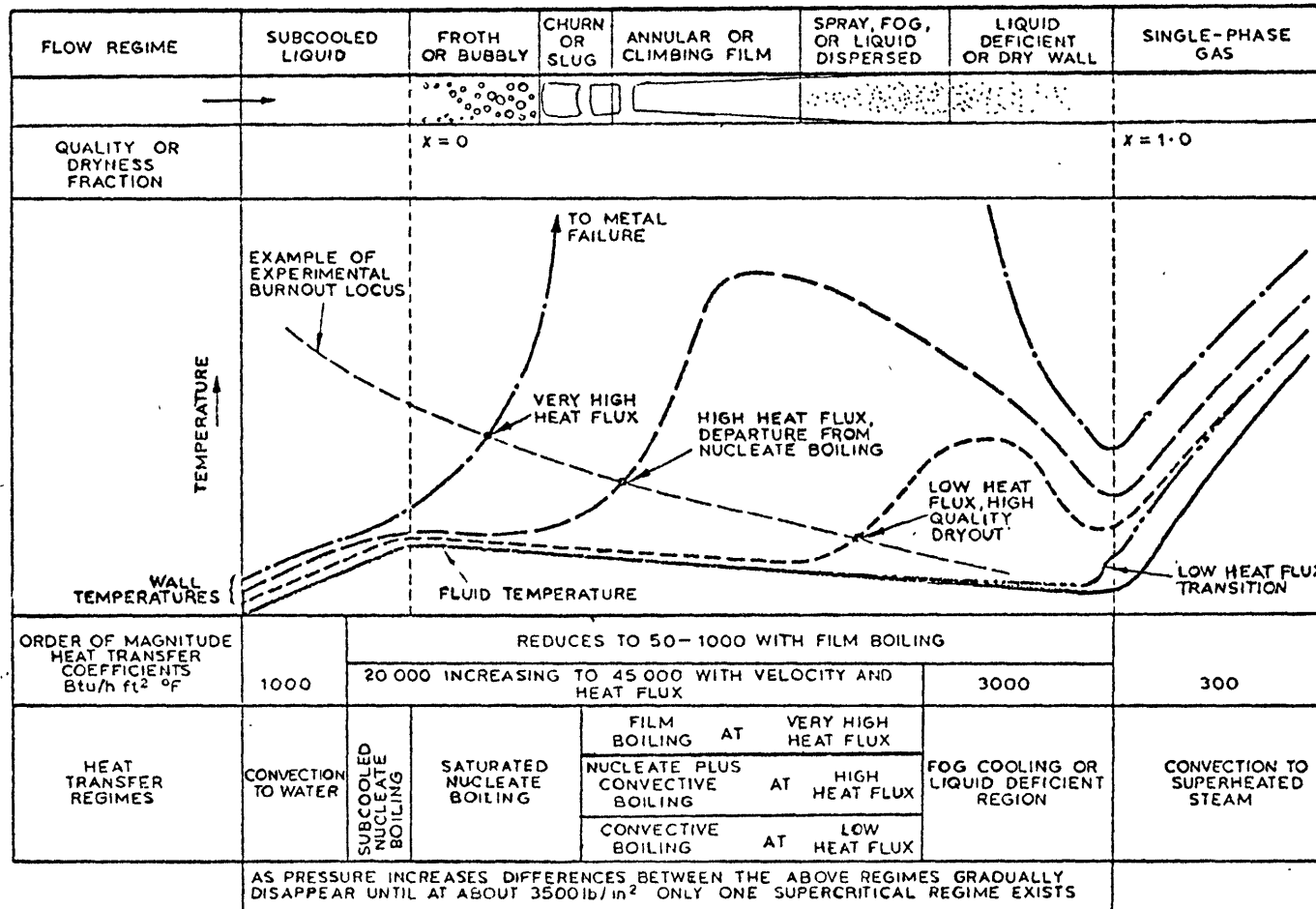


FIG.(1-2)

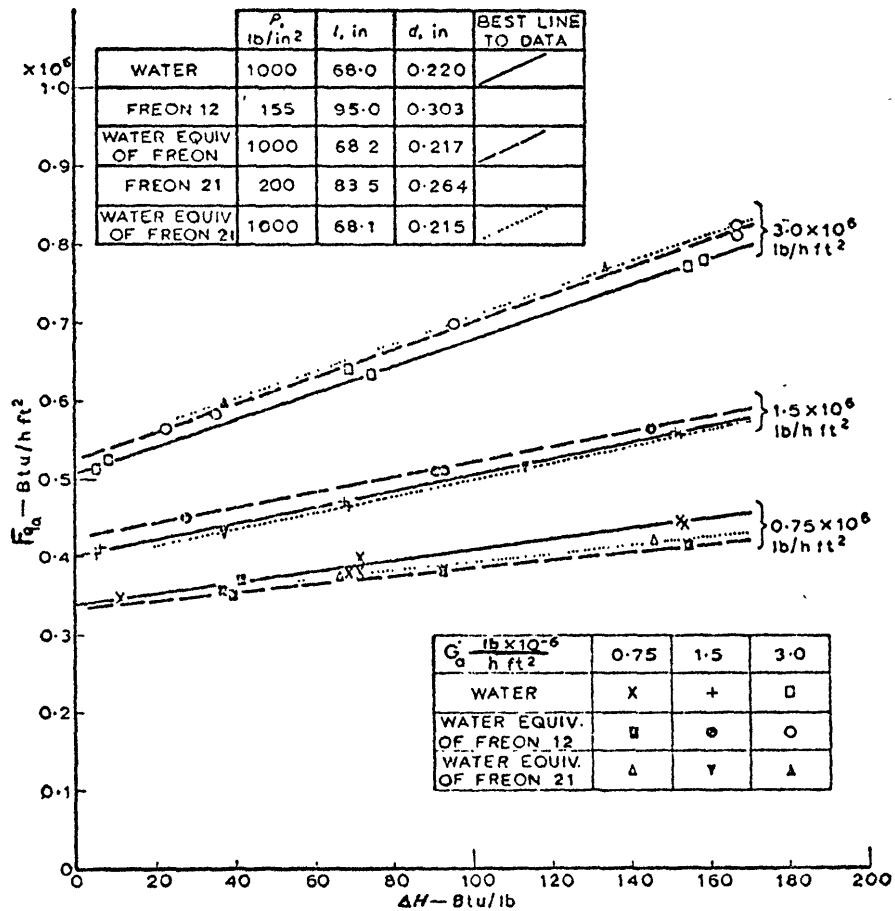


FIG. (1 - 4)

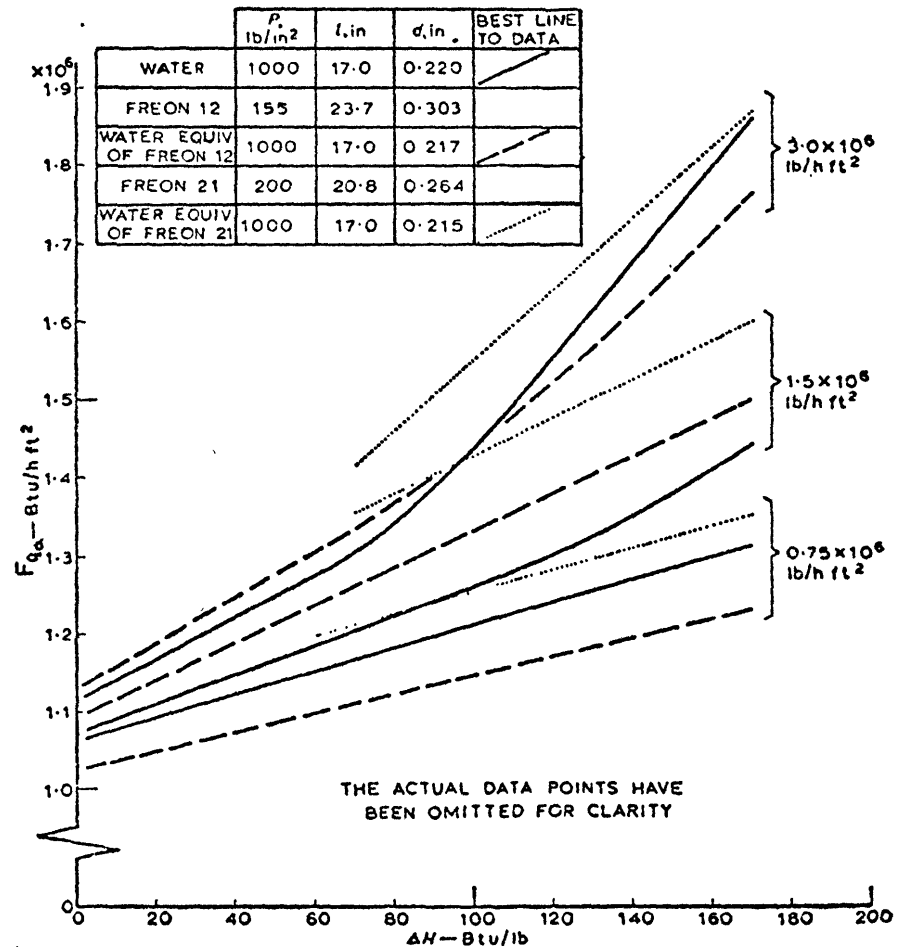
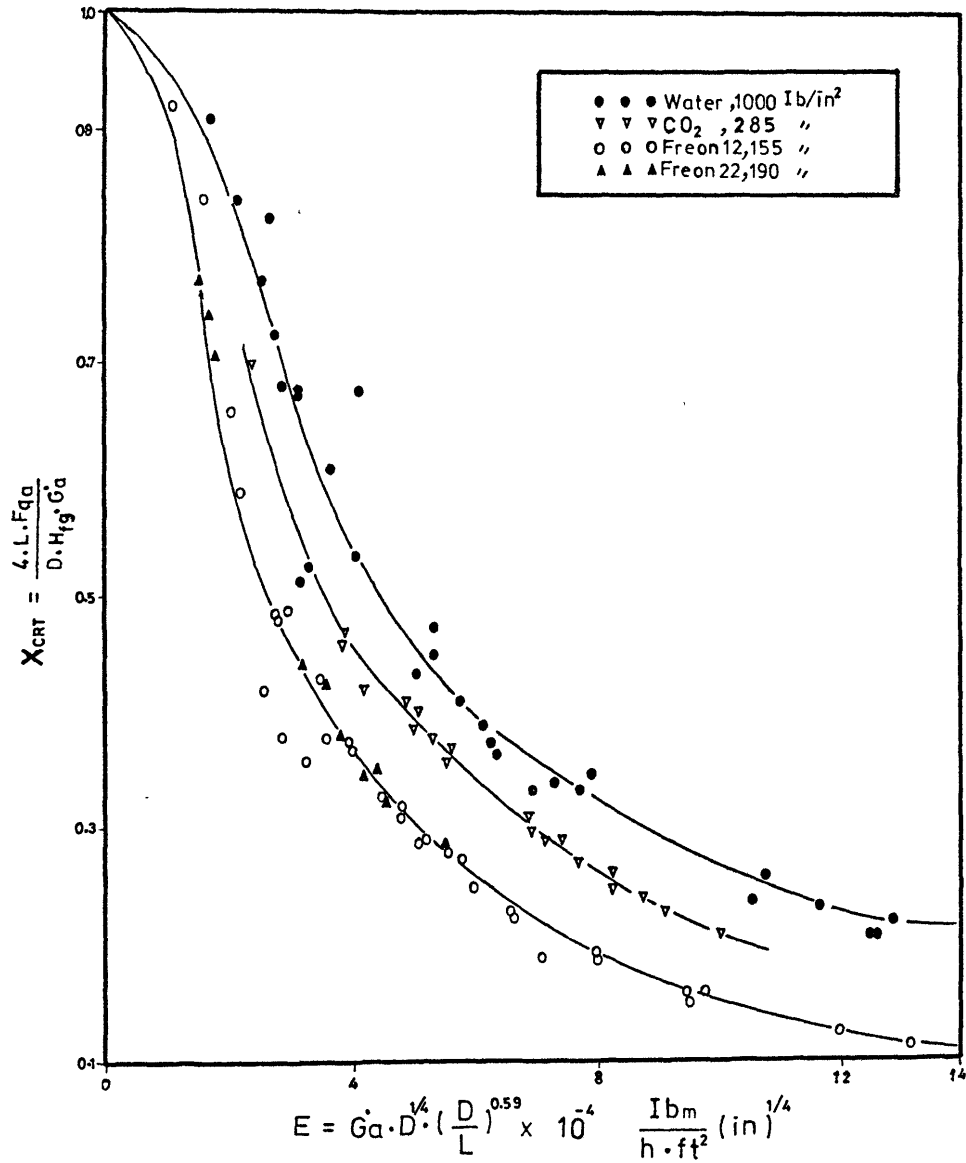
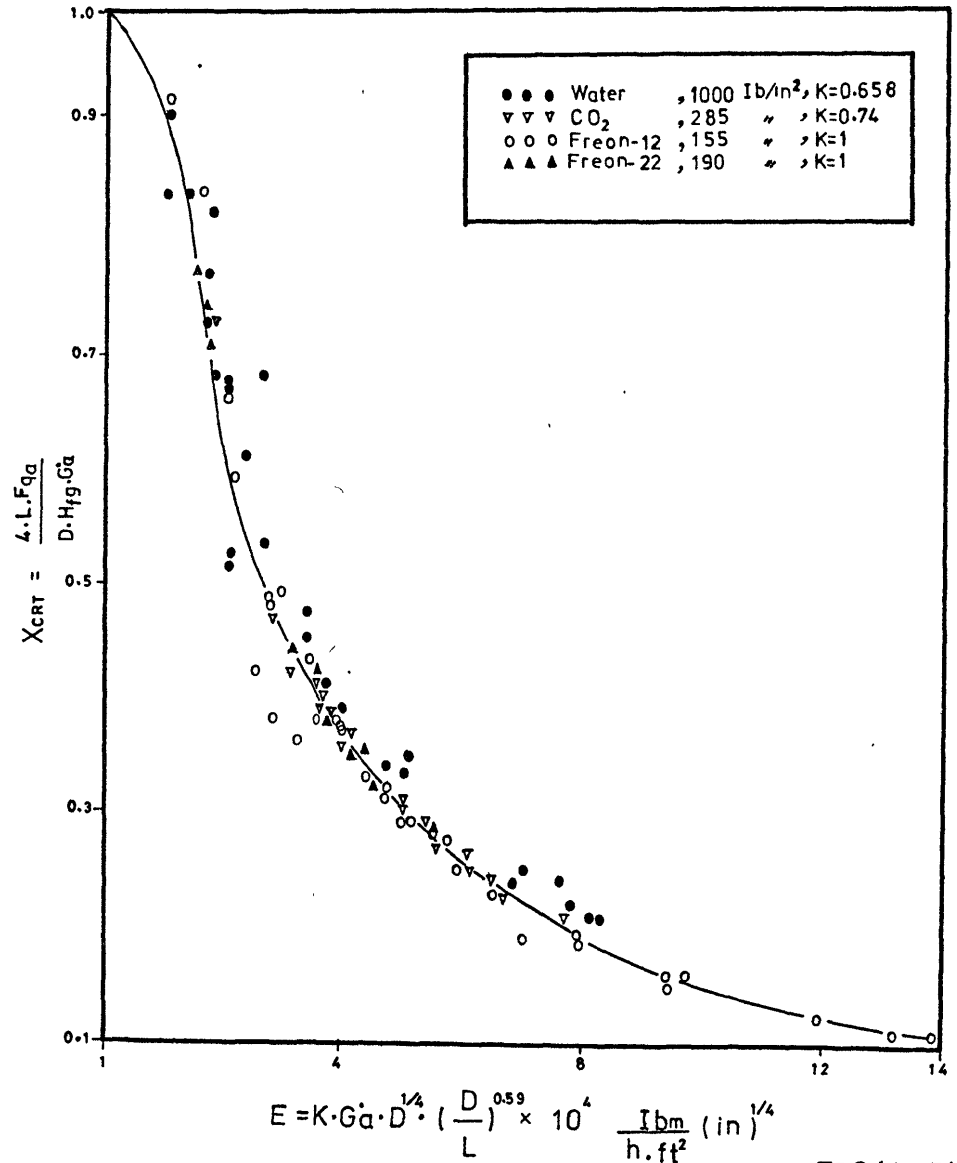


FIG (1 - 3)



FIG(1-5a)



FIG(1-5b)

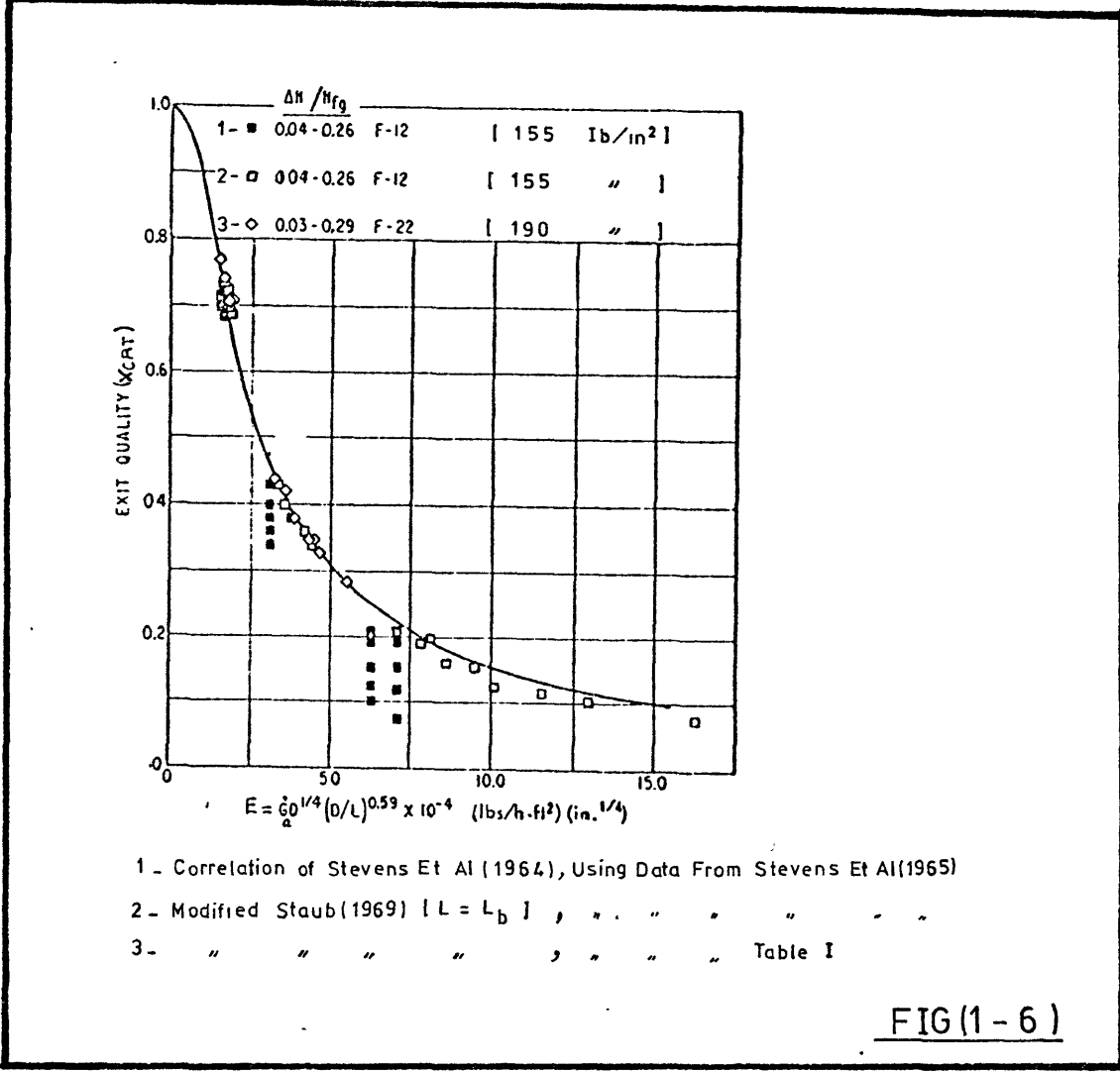


TABLE I

Critical Data Summary for Freon-22

| Inlet Mass Velocity (lb/h ft ² × 10 ⁻⁵) | Critical Heat Flux (Btu/h ft ² × 10 ⁻⁵) | Inlet Subcooling ($\Delta H / H_{fg}$) | Discharge Pressure (psig) ^a | Boiling Length L_b (in.) | Critical Discharge Quality x_{CRT} |
|---|---|---|---|----------------------------------|---|
| 3.62 | 0.191 | 0.032 | 173.5 | 58.0 | 0.770 |
| 3.80 | 0.222 | 0.110 | 177.3 | 52.5 | 0.740 |
| 7.40 | 0.230 | 0.031 | 173.5 | 56.5 | 0.44 |
| 9.00 | 0.245 | 0.032 | 172.2 | 56.0 | 0.380 |
| 7.90 | 0.268 | 0.125 | 173.1 | 46.5 | 0.425 |
| 9.70 | 0.281 | 0.120 | 173.0 | 45.0 | 0.350 |
| 3.80 | 0.230 | 0.220 | 176.2 | 46.1 | 0.705 |
| 7.85 | 0.295 | 0.226 | 175.2 | 36.9 | 0.352 |
| 9.65 | 0.310 | 0.206 | 175.1 | 35.2 | 0.286 |
| 3.80 | 0.247 | 0.291 | 176.4 | 42.9 | 0.709 |
| 7.70 | 0.313 | 0.291 | 174.9 | 31.8 | 0.328 |

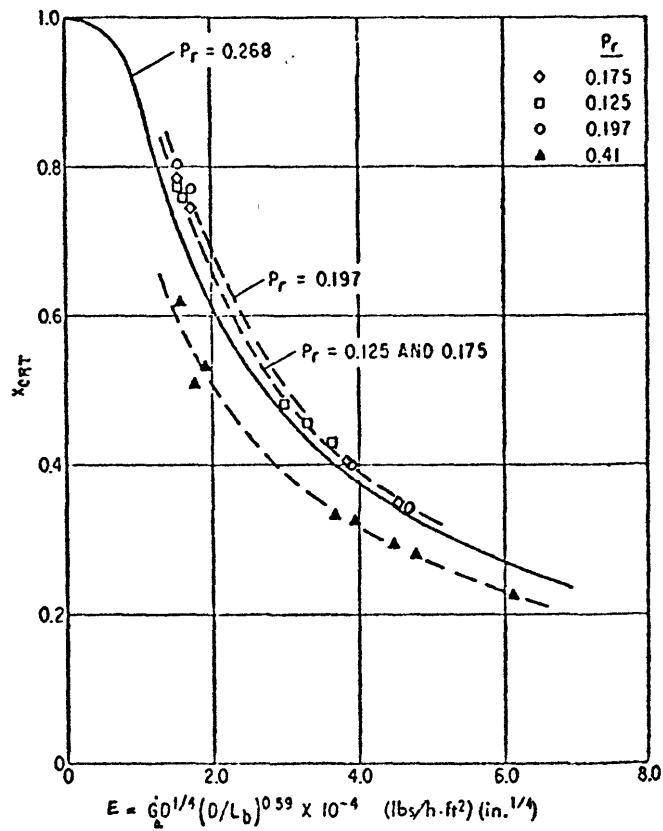


FIG. (1-7a)

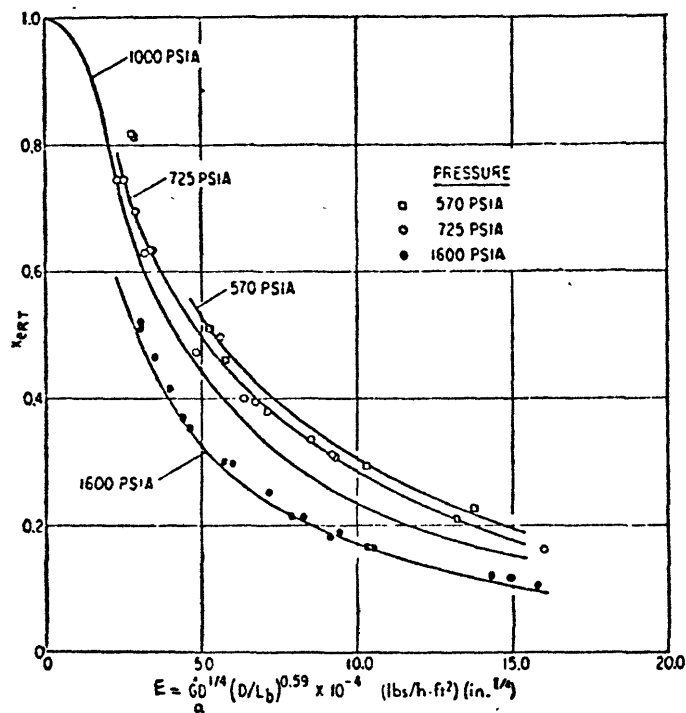


FIG. (1 - 7b)

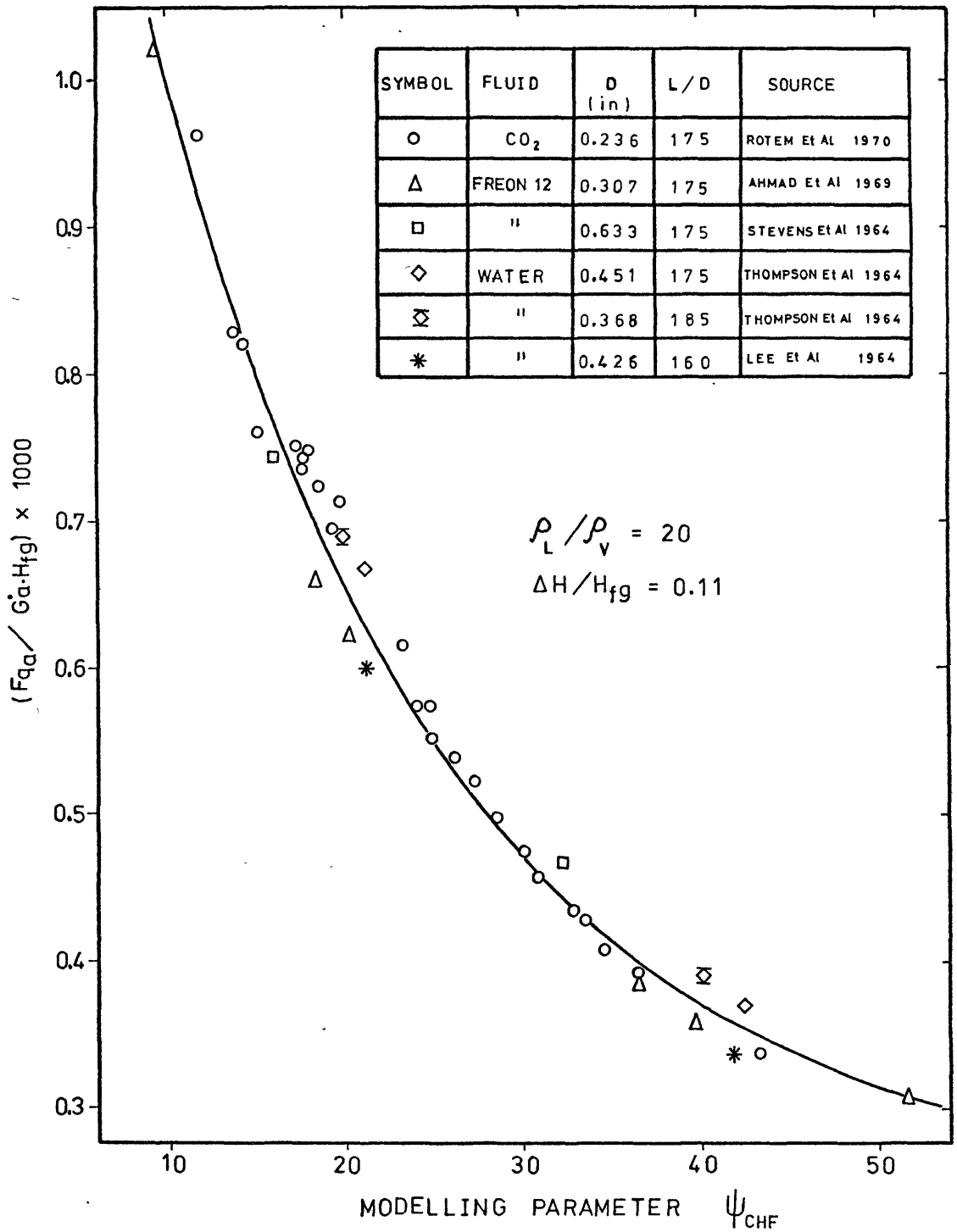


FIG. (1-8a)

CHAPTER 2SIMULATION OF CRITICAL HEAT FLUX2.1 INTRODUCTION AND DEFINITIONS

The main objective of the present chapter is to introduce a theoretical method which is developed for the simulation of the behaviour of water-boiling by Freon. The method is applied to the dimensionless groups suggested by Barnett (1964) and Ahmad (1971) for burn-out phenomenon (Section 2.2). The secondary objective is to apply the same technique referred to above to a specific type of flow, i.e. annular flow (Section 2.3).

2.2 A MATHEMATICAL MODEL FOR SIMULATING
CRITICAL HEAT FLUX

When attempting to solve a problem involving fluid flow and heat transfer it is often impossible to produce experimental conditions in which complete modelling of all the relevant parameters is attained. If the phenomena of interest can be described by a functional relationship between a number of dimensionless groups of variables, say S in number, which will be denoted by $\pi_1, \pi_2, \dots, \pi_5$ ^{etc.} then in order to provide complete modelling each group must have the same value in the model and the prototype. Suppose, however, that

because of the practical limitations upon materials and experimental conditions available to us we are able to model only $(S-r)$ of the groups the problem arises as to organising the data available so as to minimise the errors in the predictions due to the mismatch in the remaining groups. If enough data are available from model testing we can select a number of experimental points for which π_{r+1}, \dots, π_S are the same but which differ in their values of the π_1, \dots, π_r , and from these we can find a functional relationship for these groups, i.e. we have reduced the problem from one of S dimensions to one of r dimensions. Of course, the functional relations we are seeking will be different for different values of the $(\pi_{r+1} \dots \pi_S)$, but often we are only interested in predicting the behaviour of a piece of equipment for a few specified operating cases, so this limitation is acceptable.

The essence of the technique to be described is to assume that over a limited range the remaining r groups which are not correctly scaled enter in a simple way involving a number of empirical exponents. Thus if the situation is described by $f(\pi_1, \pi_2, \dots, \pi_S)$ and we are interested in determining π_1 as a function of the remaining variables we may write in general,

$$\pi_1 = F(\pi_2, \pi_3, \dots, \pi_S)$$

We suppose that the $r-1$ groups which cannot be modelled are π_2, \dots, π_r and assume that, over a limited range, they can be represented by an expression of the form $\pi_2^{n_1} \cdot \pi_3^{n_2} \dots \pi_r^{n_{r-1}}$ i.e. that

$$\pi_1 = F(\pi_2^{n_1} \cdot \pi_3^{n_2} \dots \pi_r^{n_{r-1}}), (\pi_{r+1}, \pi_{r+2}, \dots, \pi_s)$$

where A is a constant.

As an example consider Barnett's (1964) and Ahmad's (1970) equations which relate the dimensionless groups for the simulation of burn-out:

$$\frac{F_{qa} \cdot \gamma^{\frac{1}{2}}}{H_{fg} \cdot \rho_l^{\frac{1}{2}}} = F \left[\left(\frac{G_a \cdot \gamma^{\frac{1}{2}}}{\rho_l^{\frac{1}{2}}} \right), \left(\frac{D \cdot C_{pl} \cdot \rho_l^{\frac{1}{2}}}{K_l \cdot \gamma^{\frac{1}{2}}} \right), \left(\frac{H_{fg} \cdot \gamma}{\beta \cdot C_{pl}} \right), \left(\frac{\Delta H}{H_{fg}} \right), \left(\frac{\rho_l}{\rho_v} \right), \left(\frac{L}{D} \right) \right] \quad (2.1)$$

$$\frac{F_{qa} \cdot \gamma^{\frac{1}{2}}}{H_{fg} \cdot \rho_l^{\frac{1}{2}}} = F \left[\left(\frac{G_a \cdot \gamma^{\frac{1}{2}}}{\rho_l^{\frac{1}{2}}} \right), \left(\frac{D \cdot C_{pl} \cdot \rho_l^{\frac{1}{2}}}{K_l \cdot \gamma^{\frac{1}{2}}} \right), \left(\frac{C_{pl} \cdot \sigma \cdot \gamma^{\frac{1}{2}} \cdot \rho_l^{\frac{1}{2}}}{K_l} \right), \left(\frac{\Delta H}{H_{fg}} \right), \left(\frac{\rho_l}{\rho_v} \right), \left(\frac{L}{D} \right) \right] \quad (2.2)$$

$$\frac{F_{qa} \cdot \gamma^{\frac{1}{2}}}{H_{fg} \cdot \rho_l^{\frac{1}{2}}} = F \left[\left(\frac{G_a \cdot \gamma^{\frac{1}{2}}}{\rho_l^{\frac{1}{2}}} \right), \left(\frac{D \cdot C_{pl} \cdot \rho_l^{\frac{1}{2}}}{K_l \cdot \gamma^{\frac{1}{2}}} \right), \left(\frac{\mu_l \cdot C_{pl}}{K_l} \right), \left(\frac{\Delta H}{H_{fg}} \right), \left(\frac{\rho_l}{\rho_v} \right), \left(\frac{L}{D} \right) \right] \quad (2.3)$$

$$\frac{F_{qa}}{G_a \cdot H_{fg}} = F \left[\left(\frac{G_a \cdot D}{\mu_l} \right), \left(\frac{\gamma^{\frac{1}{2}} \cdot \mu_l}{D \cdot \rho_l^{\frac{1}{2}}} \right), \left(\frac{\mu_l}{\mu_v} \right), \left(\frac{\Delta H}{H_{fg}} \right), \left(\frac{\rho_l}{\rho_v} \right), \left(\frac{L}{D} \right) \right] \quad (2.4)$$

The previous equations can be put in the form (see Table 2.1):

$$\pi_1 = F(\pi_2, \pi_3, \pi_4, \pi_5, \pi_6, \pi_7) \quad (2.5)$$

Two sets of Freon-12 data are chosen, both at pressure 155 lb/in² and both at $L/D \approx 155$, thus ensuring that

π_4 , π_6 and π_7 are the same for the two sets. The only remaining independent variables are π_2 , π_3 , π_5 . π_3 will have the same value within each set (because D and the relevant fluid properties are the same) but will be different for the two different sets. By cross-plotting the remaining variables, points can be chosen which have the same values of π_5 . We thus have a number of data points, for the same values of π_4 , π_5 , π_6 , π_7 . These fall into two groups, within each of which π_3 is also the same, but all having different values of π_2 . We can therefore plot π_1 versus π_2 and produce (either by eye or by a numerical curve-fitting technique) two curves, each for a different π_3 , but both for the same π_4 , π_5 , π_6 , π_7 (Figure 2.2). So far we have made no assumptions about the functional relationships which exist except that they are smooth enough to permit the curves of Figure (2.2) to be drawn.

We now endeavour to derive a functional relationship between π_1 , π_2 and π_3 . In this particular set of experiments it turns out that the π_1 versus π_2 curves are straight lines when plotted on log-log axes, i.e.

$$\pi_1 = A \pi_2^{S_2} \quad (2.6)$$

where S_2 is the slope of the log-log plot. A and S_2 are in general functions of π_3 . It can easily be shown that equation (2.6) can be written in the alternative form

$$\pi_1 = (\pi_2 \cdot \pi_3^{n_1})^{S_2}$$

where S_2 is a function of π_3 only. In fact the variation of

S_2 with π_3 is very small ($S_2 = 0.206$ and $S_2 = 0.213$

and we shall treat it as constant. Thus we have expressed the relationship in the form

$$\pi_1 = F(\pi_2 \cdot \pi_3^{n_1}) \text{ only.}$$

We can now choose two sets of values of π_1 , π_2 and π_3 and

determine S_2 and n_1 . If we choose two values of π_2 and π_3 ,

say $\bar{\pi}_2$, $\bar{\pi}_2$, $\bar{\pi}_3$, $\bar{\pi}_3$ which represent the same value for π_1 , thus

we can show that

$$n_1 = \frac{\ln(\bar{\pi}_2/\bar{\pi}_2)}{\ln(\bar{\pi}_3/\bar{\pi}_3)} \quad (2.7)$$

and

$$S_2 = \ln \pi_1 / \ln(\bar{\pi}_2 \cdot \bar{\pi}_3^{n_1}) \quad (2.8)$$

To determine n_2 , two further sets of experimental data (Freon-12 and water at pressure 155 lb/in² and 1000 lb/in² respectively) (Table 2.2) are required. In this case the variations of π_1 with the function $(\pi_2 \times \pi_3^{n_1})$ is found for two different values of π_4 where in the above variation the terms π_5 , π_6 , and π_7 are the same in both sets of data. For these sets of experiments the relation between π_1 and $(\pi_2 \cdot \pi_3^{n_1})$ is also a straight line when plotted on log-log axes. Using the same method for determining n_1 , the following expression for n_2 is

$$n_2 = \frac{\ln\left[\frac{(\pi_2 \times \pi_3^{n_1})}{(\pi_2 \times \pi_3^{n_1})}\right]}{\ln(\pi_4/\pi_4)} \quad (2.9)$$

A computer programme "DISTORTION" was written to find n_1 and n_2 based on the method described above (see page 10).

By defining $\psi_{CHF} = \pi_2 \cdot \pi_3^{n_1} \cdot \pi_4^{n_2}$ and having determined the values of n_1 and n_2 at constant π_5 , π_6 and π_7 , the variation of ψ_{CHF} with π_1 for different fluids can be obtained. For Freon-12, Freon-21 and water the relation between ψ_{CHF} and π_1 are obtained using the computer programme SIM (see ^{note in} page 10). The results are given in Figures (2.11) to (2.22). The main objective of the curves in Figures (2.11) to (2.22) is to test the effectiveness of the proposed simulation technique, as will be shown in the preceding discussion.

The above mentioned technique has been referred to as the compensating distortion technique, used to compensate for the errors that occur in the distorted (unequal) dimensionless groups in simulating certain conditions in a prototype by a model.

Figures (2.3) and (2.4) show the relation between π_5 and n_1 and π_5 and n_2 respectively as calculated by applying the present approach. While n_1 and n_2 were reported by Ahmad to be independent of π_5 , it is found that n_1 and n_2 have

functional relationships with π_5 . n_1 increases with the increase of π_5 until it reaches a maximum value of 0.653 at $\pi_5 = 0.1$ and then decreases as shown in Figure 2.3. This is compared with a constant $n_1 = 0.667$ applying Ahmad's (1971) method for the same dimensionless groups. Figure (2.4) shows that n_2 increases with the increase of π_5 and that the curve flattens at higher values of π_5 , i.e. at values of π_5 higher than 0.2. It is found that n_2 equals 0.13 if Ahmad's method is applied to the same dimensionless groups. This is significantly lower than n_2 values found applying the present method.

Applying the present technique on Barnett's (1964) equations (2.1), (2.2) and (2.3), the relations $\pi_5 - n_1$, and $\pi_5 - n_2$ are found, Figures (2.5) to (2.10).

The examination of Figures (2.6), (2.8) and (2.10) shows that the n_2 versus π_5 curves intersect the π_5 axes at the same point ($\pi_5 = 0.124$) where $n_2 = 0$. That means that at $\pi_5 = 0.126$, $\pi_4^{n_2}$ is equal to unity and at this particular point there is no need to include π_4 in Barnett's simulation equations. This can be achieved by regulating the subcooling ratio $\Delta H/H_{fg}$ to have the value of 0.126.

Figures (2.5), (2.7) and (2.9) show the relation between n_1 and π_5 , which is the same in Barnett's three

equations.

Having determined the relation between π_5 and both n_1 and n_2 , the relation between the parameter $\psi_{CHF} (= \pi_2 \cdot \pi_3^{n_1} \cdot \pi_4^{n_2})$ and π_1 can be found.

Figures (2.11) to (2.13) show the relation between π_1 and ψ_{CHF} at $\pi_5 = 0.05, 0.118$ and 0.18 respectively at density ratio $\rho_l/\rho_v = 20$ which corresponds to pressure 155 lb/in^2 for Freon-12, 200 lb/in^2 for Freon-21 and 1000 lb/in^2 for water (see Table 2.2a). In each of Figures (2.11) to (2.13) there are two curves; the points used for curve 1 represent the results obtained applying the present method for the calculated values of n_1 and n_2 and using Ahmad's groups (Table 2.1), while the points used for curve 2 are found by taking constant values for $n_1 = 0.667$ and $n_2 = 0.13$ as reported by Ahmad (1971) and calculating π_1 and the corresponding ψ_{CHF} . Table (2.3) is a summary of the percentage R.M.S. error of the fitted curves shown in Figures (2.11) to (2.13). Using all Ahmad's data.

TABLE 2.3

| Same data is used in both cases | | | |
|-------------------------------------|------|------|------|
| π_5 | 0.05 | 0.11 | 0.18 |
| R.M.S. error, % (present method) | 1.19 | 0.51 | 0.24 |
| R.M.S. error, % (Ahmad (1971)) | 2.19 | 1.69 | 1.52 |

Table 2.3 shows clearly that the present method results in reducing the percentage R.M.S. error appreciably.

Figures (2.14), (2.15) and (2.16) show the relation between π_1 and ψ_{CHF} when the present method of calculating n_1 and n_2 is applied to Barnett's dimensionless groups, Table 2.1, at π_5 equal to 0.05, 0.11 and 0.18 respectively. The data used are for Freon-12, Freon-21 and water at density ratio $\rho_l/\rho_v = 20$ (see Table 2.2a) and the points in Figures (2.14), (2.15) and (2.16) are the results of applying the distortion technique to Barnett's equations (2.1), (2.2) and (2.3) respectively. Table 2.4 shows the percentage R.M.S. error for the simulating equations (2.1), (2.2) and (2.3).

From Tables 2.3 and 2.4 it can be noticed that applying Ahmad's dimensionless groups coupled with the present method of distortion achieves more favourable results for simulation than applying Barnett's dimensionless groups.

TABLE 2.4
Barnett's equations

| π_5 | 0.05 | 0.11 | 0.18 |
|-----------------------------------|------|------|------|
| R.M.S. error, % (equation 2.1) | 5.15 | 4.49 | 3.79 |
| R.M.S. error, % (equation 2.2) | 5.05 | 4.47 | 3.71 |
| R.M.S. error, % (equation 2.3) | 5.18 | 4.49 | 3.77 |

As an extension to the above work, the same procedure is applied, but this time at density ratio $\rho_l/\rho_v = 41$ instead of 20 as before. The results in general showed the same trend (see Figures 2.17 to 2.22).

2.3 FORMULATION OF DIMENSIONLESS GROUPS FOR AN ANNULAR FLOW MODEL

2.3.1 The model

The geometrical configuration of the proposed theoretical annular flow model is composed of the two regions as shown in Figure 2.24; the two-phase region and the saturated vapour region. At section (A) the liquid phase enters at pressure, temperature and velocity, P_i , T_i and W_i respectively. It is assumed that the system is at steady state with no waves at the liquid film surface and no liquid droplet entrainment or deposition. The heat inertia of the heated tube is ignored.

The relevant dimensionless groups are now formulated. These describe the process of burn-out and the simulation of water by Freon. The momentum, energy and continuity equations and the boundary conditions are non-dimensionalised for the model under consideration.

This approach has the advantage of showing the effects of each single parameter on the dimensionless groups, and eventually on the model as a whole. Therefore, in the cases where the groups of parameters are mismatched or have a deterring effect on the required degree of accuracy of simulation, the boundary conditions or the selected flow model can be modified to improve the degree of accuracy. Realising the complexity involved in generating such a model, we have chosen a simple annular flow model and the dimensionless groups which describe it are obtained. The effectiveness of these groups in simulating water by Freon is examined using the introduced compensating distortion technique method.

2.3.2 Governing Equations

At each cross-section of the model, both phases exist with an interface between them. The momentum, continuity and energy equations must be satisfied for each of the phases. These equations are:

$$\text{Continuity: } \frac{\partial W}{\partial z} + \frac{\partial W}{\partial y} = 0 \quad (2.10)$$

$$\text{Momentum* : } \rho W_z \frac{\partial W}{\partial z} + \rho W_y \frac{\partial W}{\partial y} = - \frac{\partial P}{\partial z} + \mu \frac{\partial^2 W}{\partial y^2} \quad (2.11)$$

* Since the effect of natural convection is neglected in this model, the gravity term in the momentum equation is assumed to have a negligible effect.

Energy:
$$\rho W_z \frac{\partial H}{\partial z} + \rho W_y \frac{\partial H}{\partial y} = W_z \frac{\partial P}{\partial z} - \frac{\partial f_{qa}}{\partial y} + \mu \left(\frac{\partial W_z}{\partial y} \right)^2 \quad (2.12)$$

2.3.3 Boundary Conditions

In order to describe the model, the velocity and the enthalpy of the fluid must be determined at each of the following:

- (a) The internal surface of the heated tube.
- (b) Channel entrance.
- (c) Interface boundaries.

The enthalpy of the fluid must also be defined at the outlet of the channel. These various boundary conditions are as follows:

At $Y = \pm D/2$:

$$W_z = 0, \quad W_y = \frac{f_{qa}}{H_{fg} \cdot \rho_l}, \quad \frac{\partial H}{\partial y} = \frac{C_{pl} \cdot f_{qa}}{K_l}, \quad H = H_{sat.l}$$

At $Z = 0$:

$$W_z = W_i, \quad \frac{\partial W_z}{\partial z} = 0, \quad H = H_i, \quad \frac{\partial H}{\partial z} = 0.$$

At the triple interface:

$$H = H_{sat.v}$$

A liquid-vapour interface:

$$\mu_v \frac{\partial W_{v.t}}{\partial n} = \mu_l \frac{\partial W_{l.t}}{\partial n}, \quad P_v - P_l = \sigma \left(\frac{1}{R_1} - \frac{1}{R_2} \right)$$

$$H = H_{sat.v}, \quad \frac{K_l}{C_{pl} \cdot \rho_v \cdot H_{fg}} \cdot \frac{\partial H}{\partial n} = W_{ln}$$

2.3.4 The Dimensionless Groups

In this section the required dimensionless groups are obtained by non-dimensionalising the conservation equations (i.e. equations (2.10), (2.11) and (2.12)) and the preceding boundary conditions.

Take:

$$\begin{aligned} z^* &= z/D, \quad Y^* = y/D, \quad W_z^* = W_z/W_i, \quad W_y^* = W_y/W_i, \\ W^*(vt, lt, ln) &= \frac{W(vt, lt, ln)}{W_i}, \quad H^* = \frac{H - H_i}{H_{fg}} \\ P^* &= \frac{P}{\rho_l \cdot W_i^2}, \quad q^* = \frac{qa}{w \cdot \rho_l \cdot H_{fg}}, \quad \rho^* = \rho / \rho_l, \quad \mu^* = \mu / \mu_l. \end{aligned} \quad (2.13)$$

Substitute (2.13) in equations (2.10), (2.11) and (2.12) and they become:

$$\frac{\partial W_z^*}{\partial z^*} + \frac{\partial W_y^*}{\partial Y^*} = 0 \quad (2.14)$$

For the liquid phase:

$$W_z^* \frac{\partial W_z^*}{\partial z^*} + W_y^* \frac{\partial W_z^*}{\partial Y^*} = - \frac{\partial P^*}{\partial z^*} + \left(\frac{\mu_l}{\rho_l \cdot W_i \cdot D} \right) \frac{\partial^2 W_z^*}{\partial Y^{*2}} \quad (2.15)$$

$$W_z^* \frac{\partial H^*}{\partial z^*} + W_y^* \frac{\partial H^*}{\partial Y^*} = \left(\frac{W_i^2}{H_{fg}} \right) W_z^* \frac{\partial P^*}{\partial z^*} - \frac{\partial q^*}{\partial Y^*} + \left(\frac{W_i \cdot \mu_l}{H_{fg} \cdot \rho_l \cdot D} \right) \left(\frac{\partial W_z^*}{\partial Y^*} \right)^2 \quad (2.16)$$

For the vapour phase:

$$W_z^* \frac{\partial W_z^*}{\partial z^*} + W_y^* \frac{\partial W_y^*}{\partial Y^*} = - \left(\frac{\rho_l}{\rho_v} \right) \frac{\partial P^*}{\partial z^*} + \left(\frac{\mu_v}{\rho_v \cdot W_i \cdot D} \right) \frac{\partial^2 W_z^*}{\partial Y^{*2}} \quad (2.17)$$

$$W_z^* \frac{\partial H^*}{\partial z^*} + W_y^* \frac{\partial H^*}{\partial Y^*} = \left(\frac{W_i^2 \cdot \rho_l}{H_{fg} \cdot \rho_v} \right) W_z^* \frac{\partial P^*}{\partial z^*} - \left(\frac{\rho_l}{\rho_v} \right) \frac{\partial q^*}{\partial Y^*} + \left(\frac{W_i \cdot \mu_v}{H_{fg} \cdot D \cdot \rho_v} \right) \left(\frac{\partial W_z^*}{\partial Y^*} \right)^2 \quad (2.18)$$

Also, the boundary conditions become:

At $Y^* = \pm \frac{1}{2}$

$$W_z^* = 0, \quad W_y^* = \frac{f_{qa}}{H_{fg} \cdot \rho_\ell \cdot W_i}, \quad \frac{\partial H^*}{\partial Y^*} = \frac{C_{p\ell} \cdot f_{qa} \cdot D}{H_{fg} \cdot K_\ell}, \quad H^* = \frac{\Delta H}{H_{fg}}$$

At $Z^* = 0$

$$W_z^* = 1, \quad \frac{\partial W_z^*}{\partial z^*} = 0, \quad H^* = 0, \quad \frac{\partial H^*}{\partial z^*} = 0.$$

At the triple interface

$$H^* = 1.$$

At liquid-vapour interface

$$\frac{\partial W_{vt}^*}{\partial n^*} = \frac{\mu_\ell}{\mu_v} \cdot \frac{\partial W_{\ell t}^*}{\partial n^*}, \quad P_v^* - P_\ell^* = \left(\frac{\sigma}{\rho_\ell \cdot W_i^2 \cdot D} \right) \cdot \left(\frac{1}{R_1^*} + \frac{1}{R_2^*} \right),$$

$$H^* = 1, \quad \frac{K_\ell}{C_{p\ell} \cdot \rho_v \cdot D \cdot W_i} \cdot \frac{\partial H^*}{\partial n^*} = W_{fn}^*$$

The dimensionless groups of properties and parameters can now be selected from the preceding boundary conditions and equations (2.15), (2.16), (2.17) and (2.18), as follows:

$$\frac{f_{qa}}{H_{fg} \cdot \rho_\ell \cdot W_i}, \quad \frac{K_\ell}{C_{p\ell} \cdot \rho_v \cdot D \cdot W_i}, \quad \frac{W_i \cdot \mu_\ell}{H_{fg} \cdot \rho_\ell \cdot D}, \quad \frac{\mu_\ell}{\mu_v}, \quad \frac{\Delta H}{H_{fg}}, \quad \frac{\rho_\ell}{\rho_v}, \quad \frac{\sigma}{\rho_\ell \cdot W_i^2 \cdot D}$$

Besides other groups which are products of two or more of the aforementioned groups:

$$\frac{\rho_\ell \cdot W_i \cdot D}{\mu_\ell}, \quad \frac{W_i^2}{H_{fg}}, \quad \frac{C_{p\ell} \cdot f_{qa} \cdot D}{H_{fg} \cdot K_\ell}, \quad \frac{\mu_v}{\rho_v \cdot W_i \cdot D}, \quad \frac{W_i^2 \cdot \rho_\ell}{H_{fg} \cdot \rho_v}, \quad \frac{W_i \cdot \mu_v}{H_{fg} \cdot \rho_v \cdot D}$$

The functional relationship that describes a solution for the annular flow model is given by $\frac{F_{qa}}{H_{fg} \cdot \rho_l \cdot W_i} = f[z^*, Y^*, \text{and groups (1), (2), (3), (4), (5), (6) and (7)}]$.

At the end of the channel where burn-out occurs, $z^* = L/D$ and $Y^* = \frac{1}{2}$. Hence, the functional relationship describing the burn-out mechanism in an annular flow model is given by:

$$\frac{F_{qa}}{H_{fg} \cdot \rho_l \cdot W_i} = f \left[\frac{K_l}{D \cdot C_{pl} \cdot \rho_v \cdot W_i}, \frac{W_i \mu_l}{H_{fg} \cdot \rho_l \cdot D}, \frac{\mu_l}{\mu_v}, \frac{\Delta H}{H_{fg}}, \frac{\rho_l}{\rho_v}, \frac{L}{D} \right] \quad (2.19)$$

Since the surface waves have been neglected in this model, it follows that the surface tension effects on the flow are neglected. Therefore, the surface tension is left out from equation (2.19). Equation (2.19) is then used to simulate burn-out in water by Freon with the aid of the compensating distortion technique described in the first part of this chapter.

2.3.5 Results and Discussions

The compensating distortion technique has been applied to the dimensionless groups in equation (2.19). In order to examine the accuracy of these groups in simulating water by Freon we used water, Freon-12 and Freon-21 data as shown in Table 2.2.

The simulation results obtained are presented

graphically in Figures (2.25) and (2.26), which show the variation of the heat flux group (i.e. $F_{qa}/(H_{fg} \cdot \rho_l \cdot W_i)$) with the critical heat flux dimensionless parameter (i.e. $\psi_{CHF} = \left(\frac{K_l}{D \cdot C_{pl} \cdot \rho_v \cdot W_i}\right) \cdot \left(\frac{W_i \mu_l}{H_{fg} \cdot \rho_l \cdot D}\right)^{n_1} \left(\frac{\mu_l}{\mu_v}\right)^{n_2}$). The degree of accuracy of simulation applying the introduced model is given by the percentage root mean square values shown in Figures (2.25) and (2.26). For π_5 (i.e. $\frac{\Delta H}{H_{fg}}$) values of 0.05, 0.11 and 0.18 and the corresponding percentage R.M.S. error values are 26.73, 24.14 and 20.78. That means that an error in the order of 20% is likely to occur. A further boundary condition needs to be added to the system to reduce the error. This could be either the rate of change of density ratio (ρ_l/ρ_v) to pressure, or the ratio between the two-phase pressure loss and the system inlet pressure. Since the hydrodynamics interrelation between the vapour and the liquid at the film surface is difficult to formulate, we directed our attention towards Barnett's number (i.e. $\gamma^{\frac{1}{2}} \mu_l / D \cdot \rho_l^{\frac{1}{2}}$) which includes the rate of change of density ratio (ρ_l/ρ_v) to pressure, parameter γ (i.e. $\gamma = \partial(\rho_l/\rho_v)/\partial P$).

The third dimensionless group in equation (2.19) (i.e. $W_i \cdot \mu_l / H_{fg} \cdot \rho_l \cdot D$, which contains parameters that appear in the remaining groups) is replaced by Barnett's group. This resulted in decreasing the percentage R.M.S. error to 3.43, 2.59 and 2.1 at $\pi_5 = 0.05, 0.11$ and 0.18 respectively

(Figure 2.26). Thus Barnett's group proved to be a significant group in this model and must be included as an integral group in the set.

In the present work, Barnett's group is applied also to Griffith's (1959) annular flow model, which is of a similar nature to the model suggested in this report.

Griffith's (1959) dimensionless groups are:

$$\frac{F_{qa}}{H_{fg} \cdot \rho_v \cdot W_i} = f \left[\left(\frac{\Delta H}{H_{fg}} \right), \frac{W_i \cdot D \cdot \rho_l}{\mu_l}, \frac{W_i \cdot D \cdot \rho_v}{\mu_v}, \frac{\rho_l}{\rho_v}, \frac{C_{pl} \cdot \mu_l}{K_l}, \frac{L}{D}, \frac{\sigma}{\rho_l \cdot W_i^2 \cdot D} \right] \quad (2.20)$$

He mentioned that the vapour Reynolds number (i.e. $W_i \cdot D \cdot \rho_v / \mu_v$) plays a significant role in the high quality region while the liquid Reynolds number dominates low quality regions. In the present analysis, the compensating technique method is applied to both cases and the corresponding percentage R.M.S. errors are calculated at $\pi_5 = 0.05, 0.11$ and 0.18 (Figures 2.27 and 2.28). It is important to note that when Barnett's group replaced the surface tension group in Griffith's model, the percentage R.M.S. errors were reduced from 72.07, 68.52, 65.75 to 1.2, 0.52 and 0.26 respectively (Figures 2.27 and 2.29) at the above mentioned π_5 values when liquid Reynolds number is considered. The percentage R.M.S. errors are also

reduced from 67.52, 64.39, 61.08 to 1.34, 0.38, 0.02 respectively (Figures 2.28 and 2.30) at the above mentioned π_5 's when the vapour Reynolds number is considered. This clearly indicates that the Barnett group has a significant influence on the degree of accuracy of simulation.

It is worthwhile to point out that better accuracy can still be achieved with further comprehension of the hydrodynamic mechanisms which govern the processes at the interface liquid surface. This will undoubtedly further the complexity in the formulation of the required model, but may result in more adequate dimensionless groups. The relation between these groups can then be studied with a view to determining those which affect the accuracy of the system.

2.4 CONCLUSION

Further improvements in simulating boiling phenomenon (Figure 2.23) in a heated channel can be achieved by modelling each boiling regime separately. Hence, the influence of the dimensionless groups developed for each region should be carefully studied and analysed. This study will determine the groups which govern the various processes in each individual regime. These groups can then be shown alongside their respective regimes. Such a method of display can then

be used to determine the dimensionless groups which control the various mechanisms in the system as a whole.

TABLE 2.1

| Pi Terms | equation no. 2.4 | equation no. 2.1 | equation no. 2.2 | equation no.2.3 |
|----------|---|--|---|--|
| π_1 | $\frac{F_{qa}}{G_a \cdot H_{fg}}$ | $\frac{F_{qa} \cdot \gamma^{\frac{1}{2}}}{H_{fg} \cdot \rho_l^{\frac{1}{2}}}$ | $\frac{F_{qa} \cdot \gamma^{\frac{1}{2}}}{H_{fg} \cdot \rho_l^{\frac{1}{2}}}$ | $\frac{F_{qa} \cdot \gamma^{\frac{1}{2}}}{H_{fg} \cdot \rho_l^{\frac{1}{2}}}$ |
| π_2 | $\frac{G_a \cdot D}{\mu_l}$ | $\frac{G_a \cdot \gamma^{\frac{1}{2}}}{\rho_l^{\frac{1}{2}}}$ | $\frac{G_a \cdot \gamma^{\frac{1}{2}}}{\rho_l^{\frac{1}{2}}}$ | $\frac{G_a \cdot \gamma^{\frac{1}{2}}}{\rho_l^{\frac{1}{2}}}$ |
| π_3 | $\frac{\gamma^{\frac{1}{2}} \cdot \mu_l}{D \cdot \rho_l^{\frac{1}{2}}}$ | $\frac{D \cdot C_{pl} \cdot \rho_l^{\frac{1}{2}}}{K_l \cdot \gamma^{\frac{1}{2}}}$ | $\frac{D \cdot C_{pl} \cdot \rho_l^{\frac{1}{2}}}{K_l \cdot \gamma^{\frac{1}{2}}}$ | $\frac{D \cdot C_{pl} \cdot \rho_l^{\frac{1}{2}}}{K_l \cdot \gamma^{\frac{1}{2}}}$ |
| π_4 | $\frac{\mu_l}{\mu_v}$ | $\frac{H_{fg} \cdot \gamma}{\beta \cdot C_{pl}}$ | $\frac{C_{pl} \cdot \sigma \cdot \gamma^{\frac{1}{2}} \cdot \rho_l^{\frac{1}{2}}}{K_l}$ | $\frac{\mu_l \cdot C_{pl}}{K_l}$ |
| π_5 | $\frac{\Delta H}{H_{fg}}$ | $\frac{\Delta H}{H_{fg}}$ | $\frac{\Delta H}{H_{fg}}$ | $\frac{\Delta H}{H_{fg}}$ |
| π_6 | $\frac{\rho_l}{\rho_v}$ | $\frac{\rho_l}{\rho_v}$ | $\frac{\rho_l}{\rho_v}$ | $\frac{\rho_l}{\rho_v}$ |
| π_7 | $\frac{L}{D}$ | $\frac{L}{D}$ | $\frac{L}{D}$ | $\frac{L}{D}$ |

a) For Figures 2.11 to 2.16: $\rho_l/\rho_v = 20$.

| Symbol | Fluid | Diameter (D) in | L/D | Pressure lb/in ² | Reference |
|--------|----------|-----------------|-------|-----------------------------|-----------------------|
| A - | Freon-12 | 0.38 | 152.1 | 155 | Stevens et al (1964) |
| B - | Freon-12 | 0.334 | 152.7 | 155 | Stevens et al (1964) |
| C - | Freon-12 | 0.452 | 155.8 | 155 | Stevens et al (1964) |
| D - | Water | 0.368 | 145.4 | 1000 | Thompson et al (1964) |
| E - | Water | 0.451 | 150.8 | 1000 | Thompson et al (1964) |
| F - | Water | 0.504 | 150.8 | 1000 | Thompson et al (1964) |
| G - | Freon-21 | 0.334 | 155.1 | 200 | Barnett et al (1965) |
| H - | Freon-21 | 0.424 | 151.7 | 200 | Barnett et al (1965) |

b) For Figures 2.17 to 2.22: $\rho_l/\rho_v = 41$.

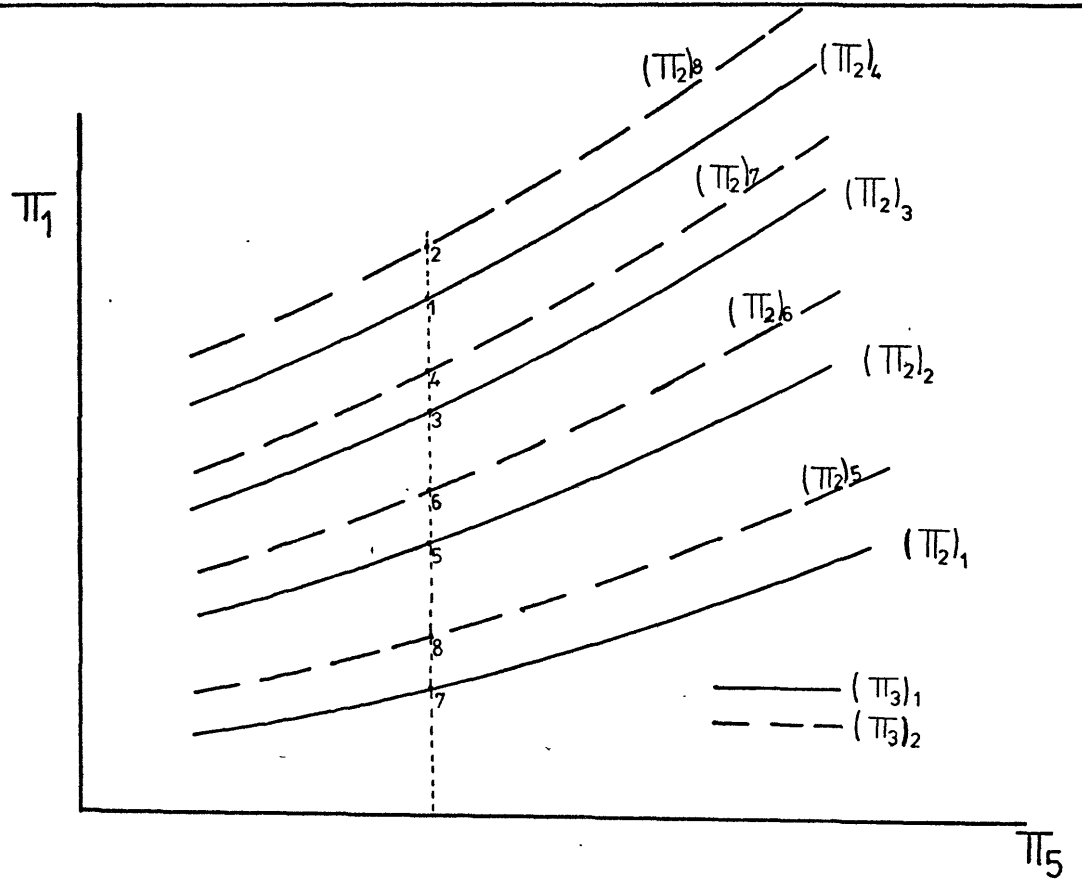
| Symbol | Fluid | Diameter (D) in | L/D | Pressure lb/in ² | Reference |
|--------|----------|-----------------|--------|-----------------------------|-----------------------|
| A - | Freon-12 | 0.303 | 150.17 | 83 | Barnett et al (1965) |
| B - | Freon-12 | 0.38 | 153.95 | 83 | Barnett et al (1965) |
| C - | Water | 0.22 | 154.55 | 560 | Thompson et al (1964) |
| D - | Freon-21 | 0.264 | 159.1 | 106 | Barnett et al (1965) |

c) Data used for calculating n1 and n2:

| Fluid | Diameter (in) | L/D | Pressure lb/in ² | Reference |
|----------|---------------|--------|-----------------------------|----------------------|
| Freon-12 | 0.303 | 156.43 | 155 | Barnett et al (1965) |
| Freon-12 | 0.452 | 155.75 | 155 | Stevens et al (1964) |
| Freon-12 | 0.55 | 130.9 | 155 | Ahmad et al (1972) |
| Water | 0.54 | 133.3 | 1000 | Janssen et al (1963) |

TABLE 2.2

Data used for testing the effectiveness of the proposed simulation technique.



$(\pi_3)_1 = \text{CONSTANT (ie } \bar{\pi}_3)$ FOR $(\pi_2)_1$ UP TO $(\pi_2)_4$
 $(\pi_3)_2 = \text{CONSTANT (ie } \bar{\pi}_3)$ FOR $(\pi_2)_5$ UP TO $(\pi_2)_8$

FIG.(2-1)

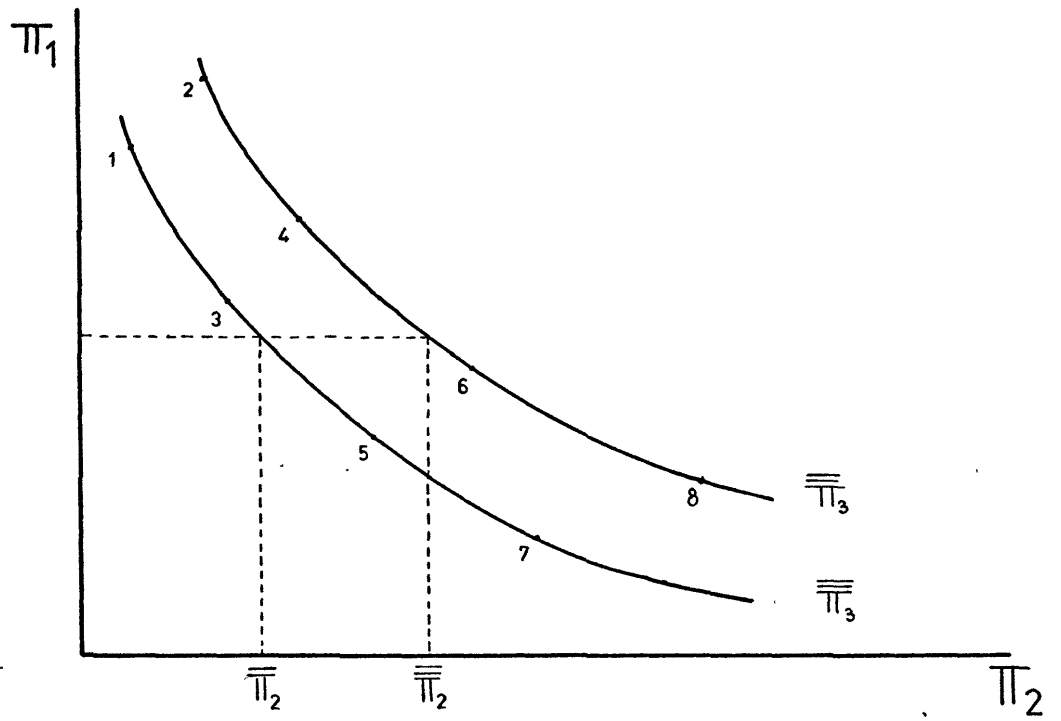
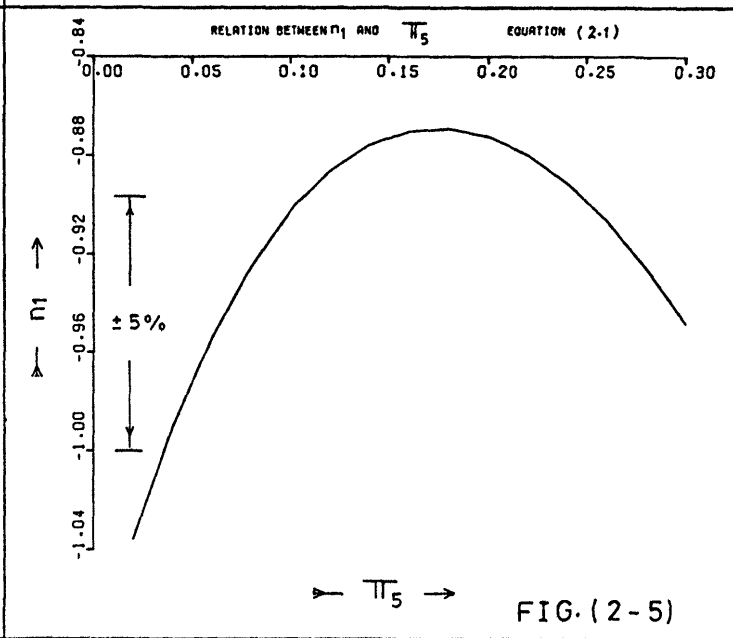
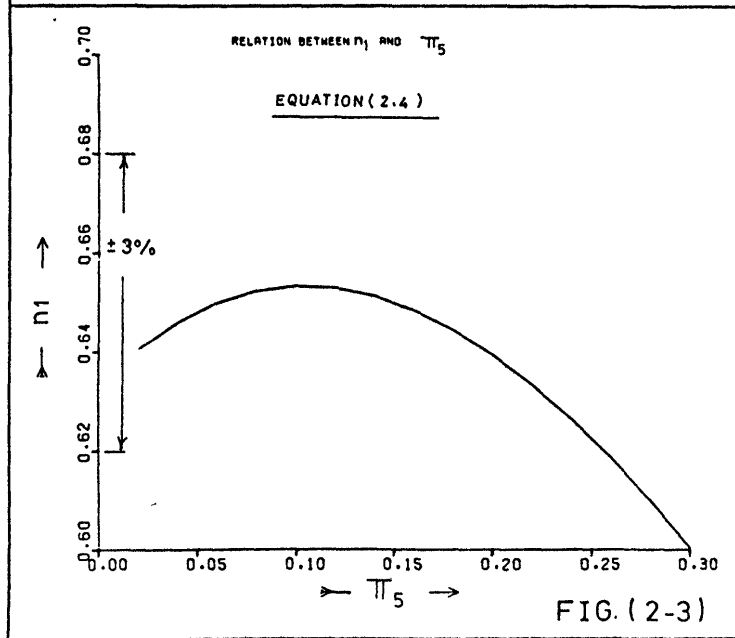
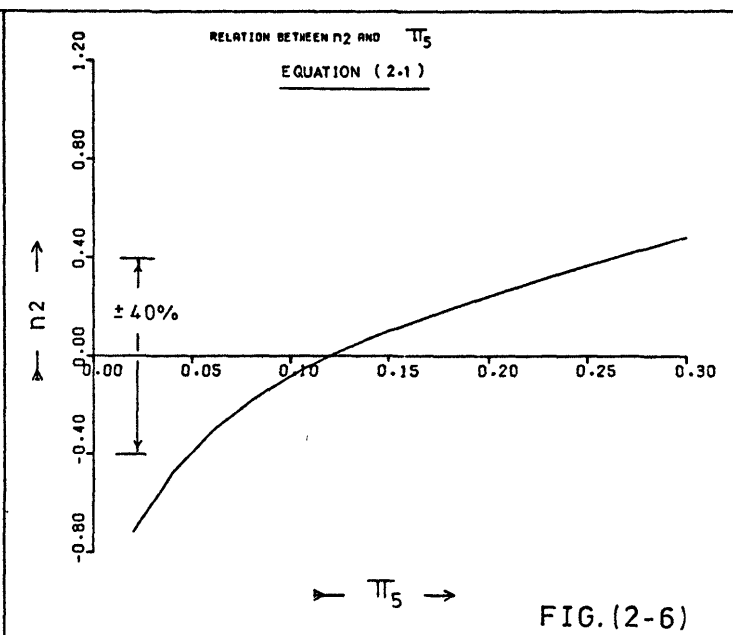
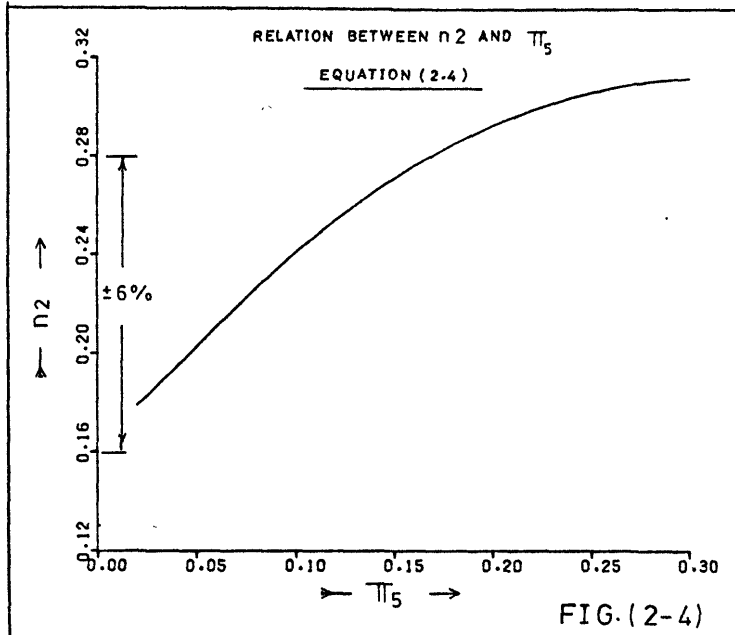


FIG.(2-2)



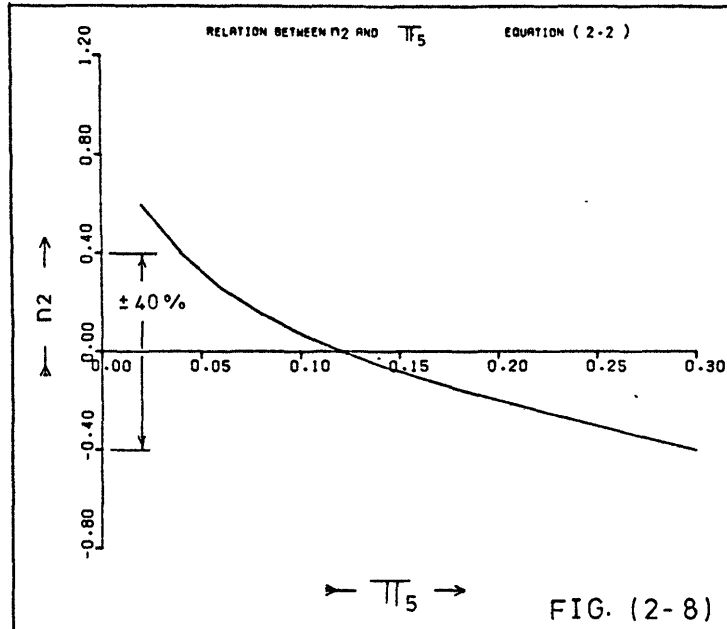


FIG. (2-8)

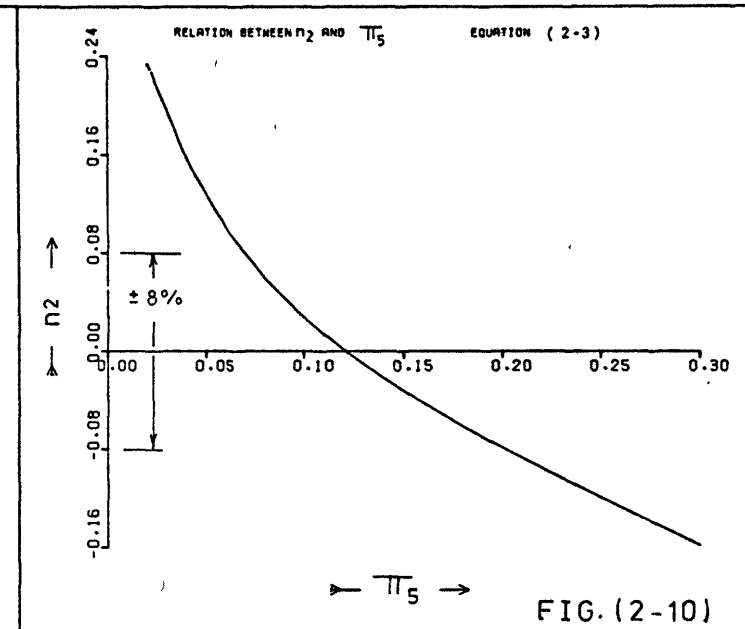


FIG. (2-10)

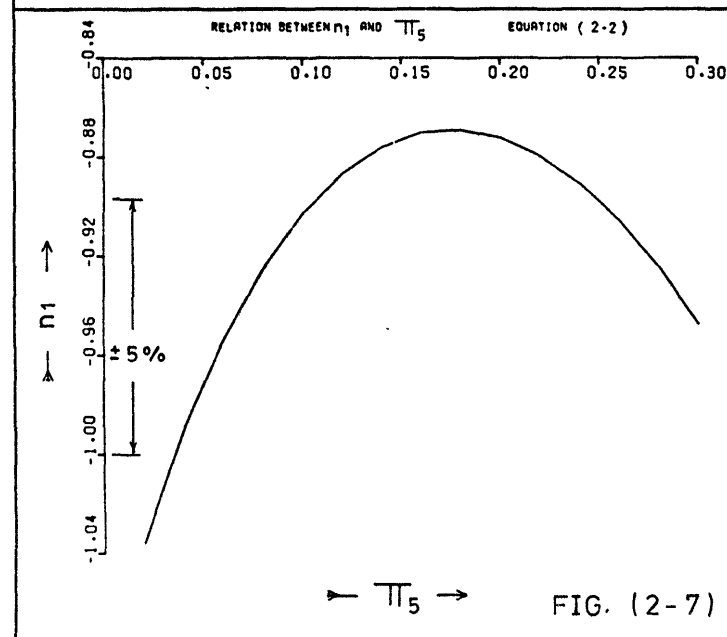


FIG. (2-7)

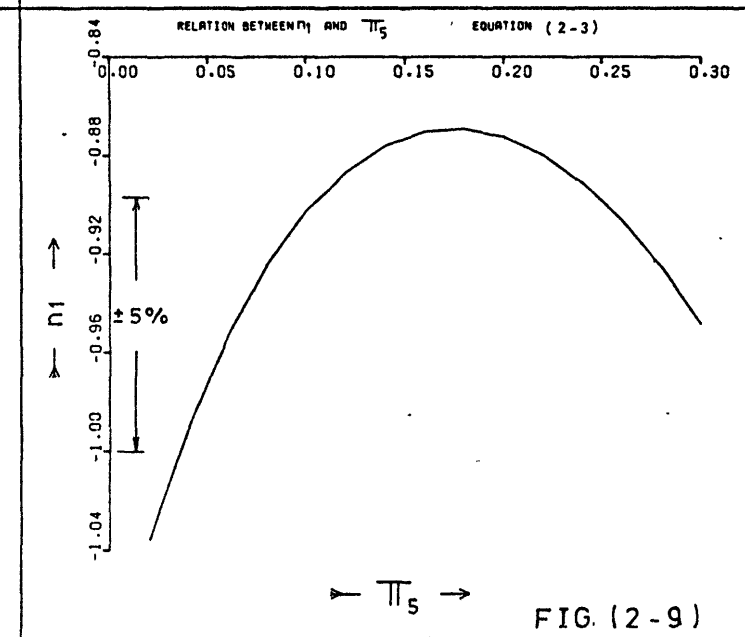
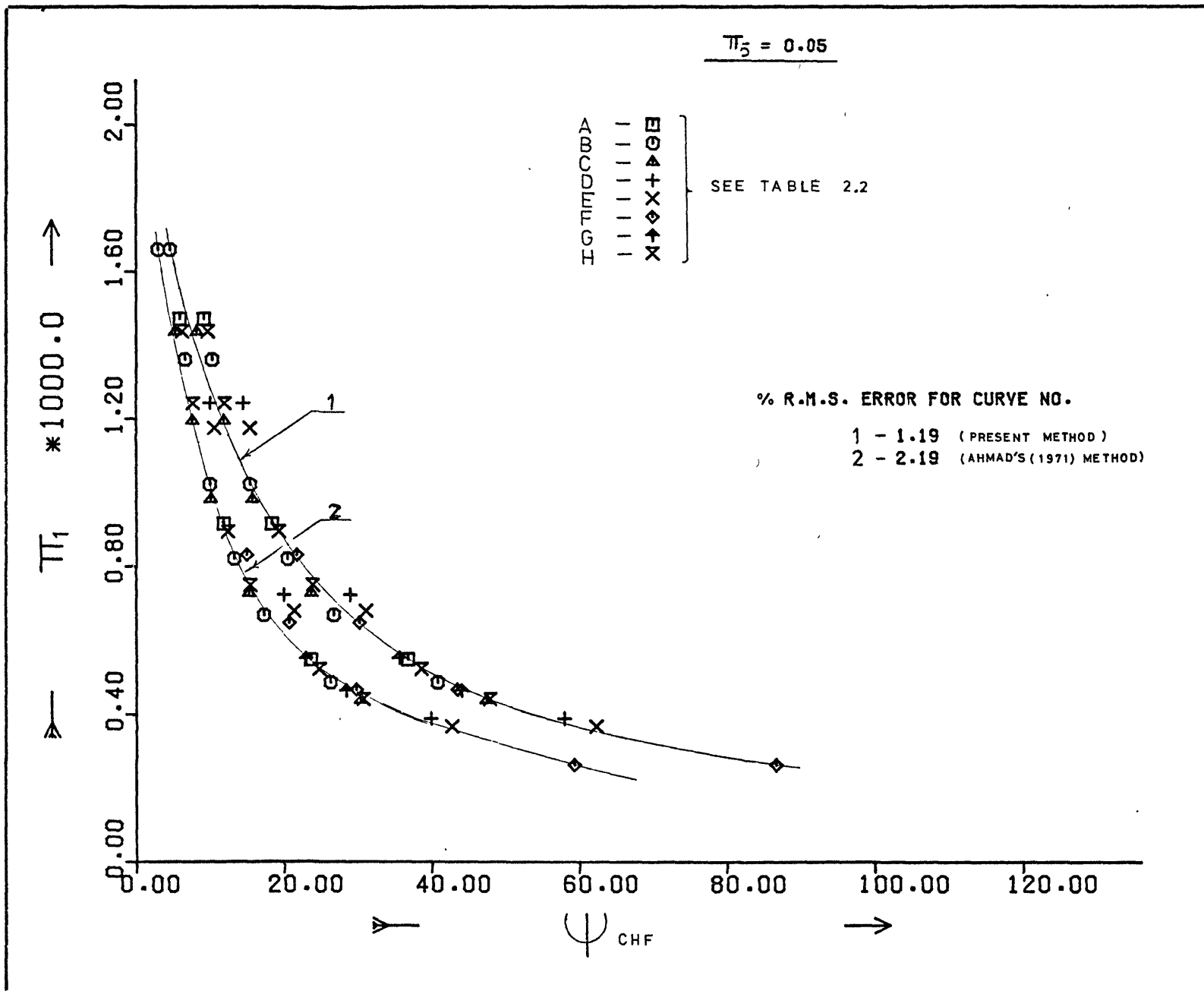


FIG. (2-9)



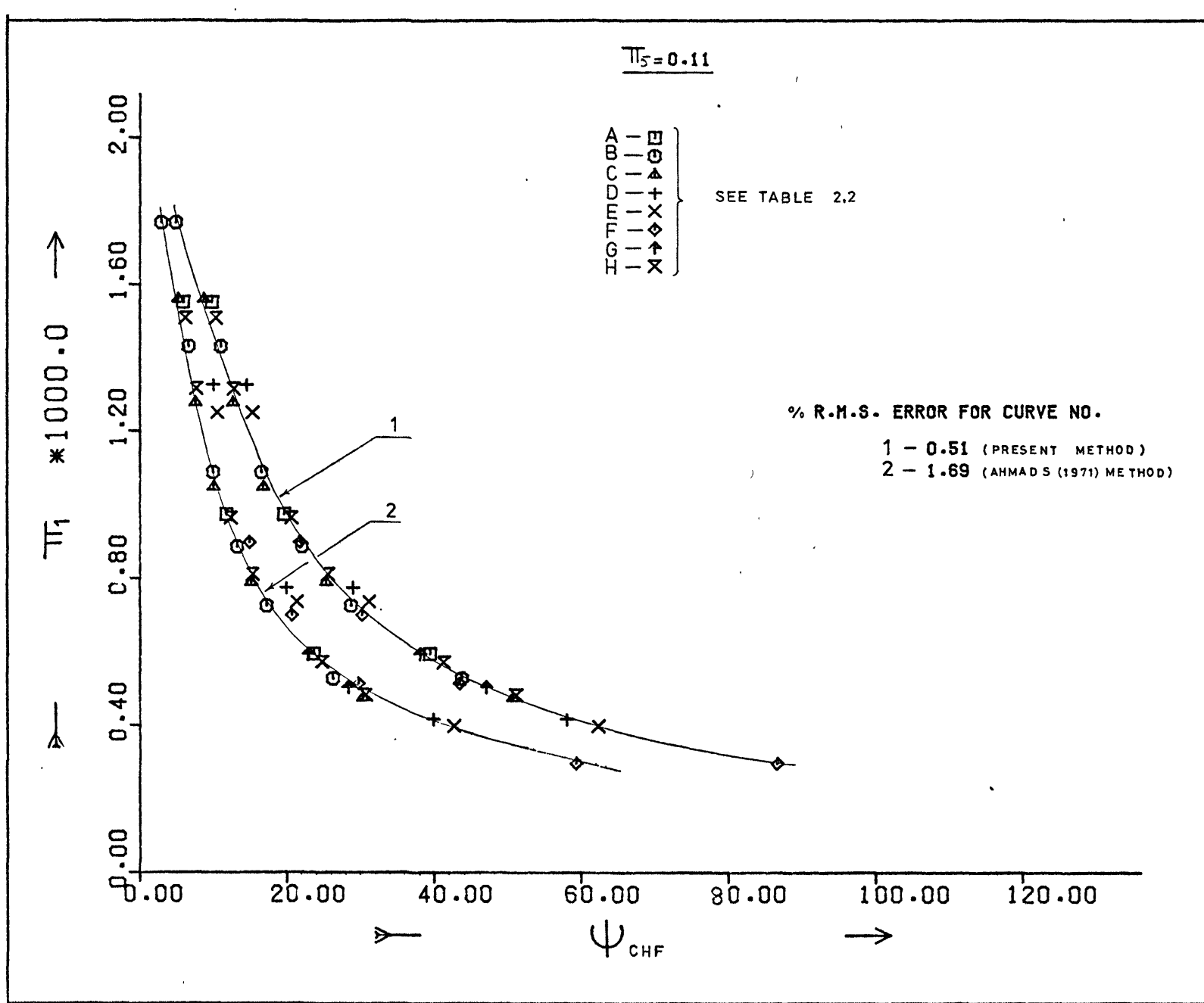


FIG (2-12)

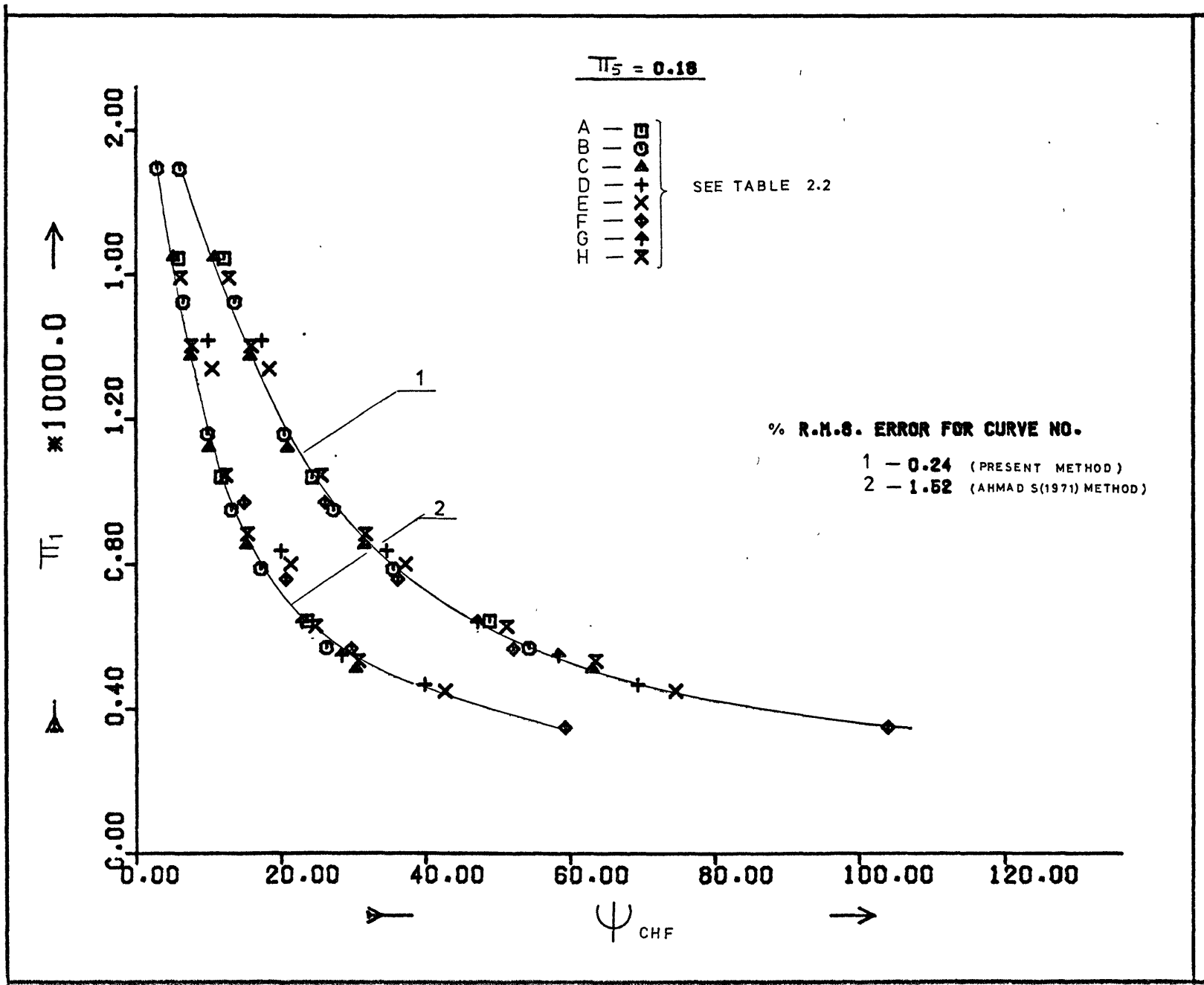
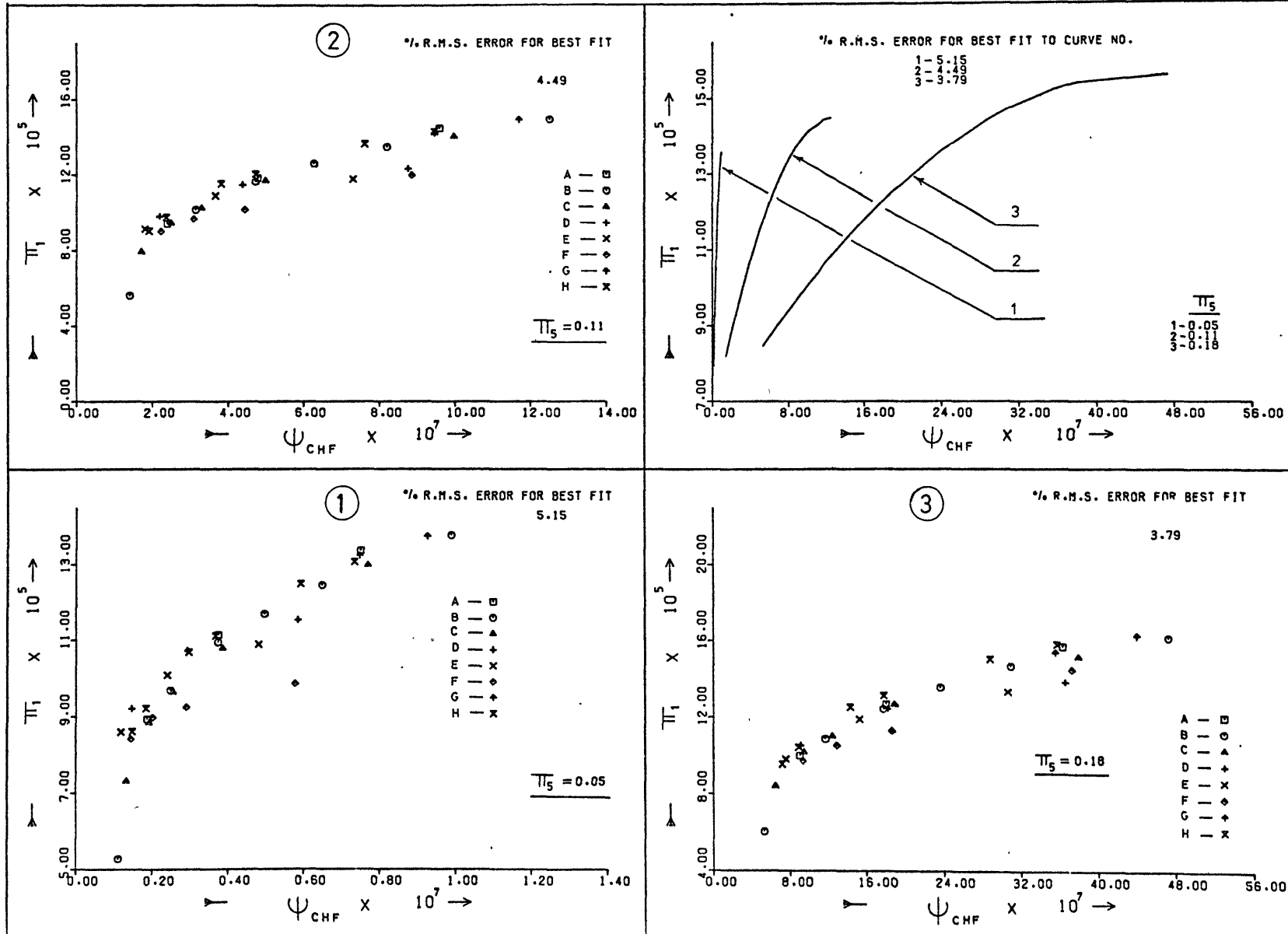


FIG (2-13)

COMPENSATING DISTORTION TECHNIQUE
 APPLIED TO
 EQUATION (2.1)



COMPENSATING DISTORTION TECHNIQUE
 APPLIED TO
 EQUATION (2.2)

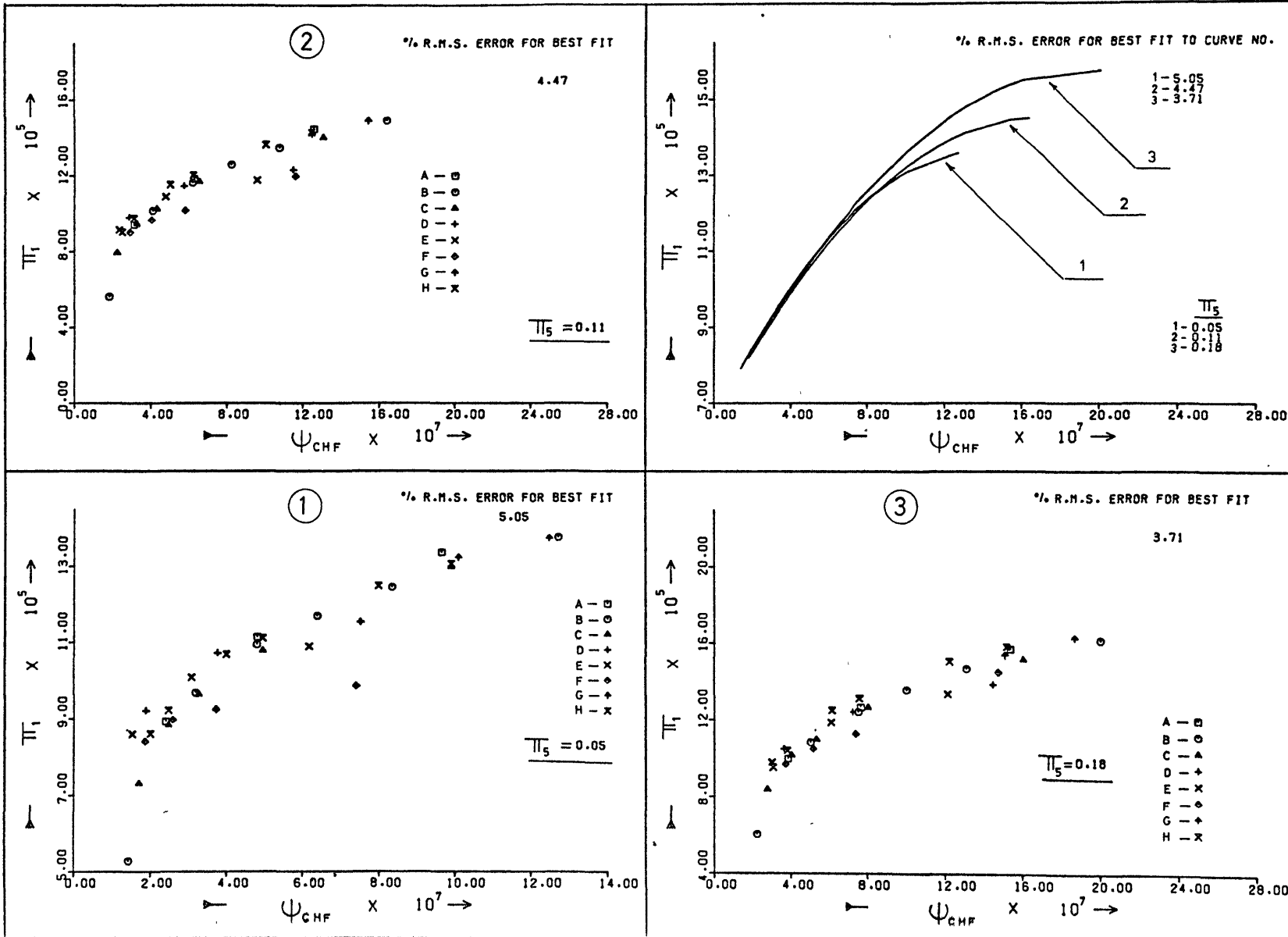


FIG (2-15)

COMPENSATING DISTORTION TECHNIQUE
 APPLIED TO
 EQUATION (2.3)

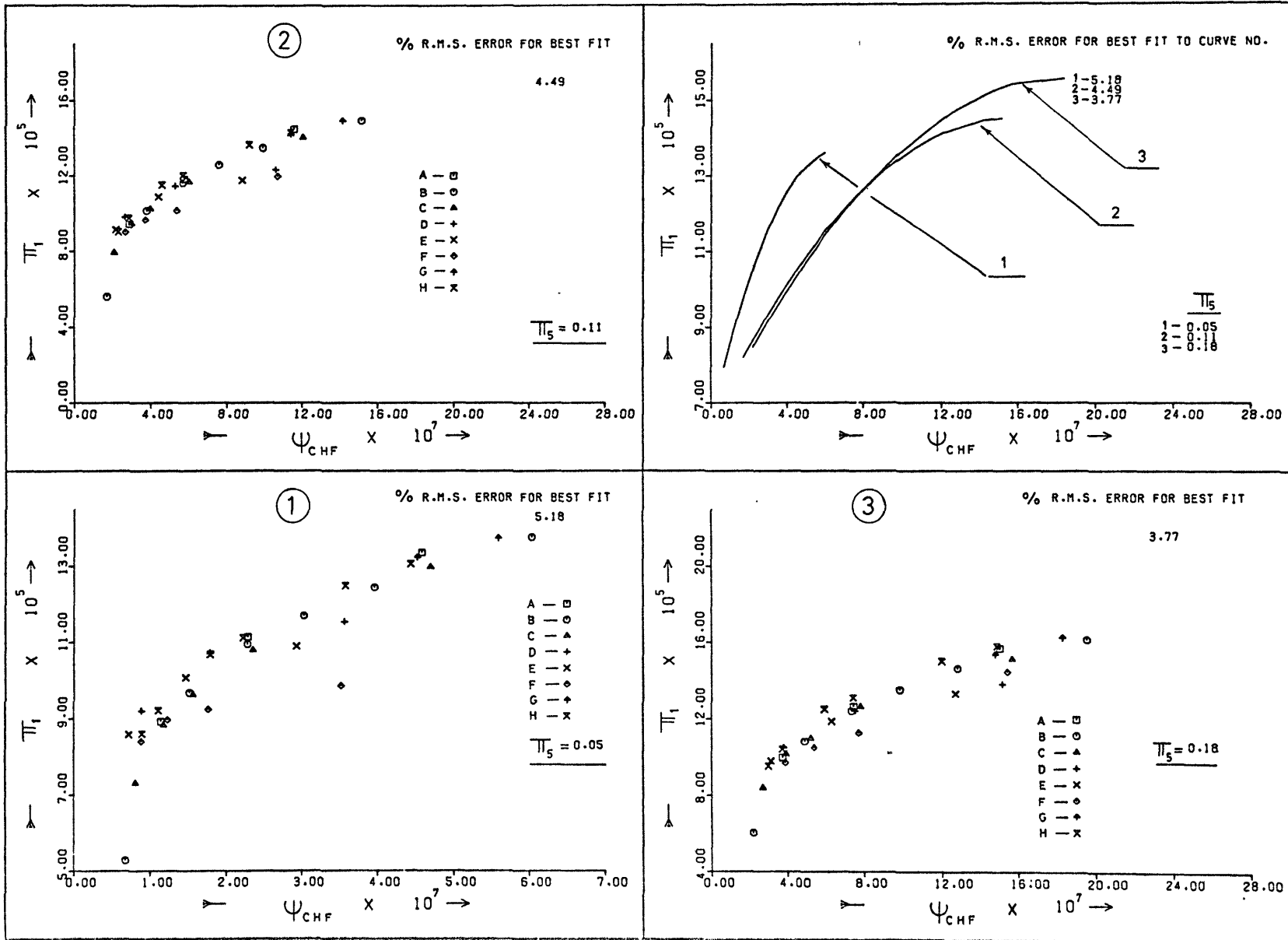


FIG (2-16)

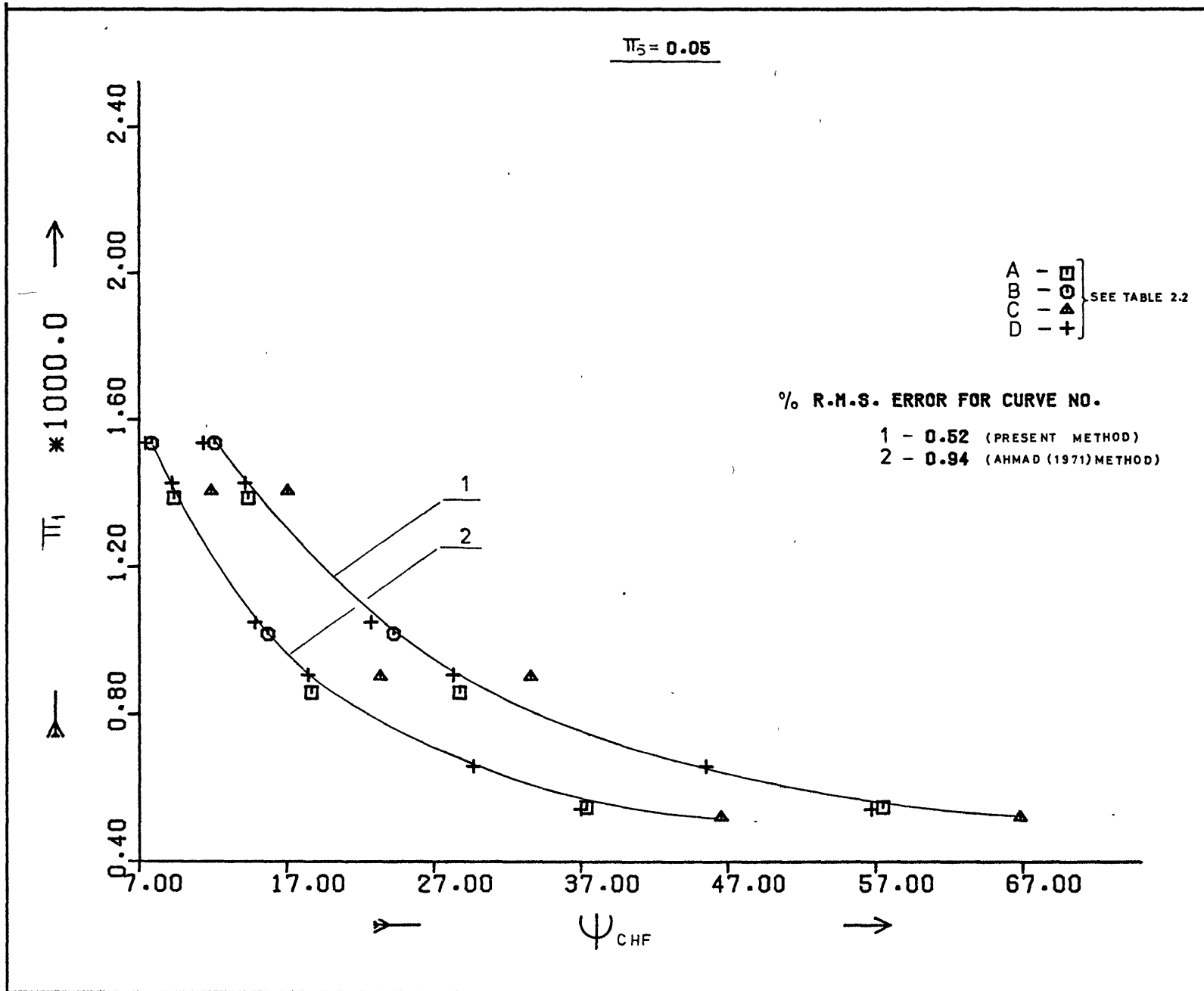


FIG (2-17)

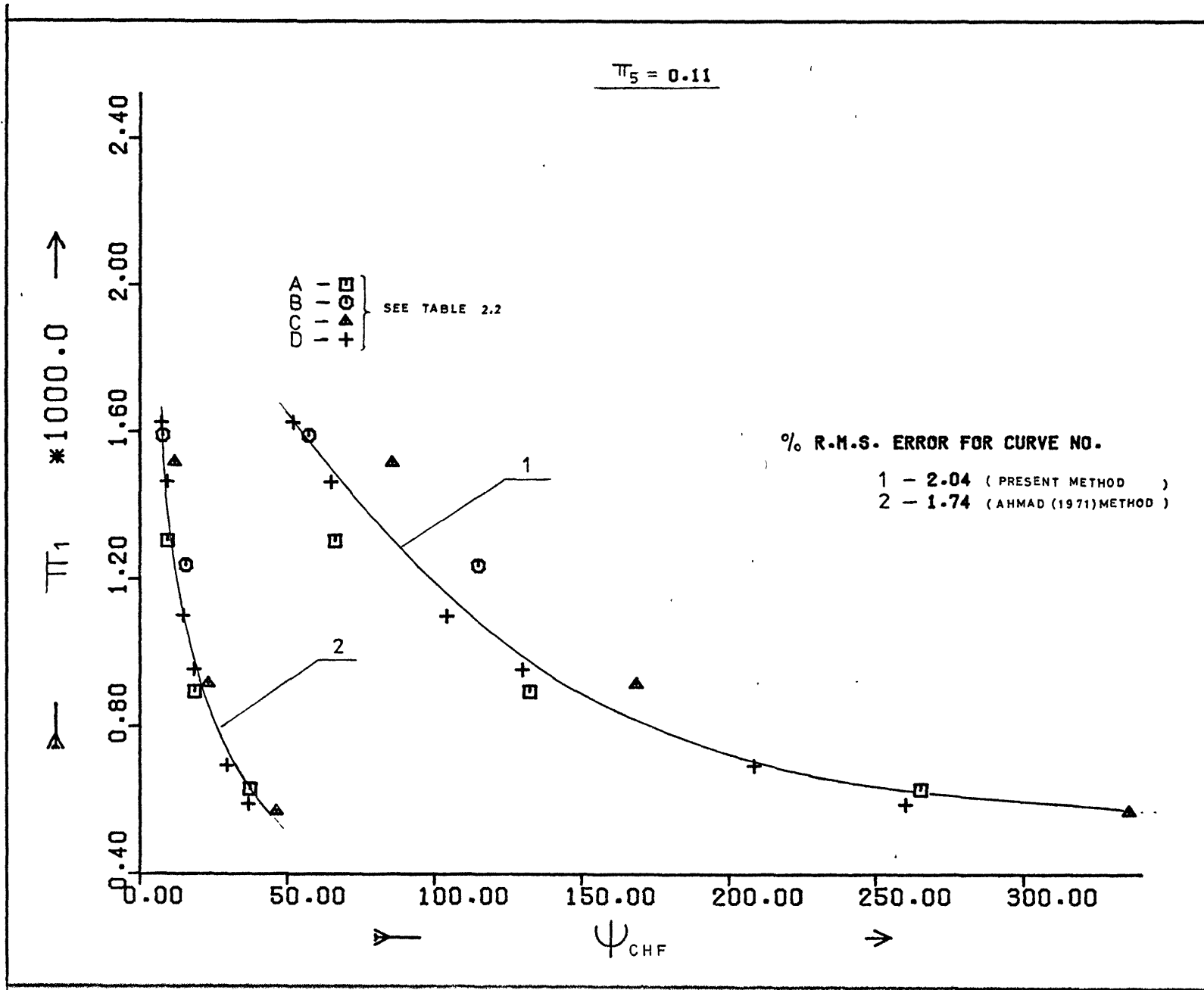


FIG (2-18)

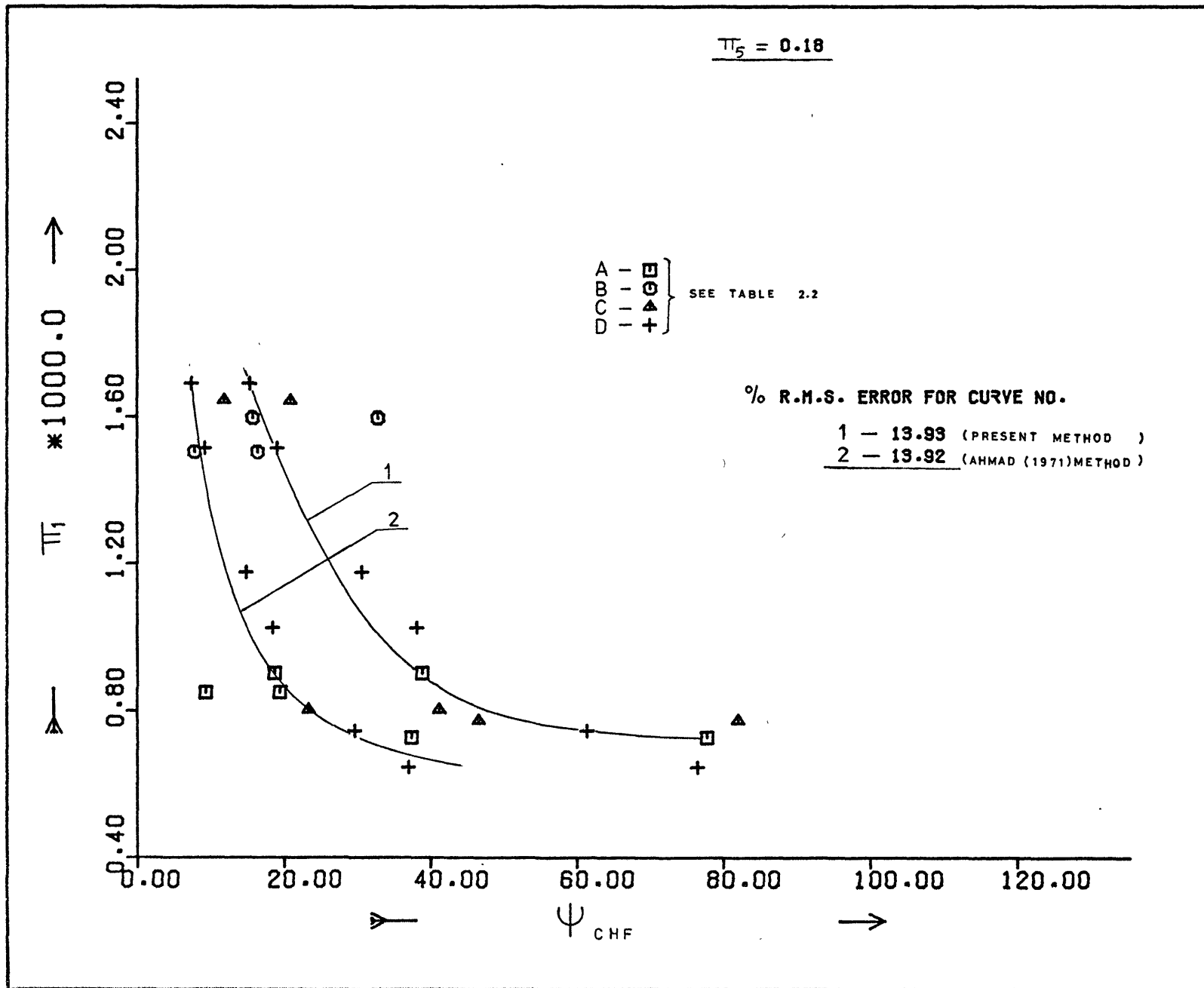


FIG (2-19)

COMPENSATING DISTORTION TECHNIQUE
 APPLIED TO
 EQUATION (2.1)

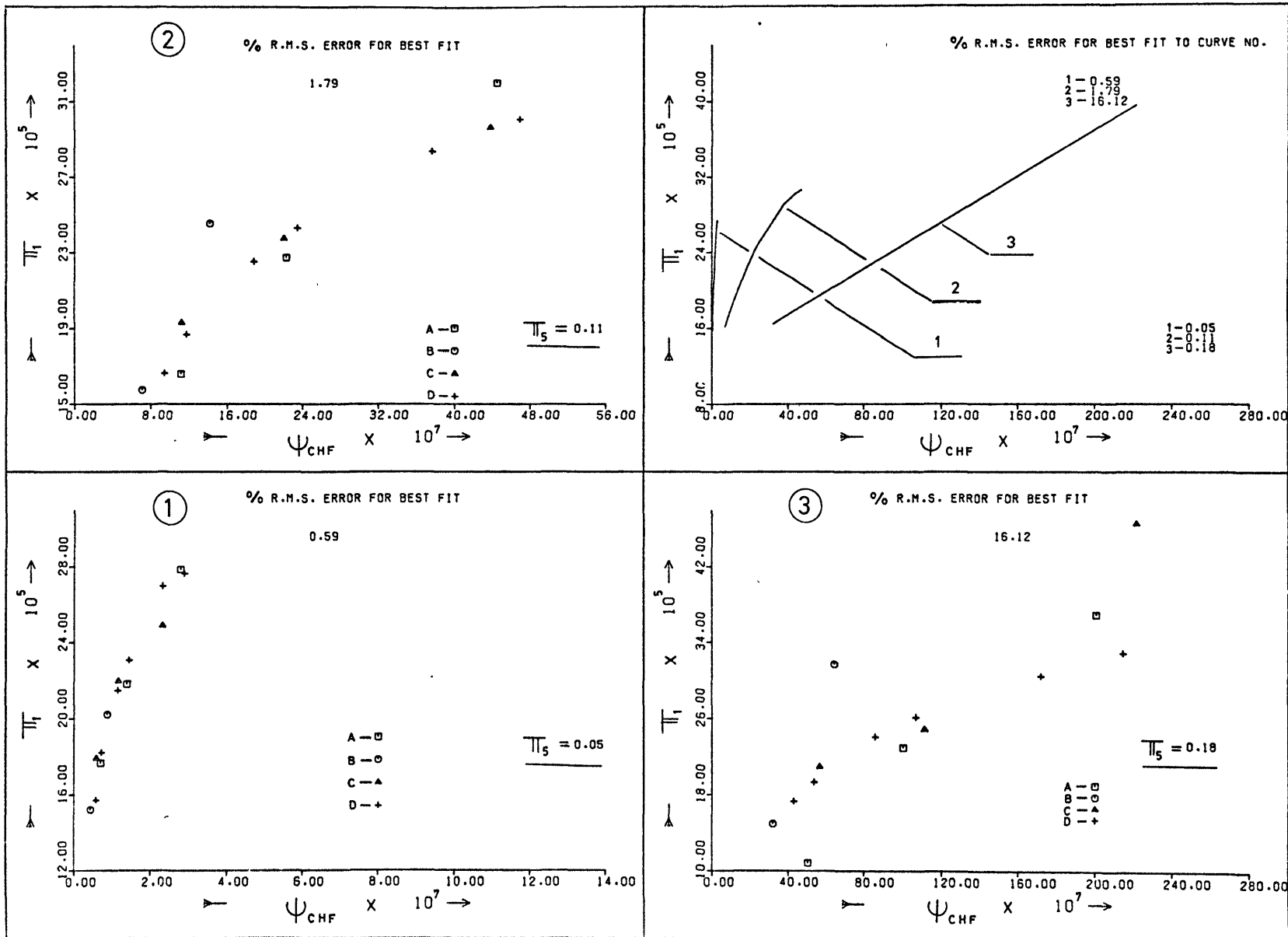
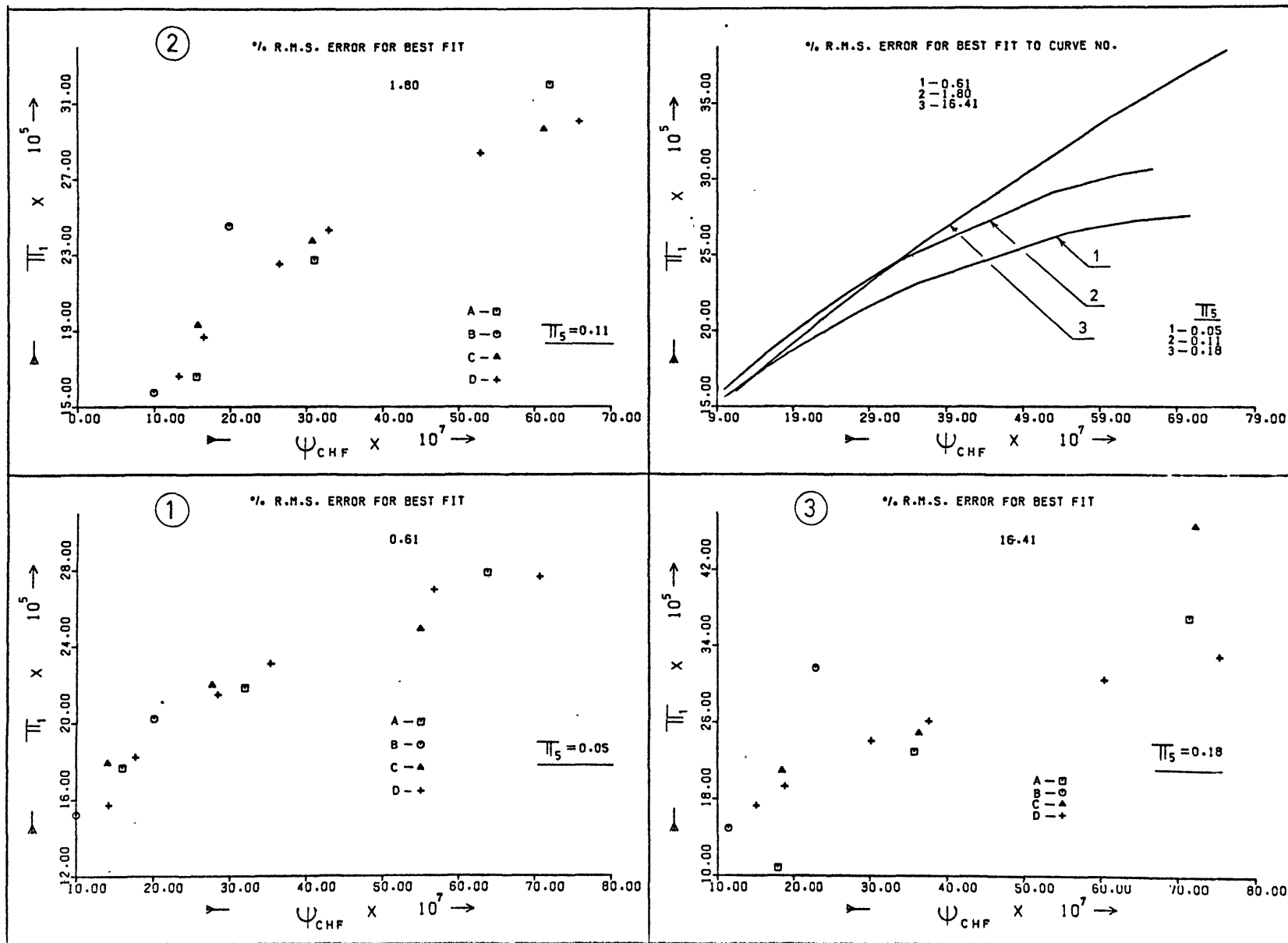


FIG. (2-20)

COMPENSATING DISTORTION TECHNIQUE
 APPLIED TO
 EQUATION (2.2)



COMPENSATING DISTORTION TECHNIQUE
 APPLIED TO
 EQUATION (3.3)

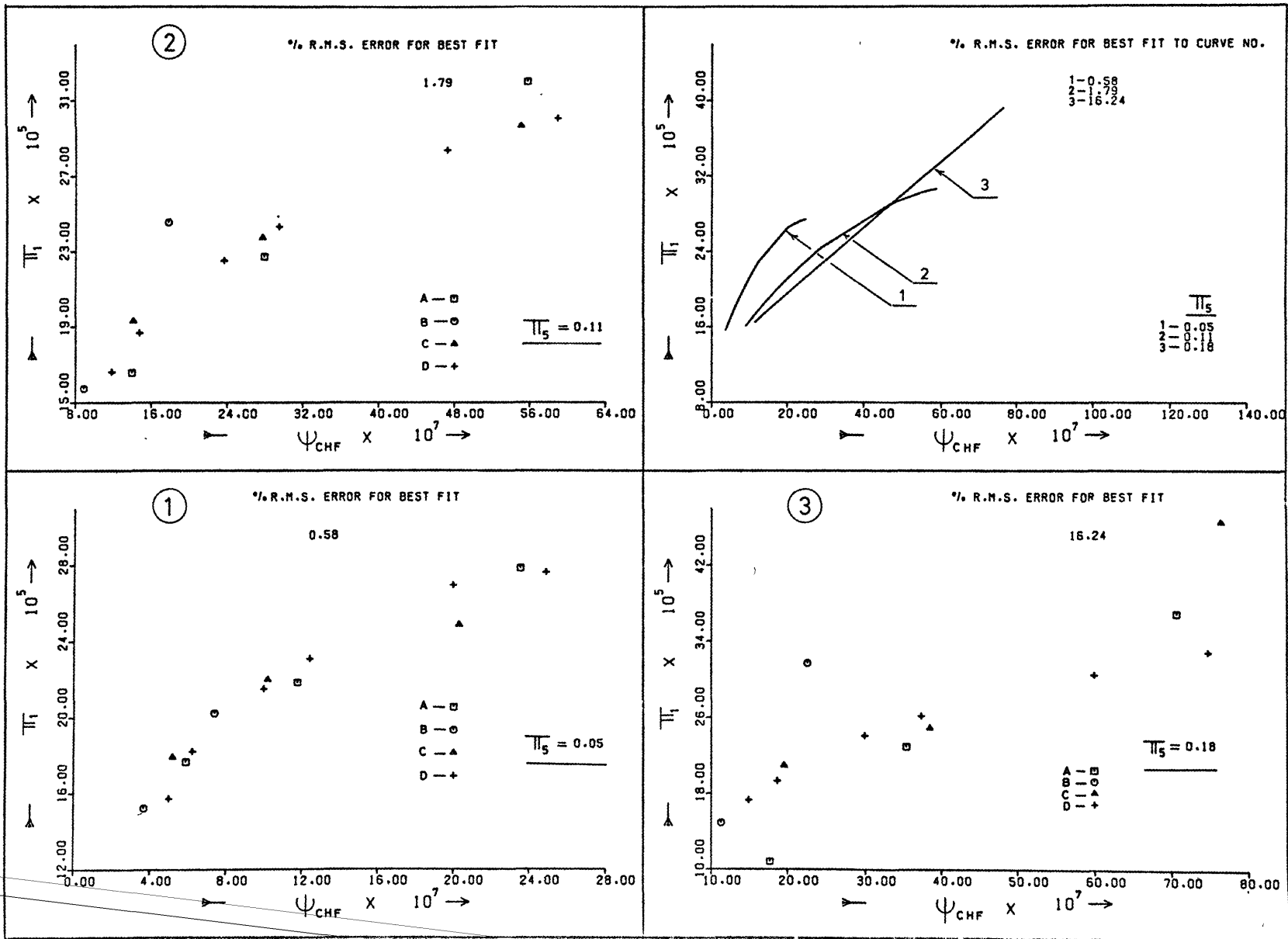


FIG. (2-22)

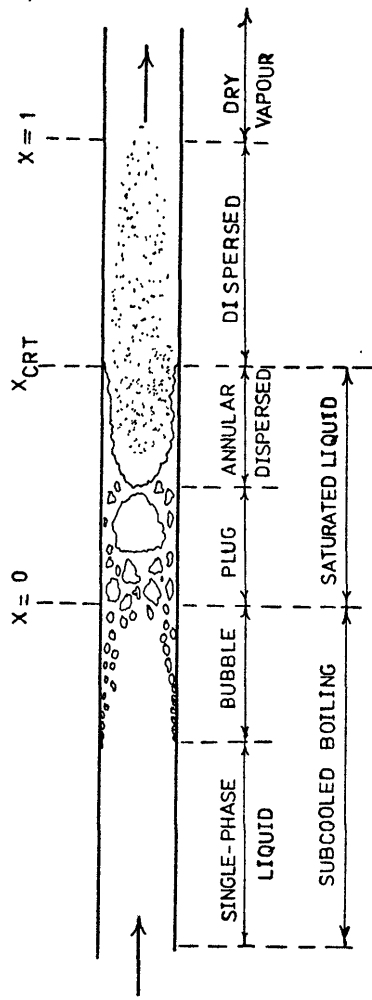


FIG. (2-23)

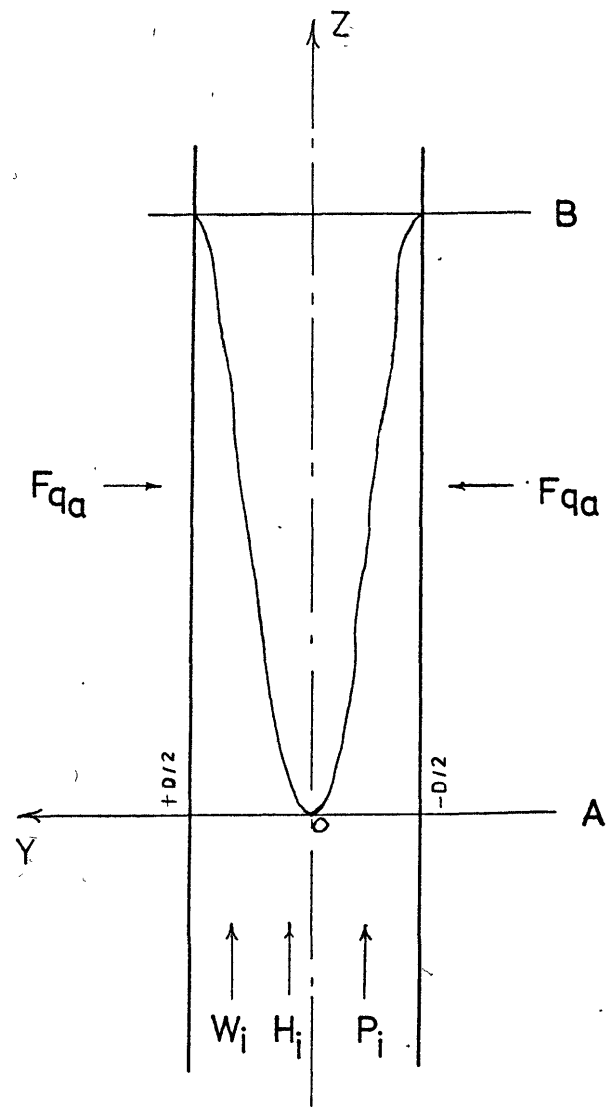


FIG. (2-24)

COMPENSATING DISTORTION TECHNIQUE
 APPLIED TO
 THE PROPOSED MODEL

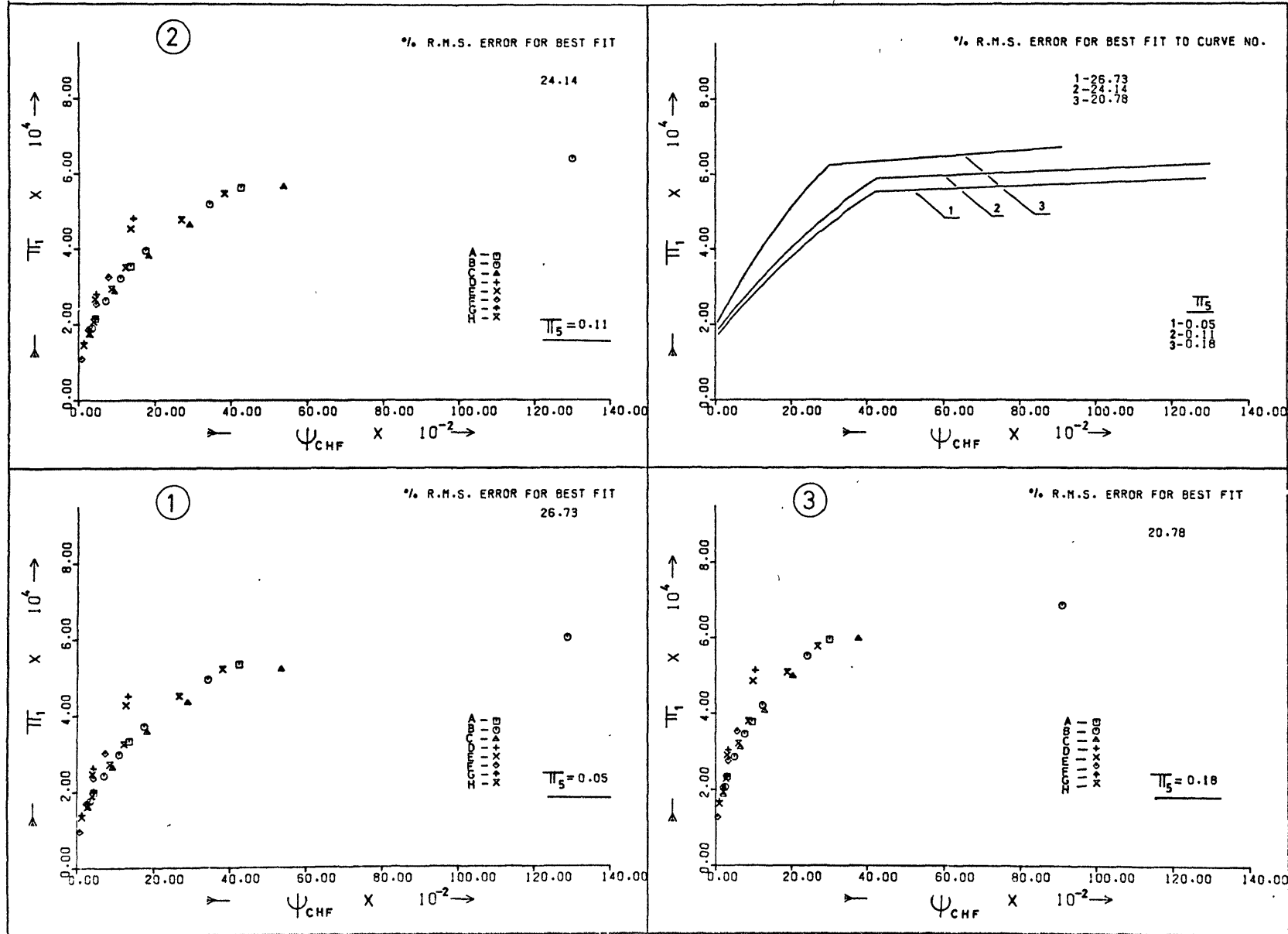
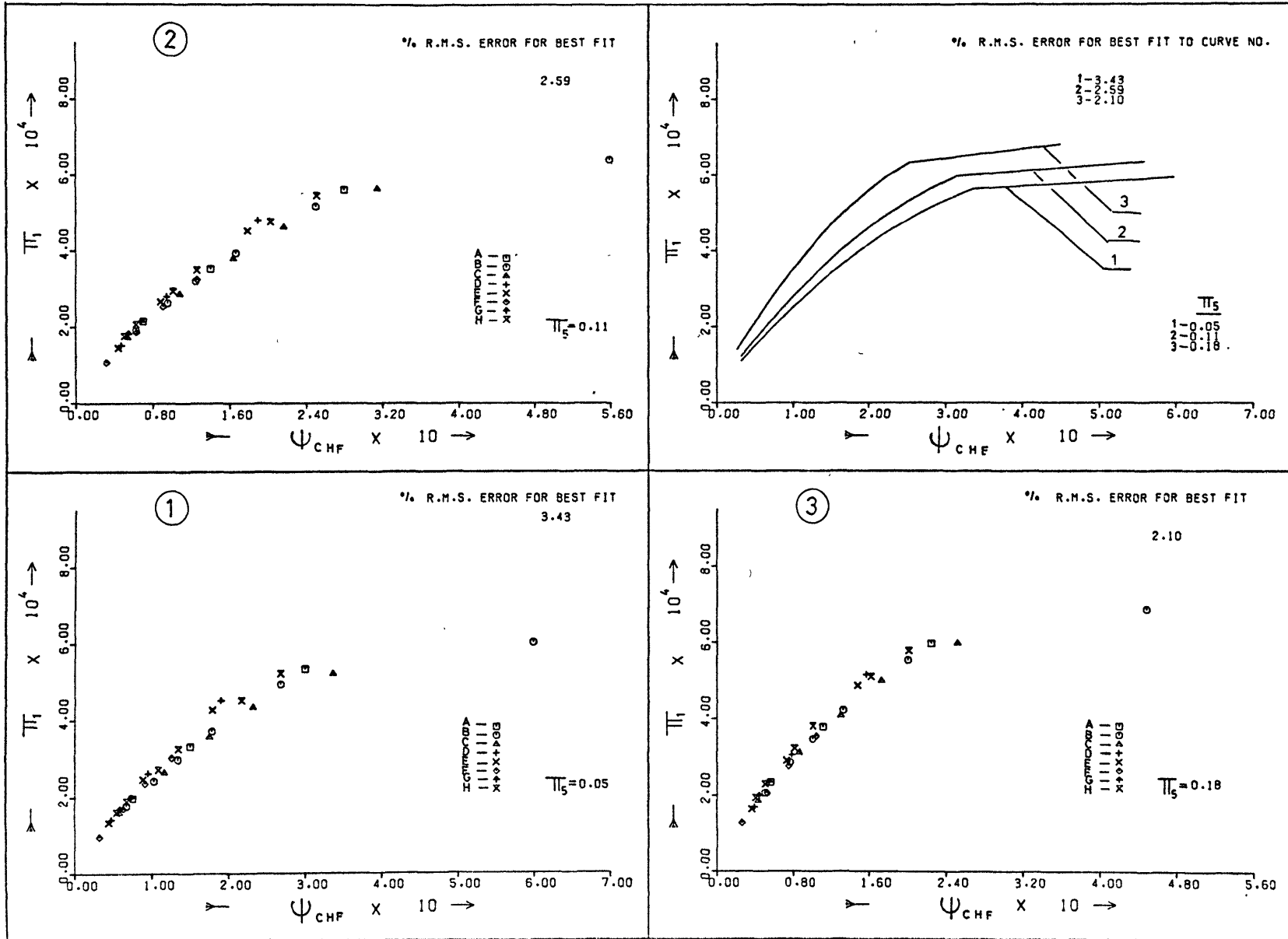
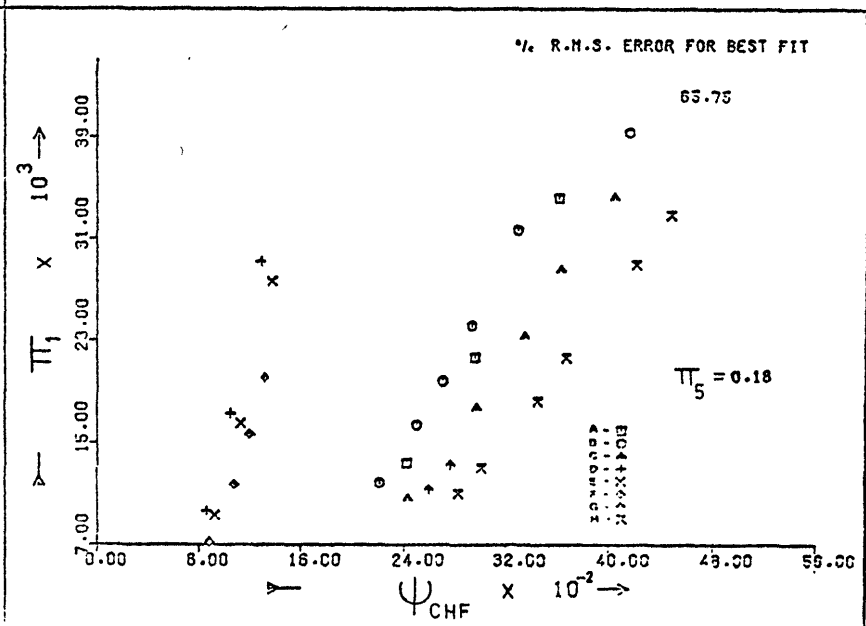
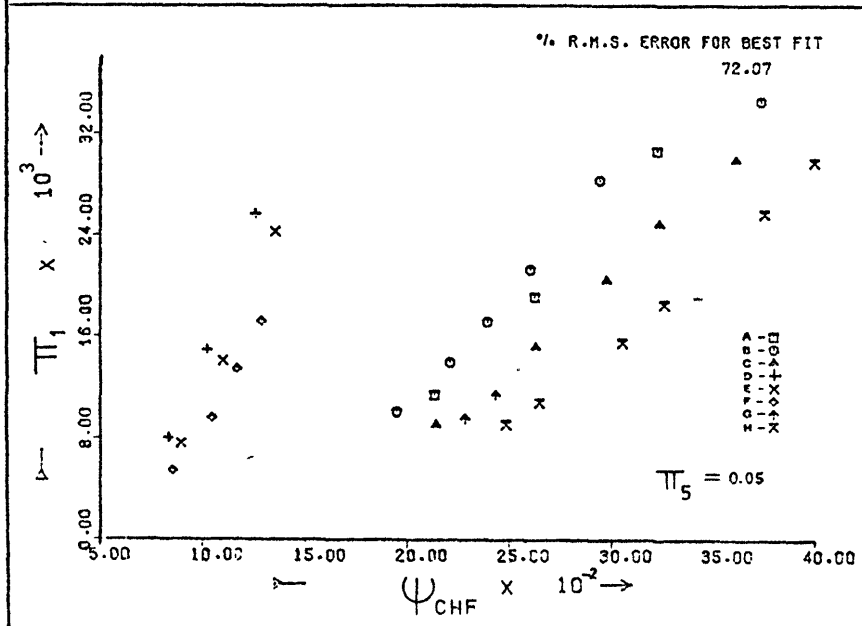
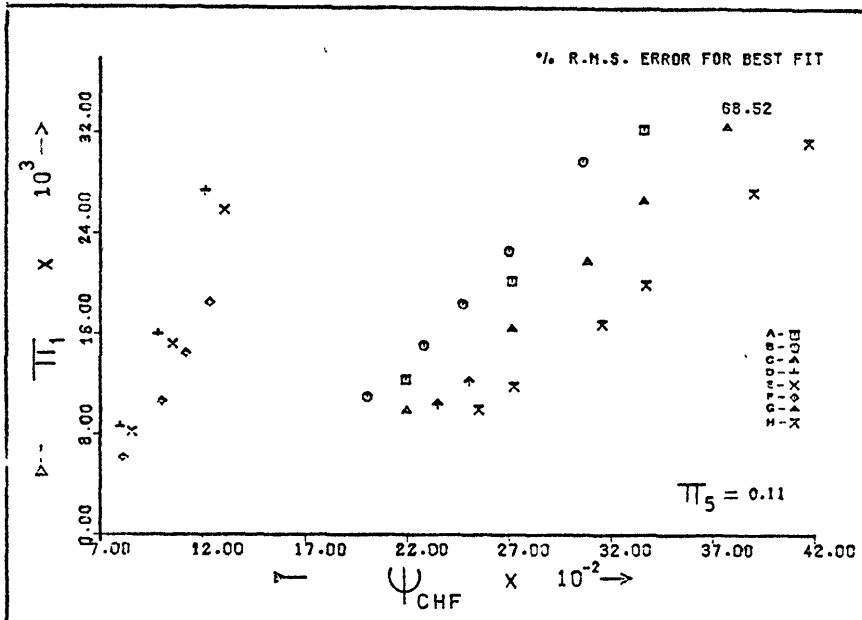


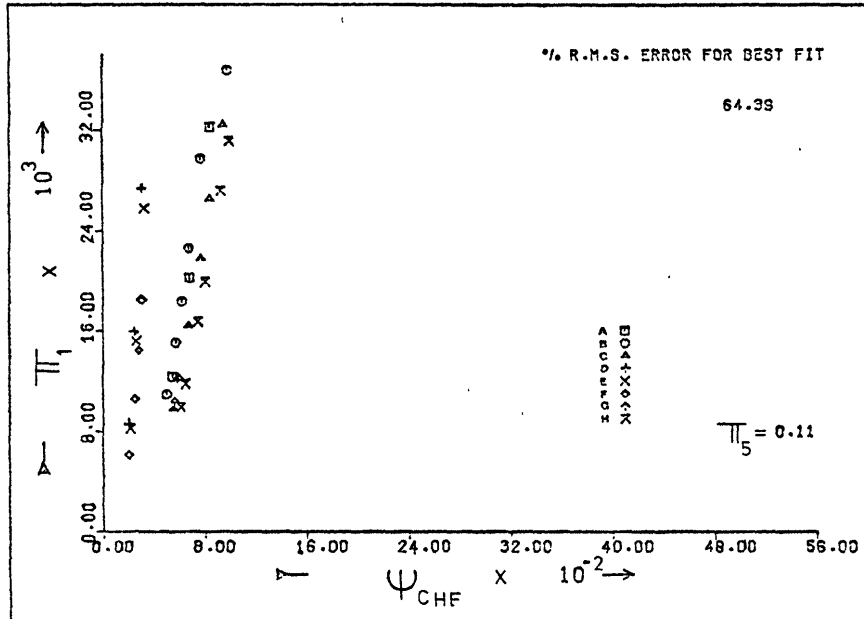
FIG. (2-25)

COMPENSATING DISTORTION TECHNIQUE
APPLIED TO
THE PROPOSED MODEL



COMPENSATING DISTORTION TECHNIQUE
 APPLIED TO
 EQUATION (2-26)





COMPENSATING DISTORTION TECHNIQUE
APPLIED TO
EQUATION (2-26)

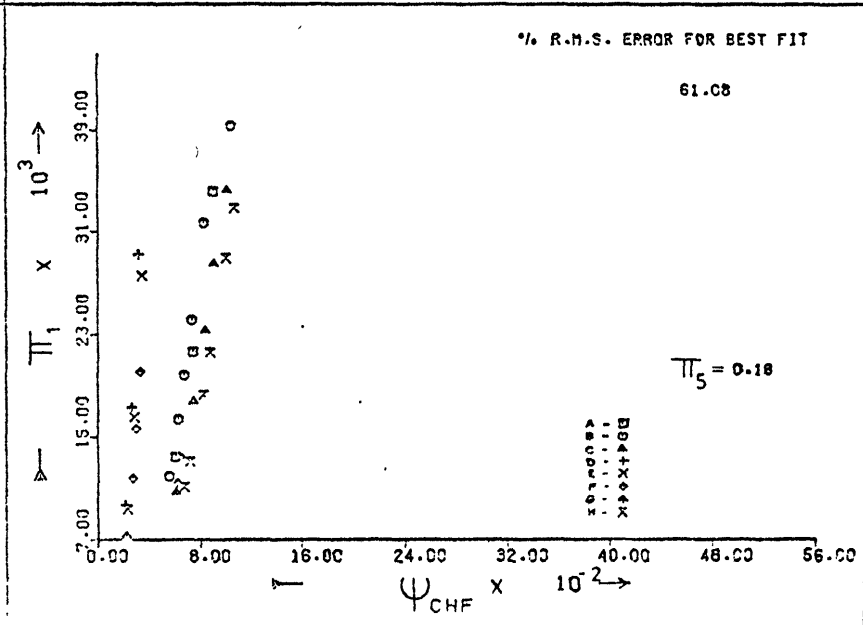
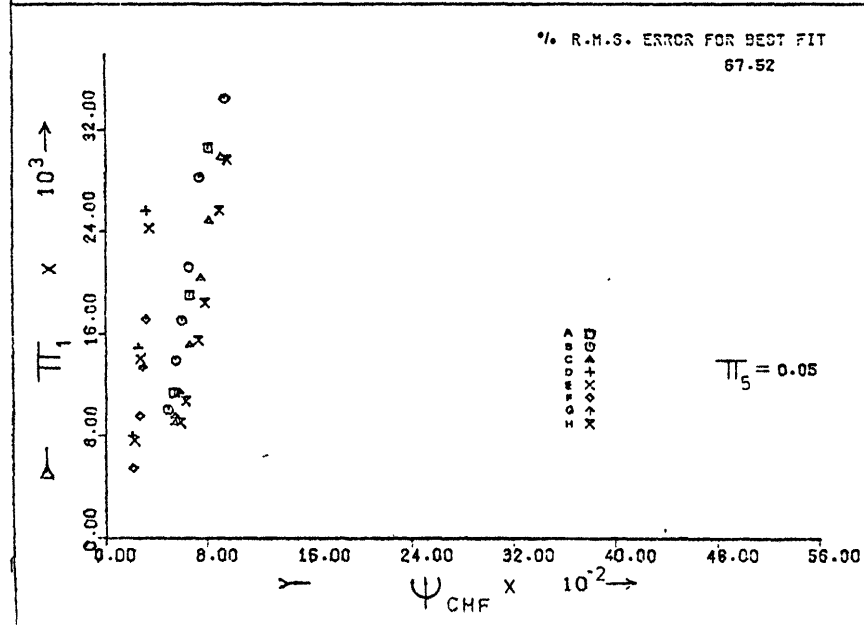


FIG. (2-28)

COMPENSATING DISTORTION TECHNIQUE
 APPLIED TO
 EQUATION (2-26)

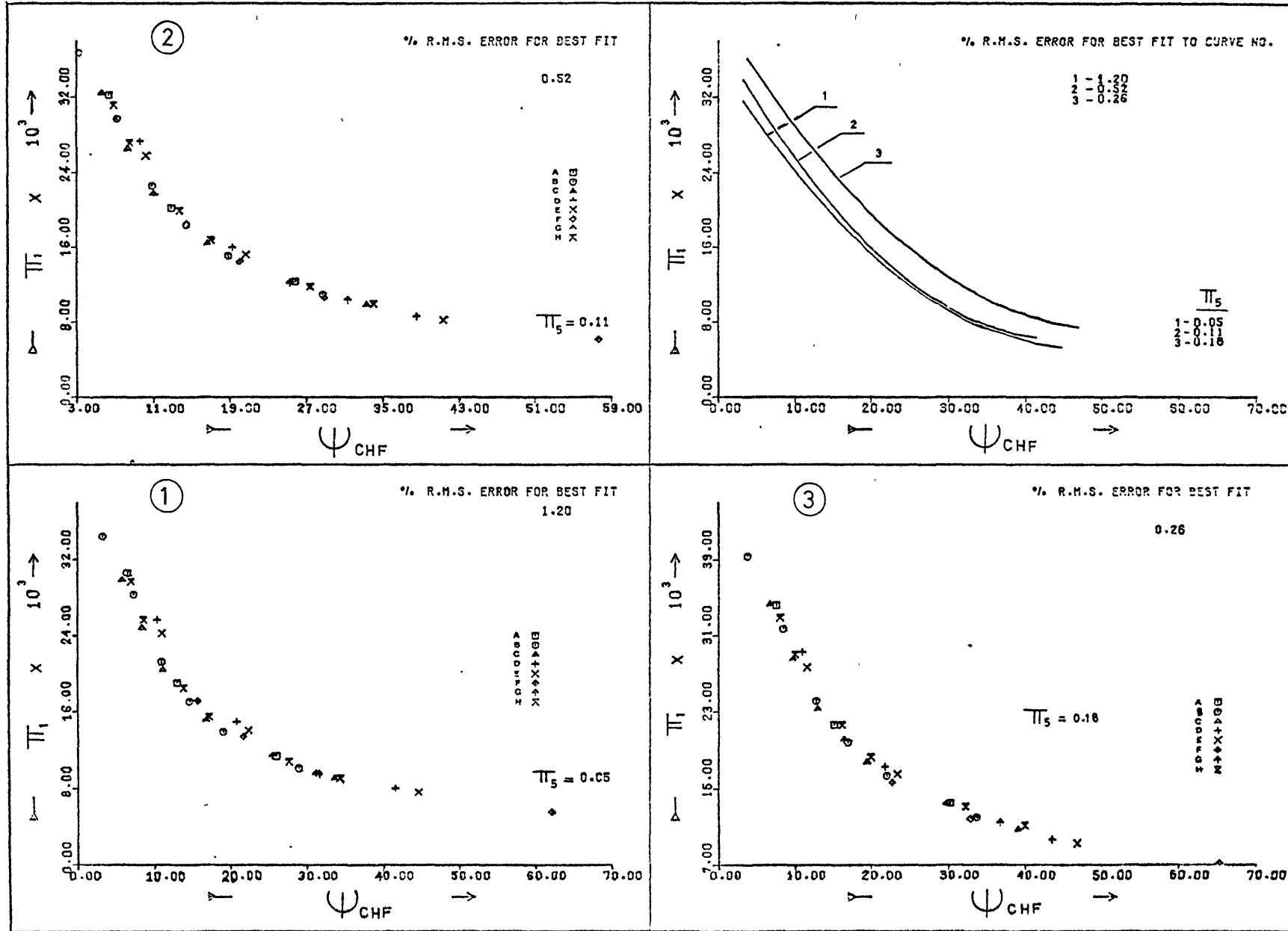


FIG. (2-29)

COMPENSATING DISTORTION TECHNIQUE
 APPLIED TO
 EQUATION (2-26)

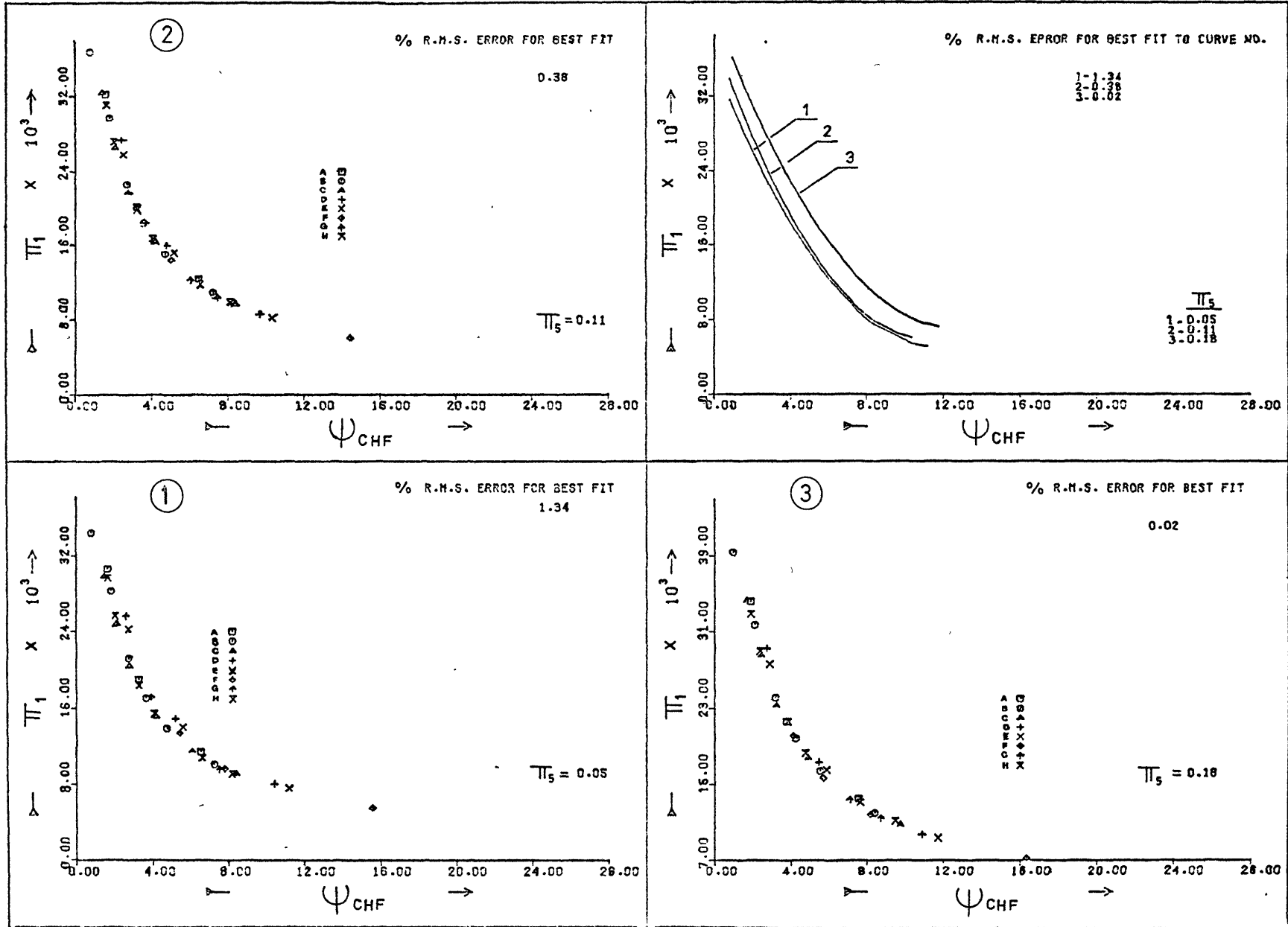


FIG. (2-30)

FALLING LIQUID FILM WITH HEAT TRANSFER
AND SURFACE WAVES

3.1 INTRODUCTION

This chapter is concerned with the behaviour of a falling liquid film with heat transfer and interfacial surface waves. Navier-Stokes equations have been solved for the wavy film model with the addition of heat transfer. A steady periodic solution which characterises the wave profile is obtained. The results include the wave properties, e.g. dimensionless wave celerity, wave length and wave number. This is a preliminary step towards the study of the effect of surface waves on the triple-phase front speed developed in Chapters 4 and 5, and to the subsequent applications of the distortion technique to simulate the triple-phase front speed in water by the use of Freon.

In the case of a wavy liquid film flowing downwards along a solid heated surface, the film has one free surface which may be in contact with either a gas or an immiscible liquid. As the liquid film is flowing down with a wavy formation there are valleys and crests. Hsu et al (1965) indicated that thermal layer penetration in the liquid film is accompanied by temperature variation at the free surface.

These temperature changes alter the free surface mechanisms, which, in turn, causes liquid to be pulled from the valleys towards neighbouring crests. This underlines the importance of surface tension in the wavy film flow configuration.

Nusselt (1916) solved the Navier-Stokes equations for wavy annular film flow flowing under gravity without including heat transfer or the effect of surface tension. Also, Duckler et al (1959) neglected the surface waves and obtained solutions for the case of smooth, non-wavy film flow. Levich (1962) proposed that all turbulent pulsations at the interface of a free flowing film are to be ignored, thus leaving there a non-turbulent layer. Kapitza (1948), Benjamin (1957) and Portalski (1964) included the effect of surface tension (capillary effects) in their solution for one-dimensional flow model. Massot et al (1966) and Rushton et al (1971) solved Navier-Stokes equations for Kapitza's model but for two-dimensional flow. Surface waves on falling films have been studied by many investigators who explained the wave patterns, e.g. Taylor et al (1963), Tailby et al (1962), Ajakaiye (1971), Ludviksson et al (1971), Krantz et al (1971), Massot (1966), Davies et al (1960), Shair (1971), Frisk (1971), Narasimhan (1971), Binnie (1972), Abi-Zadeh (1972), Pavri (1973) & Leong (1974).

3.2 MATHEMATICAL FORMULATION

The following analysis is for a wavy annular film flowing downwards on a heated surface as shown in Figure 3.1.

The following assumptions are made:

1) The shear stress along the film surface is negligible.

2) The surface waves are sinusoidal, i.e.

$$\phi = \frac{\delta - \delta_0}{\delta_0} = C_1 \sin n(z - ct) \quad (3.1)$$

3) The viscosity and thermal conductivity are constant.

4) The heat inertia is neglected.

The two-dimensional equations of motion are:

$$\frac{\partial W_z}{\partial t} + W_z \frac{\partial W_z}{\partial z} + W_y \frac{\partial W_y}{\partial y} = \nu \left[\frac{\partial^2 W_z}{\partial z^2} + \frac{\partial^2 W_z}{\partial y^2} \right] + g \beta_s (T - T_\infty) - \frac{1}{\rho_l} \cdot \frac{\partial P}{\partial z} \quad (3.2a)$$

$$\frac{\partial W_y}{\partial t} + W_z \frac{\partial W_y}{\partial z} + W_y \frac{\partial W_y}{\partial y} = \nu \left[\frac{\partial^2 W_y}{\partial z^2} + \frac{\partial^2 W_y}{\partial y^2} \right] - \frac{1}{\rho_l} \cdot \frac{\partial P}{\partial y} \quad (3.2b)$$

The continuity equation is:

$$\frac{\partial W_z}{\partial z} + \frac{\partial W_y}{\partial y} = 0 \quad (3.3)$$

Since only periodic solutions in z and t are

considered, the problem can be expressed in terms of:

$$\begin{aligned} \hat{z} &= z - ct &&) \\ & &&) \\ \hat{t} &= t &&) \end{aligned} \quad (3.4)$$

and of the following dimensionless quantities:

$$\begin{aligned} Z^* &= \frac{z}{\lambda}, \quad Y^* = \frac{y}{\delta_o}, \quad W^* = \frac{W}{W_o}, \quad v = \frac{W_y \cdot \lambda}{W_o \cdot \delta_o} \\ T^* &= \frac{t \cdot W_o \cdot \xi}{\delta_o}, \quad P^* = \frac{P}{\Omega_2 \cdot W_o^2}, \quad \alpha = \frac{c}{W_o}, \quad \xi = \frac{\delta_o}{\lambda} \\ \delta^* &= \frac{\delta}{\delta_o}, \quad F_{qa}^* = \frac{F_{qa} \cdot \delta_o}{T_{sat} \cdot K_l}, \quad \text{and } n = \frac{N_w}{\delta_o}. \end{aligned} \quad (3.5)$$

The momentum and continuity equations can now be rewritten in dimensionless forms as follows:

Continuity:

$$\frac{\partial W^*}{\partial Z^*} + \frac{\partial v}{\partial Y^*} = 0 \quad (3.6)$$

Momentum:

$$\begin{aligned} -\alpha \xi \frac{\partial W^*}{\partial Z^*} + \xi W^* \frac{\partial W^*}{\partial Z^*} + \xi v \frac{\partial W^*}{\partial Y^*} &= \frac{v}{\delta_o W_o} \left\{ \xi^2 \frac{\partial^2 W^*}{\partial Z^{*2}} + \frac{\partial^2 W^*}{\partial Y^{*2}} \right\} \\ &\quad - g \beta_s (T - T_\infty) \frac{\delta_o}{W_o^2} - \xi \frac{\partial P^*}{\partial Z^*} \end{aligned} \quad (3.7a)$$

$$-\alpha \xi^2 \frac{\partial v}{\partial Z^*} + \xi^2 W^* \frac{\partial v}{\partial Z^*} + \xi^2 v \frac{\partial v}{\partial Y^*} = \frac{v}{\delta_o W_o} \left\{ \xi^3 \frac{\partial^2 v}{\partial Z^{*2}} + \xi \frac{\partial^2 v}{\partial Y^{*2}} \right\} - \frac{\partial P^*}{\partial Y^*} \quad (3.7b)$$

The temperature distribution equation across the liquid film derived by Hewitt (1970) from one-dimensional energy equation:

$$T - T_w = \frac{F_{qa} \cdot \delta}{K_l} \left[\frac{1}{2} \left(\frac{Y}{\delta} \right)^3 - \frac{1}{8} \left(\frac{Y}{\delta} \right)^4 - \left(\frac{Y}{\delta} \right) \right]$$

is used in the present solution.

Non-dimensionalising the above equation gives:

$$T - T_w = F_{qa}^* \cdot T_{sat} \cdot \delta^* \cdot \left\{ \frac{1}{2} \left(\frac{Y^*}{\delta^*} \right)^3 - \frac{1}{8} \left(\frac{Y^*}{\delta^*} \right)^4 - \frac{Y^*}{\delta^*} \right\} \quad (3.8)$$

The buoyancy term $\left(g \beta \frac{\delta_o}{5W_o^2} (T - T_\infty) \right)$ in equation (3.7a) can be written in the form (see Appendix 1a):

$$g \beta \frac{\delta_o}{5W_o^2} (T - T_\infty) = \left(\frac{F_{qa}^{**}}{N_{Fr}^2} \right) \delta^* \left\{ \frac{1}{2} \left(\frac{Y^*}{\delta^*} \right)^3 - \frac{1}{8} \left(\frac{Y^*}{\delta^*} \right)^4 - \frac{Y^*}{\delta^*} \right\} + 16 \frac{G_r}{N_{Re}} \quad (3.9)$$

Equations (3.9) and (3.7a) yield:

$$-\alpha \xi \frac{\partial W^*}{\partial Z^*} + \xi W^* \frac{\partial W^*}{\partial Z^*} + \xi V \frac{\partial W^*}{\partial Y^*} = \frac{V}{\delta_o W_o} \left\{ \xi^2 \frac{\partial^2 W^*}{\partial Z^{*2}} + \frac{\partial^2 W^*}{\partial Y^{*2}} \right\} - \xi \frac{\partial P^*}{\partial Z^*} - 16 \frac{G_r}{N_{Re}^2} - \left(\frac{F_{qa}^{**}}{N_{Fr}^2} \right) \delta^* \left\{ \frac{1}{2} \left(\frac{Y^*}{\delta^*} \right)^3 - \frac{1}{8} \left(\frac{Y^*}{\delta^*} \right)^4 - \frac{Y^*}{\delta^*} \right\} \quad (3.7c)$$

In order to solve equations (3.7b) and (3.7c), the following boundary conditions must be satisfied:

(1) No slip and no net interfacial mass transfer at the solid-liquid interface:

$$W_z = W_y = 0 \quad \text{at } y = 0$$

In dimensionless form the boundary condition is:

$$W^* = V = 0 \quad \text{at } Y^* = 0 \quad (3.10)$$

(2) The free surface is a streamline, therefore kinematic boundary condition is:

$$\frac{\partial \delta}{\partial t} + W_z \frac{\partial \delta}{\partial z} = W_y \quad \text{at } y = \delta$$

In dimensionless form:

$$\xi \frac{\partial \delta^*}{\partial T^*} + \xi W^* \frac{\partial \delta^*}{\partial Z^*} = \xi V \quad \text{at } Y^* = \delta^* = \frac{\delta}{\delta_0} = 1 + \phi \quad (3.11)$$

(3) At the free surface the shear stresses are equal and also the normal stresses and therefore the stress condition at the free surface in dimensionless form is (see Appendix 1b):

$$P^* = -\frac{\xi^2}{N_{We}} \cdot \frac{\partial^2 \delta^*}{\partial Z^{*2}} + \frac{8}{N_{Re}} \xi \frac{\partial V}{\partial Y^*} \quad \text{at } Y^* = \delta^* \quad (3.12)$$

$$(4) \quad \frac{\partial W^*}{\partial Y^*} = 0 \quad \text{at } Y^* = \delta^* \quad (3.13)$$

We apply Kapitza's (1948) equation for the vertical velocity component:

$$W_z = \frac{3W_m}{\delta} \left(y - \frac{y^2}{2\delta} \right)$$

Introducing the dimensionless parameters (3.8) into the above equation will transform it into the following dimensionless form:

$$W^* = 3W_1^* \left\{ \frac{Y^*}{\delta^*} - \frac{1}{2} \left(\frac{Y^*}{\delta^*} \right)^2 \right\} \quad (3.14)$$

where W_1^* is the mean velocity of the film flow defined by:

$$W_1^* = \frac{1}{\delta^*} \int_0^{\delta^*} W^* dY^* \quad (3.15)$$

and

$$W_1^* = \frac{1 + \alpha\phi}{1 + \phi} \quad (\text{see Appendix 1c})$$

The Y component of velocity across the film is:

$$V = -\frac{3}{\delta^*} \cdot \frac{\partial W_1^*}{\partial Z^*} \left\{ \frac{1}{2} Y^{*2} - \frac{1}{6} \frac{Y^{*3}}{\delta^*} \right\} + 3W_1^* \frac{\partial \delta^*}{\partial Z^*} \left\{ \frac{Y^{*2}}{2\delta^{*2}} - \frac{Y^{*3}}{3\delta^{*3}} \right\} \quad (3.16)$$

and is derived from equations (3.14) and (3.6) (see Appendix 1d).

The pressure distribution equation is evaluated in terms of Y^* and Z^* by integrating equation (3.7b) with respect to Y^* and using boundary condition (3), giving the following expression for the pressure distribution across the film (see Appendix 1e):

$$P^* = \frac{4\xi}{N_{Re}} \cdot \frac{\partial V}{\partial Y^*} - \frac{6\xi}{N_{Re}} \cdot \frac{\partial W_1^*}{\partial Z^*} - \frac{\xi^2}{N_{We}} \cdot \frac{\partial^2 \delta^*}{\partial Z^{*2}} \quad (3.17)$$

The wave length and dimensionless wave celerity are obtained by averaging the equation of motion (3.7c) over the film thickness:

$$\begin{aligned} -\alpha \xi \int_0^{\delta^*} \frac{\partial W^*}{\partial Z^*} dY^* + \xi \int_0^{\delta^*} W^* \frac{\partial W^*}{\partial Z^*} dY^* + \xi \int_0^{\delta^*} V \frac{\partial W^*}{\partial Y^*} dY^* = \frac{4}{N_{Re}} \int_0^{\delta^*} \left\{ \xi^2 \frac{\partial^2 W^*}{\partial Z^{*2}} \right. \\ \left. + \frac{\partial^2 W^*}{\partial Y^{*2}} \right\} dY^* - \frac{F_{qa}^{**} \cdot \delta^*}{N_{Fr}^2} \int_0^{\delta^*} \left\{ \frac{1}{2} \left(\frac{Y^*}{\delta^*} \right)^3 - \frac{1}{8} \left(\frac{Y^*}{\delta^*} \right)^4 - \frac{Y^*}{\delta^*} \right\} dY^* \\ - 16 \int_0^{\delta^*} \frac{Gr}{N_{Re}^2} dY^* - \xi \int_0^{\delta^*} \frac{\partial P^*}{\partial Z^*} dY^* \quad (3.18) \end{aligned}$$

Substituting V and W^* (equations 3.14 and 3.16) into equation (3.18), the resulting terms in the latter equation are then integrated individually (see Appendix 1f) and multiplied by the factor $N_{Re}/12 \cdot \delta^*$:

$$\begin{aligned} & \frac{\xi^3}{N_{We}} \cdot \frac{N_{Re}}{12} \cdot \frac{\partial^3 \delta^*}{\partial Z^{*3}} + \frac{\xi^2}{12} \left[14 \frac{\partial^2 W_1}{\partial Z^{*2}} - \frac{4}{\delta^*} W_1^* \frac{\partial^2 \delta^*}{\partial Z^{*2}} \right] + \frac{N_{Re} \xi}{12} \left[\alpha \frac{\partial W_1^*}{\partial Z^*} - \frac{1}{2} \alpha \frac{W_1^*}{\delta^*} \cdot \frac{\partial \delta^*}{\partial Z^*} \right. \\ & \left. - \frac{9}{10} W_1^* \frac{\partial W_1^*}{\partial Z^*} + \frac{3}{10} \frac{W_1^{*2}}{\delta^*} \cdot \frac{\partial \delta^*}{\partial Z^*} \right] - \frac{8}{12} \frac{\xi^2}{\delta^*} \cdot \frac{\partial W_1^*}{\partial Z^*} \cdot \frac{\partial \delta^*}{\partial Z^*} - \frac{W_1^*}{\delta^{*2}} + \frac{1}{30} \frac{N_{Re}}{N_{Fr}^2} F_{qa}^{**} \delta^* \\ & - \frac{4}{3} \frac{Gr}{N_{Re}} = 0 \end{aligned} \quad (3.19)$$

Hence, using the expression for δ^* and W_1^* in terms of the dimensionless displacement parameter ϕ (i.e. $\delta^* = 1+\phi$ and $W_1^* = \frac{1+\alpha\phi}{1+\phi}$) in equation (3.19) and neglecting the quadratic and higher powers of ϕ , the following linearised equation of motion is obtained:

$$\begin{aligned} & \frac{N_{Re} \xi^*}{12} \frac{\xi^*}{N_{We}} \phi'''' + \frac{\xi^2}{6} [7\alpha - 9] \phi'' + \frac{N_{Re} \xi}{12} \left[\alpha^2 - \frac{12}{5} \alpha + \frac{6}{5} \right] \phi' \\ & + \left[(3-\alpha) + \frac{1}{30} \frac{N_{Re}}{N_{Fr}^2} F_{qa}^{**} \right] \phi - \frac{4}{3} \frac{Gr}{N_{Re}} + \frac{1}{30} \frac{N_{Re}}{N_{Fr}^2} F_{qa}^{**} - 1 = 0 \end{aligned} \quad (3.20a)$$

Since the mean value of ϕ is zero for periodic solution, the constant term in equation (3.20a) must be equal to zero, i.e.

$$\frac{F_{qa}^{**}}{30} \cdot \frac{N_{Re}}{N_{Fr}^2} = 1 + \frac{4}{3} \frac{Gr}{N_{Re}}$$

Therefore equation (3.20a) reduces to:

$$\begin{aligned} & \frac{N_{Re} \xi^3}{12} \cdot \frac{\xi^3}{N_{We}} \cdot \phi'''' + \frac{\xi^2}{6} [7\alpha - 9] \phi'' + \frac{N_{Re} \xi}{12} \left[\alpha^2 - \frac{12\alpha}{5} + \frac{6}{5} \right] \phi' \\ & + \left[3 - \alpha + \frac{1}{30} \frac{N_{Re}}{N_{Fr}^2} F_{qa}^{**} \right] \phi = 0 \end{aligned} \quad (3.20b)$$

Substituting for ϕ , ϕ' , ϕ'' and ϕ''' in equation (3.20b) from Appendix 3 gives:

$$\begin{aligned}
 & - \frac{N_{Re}}{12} \cdot \frac{\xi^3}{N_{We}} \cdot Cl. \left(\frac{N_w}{\xi} \right)^3 \cos \frac{N_w}{\xi} (Z^* - \alpha T^*) - \frac{\xi^2}{6} [7\alpha - 9] \cdot Cl. \left(\frac{N_w}{\xi} \right)^2 \\
 & \sin \frac{N_w}{\xi} (Z^* - \alpha T^*) + \frac{N_{Re}}{12} \xi \left[\alpha^2 - \frac{12\alpha}{5} + \frac{6}{5} \right] \cdot Cl. \frac{N_w}{\xi} \cos \frac{N_w}{\xi} (Z^* - \alpha T^*) \\
 & + \left[3 - \alpha + \frac{1}{30} \frac{N_{Re}}{N_{Fr}^2} F_{qa}^{**} \right] \cdot Cl. \sin \frac{N_w}{\xi} (Z^* - \alpha T^*) = 0 \quad (3.21)
 \end{aligned}$$

For a sinusoidal equation the sine and the cosine terms have to be equal, correspondingly.

(a) Equal cosine terms from equation (3.21):

$$\begin{aligned}
 & \frac{N_{Re}}{12} \cdot \frac{\xi^3}{N_{We}} \cdot Cl. \left(\frac{N_w}{\xi} \right)^3 \cos \frac{N_w}{\xi} (Z^* - \alpha T^*) \\
 & = \frac{N_{Re}}{12} \xi \left[\alpha^2 - \frac{12}{5} \alpha + \frac{6}{5} \right] \cdot Cl. \frac{N_w}{\xi} \cos \frac{N_w}{\xi} (Z^* - \alpha T^*) \\
 \therefore N_{We} & = \frac{N_w^2}{\left(\alpha^2 - \frac{12}{5} \alpha + \frac{6}{5} \right)} \quad (3.22)
 \end{aligned}$$

(b) Equal sine terms from equation (3.21):

$$\begin{aligned}
 & \frac{\xi^2}{6} [7\alpha - 9] \cdot Cl. \frac{N_w^2}{\xi^2} \sin \frac{N_w}{\xi} (Z^* - \alpha T^*) \\
 & = \left[3 - \alpha + \frac{1}{30} \frac{N_{Re}}{N_{Fr}^2} F_{qa}^{**} \right] \cdot Cl. \sin \frac{N_w}{\xi} (Z^* - \alpha T^*) \\
 \therefore N_w^2 & = \frac{6 \left[3 - \alpha + \frac{1}{30} \frac{N_{Re}}{N_{Fr}^2} F_{qa}^{**} \right]}{(7\alpha - 9)} \quad (3.23)
 \end{aligned}$$

From equations (3.22) and (3.23), N_{We} is given by:

$$N_{We} = \frac{6 \left[3 - \alpha + \frac{1}{30} \frac{N_{Re}}{N_{Fr}^2} \cdot F_{qa}^{**} \right]}{\left[7\alpha - 9 \right] \left[\alpha^2 - \frac{12}{5} \alpha + \frac{6}{5} \right]} \quad (3.24)$$

Since the dimensionless wave number is defined as $N_w = \frac{2\pi\delta_o}{\lambda}$,

The wave length λ can be obtained from equation (3.23)

$$\lambda = 2\pi\delta_o \sqrt{\frac{(7\alpha - 9)}{6 \left[3 - \alpha + \frac{1}{30} \frac{N_{Re}}{N_{Fr}^2} F_{qa}^{**} \right]}} \quad (3.25)$$

Also, from equation (3.23):

$$\lambda = 2\pi\delta_o \sqrt{\frac{1}{\left(\alpha^2 - \frac{12}{5} \alpha + \frac{6}{5} \right) \cdot N_{We}}} \quad (3.26)$$

3.3 DISCUSSION

Equation (3.24) gives the relation between Weber number (N_{We}), the dimensionless wave celerity (α), Reynolds number N_{Re} , Froude number N_{Fr} and the dimensionless heat flux quantity F_{qa}^{**} . In the case where no heat is added (i.e. $F_{qa}^{**} = 0$) equation (3.24) becomes:

$$N_{We} = \frac{6[3 - \alpha]}{\left[7\alpha - 9 \right] \left[\alpha^2 - \frac{12}{5} \alpha + \frac{6}{5} \right]}$$

Figure 3.2 shows the relation between Weber number and the dimensionless wave celerity α if heat transfer is not assumed, this is to compare it with the theoretical work of Kapitza (1948), Massot et al (1966), Rushton et al (1971) and the experimental results given by Kapitza (1948), Stainthorp et al (1965) and Jones et al (1966). It is noticed from Figure 3.2 that although our present theoretical results are slightly nearer to the experimental data, there is still a considerable discrepancy.

Figure 3.3 shows the relation between Weber number (We) and the dimensionless wave celerity (α) with heat transfer for different values of the dimensionless group $(N_{Re} F_{qa}^{**}/30N_{Fr}^2)$, equation (3.24). At $(N_{Re} F_{qa}^{**})/(30N_{Fr}^2)$ equal to zero there is no heat transfer between the solid surface and the film.

As the dimensionless group increases, the maximum value of the dimensionless celerity increases at the same average velocity. This indicates that the dimensionless group $N_{Re} \cdot F_{qa}^{**}/N_{Fr}^2$ is a significant parameter when plotting the relation between Weber number and the dimensionless wave celerity (α) - a result which has important implications for modelling.

Kapitza (1948) suggests that the value of the dimensionless wave amplitude ($C1$) is that which provides the

least viscous dissipation of the mechanical energy. To determine such value of Cl, Kapitza minimised a simplified expression of the viscous dissipation, namely $\mu\left(\frac{\partial W}{\partial y}\right)$, while Massot et al (1966) minimised the viscous energy dissipation, namely $2\left[\left(\frac{\partial W}{\partial z}\right)^2 + \left(\frac{\partial W}{\partial y}\right)^2\right] + \left[\frac{\partial W}{\partial z} + \frac{\partial W}{\partial y}\right]^2 - \frac{3}{2}\left[\frac{\partial W}{\partial z} + \frac{\partial W}{\partial y}\right]^2$. Figure 3.4 shows the results of the above approaches and the experimental results for determining the dimensionless wave amplitude (Cl).

From Figure 3.4 Kapitza's method showed that the dimensionless wave amplitude (Cl) has a constant value of 0.46, while Massot et al showed that Cl has a decreasing function with Weber number. However, it appears from the experimental results that Cl increases with the increase of Weber number. Realising the discrepancy between the theoretical and practical results, see Figure 3.4, Massot et al stated that since no justification of these theoretical assertions were given, therefore both theoretical results are questionable.

Hatton et al (1971) showed that ^{experimentally} buoyancy forces cause reversed flow when films flow downwards over a heated surface (Figure 3.5). That is why, in the present analysis, it was considered necessary to include the effect of buoyancy forces in the solution of the equation of motion. This inclusion is to account for the forces which cause the

recirculation zones in the downwards heated film flow created by natural and forced convection.

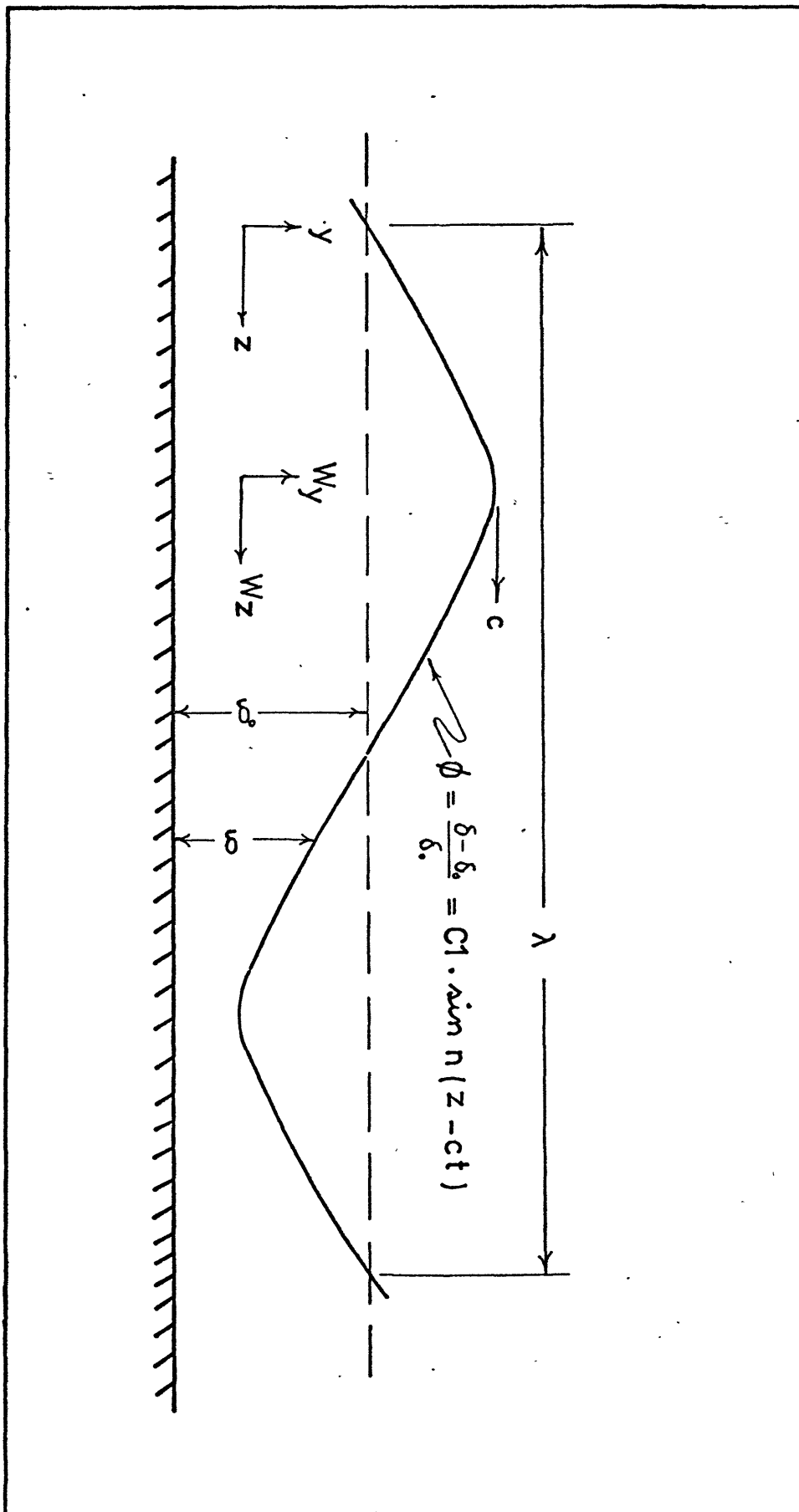


FIG.(3-1)

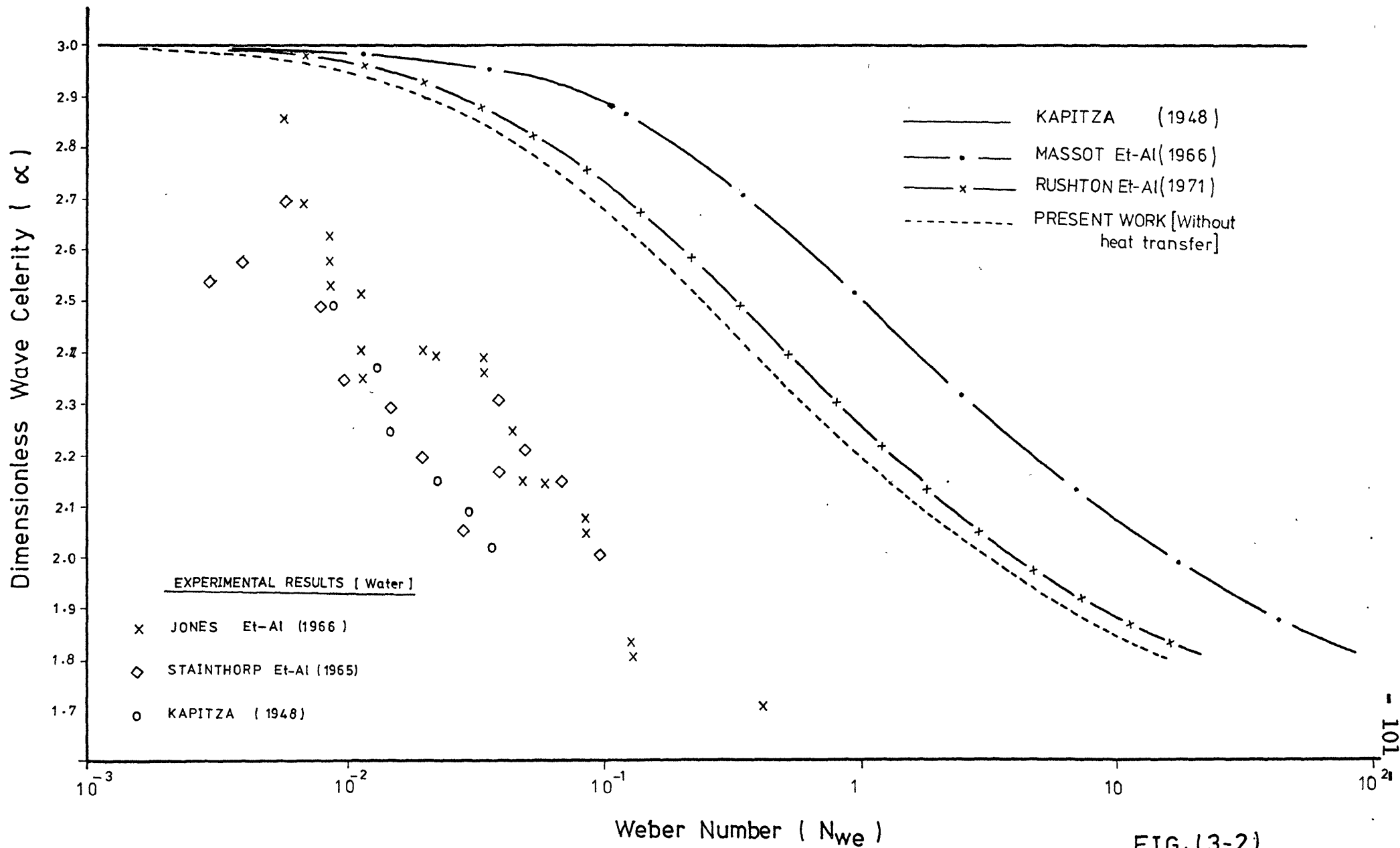
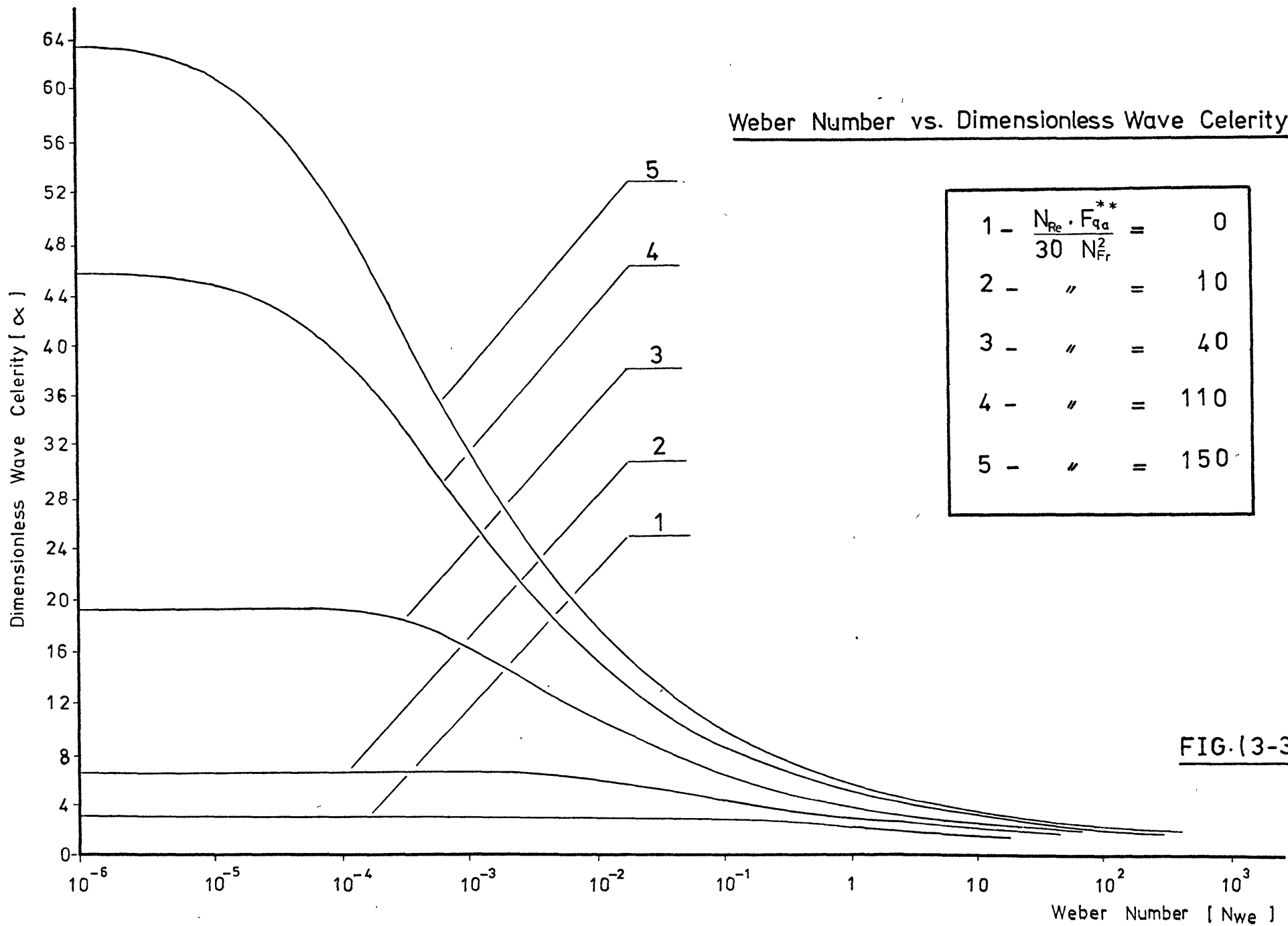


FIG. (3-2)



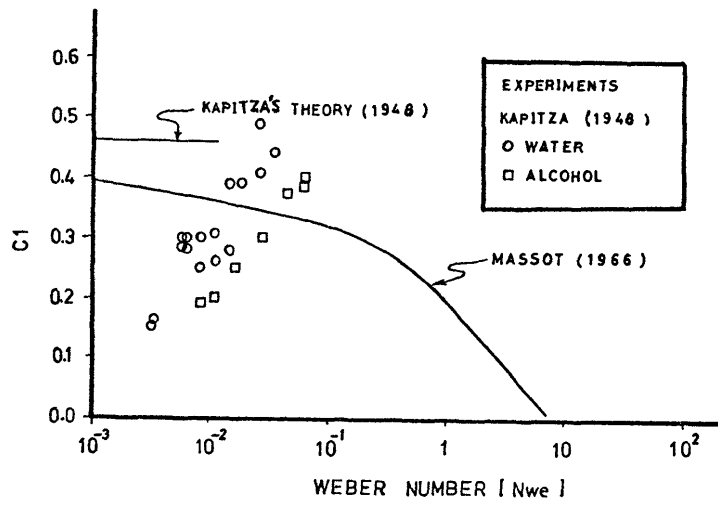


FIG.(3-4)

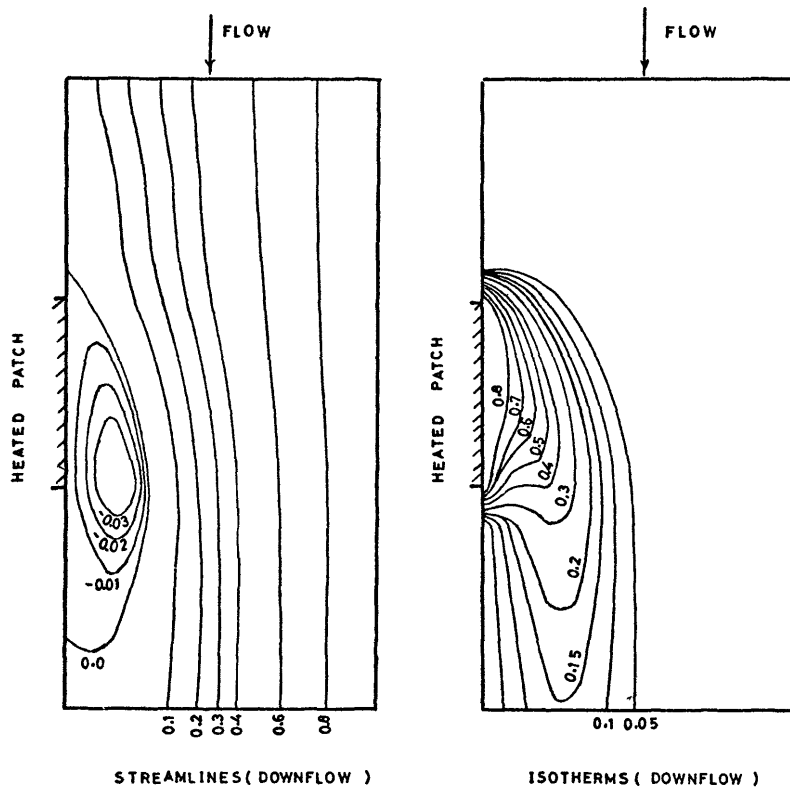


FIG.(3-5)

CHAPTER 4SIMULATION OF THE EFFECT OF WAVES ON THE
MOTION OF THE TRIPLE-PHASE FRONT OF A DRY
PATCH IN A WAVY FILM BY THE USE OF FREON4.1 INTRODUCTION

When thin films of liquid flow over a solid surface, there is always a possibility that a dry patch could develop. The first part of this chapter deals with the motion of the triple-phase front as this determines if the dry patch could be re-wetted, enlarged or become stable (Section 4.2). The heated solid surface is the internal surface of a horizontal tube and the thin film is motivated by vapour of the same substance. The film flow is under the influence of the shear which is applied by an interface vapour stream, the gravity force being neglected. The formation of waves on the liquid film surface is a significant feature of film flow due to its role in controlling the rate of heat and mass transfer, and also the movement of the triple-phase front; Zuber (1966), Wedekind et al (1968), Wedekind (1971) and Mariy et al (1974).

In the second part of this chapter we apply the compensating distortion technique to simulate the triple-phase front motion in water by Freon (Section 4.4).

4.2 THE MODEL

Assume that the triple-phase stagnation point of a dry patch of a shape similar to that suggested by Hartley and Murgatroyd (1964) and later photographed by Thompson (1970) and El-Shanawany (1974) would behave in a similar way to the edge of the annular liquid film at the end of the region of two-phase flow in a straight tubular steam generator. Figure 4.1a shows the cross section of the film and the triple-phase front where θ is the contact angle. According to Hartley and Murgatroyd (1964), for each contact angle there is a unique value of the critical thickness δ_c ; when the film becomes thicker than δ_c , the kinetic head overcomes the capillary force at the stagnation point and this point advances to re-wet the dry patch.

Assume a film front, Figure 4.1a, which, in the absence of waves, is just stable and of thickness δ_c , the heat supplied being just sufficient to evaporate the incoming liquid at the triple-phase front. Now, if we assume that harmonic waves exist on the film surface, as shown in Figure 4.1b, the film thickness will increase at the triple-phase point when the waves reach it. The static and dynamic forces will overcome the capillary forces and the triple-phase front will move forward over the heated surface. The subsequent

advance and retreat of the front will depend on whether the excess liquid is evaporated before the next wave arrives. In the proper circumstances the front will, on average, move forward and re-wet the surface.

Now, the objectives are to find the effect of surface waves on the triple-phase front motion; hence, to find the rewetting speed at different values of heat-flux, mass velocity, subcooling and dimensionless wave amplitude. Also, to simulate the above result by Freon-12 and to determine the simulation errors. To simplify the model the inertia of the solid surface has been neglected.

• Wedekind (1968) related the interface (triple) point oscillations to the liquid waves which propagate along the liquid annulus in the annular flow regime. Those waves which reach the triple-phase front appear to "wash up" and "recede" from the dry tube wall much as surface waves on a lake interact with the beach.

The effect of heat flux and excess liquid on the interface triple front oscillations can be as follows:

From an energy consideration, the time required and the distance along the dry wall along which the wave advances, are both directly proportional to the amount of

liquid present in the wave and are inversely proportional to the heat flux. Therefore, with waves of comparable volumes the interface-front movement is expected to decrease as the heat flux increases.

Let the distance travelled by the triple-phase front per unit time:

$$\eta(t) \propto \dot{m}_2(t)$$

Also, $\eta(t) \propto 1/f_{qi}$

$$\therefore \eta(t) = K \frac{\dot{m}_2(t)}{f_{qi}}$$

Where: $\dot{m}_2(t)$ is the mass of excess liquid supplied by the wave per unit time, lb/hr.

f_{qi} is the heat flux between the tube wall and fluid, Btu/hr.ft.

4.3 ANALYTICAL SOLUTION

In order to get the interface (triple-front) movement, the continuity and the energy equations are considered and solved for the region near the interface triple front.

Continuity equation:

$$\frac{d}{dt} \int_{z=0}^{z=\eta(t)} (\rho_l A + \rho_v A') dz = m_t(z,t)_{z=0} - m_t(z,t)_{z=\eta(t)} \quad (4.1)$$

where: (see Figures 4.1 and 4.3)

$$A_t = A + A'$$

A = Cross-sectional area occupied by liquid phase, ft

A' = Cross-sectional area occupied by vapour phase, ft

$m(z,t)$ = Local instantaneous mass flow rate of liquid phase, lb/h.

$\alpha(z,t)$ = void fraction = A'/A_t .

ρ_ℓ = liquid density, lb/ft³.

ρ_v = vapour density, lb/ft³.

Introducing the void fraction into the continuity equation we get.

$$\frac{d}{dt} \int_{z=0}^{z=\eta(t)} [\rho_\ell + (\rho_v - \rho_\ell)\alpha] A_t dz = m_t(z,t)_{z=0} - m_t(z,t)_{z=\eta(t)} \quad (4.2)$$

Applying Leibnitz theorem*, equation (4.2) becomes:

$$\begin{aligned} \int_{z=0}^{z=\eta(t)} \frac{d}{dt} [\rho_\ell + (\rho_v - \rho_\ell)\alpha] A_t dz + [\rho_\ell + (\rho_v - \rho_\ell)\alpha] A_t \frac{d}{dt} \eta(t) \\ = m_t(z,t)_{z=0} - m_t(z,t)_{z=\eta(t)} \end{aligned} \quad (4.3)$$

where: $A_t = A' + A$

Multiply (4.3) by H_v (specific enthalpy of the vapour):

* If $\phi = \int_{\psi_t}^{\psi_E} h(\psi, x) d\psi$

$$\therefore \frac{d\phi}{dx} = \int_{\psi_t}^{\psi_E} \frac{dh}{dx} d\psi + h(\psi_E, x) \frac{d\psi_E}{dx} - h(\psi_t, x) \frac{d\psi_t}{dx}$$

where $h(\psi_t, x) \frac{d\psi_t}{dx} = 0$ if ψ_t is a specified value.

$$\begin{aligned} \therefore \int_{z=0}^{z=\eta(t)} \frac{d}{dt} \left[\rho_{\ell} H_v + (\rho_v H_v - \rho_{\ell} H_v) \alpha \right] A_t dz + \left[\rho_{\ell} H_v + (\rho_v H_v \right. \\ \left. - \rho_{\ell} H_v) \alpha \right] A_t \frac{d}{dt} \eta(t) = H_v m_t(z, t)_{z=0} - H_v m_t(z, t)_{z=\eta(t)} \end{aligned} \quad (4.4)$$

Energy equation:

Neglect the changes in kinetic energy and viscous dissipation. Furthermore, the only heat transfer that will be considered is the internal average surface heat flux (f_{qi}):

$$\begin{aligned} \frac{d}{dt} \int_{z=0}^{z=\eta(t)} \left[\rho_{\ell} H_{\ell} A + \rho_v H_v A' \right] dz = \int_{z=0}^{z=\eta(t)} f_{qi} dz + \left[H_{\ell} m_{\ell}(z, t) \right. \\ \left. + H_v m_v(z, t) \right]_{z=0} - \left[H_v m_t(z, t) \right]_{z=\eta(t)} \end{aligned} \quad (4.5)$$

where f_{qi} is the radial heat supplied to the liquid from the internal surface of the pipe.

Introducing the local flow quality x and local void fraction (α) to equation (4.5), we get:

$$\begin{aligned} \frac{d}{dt} \int_{z=0}^{z=\eta(t)} \left[\rho_{\ell} H_{\ell} + (\rho_v H_v - \rho_{\ell} H_{\ell}) \alpha \right] A_t dz = \int_{z=0}^{z=\eta(t)} f_{qi} dz \\ + \left[\left\{ H_{\ell} + (H_v - H_{\ell}) x \right\} m_t(z, t) \right]_{z=0} - \left[H_v m_t(z, t) \right]_{z=\eta(t)} \end{aligned} \quad (4.6)$$

Again applying Leibnitz theorem to equation (4.6) we get:

$$\begin{aligned}
 & \int_{z=0}^{z=\eta(t)} \frac{d}{dt} \left[\rho_{\ell} H_{\ell} + (\rho_{\ell} H_{\ell} - \rho_{\ell} H_{\ell}) \alpha \right] A_t dz + \left[\rho_{\ell} H_{\ell} + (\rho_{\ell} H_{\ell} - \rho_{\ell} H_{\ell}) \alpha \right] \\
 & \cdot A_t \frac{d}{dt} \eta(t) = \int_{z=0}^{z=\eta(t)} f_{qi} dz + \left[\left\{ H_{\ell} + (H_{\ell} - H_{\ell}) x \right\} m_t(z, t) \right]_{z=0} \\
 & - \left[H_{\ell} m_t(z, t) \right]_{z=\eta(t)} \quad (4.7)
 \end{aligned}$$

Subtracting (4.4) from (4.7):

$$\begin{aligned}
 & \int_{z=0}^{z=\eta(t)} \frac{d}{dt} \left[\rho_{\ell} (H_{\ell} - H_{\ell}) - \rho_{\ell} (H_{\ell} - H_{\ell}) \alpha \right] A_t dz + \left[\rho_{\ell} (H_{\ell} - H_{\ell}) \right. \\
 & \left. - \rho_{\ell} (H_{\ell} - H_{\ell}) \alpha \right] A_t \frac{d}{dt} \eta(t) = \int_{z=0}^{z=\eta(t)} f_{qi} dz + m_t(z, t)_{z=0} \\
 & \cdot \left[H_{\ell} + H_{\ell} x - H_{\ell} x - H_{\ell} \right]
 \end{aligned}$$

$$\begin{aligned}
 \therefore & \int_{z=0}^{z=\eta(t)} \frac{d}{dt} \left[\rho_{\ell} (H_{\ell} - H_{\ell}) - \rho_{\ell} (H_{\ell} - H_{\ell}) \alpha \right] A_t dz + \left[\rho_{\ell} (H_{\ell} - H_{\ell}) \right. \\
 & \left. - \rho_{\ell} (H_{\ell} - H_{\ell}) \alpha \right] A_t \frac{d}{dt} \eta(t) = \int_{z=0}^{z=\eta(t)} f_{qi} dz + m_t(z, t)_{z=0} \\
 & \cdot \left[(H_{\ell} - H_{\ell}) - x(H_{\ell} - H_{\ell}) \right]
 \end{aligned}$$

$$\begin{aligned}
 & \rho_{\ell} (H_{\ell} - H_{\ell}) A_t \left[\int_{z=0}^{z=\eta(t)} \frac{d}{dt} (1 - \alpha) dz + (1 - \alpha) \frac{d}{dt} \eta(t) \right] \\
 & = \int_{z=0}^{z=\eta(t)} f_{qi} dz + m_t(z, t)_{z=0} (H_{\ell} - H_{\ell}) (1 - x)
 \end{aligned}$$

$$\begin{aligned} & \rho_{\ell}(H_{\ell}-H_v)A_t \left[\int_{z=0}^{z=\eta(t)} \frac{d}{dt}(-\alpha) dz + (-\alpha) \frac{d}{dt} \eta(t) + \frac{d}{dt} \eta(t) \right] \\ & = \int_{z=0}^{z=\eta(t)} f_{qi} dz + m_t(z, t)_{z=0} (H_{\ell}-H_v)(1-x) \end{aligned} \quad (4.8)$$

Applying Leibnitz theorem to equation (4.8):

$$\begin{aligned} \therefore & \rho_{\ell}(H_{\ell}-H_v)A_t \left[\frac{d}{dt} \eta(t) - \frac{d}{dt} \int_{z=0}^{z=\eta(t)} \alpha dz \right] \\ & = \int_{z=0}^{z=\eta(t)} f_{qi} dz + m_t(z, t)_{z=0} (H_{\ell}-H_v)(1-x) \end{aligned}$$

or,

$$\begin{aligned} & \rho_{\ell}(H_v-H_{\ell})A_t \left[\frac{d}{dt} \eta(t) - \frac{d}{dt} \int_{z=0}^{z=\eta(t)} \alpha dz \right] + \int_{z=0}^{z=\eta(t)} f_{qi} dz \\ & = m_t(z, t)_{z=0} (H_v-H_{\ell})(1-x) \end{aligned} \quad (4.9)$$

Assuming that the mean void fraction:

$$\bar{\alpha} = \frac{1}{\eta(t)} \int_{z=0}^{z=\eta(t)} \alpha dz$$

$$\begin{aligned} \therefore & \rho_{\ell}(H_v-H_{\ell})A_t \left[\frac{d}{dt} \eta(t) - \frac{d}{dt} \{ \bar{\alpha} \eta(t) \} \right] + f_{qi} \eta(t) \\ & = (H_v-H_{\ell})(1-x) m_t(z, t)_{z=0} \end{aligned}$$

$$\rho_{\ell} A_t (H_v-H_{\ell}) \left[\frac{d}{dt} \eta(t) (1-\bar{\alpha}) \right] + f_{qi} \eta(t) = (H_v-H_{\ell})(1-x) m_t(z, t)_{z=0} \quad (4.10)$$

Divide (4.10) by $\rho_{\ell} A_t (H_v-H_{\ell})(1-\bar{\alpha})$:

$$\therefore \frac{d}{dt} \eta(t) + \frac{f_{qi}}{\rho_{\ell} A_t (H_v - H_{\ell}) (1-\bar{\alpha})} \eta(t) = \frac{(1-x)}{\rho_{\ell} (1-\bar{\alpha}) A_t} m_t(z, t)_{z=0} \quad (4.11)$$

Calculation of $m_t(z, t)_{z=0}$:

The assumed harmonic wave is:

$$\phi = C1 \sin n Z1$$

where: $n = 2\pi/\lambda$

$$Z1 = z - ct$$

Now, by shifting the axis to Z and Y as shown in Figure (4.3a), the wave equation becomes:

$$\phi = C1 \sin \frac{2\pi}{\lambda} (z - \frac{\lambda}{4}) + C1$$

Or,

$$\phi = -C1 \cos (\frac{2\pi}{\lambda} z) + C1 \quad (4.12)$$

where:

$$\phi = \frac{\delta - \delta_c}{\delta_c} \quad (\text{Figure 4.3b})$$

$$\therefore \frac{\delta - \delta_c}{\delta_c} = -C1 \cos (\frac{2\pi}{\lambda} z) + C1 \quad (4.13)$$

$$\begin{aligned} \delta_r = \delta - \delta_c &= -\delta_c C1 \cos(\frac{2\pi}{\lambda} z) + \delta_c C1 \\ &= -\overset{*}{A} \cos(\frac{2\pi}{\lambda} z) + \overset{*}{A} \end{aligned}$$

where $Z = Ct$ and $\overset{*}{A} = \delta_c C1$.

$$\therefore \delta_r = -\overset{*}{A} \cos (\frac{2\pi}{\lambda} ct) + \overset{*}{A} \quad (4.14)$$

From Figure (4.3c) we have:

$$\begin{aligned} A_2 &= \pi(R - \delta_c)^2 - \pi(R - \delta_c - \delta_r)^2 \\ &= -\pi\delta_r^2 + 2\pi\delta_r(R - \delta_c) \end{aligned} \quad (4.15)$$

Excess rate of flow due to the presence of the wave $\dot{m}_2 = \rho_\ell CA_2$:

$$= \rho_\ell C \left[-\pi\delta_r^2 + 2\pi\delta_r(R - \delta_c) \right] \quad (4.16)$$

Therefore the total rate of flow = $\dot{m}_1 + \dot{m}_2$:

$$= \dot{m}_t = \dot{m}_1 + \rho_\ell C \left[-\pi\delta_r^2 + 2\pi\delta_r(R - \delta_c) \right]$$

But:

$$\delta_r^2 = \left[\overset{*}{A} - \overset{*}{A} \cos\left(2\frac{\pi ct}{\lambda}\right) \right]^2 = \overset{*}{A}^2 \cos^2 \frac{2\pi ct}{\lambda} + \overset{*}{A}^2 - 2\overset{*}{A}^2 \cos \frac{2\pi ct}{\lambda}$$

$$\begin{aligned} \therefore \dot{m}_t &= \dot{m}_1 + \rho_\ell C \left[2\pi(R - \delta_c) \left(-\overset{*}{A} \cos \frac{2\pi ct}{\lambda} + \overset{*}{A} \right) - \pi \left(\overset{*}{A}^2 \cos^2 \frac{2\pi ct}{\lambda} + \overset{*}{A}^2 \right. \right. \\ &\quad \left. \left. - 2\overset{*}{A}^2 \cos \frac{2\pi ct}{\lambda} \right) \right] \end{aligned} \quad (4.17)$$

$$\text{Let } S = \frac{f_{qi}}{\rho_\ell (1-\alpha) A_t (H_v - H_\ell)}, \quad B = \frac{(1-x)}{\rho_\ell (1-\alpha) A_t}, \quad \hat{P} = \dot{m}_1 \quad) \quad (4.18)$$

$$\hat{Z} = 2\pi\rho_\ell CA(R - \delta_c), \quad \text{and } \hat{Y} = \pi\rho_\ell CA^2 \quad)$$

$$\therefore \dot{m}_t = \hat{P} + \hat{Z} \left(-\cos \frac{2\pi ct}{\lambda} + 1 \right) - \hat{Y} \left(\cos^2 \frac{2\pi ct}{\lambda} + 1 - 2\cos \frac{2\pi ct}{\lambda} \right) \quad (4.19)$$

Substituting in equation (4.11):

$$\frac{d\eta}{dt} + S\eta = B \left[\hat{P} + \hat{Z} \left(-\cos \frac{2\pi ct}{\lambda} + 1 \right) - \hat{Y} \left(\cos^2 \frac{2\pi ct}{\lambda} + 1 - 2\cos \frac{2\pi ct}{\lambda} \right) \right] \quad (4.20)$$

($\eta(t)$ is written as η for simplicity.)

If the film is free of surface waves and the triple-phase front is stationary, then:

$$d\eta/dt = 0 \quad (4.21)$$

From equations (4.11), (4.19) and (4.22):

$$\hat{z}_i = \eta_o = \hat{B}P/S \quad (4.22)$$

which is the initial boundary condition at $t = 0$. Equation (4.20) is solved by third order Runge-Kutta method* in order to obtain the relation between the interface triple point position and time per one wave period and the average rewetting speed for different values of surface heat flux (F_{qa}), mass velocity (G'_a), subcooling (ΔH) and dimensionless wave amplitude (Cl).

4.4 NUMERICAL SOLUTION

It is recognised that equation (4.20) can be solved analytically. However, we have chosen to apply Runge-Kutta, so as to take advantage of the available computer facility in processing and plotting extensive results in a rather convenient

* Third order Runge-Kutta method:

$$y_{n+1} = y_n + \frac{h}{6}(f_o + 4f_1 + f_2)$$

where

$$f_o = f(x_n, y_n)$$

$$f_1 = f(x_n + h/2, y_n + hf_o/2)$$

$$f_2 = f(x_n + h, y_n + 2hf_1 - hf_o)$$

way, and also to establish this method for further developments of the present theory. The relation between the triple-phase front position during the time of two wave periods and the average rewetting speed for different values of surface heat-flux, mass velocity and dimensionless wave amplitude and sub-cooling has been found, as follows:

(i) Select an existing water burn-out data for a uniformly heated round tube (i.e. F_{qa} , G_a , ΔH , L and D).

(ii) The surface tension is calculated from the following equation (Reid and Sherwood (1966)):

$$\sigma = 2.204 \times 10^{-3} P_c^{2/3} T_c^{1/3} (0.133\alpha_c - 0.281)(1 - T_r)^{11/9} \quad (4.23)$$

where: P_c = critical pressure of the fluid substance (atmosphere).

T_c = critical temperature of the fluid substance ($^{\circ}K$)

α_c = Riede factor (dimensionless).

$T_r = T/T_c$.

(iii) The film thickness δ_c which is the minimum undisturbed film thickness (a smooth film free from waves) is calculated from the equation derived by Zuber and Staub (1966) for minimum film thickness with heat transfer:

$$\frac{\rho_l}{15} \left[\frac{g(\rho_v - \rho_l)}{\rho_l \cdot v_l} \right]^2 \delta_c^4 = \frac{\sigma(1 - \cos\theta_c)}{\delta_c} + \frac{d\sigma}{dT} \cdot \frac{F_{qa}}{K_l} \cos\theta + \rho_v \left[\frac{F_{qa}}{\rho_v (H_v - H_l)} \right]^2 \frac{\rho_v - \rho_l}{\rho_l} \cos^2\theta \quad (4.24)$$

Equation (4.23) is used to calculate the thermocapillary term in equation (4.24). However, it should be mentioned here that the minimum film thickness δ_c when calculated applying Hartley and Murgatroyd (1964) equation for isothermal flow shows that it has a lower value than that obtained from equation (4.24).

- (iv) The contact angle is calculated from the equation given by Newman and Searle (1951):

$$\cos\theta = 1 - \frac{\delta_c^2 g \rho_l}{2g_o \sigma}$$

- (v) The mean void fraction is calculated from the equation given by Smith (1971):

$$\bar{\alpha} = \left\{ 1 + \frac{0.4\rho_v}{\rho_l} \left(\frac{1}{x} - 1\right) + \frac{0.6\rho_v}{\rho_l} \left(\frac{1}{x} - 1\right) \left[\frac{\frac{\rho_l}{\rho_v} + 0.4\left(\frac{1}{x} - 1\right)}{1 + 0.4\left(\frac{1}{x} - 1\right)} \right]^{\frac{1}{2}} \right\}^{-1}$$

The calculated $\bar{\alpha}$ is in agreement with values found by Levy (1960) and Fujie (1964).

- (vi) The relation between flow quality X, surface heat-flux F_{qa} , the mass velocity \dot{G}_a and subcooling ΔH is given by Stevens and Macbeth (1971) as:

$$X = \frac{4L}{D} \cdot \frac{F_{qa}}{G_a \cdot H_{fg}} - \frac{\Delta H}{H_{fg}}$$

(vii) The wave length (λ) and the dimensionless wave celerity (α) are calculated from equations (3.26) and (3.24), i.e.

$$\lambda = 2\pi \delta_o \sqrt{\frac{1}{N_{We}(\alpha^2 - \frac{12}{5}\alpha + \frac{6}{5})}}$$

$$N_{We} = \frac{6 \left[3 - \alpha + \frac{1}{30} \frac{N_{Re}}{N_{Fr}^2} \Phi \right]}{(7\alpha - 9)(\alpha^2 - \frac{12}{5}\alpha + \frac{6}{5})} \quad (\text{see Appendix 3b})$$

(viii) Equation (4.20) can now be solved to obtain the relation between the triple-phase front position during the time of two periods and the average rewetting speed for the given burn-out data.

(ix) The simulation dimensionless groups given by Ahmad (1971) are used to predict the Freon burn-out data which corresponds to the selected water burn-out data. These dimensionless groups (which should be the same for both water and Freon-12) are (see Chapter 2):

$$\pi_1 = \frac{F_{qa}}{G_a \cdot H_{fg}} \quad (\text{I})$$

$$\psi_{CHF} = \frac{G_a \cdot D}{\mu_\ell} \cdot \left(\frac{\gamma^{1/2} \cdot \mu_\ell}{D \cdot \rho_\ell^{1/2}} \right)^{n_1} \cdot \left(\frac{\mu_\ell}{\mu_v} \right)^{n_2} \quad (\text{II})$$

$$\pi_5 = \frac{\Delta H}{H_{fg}} \quad (\text{III}) \quad (4.25)$$

$$\pi_6 = \frac{\rho_l}{\rho_v} \quad (IV)$$

$$\pi_7 = \frac{L}{D} \quad (V) \quad (4.25)$$

where the relation between π_5 and the measures of distortion n_1 and n_2 are found applying the distortion method described in Chapter 2.

We start by assuming that $D_{\text{Freon-12}} = D_{\text{water}}$; knowing π_7 from existing water burn-out data L_{Freon} can be deduced (equation 4.25-V). The Freon system pressure is deduced from equation (4.25-IV) and hence the Freon subcooling is found from equation (4.25-III). Knowing π_1 and ψ_{CHF} for water, the surface heat flux and the mass velocity of Freon are found from equation (4.25-I) and (4.25-II) respectively.

(x) Repeating steps (ii) to (viii) with the new Freon burn-out data, step (ix) can be determined for the calculated Freon data.

(xi) The effect of increasing or decreasing the surface heat flux F_{qa} , mass velocity G_a , subcooling ΔH and the dimensionless wave amplitude Cl on the average dimensionless rewetting speed can be obtained by increasing or decreasing the value of one of the parameters while keeping the other three parameters constant

and repeating steps (ii) to (x).

A computer programme (SIMGI) is developed (see page 10) to obtain the relation between the triple-phase front speed and the four parameters (F_{qa} , G_a , ΔH and Cl).

Results on water burn-out in uniformly heated round tubes as reported by Thompson and Macbeth (1964) are used in the calculations. Although we applied the results at different runs, nevertheless the results of one run are reported here as demonstrative example of the application of the present theory, as follows:

| <u>Run No. 679.03</u> | | <u>Thompson et al (1964)</u> | |
|---|----------------------|------------------------------|--|
| <u>Substance</u> | <u>Water</u> | | |
| Pressure | 1000 psia | | |
| Temperature | 545 | $^{\circ}F$ | |
| Surface Heat Flux | 0.6069×10^6 | Btu/hr.ft ² | |
| Mass Velocity | 0.7400×10^6 | lb/hr.ft ² | |
| Subcooling | 72.8 | Btu/lb. | |
| Diameter | 0.038 | ft. | |
| Length | 5.667 | ft. | |
| <hr/> | | | |
| <u>Physical property data for water at 1000 lb/in² (Andersen et al</u> | | | |
| <u>Data are also collected from Technical Bulletin (DUPONT) C-30 (1969)):</u> | | | |
| Liquid Density | 46.3 | lb/ft ³ | |
| Vapour Density | 2.244 | lb/ft ³ | |
| Liquid Viscosity | 0.227 | lb/hr.ft. | |

| | | |
|---|----------|-------------------------|
| Vapour Viscosity | 0.0464 | lb/hr.ft. |
| Liquid thermal conductivity | 0.3272 | Btu/hr.ft. °F |
| Vapour thermal conductivity | 0.0365 | Btu/hr.ft. °F |
| Liquid specific heat | 1.295 | Btu/lb. °F |
| Vapour specific heat | 1.178 | Btu/lb. °F |
| Latent heat | 649.4 | Btu/lb. |
| Surface tension | 0.0395 | lb/sec ² . |
| $\Upsilon = (-d(\rho_l / \rho_v) / dP)$ | 0.02695 | in ² /lb. |
| $\beta = (dT/dP)$ | 0.1215 | °F.in ² /lb. |
| Coefficient of expansion | 0.000416 | 1/°R |

4.5 RESULTS AND DISCUSSION

4.5.1 Triple-phase front motion for Water and Freon

The main parameters considered in the present work which are thought to affect the motion of the triple-phase front are the mass velocity, the dimensionless wave amplitude, the surface heat-flux and the subcooling. The values of F_{qa} , G'_a and ΔH for burn-out conditions as reported by Thompson et al (1964) are taken, and Cl value is assumed. To demonstrate the effect of these four parameters, three are kept constant while different values are allocated to the fourth. As, for example, take the case where $F_{qa} = 0.6069 \times 10^6$ Btu/hr.ft², $G'_a = 0.740 \times 10^6$ lb/hr.ft², and $\Delta H = 72.8$ Btu/lb from run (679.03), Thompson et al (1964), assuming Cl = 0.4. Then

seven different surface heat flux values for water at 1000 lb/in² are considered and fed to the programme (SIMGI).

Further, this programme predicts the corresponding simulating Freon-12 surface heat flux values at pressure 155 lb/in² applying the simulation technique as mentioned previously in Section 4.5, part (ix) (see Table 4.1a).

TABLE 4.1a

| Values | Water Surface Heat Flux (BTU/hr.ft ²) | Corresponding Freon-12 Surface Heat Flux (BTU/hr.ft ²) |
|--------|---|--|
| 1 | 0.519 x 10 ⁶ | 0.284 x 10 ⁵ |
| 2 | 0.557 x 10 ⁶ | 0.304 x 10 ⁵ |
| 3 | 0.607 x 10 ⁶ | 0.331 x 10 ⁵ |
| 4 | 0.657 x 10 ⁶ | 0.359 x 10 ⁵ |
| 5 | 0.699 x 10 ⁶ | 0.383 x 10 ⁵ |
| 6 | 0.707 x 10 ⁶ | 0.386 x 10 ⁵ |
| 7 | 0.757 x 10 ⁶ | 0.413 x 10 ⁵ |

The results are shown in Figures (4.4a) and (4.5a), where the triple-phase front position is plotted versus the time of two successive wave periods. It can be seen from Figures (4.4a) and (4.5a) that the triple-phase front moves either forward or backward depending on the surface heat flux.

When the surface heat flux is relatively high, the triple-phase front moves backward initially at higher speed, then it slows down and then afterwards the motion accelerates

again. When the surface heat flux is relatively small, the forward movement of the triple-phase front is such that it starts with slower speed, then accelerates and then it decelerates. This phenomenon could be explained by considering the mass of fluid fed to the triple-phase front region by the incoming harmonic liquid waves. It is shown also that an increase in surface heat flux results in a decrease in the wave period. The forward displacement of the liquid front after two waves increases with the decrease of surface heat flux while the reverse occurs when the motion is backward. It is obvious that at a particular value of surface heat flux the triple front oscillates around its original position (curve (5) in Figures (4.4a) and (4.5a)).

Figures (4.4b) and (4.5b) show the position of the triple-phase front during the motion of two waves this time; the mass velocity G_a' is considered for water at pressure 1000 lb/in^2 and seven different values are taken maintaining the other three parameters constant and the corresponding simulating Freon-12 values at pressure 155 lb/in^2 calculated applying the simulation technique described in Section (4.5), part (ix), given in Table (4.1b).

An increase in G_a' results in an increase in the distance moved by the triple-phase front during a wave period

TABLE 4.1b

| Values | Water Mass Velocity (lb/hr.ft ²) | Corresponding Freon-12 Mass Velocity (lb/hr.ft ²) |
|--------|---|--|
| 1 | 0.574 x 10 ⁶ | 0.367 x 10 ⁶ |
| 2 | 0.605 x 10 ⁶ | 0.387 x 10 ⁶ |
| 3 | 0.628 x 10 ⁶ | 0.401 x 10 ⁶ |
| 4 | 0.646 x 10 ⁶ | 0.414 x 10 ⁶ |
| 5 | 0.688 x 10 ⁶ | 0.440 x 10 ⁶ |
| 6 | 0.730 x 10 ⁶ | 0.467 x 10 ⁶ |
| 7 | 0.711 x 10 ⁶ | 0.493 x 10 ⁶ |

and results in a decrease in the wave period, until a value of G_a is reached at which the triple-phase front oscillates about its original position (curve (3), Figures (4.4b) and (4.5b)). A further increase in the mass velocity results in rewetting the dry area. Also as expected, when keeping F_{qa} , ΔH and Cl constant, it is found that the triple-phase front moves backwards at relatively low mass velocities.

Figures (4.6a) and (4.7a) show the relation between the triple-phase front position and the period of wave travel at different subcooling values; for water at pressure 1000 lb/in² and the corresponding simulated Freon-12 subcooling values at 155 lb/in² are shown in Table (4.1c).

The trend is that the maximum travel of the triple-phase front is proportional to the subcooling. The shape of

TABLE 4.1c

| Values | Water Subcooling Values Btu/lb. | Corresponding Freon-12 Subcooling Values Btu/lb. |
|--------|------------------------------------|---|
| 1 | 0.0 | 0.0 |
| 2 | 24.8 | 2.12 |
| 3 | 36.8 | 3.14 |
| 4 | 52.8 | 4.50 |
| 5 | 68.8 | 5.87 |
| 6 | 84.8 | 7.24 |
| 7 | 100.8 | 8.60 |

the curves is typical of the results of the present study, insofar as motion is slower at the start and end of the wave period when the net motion is forward, except for the case at high subcooling values. At lower subcooling the triple-phase front starts with backward motion and then advances afterwards.

Figures (4.6b) and (4.7b) show the position of the triple-phase front during the motion of two waves this time, the dimensionless wave amplitude C_1 is considered and seven different values are taken for water and the simulating Freon-12 at pressure 1000 psia and 155 psia respectively;

1. $C_1 = 0.04$
2. $C_1 = 0.13$
3. $C_1 = 0.25$

4. $C1 = 0.37$
5. $C1 = 0.49$
6. $C1 = 0.61$
7. $C1 = 0.64$

From Figures (4.6b) and (4.7b) it is obvious that the change of the dimensionless wave amplitude does not affect the time needed for the triple-phase front to go to its outermost position, but significantly affects the distance moved by the triple front during the period of one wave. As $C1$ increases the maximum distance moved by the triple-phase front increases. The motion of the triple front is slower at both the beginning and near the end.

Figures (4.8a) and (4.8b) show the relation between the rewetting average velocity per wave period and the four parameters, i.e. F_{qa} , G_a , ΔH and $C1$, for 1000 psia and 155 psia respectively. From these figures the rewetting average velocity per wave period increases with the increase of $C1$ or G_a or ΔH and decreases with the increase of F_{qa} . F_{qa} and G_a have a greater effect on the rewetting average velocity than the effect of both ΔH and $C1$.

By increasing the range of the four parameters, F_{qa} , G_a , ΔH and $C1$, it was found that the relation of the

rewetting average speed with F_{qa} , ΔH and Cl remains linear while for G'_a it is only linear at the higher mass velocities. Figure (4.9) shows the relation between the rewetting average velocity and the mass velocity for water and the simulating Freon-12.

4.5.2 Errors in the simulation of the triple-phase front speed

Now, to assess the accuracy of the simulating Freon triple-phase front velocity, and to find the simulation percentage R.M.S. error and the standard deviation with the intention of further developing the above-mentioned method, the following procedure is followed:

The dimensionless triple-phase front speeds:

$$SP = \frac{\eta_m / t_p}{w_o}$$

where: η_m = distance travelled by the triple-phase front at the end of each period

t_p = time of one period

w_o = mean film velocity

are calculated for water, and the corresponding Freon values for run 679.03 (Thompson et al (1964), Table (4.1)) for the conditions stated in Table (4.2). The results of the calculations are plotted in Figures (4.10a, b, c and d) and also shown in Table (4.2).

TABLE 4.2

| Dimensionless Group | Parameter under test in this group | Simulation % R.M.S. Error |
|--|---|---------------------------|
| $\pi_1 = \frac{F_{qa}}{G_a \times H_{fg}}$ | Surface heat flux F_{qa} For water: $0.171 \times 10^6 \leq F_{qa} \leq 0.699 \times 10^6$ For Freon-12: $0.933 \times 10^4 \leq F_{qa} \leq 0.383 \times 10^5$ | 32.5 |
| $\psi_{CHF} = \frac{G_a \cdot D \cdot \gamma^{\frac{1}{2}} \cdot \mu_l}{\mu_l \cdot D \cdot \rho_l^{\frac{1}{2}}} \cdot (\mu_l / \mu_v)^{n_1}$ | Mass Velocity G_a For water: $0.52 \times 10^6 \leq G_a \leq 0.252 \times 10^7$ For Freon-12: $0.333 \times 10^6 \leq G_a \leq 0.161 \times 10^7$ | 35.3 |
| $\pi_5 = \frac{\Delta H}{H_{fg}}$ | Subcooling ΔH For water: $24.8 \leq \Delta H \leq 108.8$ For Freon-12: $2.12 \leq \Delta H \leq 8.6$ | 35.0 |
| C1 | Dimensionless wave amplitude C1 For water and Freon-12 $0.4 \leq C1 \leq 0.64$ | 32.1 |

It can be seen that the % R.M.S. error is between 32.5 and 35%.

Data of other runs of Thompson et al (1964) experiments were also used and in all cases the R.M.S. error

was around 35%. We have chosen two runs from Thompson et al (1964), i.e.

| <u>Run 218.03</u> | | <u>Run 352.03</u> | |
|-------------------|-----------------------------------|-------------------|-----------------------------------|
| F_{qa} | = 464000.0 Btu/hr.ft ² | F_{qa} | = 516500.0 Btu/hr.ft ² |
| G_a | = 1400000.0 lb/hr.ft ² | G_a | = 870000.0 lb/gr.ft ² |
| ΔH | = 68.1 Btu/lb. | ΔH | = 78.6 Btu/lb. |
| D | = 0.22 in. | D | = 0.368 in. |
| L | = 68.0 in. | L | = 79.0 in. |

and the results of the calculations are shown in Figures (4.11) and (4.12) respectively.

It must be noted that throughout the calculations a unity diameter ratio (i.e. D_{Freon}/D_{water}) has been considered. The percentage R.M.S. error as found above is too high to be acceptable. Therefore it is thought to either undertake improvements to the method presented or to investigate the effect of the diameter ratio (D_{Freon}/D_{water}).

In order to test the effect of the diameter ratio on the simulation percentage R.M.S. error when changing one of the four parameter (i.e. F_{qa} , G_a , ΔH or Cl) while the other three are kept constant, different burn-out data taken from Thompson et al (1964) were tested for diameter ratios $1.5 \geq \frac{D_{Freon}}{D_{water}} \geq 0.55$. The results are shown in Figures (4.13) and (4.14) for runs 679.03 and 218.03, Thompson et al (1964), where the diameter ratio is plotted versus percentage R.M.S.

error and standard deviation. The condition at which the calculations were made are tabulated in Table (4.3).

TABLE 4.3

| Run Number 679.03 | | | | |
|-------------------|-------------------------------|------------------------|----------------------------|---|
| Figure | Parameter under investigation | Minimum % R.M.S. Error | Minimum Standard Deviation | Diameter Ratio for minimum % RMS & St. Dev. |
| 4.13a | F_{qa} (in π_1) | 1.46 | 0.11×10^{-2} | 0.68 |
| 4.13b | G_a (in ψ_{CHF}) | 4.22 | 0.07×10^{-2} | 0.69 |
| 4.13c | ΔH (in π_5) | 7.50 | 1.10×10^{-2} | 0.67 |
| 4.13d | Cl | 0.75 | 0.14×10^{-2} | 0.68 |
| Run Number 218.03 | | | | |
| Figure | Parameter under investigation | Minimum % R.M.S. Error | Minimum Standard Deviation | Diameter Ratio for minimum % RMS & St. Dev. |
| 4.14a | F_{qa} (in π_1) | 1.085 | 0.48×10^{-2} | 0.69 |
| 4.14b | G_a (in ψ_{CHF}) | 1.11 | 0.42×10^{-2} | 0.68 |
| 4.14c | ΔH (in π_5) | 6.94 | 2.54×10^{-2} | 0.67 |
| 4.14d | Cl | 0.05 | 0.02×10^{-2} | 0.68 |

Examination of the Figures (4.13) and (4.14) showed that for all tested cases the curves showed the same trend. Starting from a diameter ratio equal to 0.55, the percentage R.M.S. error decreases with the increase of the diameter ratio to a minimum at diameter ratio ≈ 0.68 and then the error increases rapidly with further increase in the diameter ratio.

From the results obtained it can be said that for the simulation of the water triple-phase front movement by the use of Freon with minimum % R.M.S. error, the diameter ratio $D_{\text{Freon}}/D_{\text{water}}$ must be equal to 0.68. The minimum percentage R.M.S. error is achieved by the variation of Cl maintaining F_{qa} , G_a and ΔH constant.

The dimensionless triple front speed for Freon-12 and water is plotted versus the dimensionless simulating groups of equation (4.25) (ψ_{CHF} , π_1 and π_5) and the dimensionless wave amplitude Cl, at diameter ratio 0.68, Figure (4.15), which shows that applying the simulation technique at diameter ratio 0.68 resulted in obtaining an accurate simulation.

As a further study of the dimensionless groups which are amended by distortion factors, so as to simulate the triple-phase front speed for water by Freon, the dimensionless groups developed in Chapter 2 for an annular flow model are used. These groups are:

$$\begin{aligned}\pi_1 &= \frac{F_{qa}}{H_{fg} \cdot \rho_l \cdot w_i} \\ \psi_{\text{CHF}} &= \frac{K_l}{D \cdot C_{pl} \cdot \rho_v \cdot w_i} \cdot \left(\frac{\gamma^{1/2} \cdot \mu_l}{D \cdot \rho_l^{1/2}} \right)^{n_1} \cdot \left(\frac{\mu_l}{\mu_v} \right)^{n_2} \\ \pi_5 &= \frac{\Delta H}{H_{fg}} \\ \pi_6 &= \frac{\rho_l}{\rho_v} \\ \pi_7 &= L/D\end{aligned}$$

Figure (4.16) shows the dimensionless triple-phase front speed for water and the simulating Freon-12 plotted versus the above annular flow model dimensionless groups π_1 , ψ_{CHF} and π_5 , and the dimensionless wave amplitude Cl at diameter ratio $D_{Freon}/D_{water} = 1$ for run 679.03, Thompson et al (1964). This resulted in a simulation error of 32% (Table (4.4)). The resulting simulation errors did not change considerably from those obtained by applying the earlier dimensionless groups of equation (4.25) at the same diameter ratio. Also, it has been noticed that by changing the diameter ratio D_{Freon}/D_{water} for all tested cases starting from a ratio of 0.55 the percentage R.M.S. error decreased. The percentage R.M.S. error reached a minimum at diameter ratio of about 0.68. Further increase in the diameter ratio resulted in an increase in the percentage R.M.S. error which is similar to the earlier case when the dimensionless groups of equation (4.25) were used.

Figure (4.17) shows the relation between the dimensionless triple-phase front speed and the annular dimensionless groups π_1 , ψ_{CHF} , π_5 and the dimensionless amplitude Cl at diameter ratio $D_{Freon}/D_{water} = 0.68$. From this figure it is clear that accurate simulations are obtained at diameter ratio equal to 0.68. The percentage R.M.S. error

obtained for each of the dimensionless groups (i.e. π_1 , ψ_{CHF} , π_5 and Cl) at diameter ratio 0.68 are given in Table (4.4).

It can be concluded that the minimum simulation error is achieved when simulating the triple-phase front speed using the method described in this chapter at a diameter ratio of 0.68.

In the following chapter, further improvements are applied to the model described in this chapter to reduce the simulation errors.

TABLE 4.4

| Figure | Parameter under investigation | % R.M.S. Error | Standard Deviation | Diameter Ratio |
|--------|-------------------------------|----------------|--------------------|----------------|
| 4.16a | F_{qa} | 32.03 | 0.195 | 1 |
| 4.16b | G'_a | 34.00 | 0.159 | 1 |
| 4.16c | ΔH | 34.90 | 0.060 | 1 |
| 4.16d | Cl | 31.70 | 0.058 | 1 |
| 4.17a | F_{qa} | 2.12 | 0.0035 | 0.68 |
| 4.17b | G'_a | 7.87 | 0.0029 | 0.68 |
| 4.17c | ΔH | 9.24 | 0.0111 | 0.68 |
| 4.17d | Cl | 0.40 | 0.0007 | 0.68 |

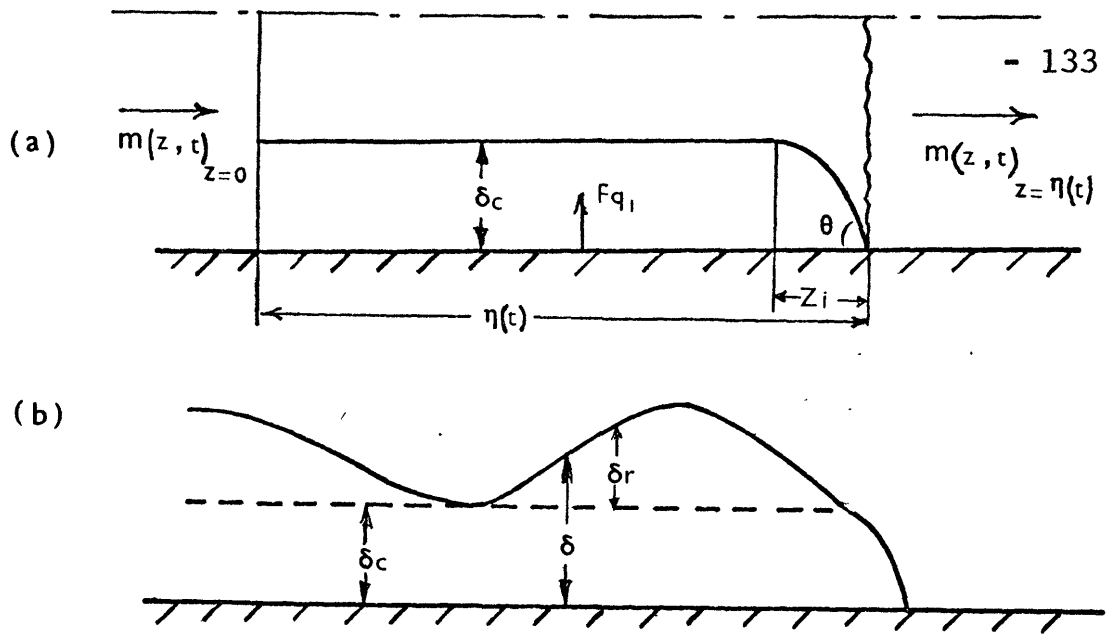
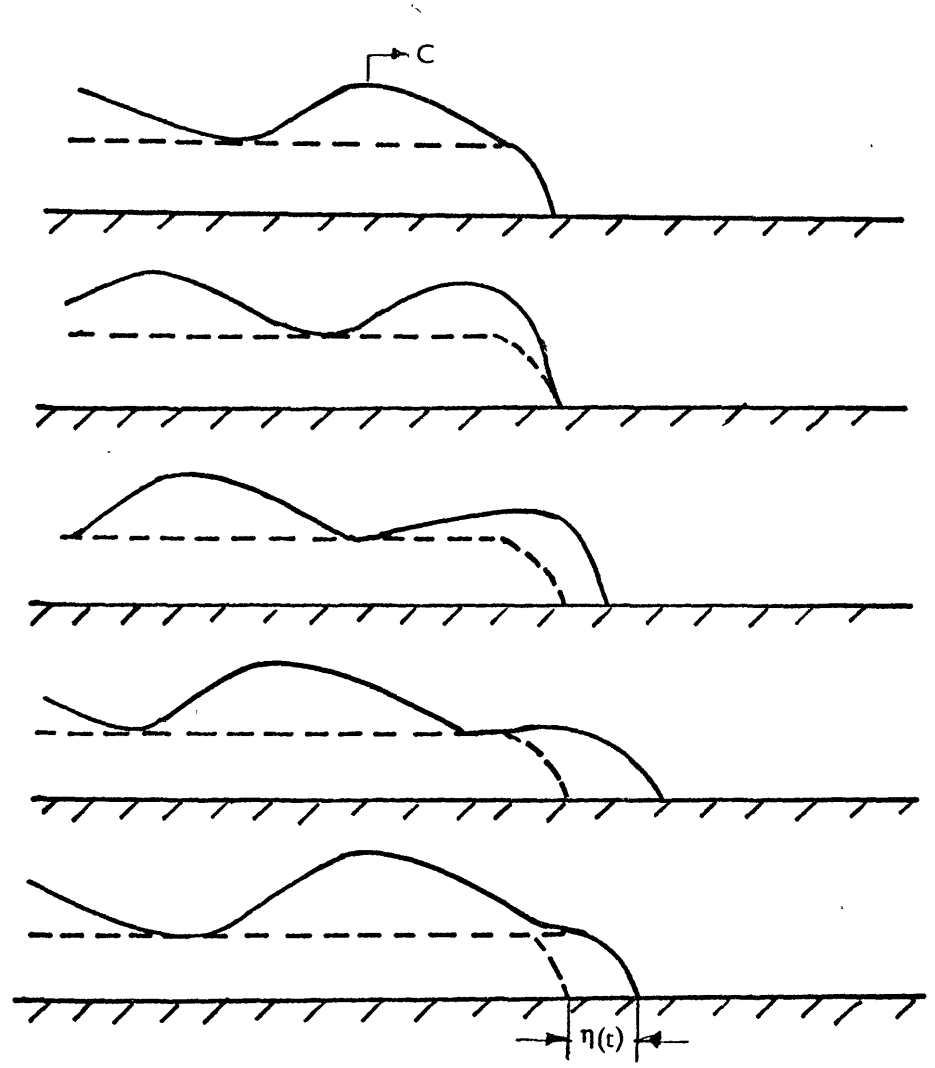


FIG (4.1)



Schematic Motion of Triple-phase Front
During One Wave Period

FIG (4.2)

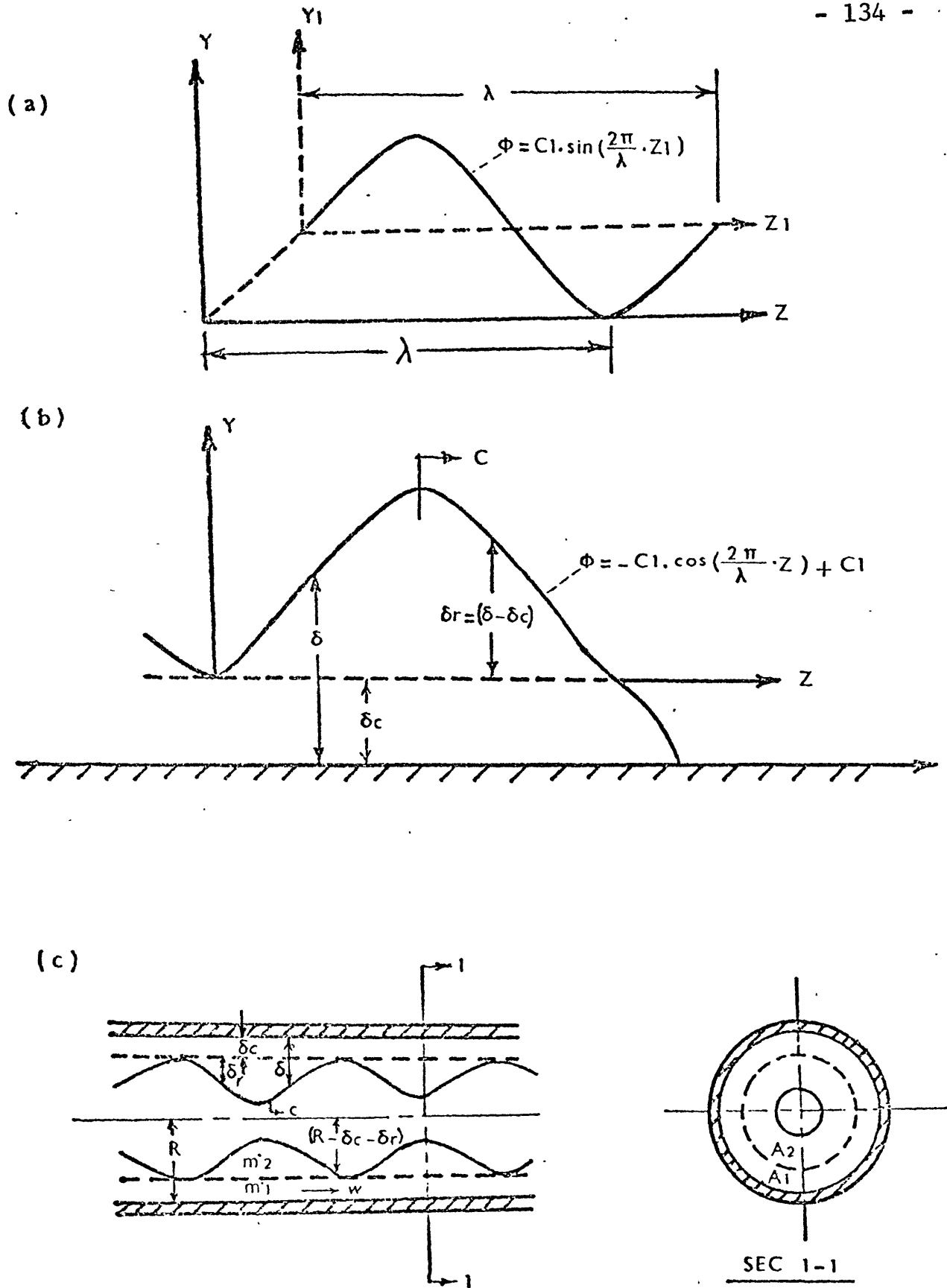


FIG. (4-3)

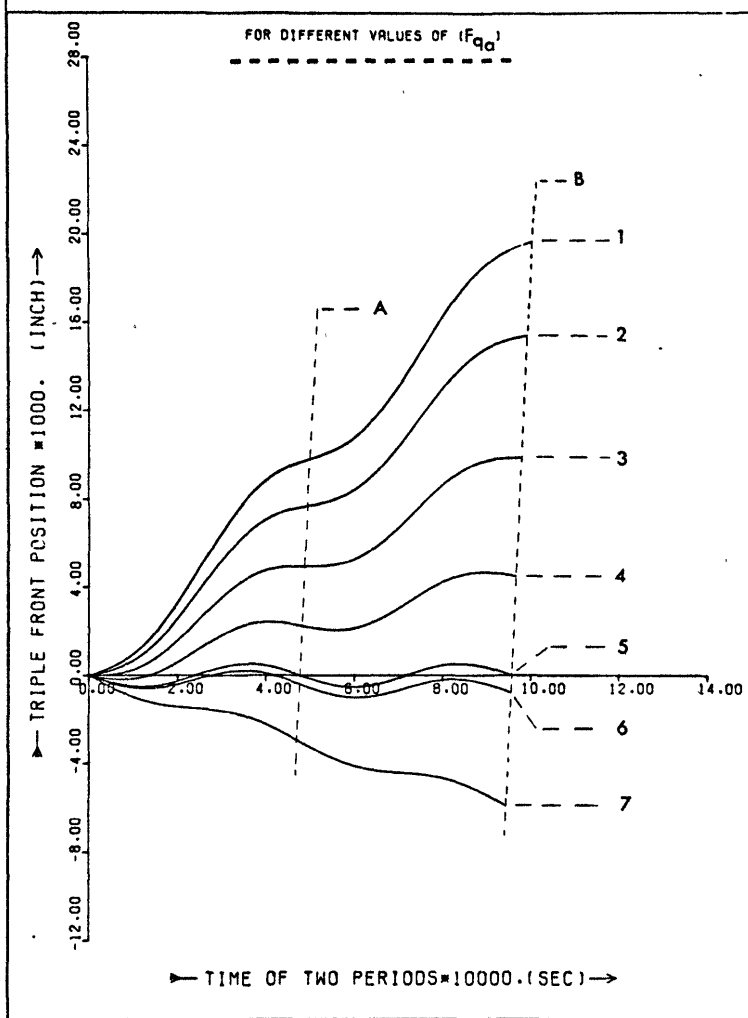
Figure (4.4a): Interface triple phase front position during two waves for different values of F_{qa} . Water at pressure = 1000 lb/in². Constant parameters: $G_a = 0.740 \times 10^6$ lb/h.ft²; $\Delta H = 72.8$ Btu/lb.; Cl = 0.4. Contour line of: A) one wave period, B) two wave periods.

| | | | | |
|----|----------|---|---------------------|-----------------------|
| 1. | F_{qa} | = | 0.519×10^6 | Btu/h.ft ² |
| 2. | F_{qa} | = | 0.557×10^6 | Btu/h.ft ² |
| 3. | F_{qa} | = | 0.607×10^6 | Btu/h.ft ² |
| 4. | F_{qa} | = | 0.657×10^6 | Btu/h.ft ² |
| 5. | F_{qa} | = | 0.669×10^6 | Btu/h.ft ² |
| 6. | F_{qa} | = | 0.707×10^6 | Btu/h.ft ² |
| 7. | F_{qa} | = | 0.757×10^6 | Btu/h.ft ² |

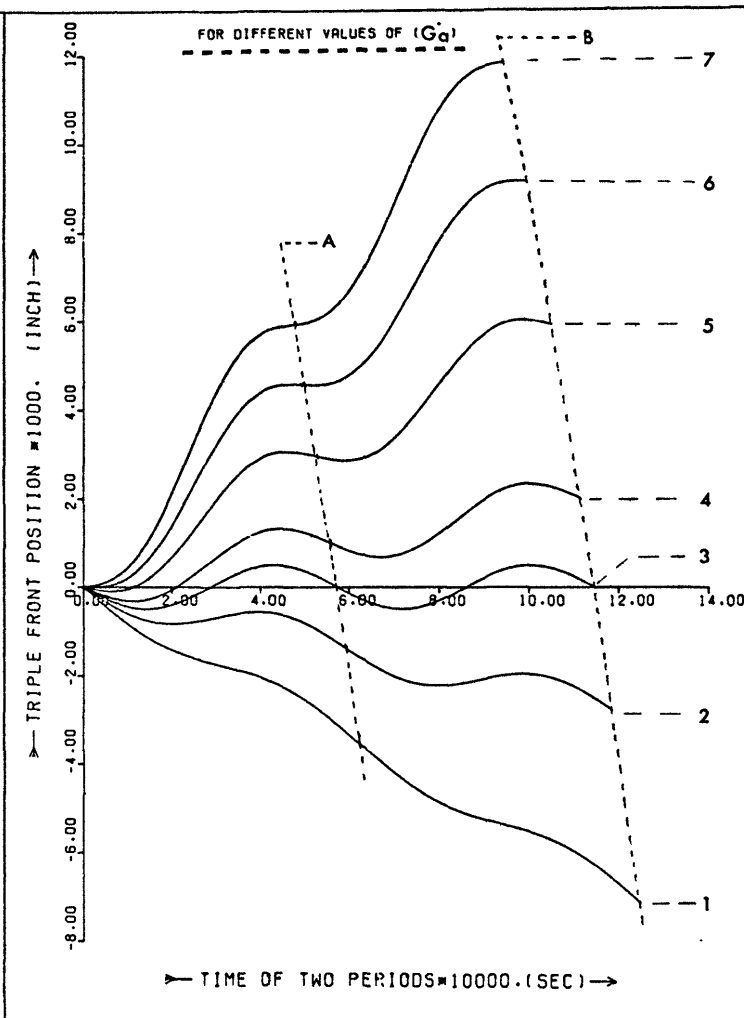
Figure (4.4b): Interface triple front position during two waves for different values of G_a . Water at pressure = 1000 lb/in². Constant parameters: $F_{qa} = 0.6069 \times 10^6$ Btu/h.ft²; $\Delta H = 72.8$ Btu/lb.; Cl = 0.4. Contour line of: A) one wave period, B) two wave periods.

| | | | | |
|----|-------|---|---------------------|----------------------|
| 1. | G_a | = | 0.574×10^6 | lb/h.ft ² |
| 2. | G_a | = | 0.605×10^6 | lb/h.ft ² |
| 3. | G_a | = | 0.628×10^6 | lb/h.ft ² |
| 4. | G_a | = | 0.646×10^6 | lb/h.ft ² |
| 5. | G_a | = | 0.688×10^6 | lb/h.ft ² |
| 6. | G_a | = | 0.730×10^6 | lb/h.ft ² |
| 7. | G_a | = | 0.771×10^6 | lb/h.ft ² |

 INTERFACE TRIPLE FRONT POSITION DURING TWO WAVES



FIG(4-4a)



FIG(4-4b)

Figure (4.5a): Interface triple front position during two successive waves for different values of F_{qa} . Freon-12 at pressure = 155 lb/in². Constant parameters: $G_a = 0.473 \times 10^6$ lb/h.ft².; $\Delta H = 6.21$ Btu/lb.; $Cl = 0.4$. Contour lines of: A) one wave period, B) two wave periods.

| | | | | |
|----|----------|---|---------------------|-----------------------|
| 1. | F_{qa} | = | 0.284×10^5 | Btu/h.ft ² |
| 2. | F_{qa} | = | 0.304×10^5 | Btu/h.ft ² |
| 3. | F_{qa} | = | 0.331×10^5 | Btu/h.ft ² |
| 4. | F_{qa} | = | 0.359×10^5 | Btu/h.ft ² |
| 5. | F_{qa} | = | 0.383×10^5 | Btu/h.ft ² |
| 6. | F_{qa} | = | 0.386×10^5 | Btu/h.ft ² |
| 7. | F_{qa} | = | 0.413×10^5 | Btu/h.ft ² |

Figure (4.5b): Interface triple front position during two successive waves for different values of G_a . Freon-12 at pressure = 155 lb/in². Constant parameters: $F_{qa} = 0.331 \times 10^5$ Btu/h.ft²; $\Delta H = 6.21$ Btu/lb.; $Cl = 0.4$. Contour lines of: A) one wave period, B) two wave periods.

| | | | | |
|----|-------|---|---------------------|----------------------|
| 1. | G_a | = | 0.367×10^6 | lb/h.ft ² |
| 2. | G_a | = | 0.387×10^6 | lb/h.ft ² |
| 3. | G_a | = | 0.401×10^6 | lb/h.ft ² |
| 4. | G_a | = | 0.414×10^6 | lb/h.ft ² |
| 5. | G_a | = | 0.440×10^6 | lb/h.ft ² |
| 6. | G_a | = | 0.467×10^6 | lb/h.ft ² |
| 7. | G_a | = | 0.493×10^6 | lb/h.ft ² |

INTERFACE TRIPLE FRONT POSITION DURING TWO WAVES

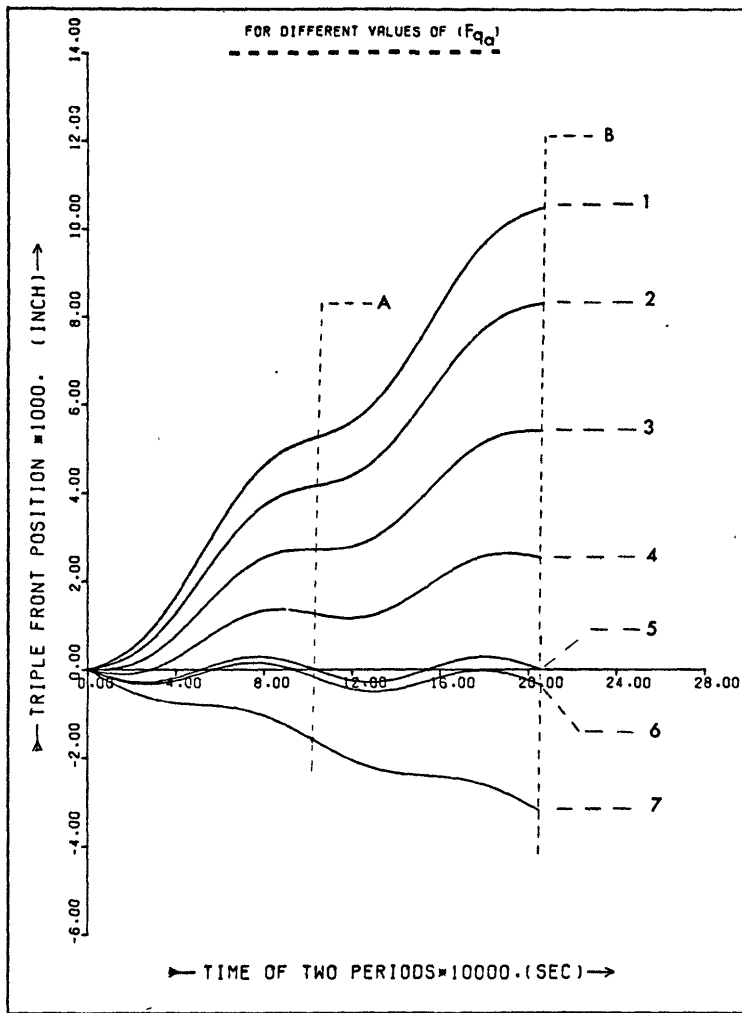


FIG.(4-5a)

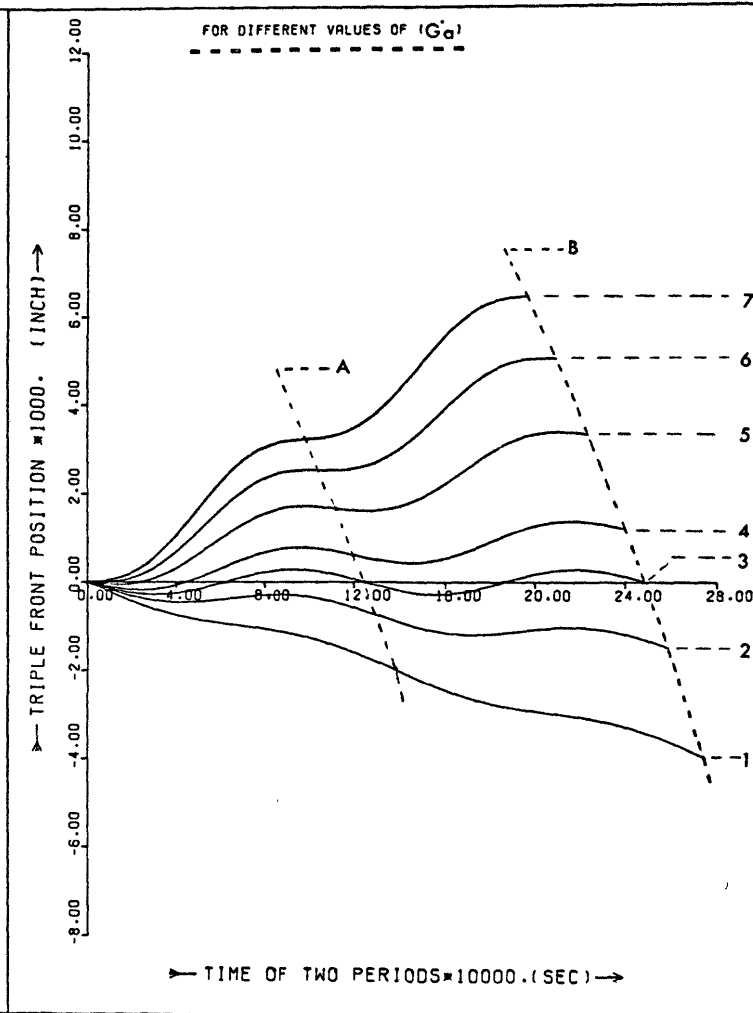


FIG.(4-5b)

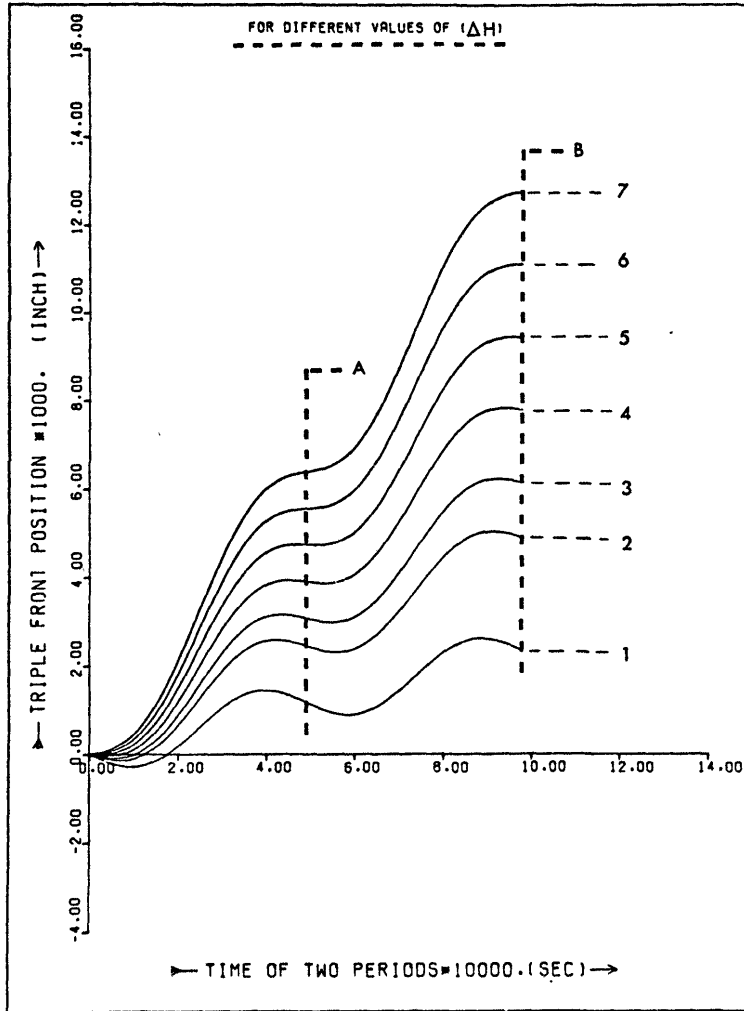
Figure(4.6a) Interface triple front position during two successive waves for different values of ΔH . Water at pressure = 1000 lb/in². Constant parameters: $F_{qa} = 0.6069 \times 10^6$ Btu/h.ft²; $G_a = 0.740 \times 10^6$ lb/h.ft²; $C1 = 0.4$. Contour line of: A) one wave period; B) two waves period.

1. $\Delta H = 0.0$ Btu/lb.
2. $\Delta H = 24.8$ Btu/lb.
3. $\Delta H = 36.8$ Btu/lb.
4. $\Delta H = 52.8$ Btu/lb.
5. $\Delta H = 68.8$ Btu/lb.
6. $\Delta H = 84.8$ Btu/lb.
7. $\Delta H = 100.8$ Btu/lb.

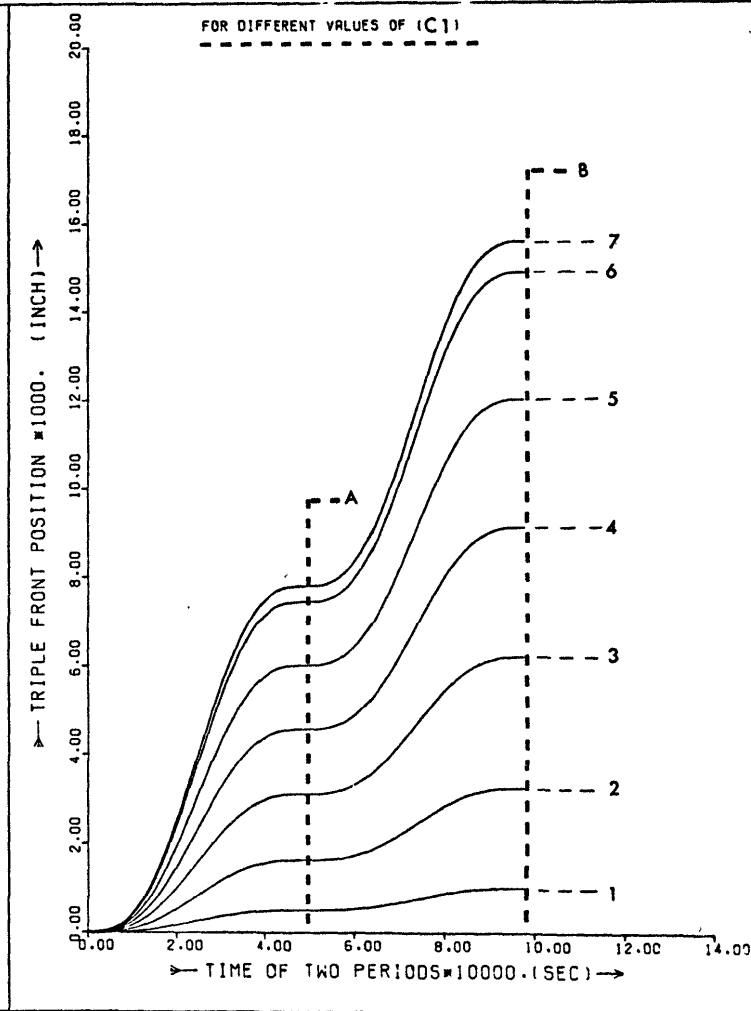
Figure(4.6b) Interface triple front position during two successive waves for different values of $C1$. Water at pressure = 1000 lb/in². Constant parameters: $F_{qa} = 0.6069$ Btu/h.ft²; $G_a = 0.740 \times 10^6$ lb/h.ft²; $\Delta H = 72.8$ Btu/lb. Contour line of: A) one wave period; B) two waves period.

1. $C1 = 0.04$
2. $C1 = 0.13$
3. $C1 = 0.25$
4. $C1 = 0.37$
5. $C1 = 0.49$
6. $C1 = 0.61$
7. $C1 = 0.64$

 INTERFACE TRIPLE FRONT POSITION DURING TWO WAVES



FIG(4-6a)



FIG(4-6b)

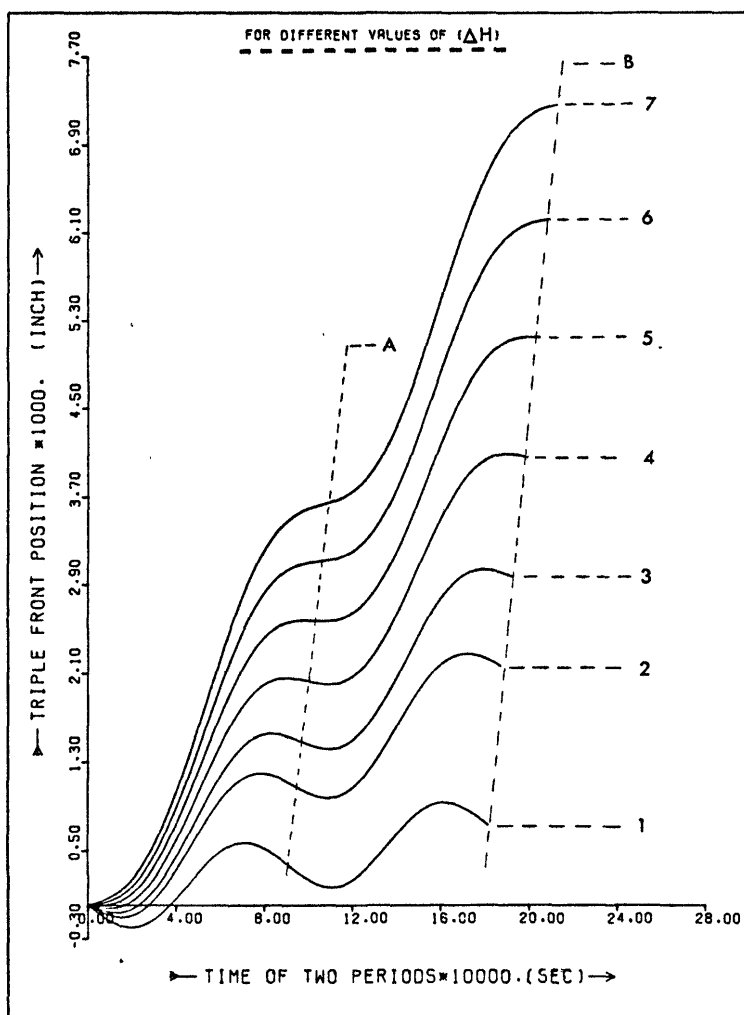
Figure (4.7a) Interface triple front position during two successive waves for different values of ΔH . Freon-12 at pressure = 155 lb/in². Constant parameters: $F_{qa} = 0.331 \times 10^5$ Btu/h.ft³; $G_a = 0.473 \times 10^6$ lb/h.ft²; $C1 = 0.4$. Contour line of: A) one wave period; B) two waves period.

- | | | |
|----|-------------------|---------|
| 1. | $\Delta H = 0.0$ | Btu/lb. |
| 2. | $\Delta H = 2.12$ | Btu/lb. |
| 3. | $\Delta H = 3.14$ | Btu/lb. |
| 4. | $\Delta H = 4.50$ | Btu/lb. |
| 5. | $\Delta H = 5.87$ | Btu/lb. |
| 6. | $\Delta H = 7.24$ | Btu/lb. |
| 7. | $\Delta H = 8.60$ | Btu/lb. |

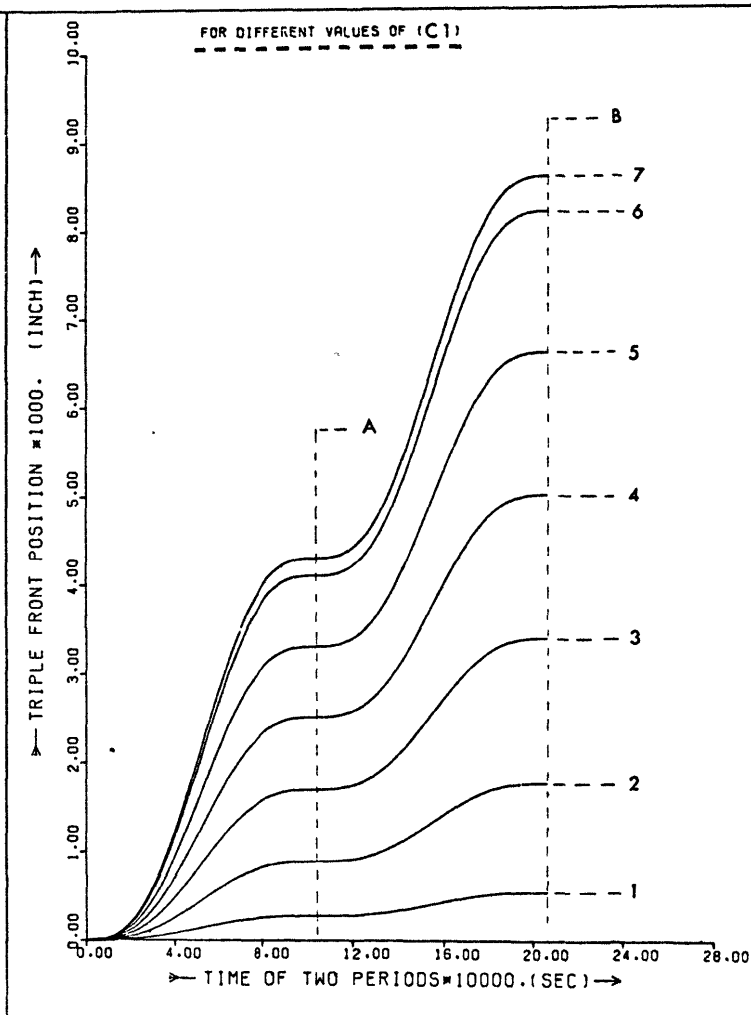
Figure (4.7b) Interface triple front position during two successive waves for different values of $C1$. Freon-12 at pressure = 155 lb/in². Constant parameters: $F_{qa} = 0.331 \times 10^5$ Btu/h.ft²; $G_a = 0.473 \times 10^6$ lb/h.ft²; $\Delta H = 6.21$ Btu/lb. Contour line of; A) one wave period; B) two waves period.

- | | |
|----|-------------|
| 1. | $C1 = 0.04$ |
| 2. | $C1 = 0.13$ |
| 3. | $C1 = 0.25$ |
| 4. | $C1 = 0.37$ |
| 5. | $C1 = 0.49$ |
| 6. | $C1 = 0.61$ |
| 7. | $C1 = 0.64$ |

INTERFACE TRIPLE FRONT POSITION DURING TWO WAVES



FIG(4-7a)



FIG(4-7b)

INTERFACE TRIPLE FRONT SPEED
VERSUS (QA,GA,C1,DELH)

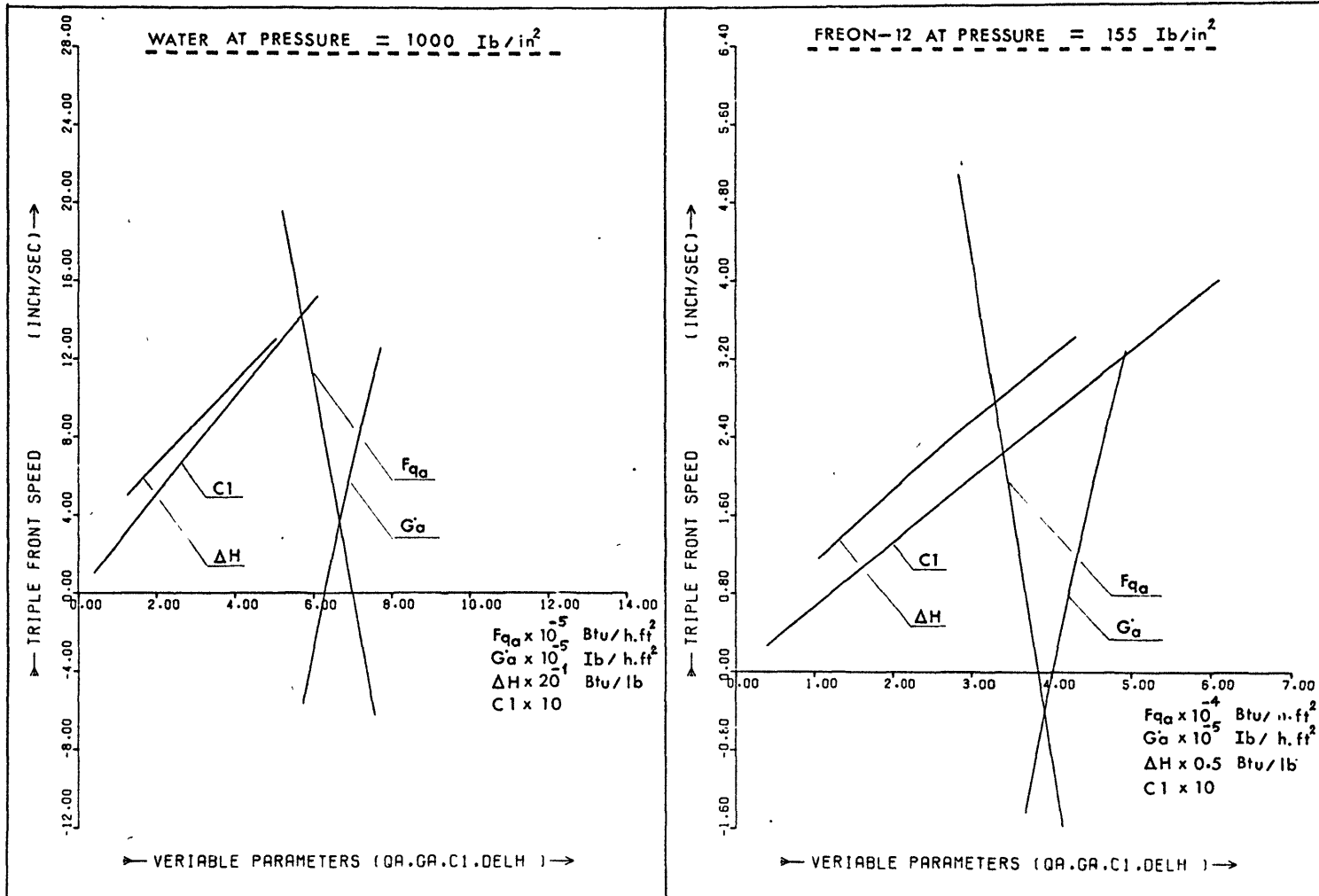


FIG. (4-8a)

FIG.(4-8b)

TRIPLE PHASE FRONT SPEED VS. MASS VELOCITY

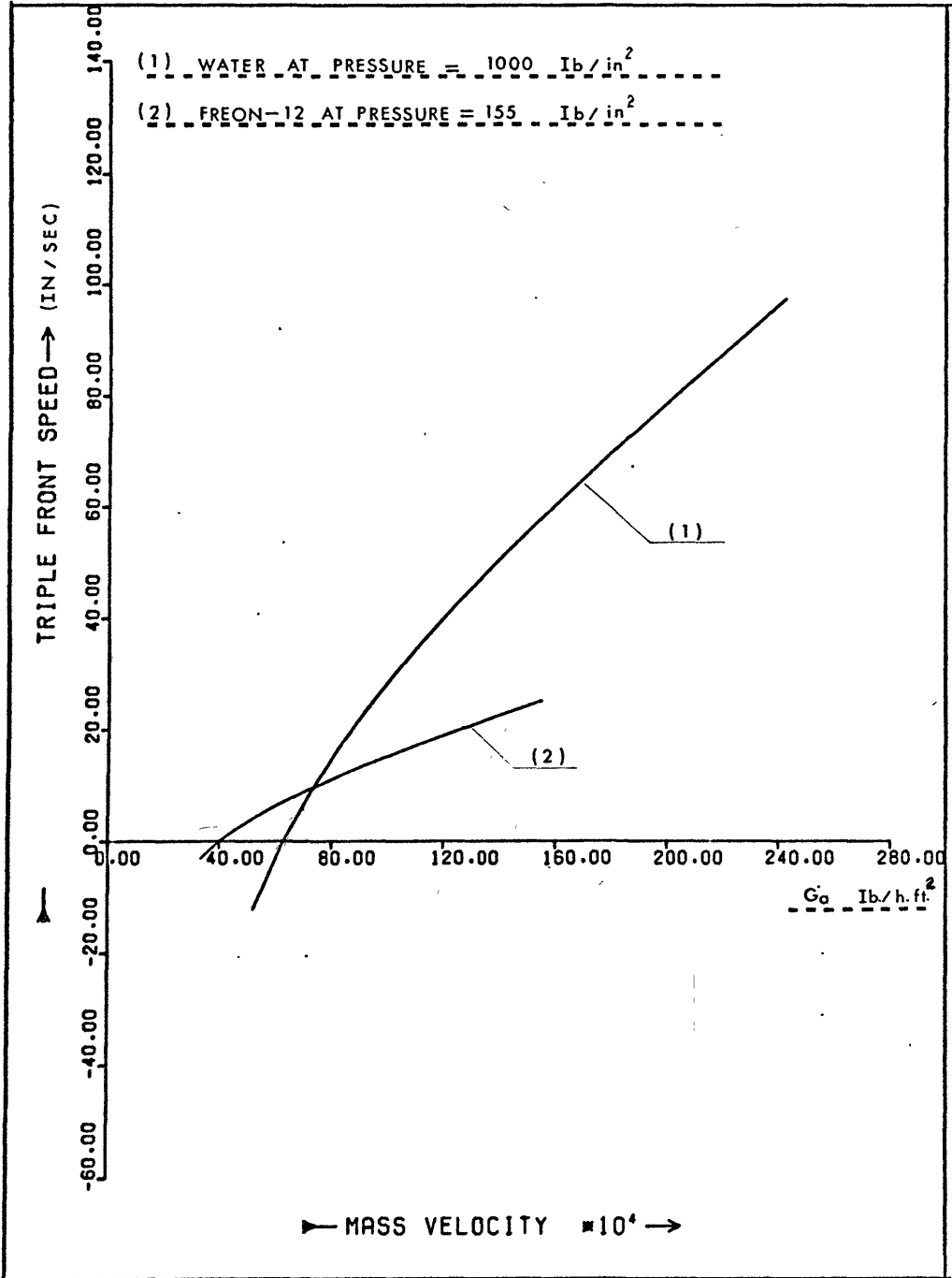
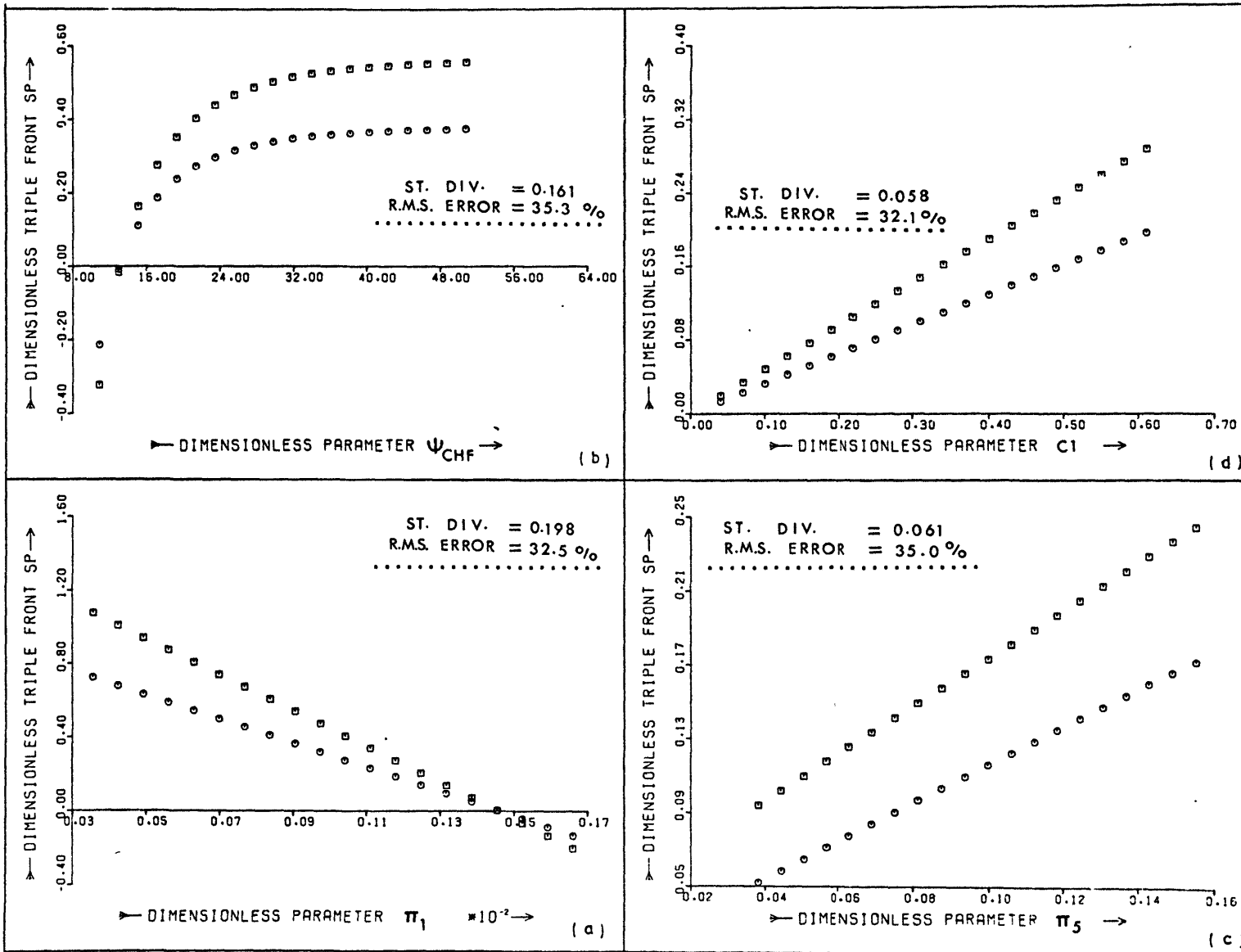


FIG.(4-9)

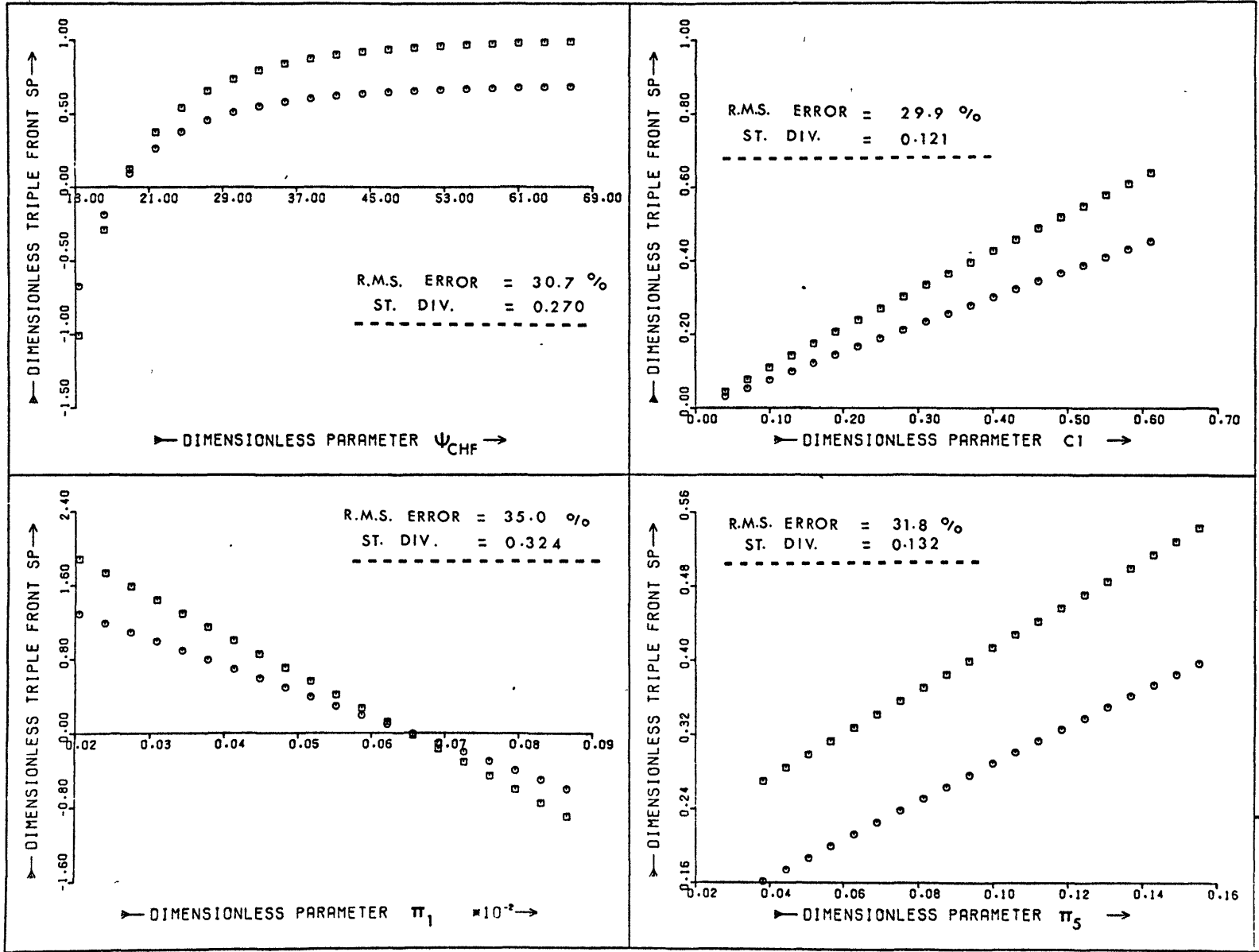
DIMENSIONLESS PARAMETERS π_1, ψ_{CHF}, π_5 VERSUS DIMENSIONLESS TRIPLE FRONT SPEED (SP)



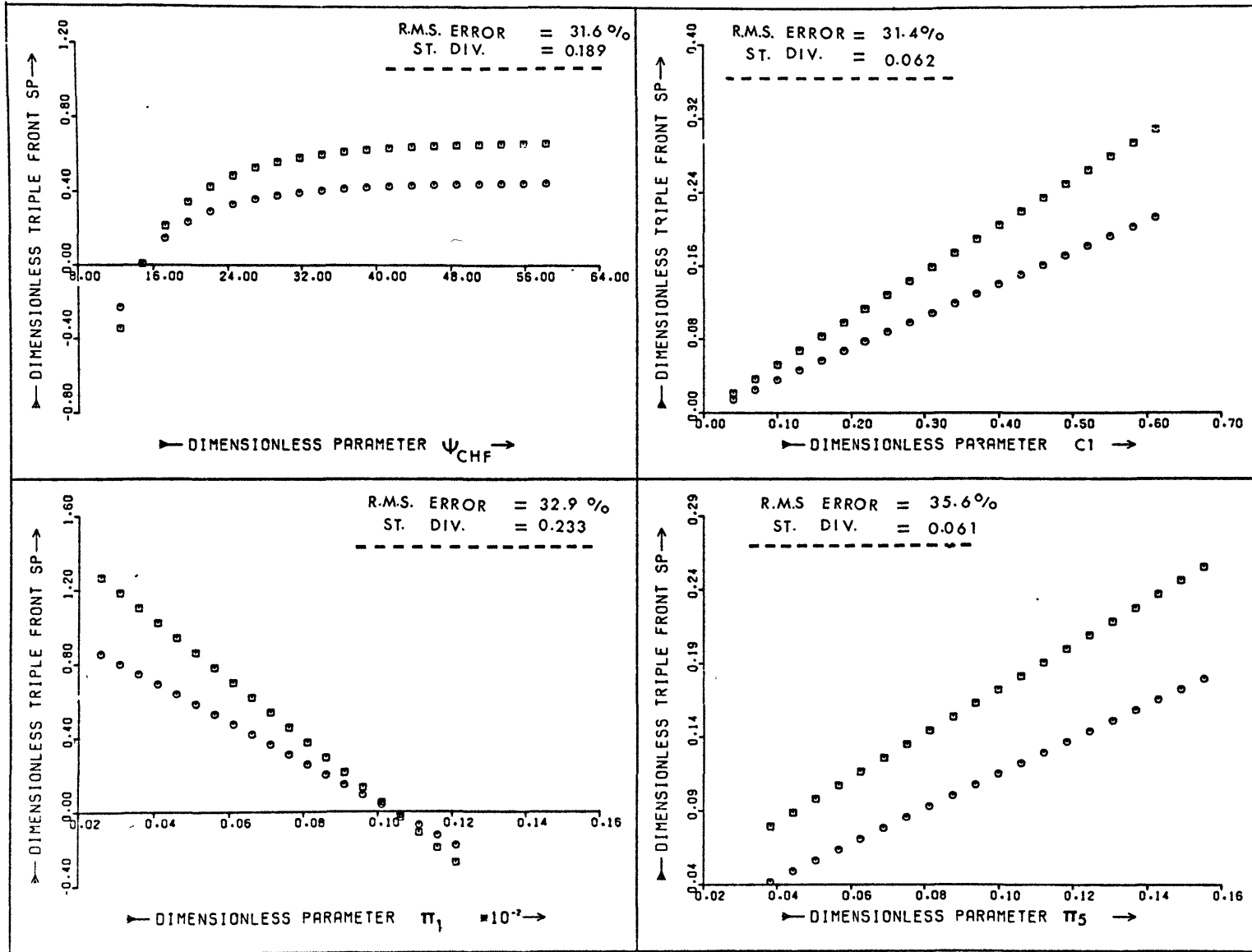
Water
 Freon-12

 FIG.(4-10)

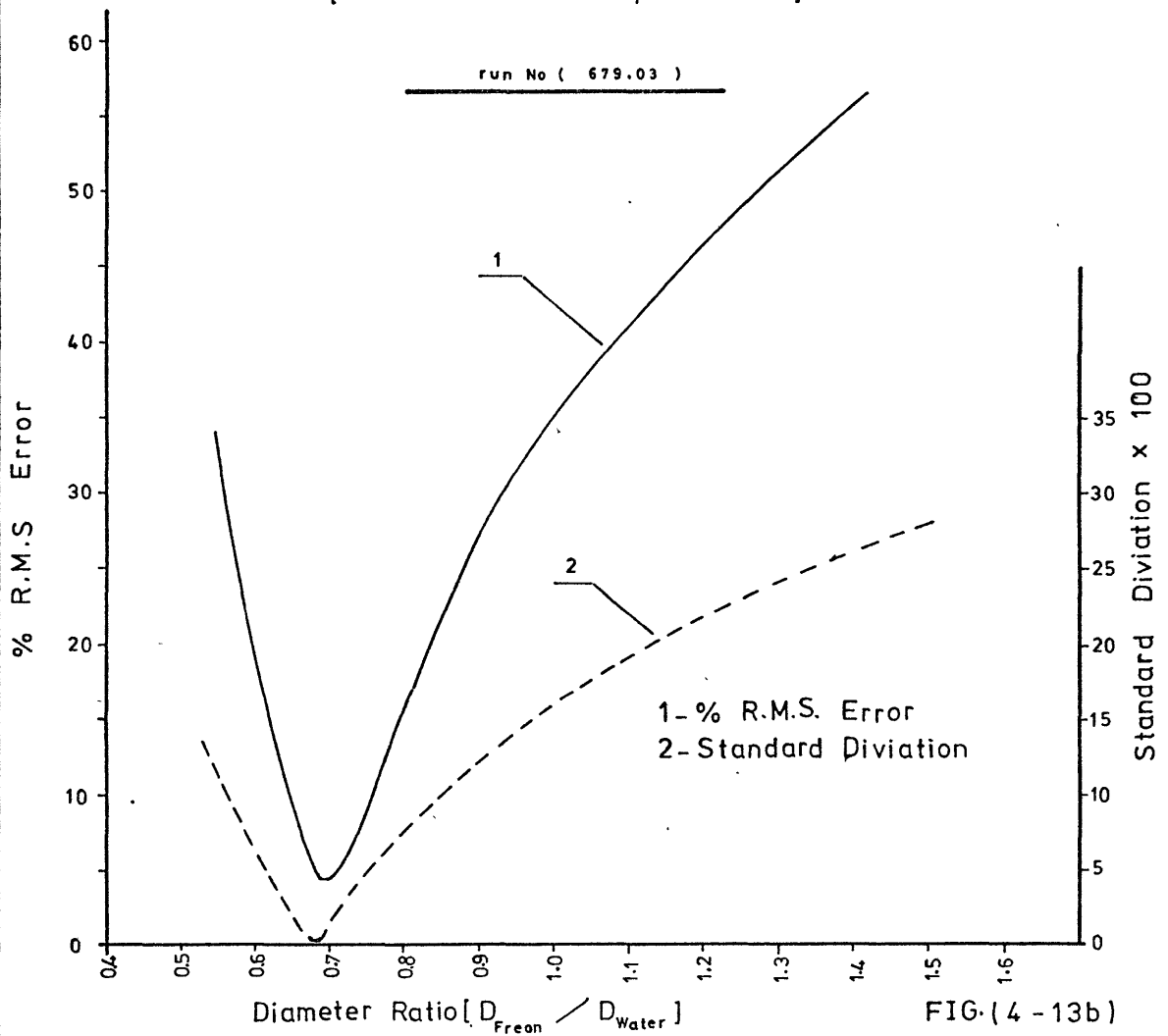
DIMENSIONLESS PARAMETERS (π_1, ψ_{CHF}, π_5) VERSUS DIMENSIONLESS TRIPLE FRONT SPEED (SP)



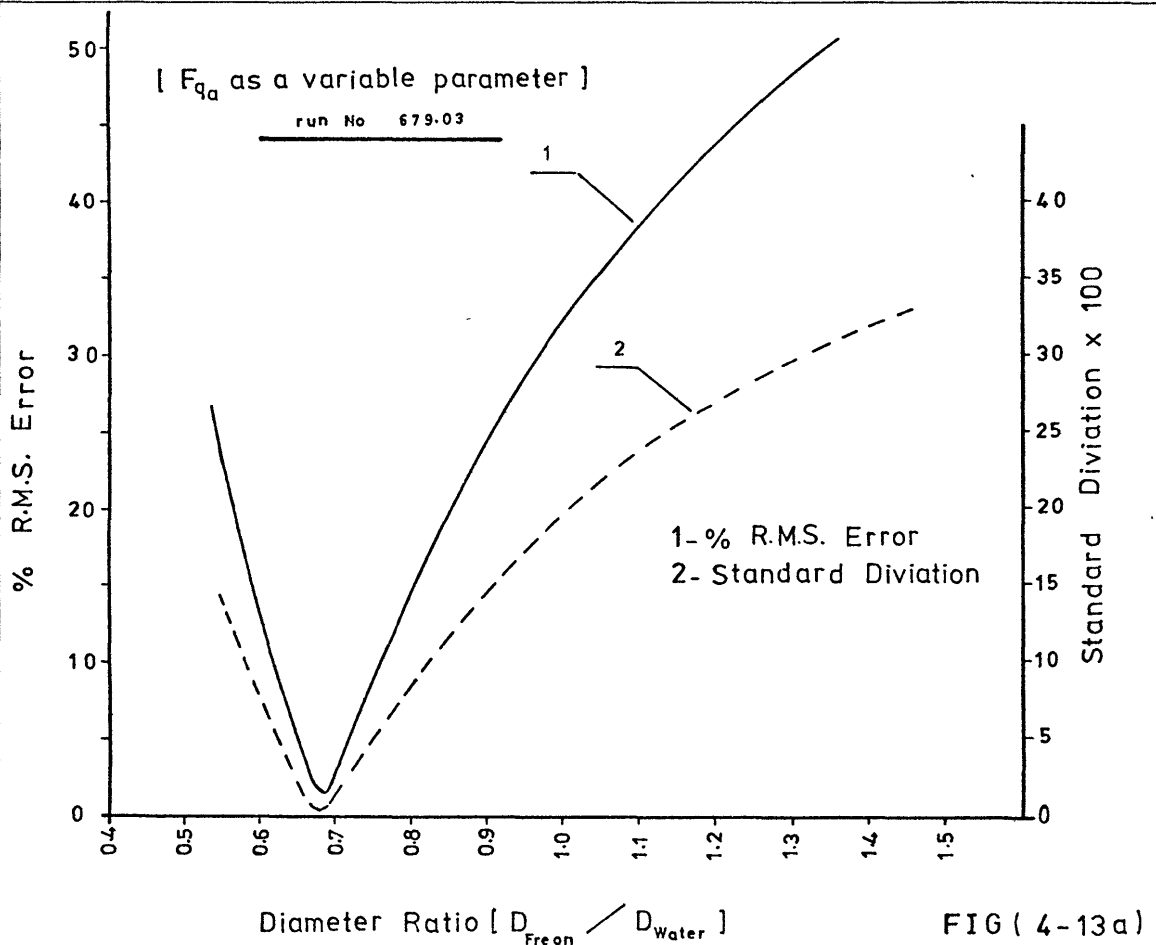
DIMENSIONLESS PARAMETERS (Ψ_{CHF} , Π_1 , Π_5) VERSUS DIMENSIONLESS TRIPLE FRONT SPEED (SP)

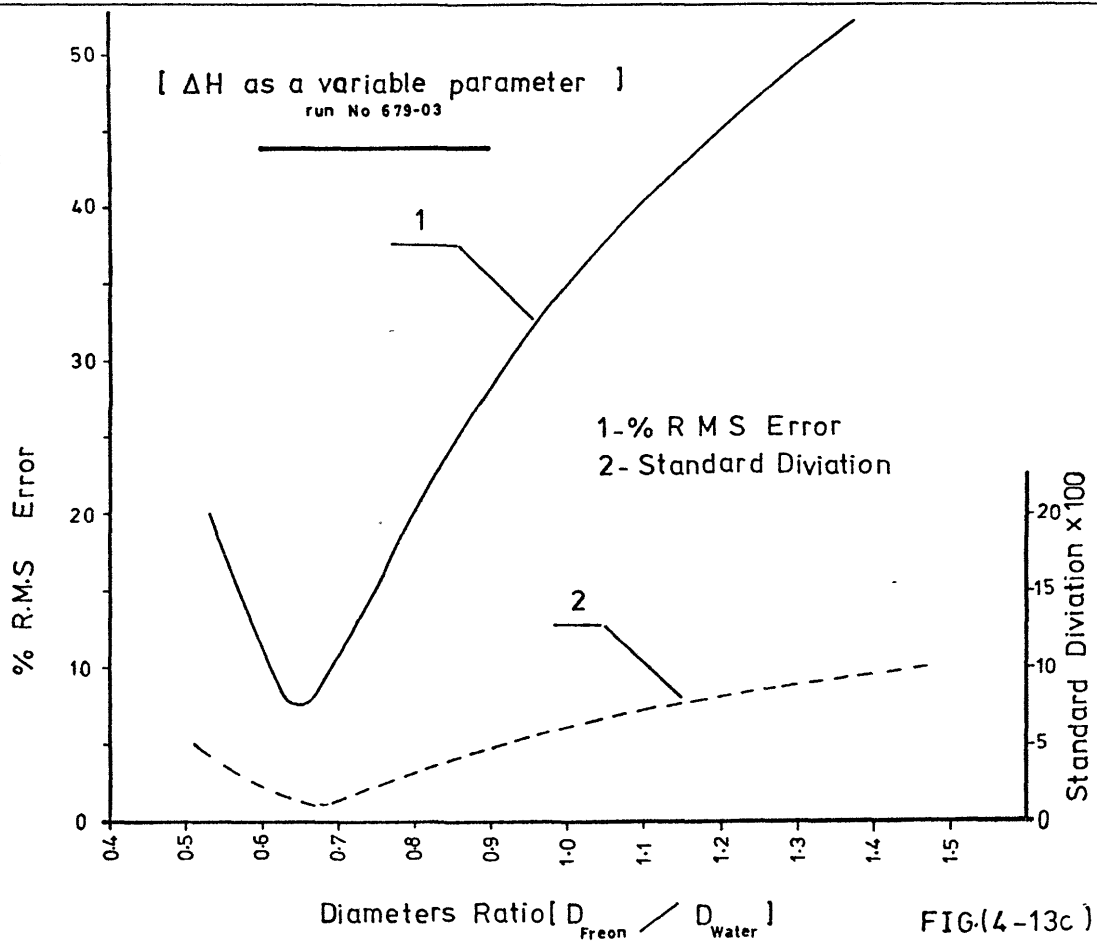
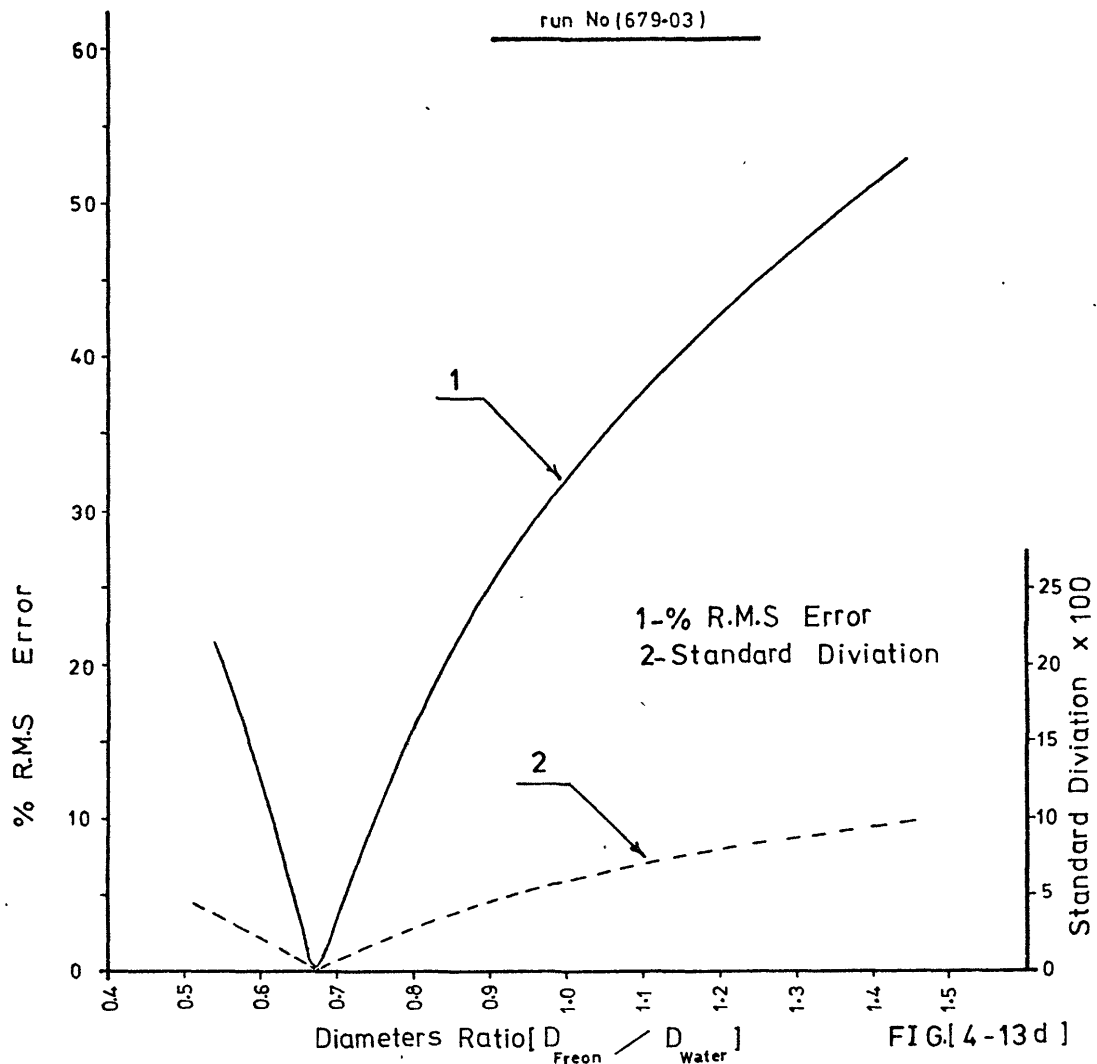


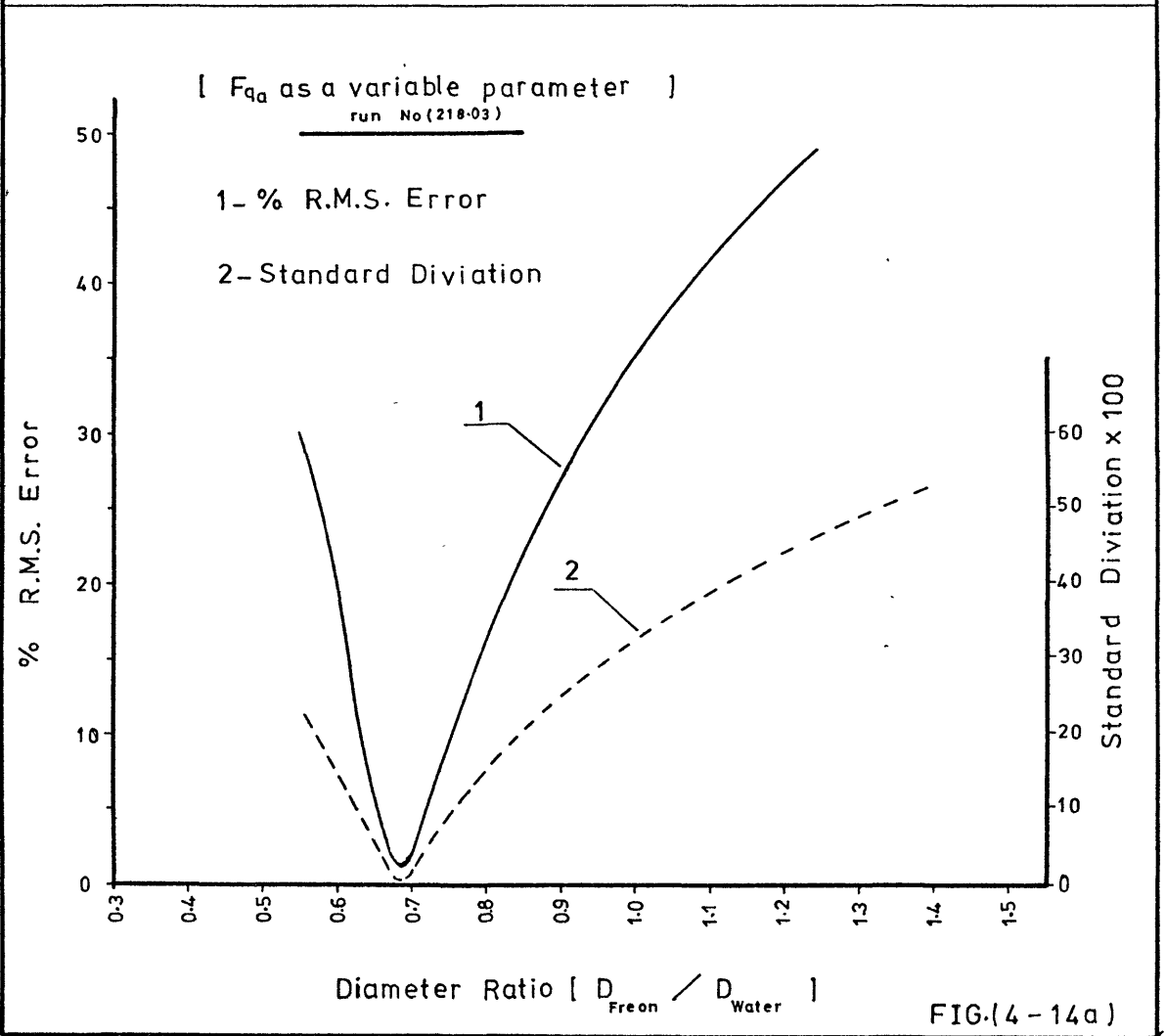
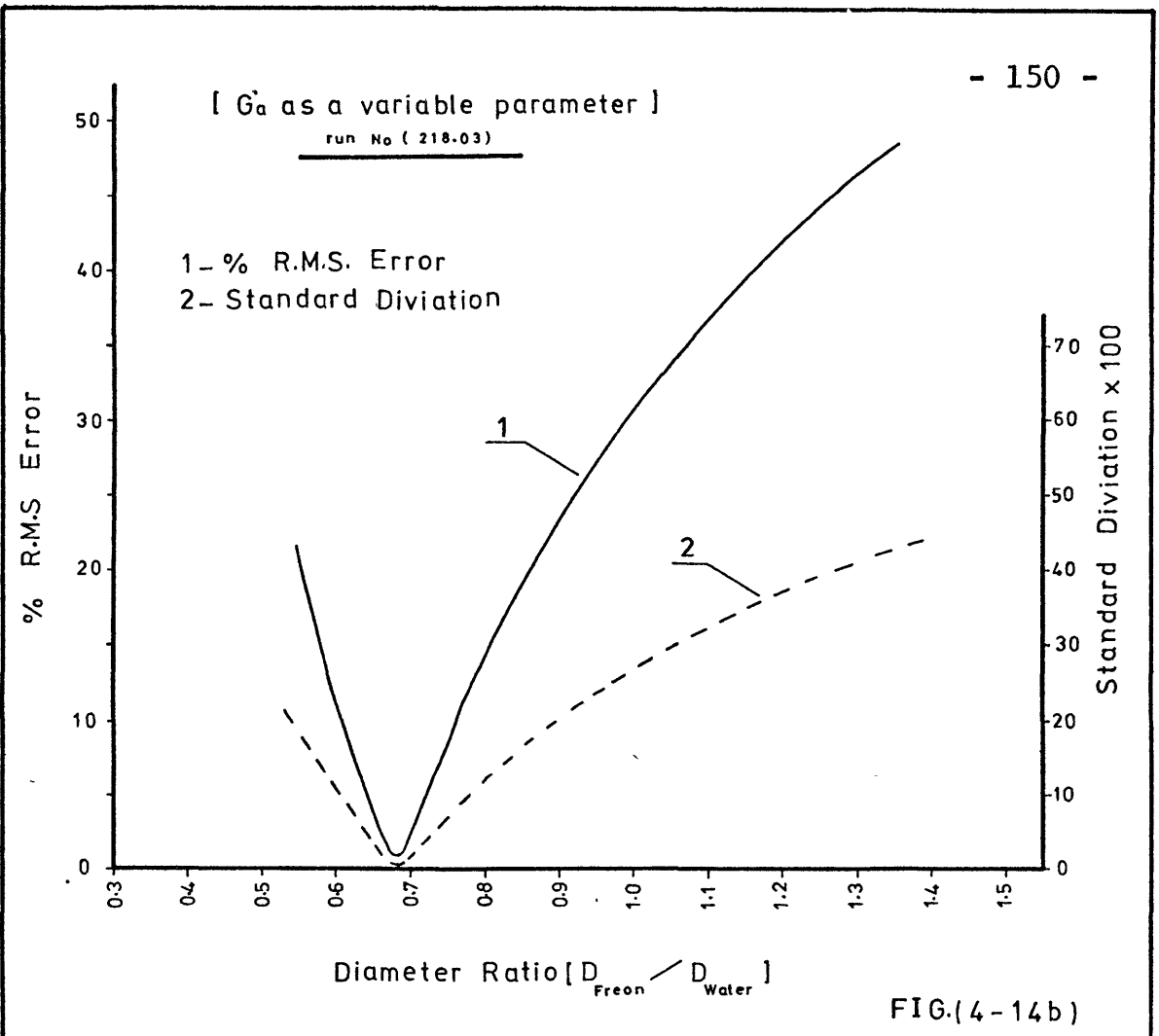
[G_a as a variable parameter]

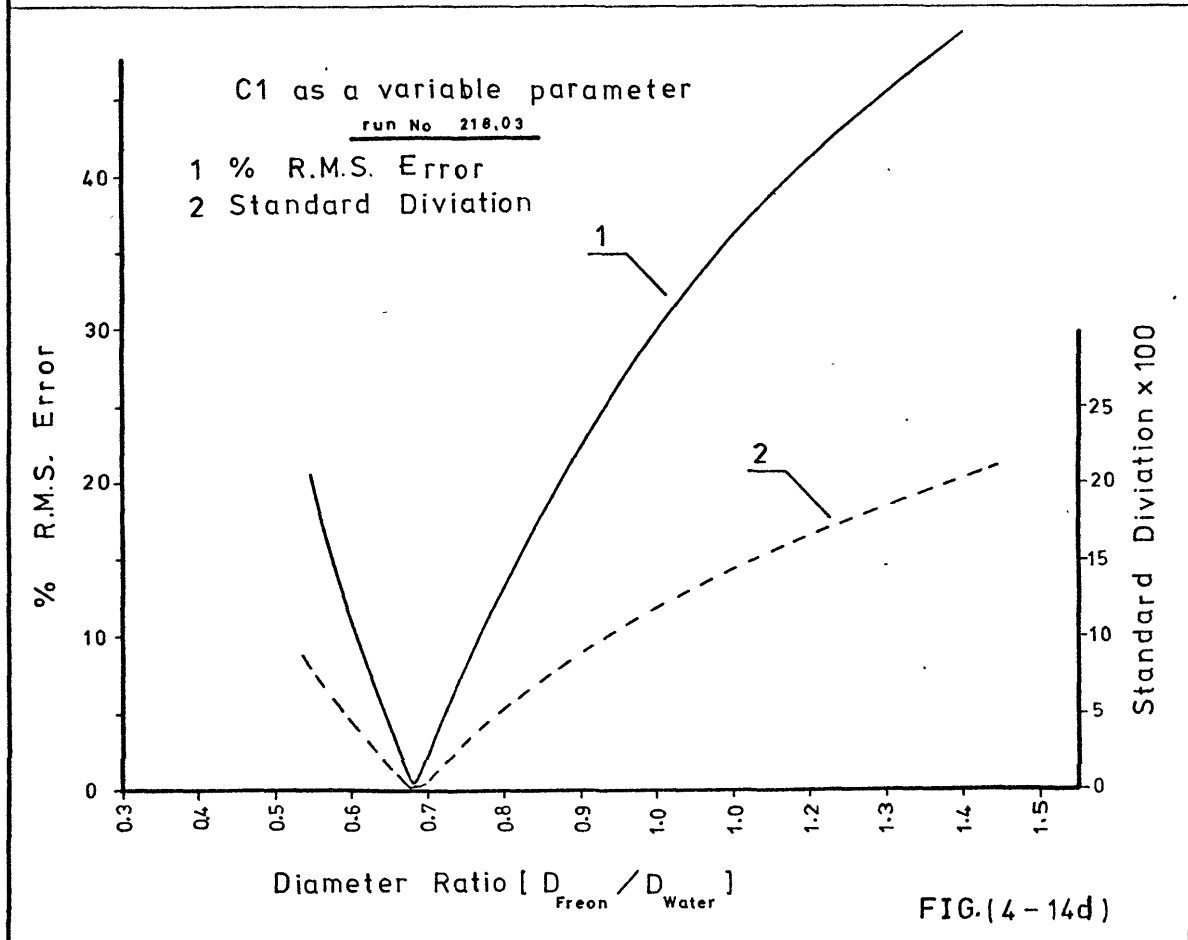
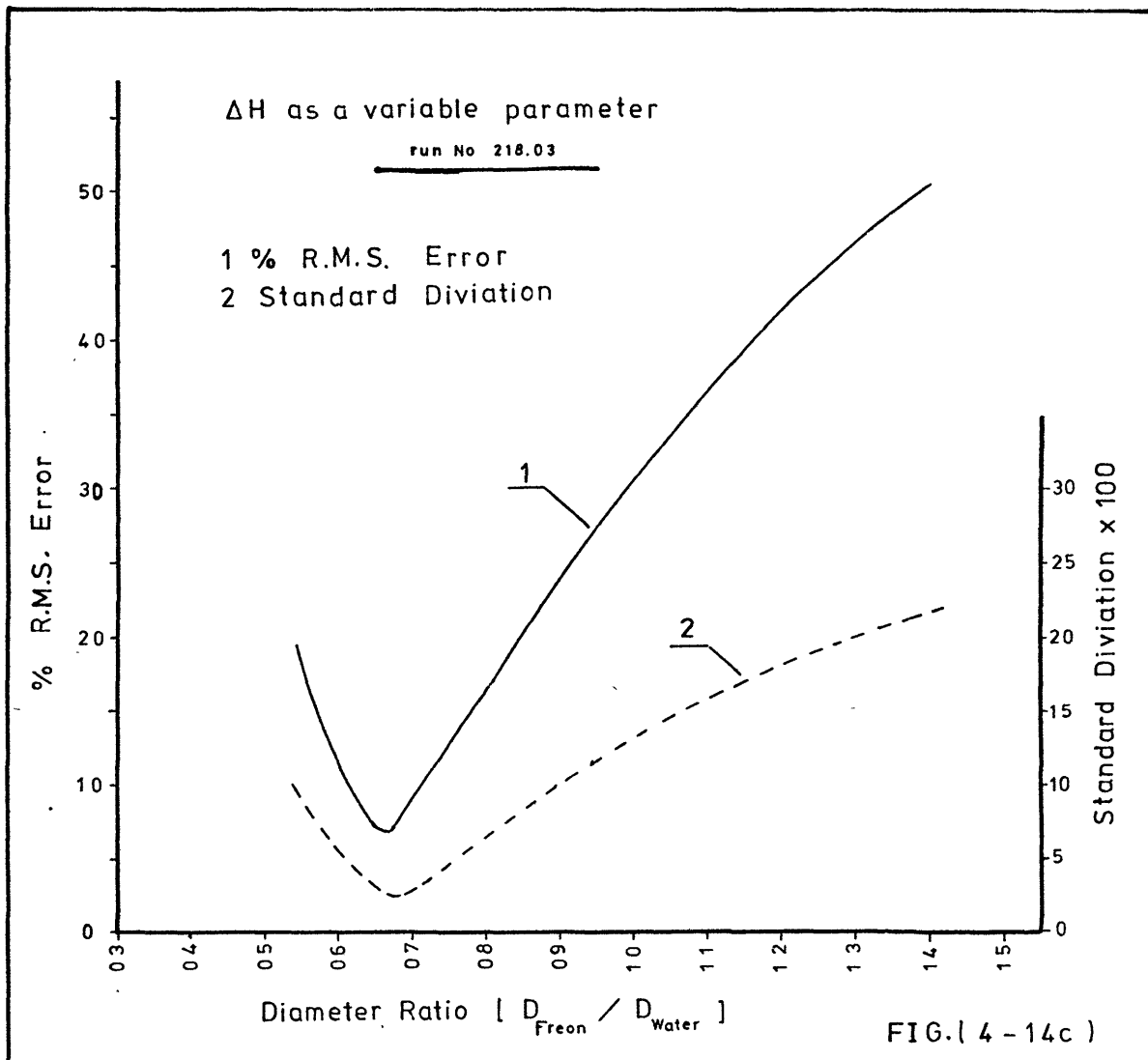


[F_{qa} as a variable parameter]









DIMENSIONLESS PARAMETERS ($\pi_1, \psi_{CHF}, \pi_5, C_1$) VERSUS DIMENSIONLESS TRIPLE FRONT SPEED (SP)

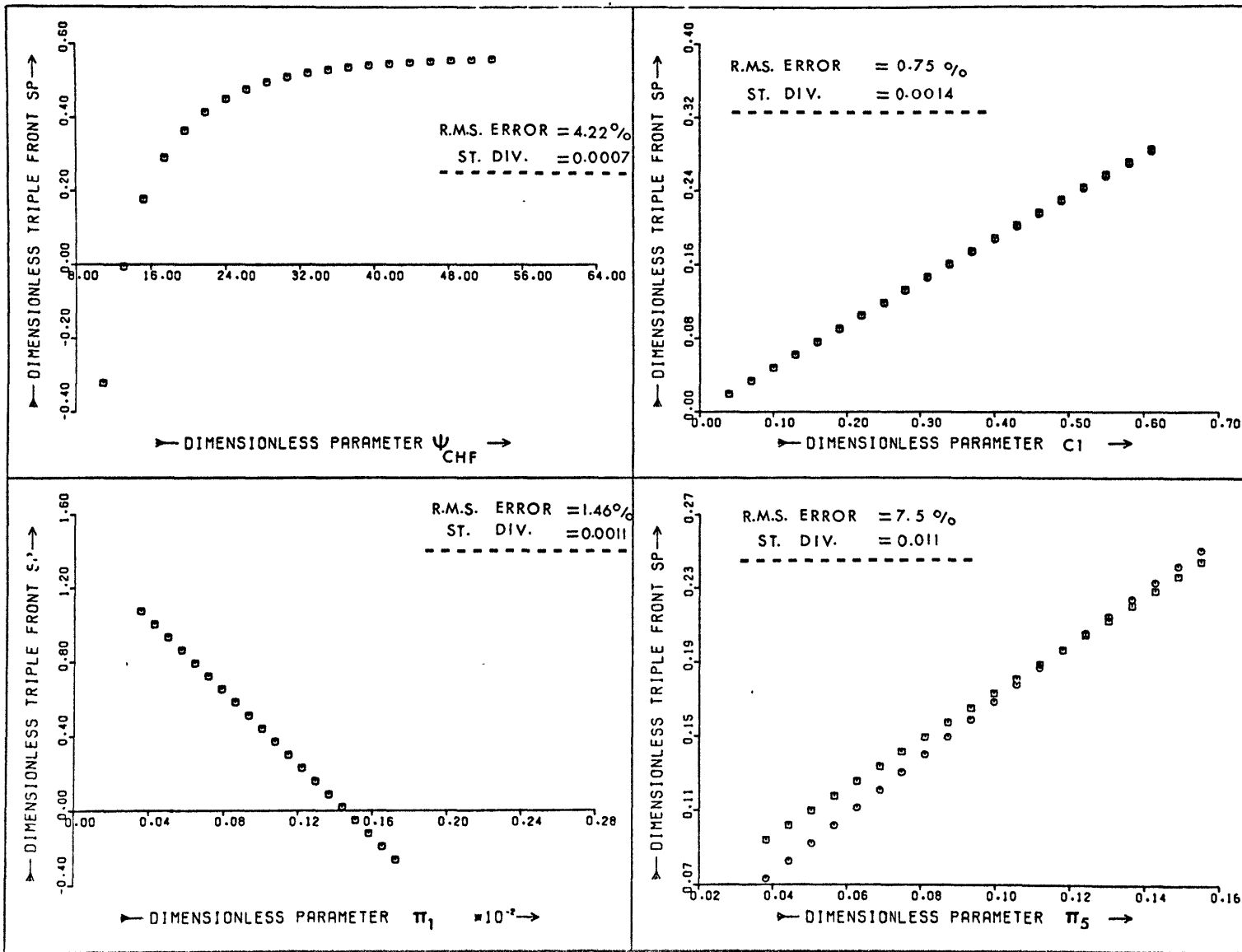
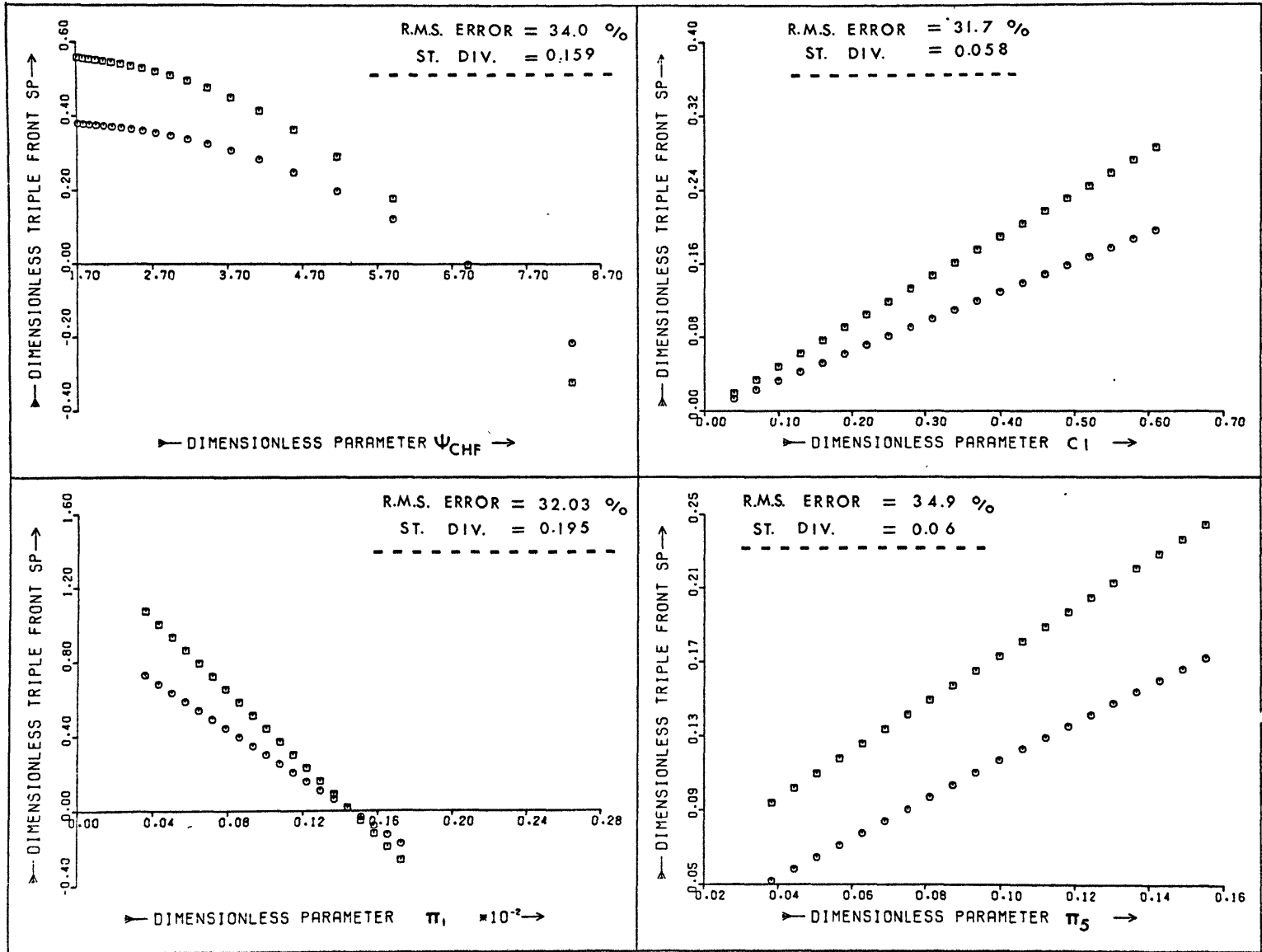


FIG.(4-15)

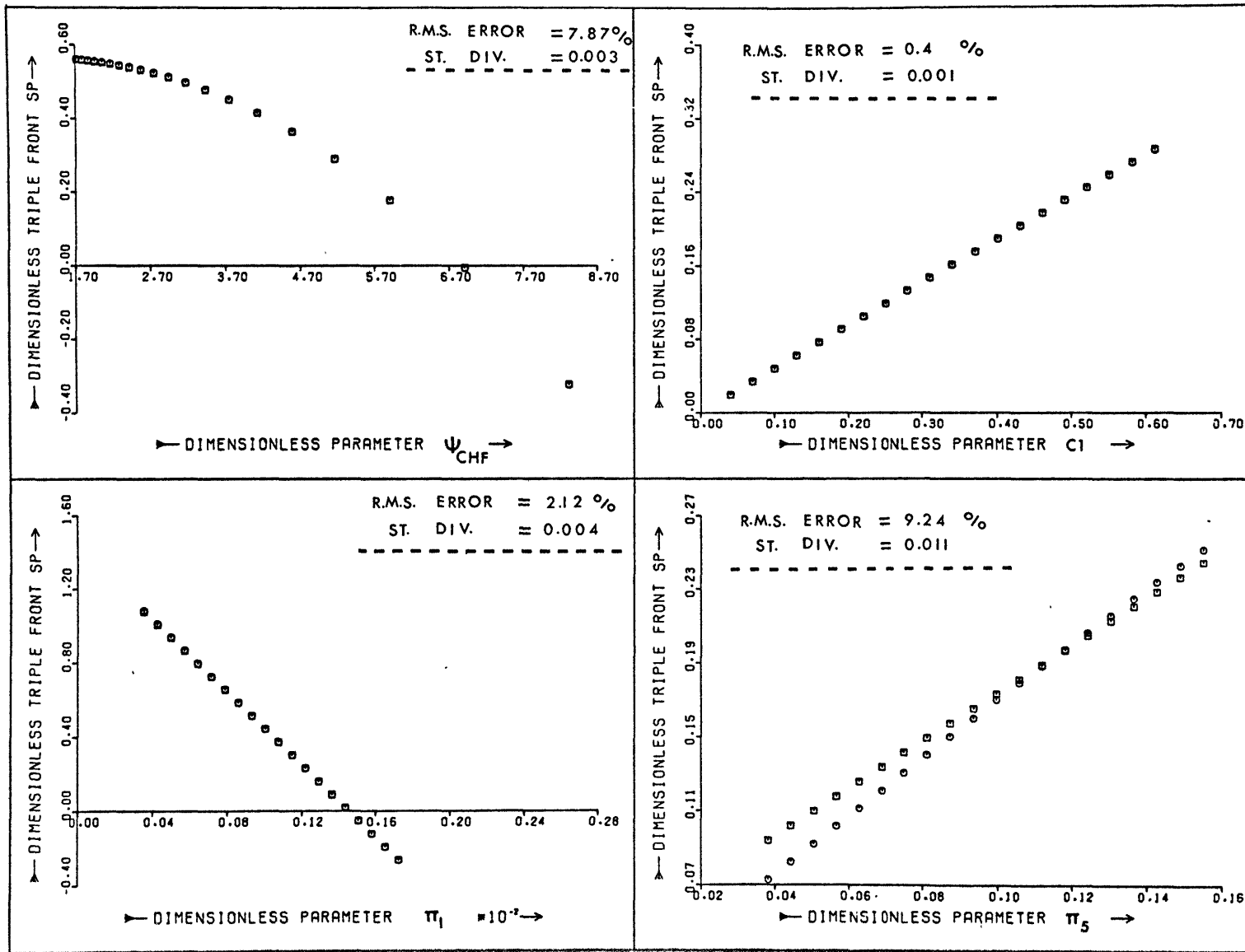
DIMENSIONLESS PARAMETERS ($\pi_1, \psi_{CHF}, \pi_5, C_1$) VERSUS DIMENSIONLESS TRIPLE FRONT SPEED (SP)



□ Water
 ○ Freon-12
 - - - - -

FIG (4-16)

DIMENSIONLESS PARAMETERS ($\pi_1, \psi_{CHF}, \pi_5, C_1$) VERSUS DIMENSIONLESS TRIPLE FRONT SPEED (SP)



CHAPTER 5

A MODIFIED METHOD TO SIMULATE THE EFFECT OF WAVES ON THE MOTION OF THE TRIPLE-PHASE FRONT OF A DRY PATCH FORMED IN A THIN MOTIVATED LIQUID FILM

5.1 INTRODUCTION

In the preceding chapter, the values of the wave length and the wave celerity applied to the solution were taken from a single-phase model (Chapter 3).

The effectiveness of the simulation if represented by percentage R.M.S. error was 35% at a unity diameter ratio. Due to such relatively high percentage error and in a trial to achieve better results, the values of single-phase wave length and celerity were exchanged by values obtained from a two-phase model. Moreover, the interface shear forces between the two phases were considered. We neglected the body forces on the film due to vapour formation, the slip between the liquid film and the tube wall, entrained liquid droplets in the vapour core, vapour bubbles in the liquid film and the thermal inertia of the heated solid surface.

5.2 THE MODEL

Consider the part of the annular liquid film near the end of the two-phase flow regime in a straight tubular

steam generator. The free interfacial film surface is idealised by assuming it to constitute advancing harmonic waves.

At the triple-phase front the waves increase the film thickness periodically and the static and dynamic forces overcome the capillary forces. Hence the triple-phase front moves forward or backward over the heated surface. This model is similar to the model introduced in the preceding chapter, but with one exception; that here the interfacial shear stress is considered, hence other values for the wave length and celerity are obtained.

5.3 GOVERNING EQUATIONS

Consider an annular two-phase flow in a heated tube with interfacial sinusoidal wave as shown in Figure (5.1).

Following Tippet's (1964) approach, we have:

Continuity equations:

$$\begin{aligned} \frac{\partial^2 \phi_l}{\partial z^2} + \frac{\partial^2 \phi_l}{\partial y^2} &= 0 & 0 < y \leq \delta_o &) \\ & & &) \\ \frac{\partial^2 \phi_v}{\partial z^2} + \frac{\partial^2 \phi_v}{\partial y^2} &= 0 & \delta_o \leq y < \delta_o + l'' &) \end{aligned} \quad (5.1)$$

where:

$$\begin{aligned} -\frac{\partial \phi_l}{\partial z} &= W_{l,z} = \text{the component of liquid velocity} \\ & & & \text{in the z-direction} \\ -\frac{\partial \phi_v}{\partial z} &= W_{v,z} = \text{the component of vapour velocity} \\ & & & \text{in the z-direction} \end{aligned}$$

$$-\frac{\partial \phi_l}{\partial y} = W_{l,y} = \text{the component of liquid velocity in the y-direction}$$

$$-\frac{\partial \phi_v}{\partial y} = W_{v,y} = \text{the component of vapour velocity in the y-direction}$$

The boundary conditions are:-

i) the liquid film:

$$\text{Lim}\left(-\frac{\partial \phi_l}{\partial y}\right)\Big|_{y \rightarrow \delta_0^-} = \delta_1' \cos\left(\frac{2\pi}{\lambda} \cdot z - wt\right) + w\delta_1 \cdot \sin\left(\frac{2\pi}{\lambda} \cdot z - wt\right) \quad (5.2)$$

$$-\left(\frac{\partial \phi_l}{\partial y}\right)_{y=0} = 0 \quad (5.3)$$

ii) in the vapour core:

$$\begin{aligned} \text{Lim}\left(-\frac{\partial \phi_v}{\partial y}\right)\Big|_{y \rightarrow \delta_0^+} &= \text{Lim}\left[\frac{\partial \delta}{\partial t} + \frac{\partial \delta}{\partial z} \left(\frac{\partial z}{\partial t}\right)\right]_{y=\delta_0^+} \\ &= \delta_1' \cdot \cos\left(\frac{2\pi}{\lambda} \cdot z - wt\right) + \left(w - \frac{2\pi}{\lambda} \cdot W_{v,l}\right) \\ &\quad \cdot \delta_1 \sin\left(\frac{2\pi}{\lambda} \cdot z - wt\right) \end{aligned} \quad (5.4)$$

$$-\frac{\partial \phi_v}{\partial z} = W_{l,v} \quad y = \delta_0 + l'' \quad (5.5)$$

iii) At $y = \delta_0 + l''$ the effective core to film relative velocity is $W_{l,v}$ and the coordinate system is considered to be moving so that $W_{l,v} = 0$. The interfacial waves are assumed to be of the general sinusoidal form, i.e.

$$\delta_r(z,t) = \delta_1 \cdot \cos\left(\frac{2\pi}{\lambda} \cdot z - wt\right) \quad (5.6)$$

where: $w = \text{frequency of interfacial waves (1/sec)}$
 $= 2\pi c/\lambda$

$c = \text{wave celerity}$

$$\delta_1 = \delta_m - \delta_o$$

$$\delta_r = \delta - \delta_c$$

Tippet (1964) considered the local pressure in the film and in the core using the momentum equation, then applying the force balance at the interface together with the mixing length theory (Schlichting, 1968), the following relations were found for the effective relative velocity between the vapour core and the liquid film ($W_{l,v}$), wave length (λ), film thickness (δ_c) and the wave frequency (w):

$$W_{l,v} = \frac{K_2}{K} \left(\frac{1}{2} \cdot \phi_{\text{TPF}} \cdot f_F \right)^{\frac{1}{2}} \cdot \frac{G_a}{\rho_l} \left[1 + \sqrt{\frac{\rho_l}{\rho_v}} \right] \quad (5.7)$$

$$\lambda = \frac{K_3 \cdot \sigma}{\rho_v \cdot W_{l,v}^2} \cdot \left(1 + \frac{\rho_v}{\rho_l} \right) \quad (5.8)$$

$$\delta_c = \frac{2 \cdot K_3 \cdot K_4 \cdot \sigma \cdot \rho_l (1 + \rho_l / \rho_v)}{\phi_{\text{TPF}} \cdot f_F \cdot G_a \cdot (1 + \sqrt{\rho_l / \rho_v})^2} \quad (5.9)$$

$$w = \frac{2\pi c}{\lambda} = \frac{2\pi}{\lambda} \cdot \left[\frac{\rho_v W_v \tanh\left(\frac{2\pi}{\lambda} \cdot \ell''\right) + \rho_l W_l \coth\left(\frac{2\pi}{\lambda} \cdot \delta_c\right)}{\rho_v \tanh\left(\frac{2\pi}{\lambda} \cdot \ell''\right) + \rho_l \coth\left(\frac{2\pi}{\lambda} \cdot \delta_c\right)} \right] \quad (5.10)$$

where: $K_2 = K = 0.4$

$$\ell'' = K_2 \cdot \delta_c$$

$$2\pi < K_3 < 3\pi$$

$$5 > K_1 \geq 1$$

$$K_4 = 1/K_1$$

$$\phi_{\text{TPF}} = \text{Two-phase friction multiplier } (dP/dz)_{\text{TPF}} / (dP/dz)$$

f_F = friction factor.

ℓ'' = mixing length of turbulent diffusion.

Rewrite the equation (4.20) of the triple-phase front speed:

$$\frac{d\eta}{dt} + S\eta = B \left[P + Z \left(-\cos \frac{2\pi ct}{\lambda} + 1 \right) - Y \left(\cos^2 \frac{2\pi ct}{\lambda} + 1 - 2 \cos \frac{2\pi ct}{\lambda} \right) \right] \quad (4.20)$$

5.4 SOLUTION

We solved equations (5.7), (5.8), (5.9), (5.10) and (4.20) numerically to find the interface triple-front displacement due to the film surface waves and also to find the effect of the various parameters F_{qa} , G_a , Cl and ΔH on the movement of the triple-phase front.

The same data as used in Chapter 4 are applied, i.e. data collected from runs 679.03, 218.03 and 352.02, Thompson et al (1964).

As mentioned before, the constants K_3 and K_1 used in equations (5.8) and (5.9) have the values $2\pi < K_3 < 3\pi$ and $5 > K_1 \geq 1$ respectively. To test the influence of these constants on the calculated values of the triple front speed, three programme runs were carried out for different values of K_1 and K_3 as follows:

$$\begin{array}{lll}
 \text{(i)} & K_1 = 1.1 & K_3 = 2.9\pi \quad \dots \quad K_5 = 8.28 \\
 \text{(ii)} & K_1 = 1.5 & K_3 = 2.5\pi \quad \dots \quad K_5 = 5.23 \\
 \text{(iii)} & K_1 = 4.9 & K_3 = 2.1\pi \quad \dots \quad K_5 = 1.35
 \end{array}$$

where $K_5 = K_3/K_1$.

The results showed that the triple front speed did not depend significantly on K_5 . Also, the film thickness (equation (5.9)) was shown to be more sensitive to these constants than the wave length (equation (5.8)). However, we have chosen the values $K_1 = 1.1$ and $K_3 = 3\pi$ which gave a film thickness comparable with that found by Staub et al (1966).

5.5 RESULTS AND DISCUSSION

5.5.1 Triple-phase front motion

To demonstrate the effect of the four parameters F_{qa} , G_a , Cl and ΔH on the triple front speed, three parameters are kept constant while different values of the fourth are considered. All the results are presented such that the triple-phase front position is shown during the period of two successive waves. The procedure of calculations is as follows:

- (i) Experimental data for water at 1000 lb/in^2 are obtained from Thompson et al (1964), F_{qa} , G_a , and ΔH .

(ii) Applying the same technique as mentioned in Section (4.5), the corresponding values of the four parameters F_{qa} , G_a , Cl and ΔH are found for Freon-12 which would simulate the water at burn-out.

(iii) Then the triple-phase front speed of water and the simulating Freon are found applying the corresponding parameters in (i) and (ii).

Table (5.1) shows the groups of the four parameters chosen for the calculation of the triple-phase front position during the period of two successive waves for water and the simulating Freon. The results are shown plotted in Figures (5.2) to (5.5).

TABLE 5.1

| Parameter under investigation (for water at 1000 lb/in ²) | Fig. | Corresponding simulated values for Freon-12 (at 155 lb/in ²) | Fig. |
|---|--|--|--------|
| Surface Heat Flux (F_{qa}) | (5.2a) | Surface Heat Flux (F_{qa}) | (5.3a) |
| 1. 0.519×10^6 Btu/h.ft ² | | 1. 0.284×10^5 Btu/h.ft ² | |
| 2. 0.557×10^6 Btu/h.ft ² | | 2. 0.304×10^5 Btu/h.ft ² | |
| 3. 0.607×10^6 Btu/h.ft ² | | 3. 0.331×10^5 Btu/h.ft ² | |
| 4. 0.657×10^6 Btu/h.ft ² | | 4. 0.359×10^5 Btu/h.ft ² | |
| 5. 0.699×10^6 Btu/h.ft ² | | 5. 0.383×10^5 Btu/h.ft ² | |
| 6. 0.707×10^6 Btu/h.ft ² | | 6. 0.386×10^5 Btu/h.ft ² | |
| 7. 0.757×10^6 Btu/h.ft ² | 7. 0.413×10^5 Btu/h.ft ² | | |
| Mass Velocity (G_a) | (5.2b) | Mass Velocity (G_a) | (5.3b) |
| 1. 0.574×10^6 lb/hr.ft ² | | 1. 0.367×10^6 lb/hr.ft ² | |
| 2. 0.605×10^6 lb/hr.ft ² | | 2. 0.387×10^6 lb/hr.ft ² | |

TABLE 5.1 (continued)

| Parameter under investigation (for water at 1000 lb/in ²) | Fig. | Corresponding simulated values for Freon-12 (at 155 lb/in ²) | Fig. |
|--|--------|--|--------|
| Mass Velocity (G'_a) 3. 0.628×10^6 lb/hr.ft ² 4. 0.646×10^6 lb/hr.ft ² 5. 0.688×10^6 lb/hr.ft ² 6. 0.730×10^6 lb/hr.ft ² 7. 0.771×10^6 lb/hr.ft ² | (5.2b) | Mass Velocity (G'_a) 3. 0.410×10^6 lb/hr.ft ² 4. 0.414×10^6 lb/hr.ft ² 5. 0.440×10^6 lb/hr.ft ² 6. 0.467×10^6 lb/hr.ft ² 7. 0.493×10^6 lb/hr.ft ² | (5.3b) |
| Subcooling (ΔH) 1. 0.00 Btu/lb 2. 24.8 Btu/lb 3. 36.8 Btu/lb 4. 52.8 Btu/lb 5. 68.8 Btu/lb 6. 84.8 Btu/lb 7. 100.8 Btu/lb | (5.4a) | Subcooling (ΔH) 1. 0.00 Btu/lb 2. 2.12 Btu/lb 3. 3.14 Btu/lb 4. 4.50 Btu/lb 5. 5.87 Btu/lb 6. 7.24 Btu/lb 7. 8.60 Btu/lb | (5.5a) |
| Dimensionless Wave Amplitude (C_1) 1. $C_1 = 0.04$ 2. $C_1 = 0.13$ 3. $C_1 = 0.25$ 4. $C_1 = 0.37$ 5. $C_1 = 0.49$ 6. $C_1 = 0.61$ 7. $C_1 = 0.67$ | (5.4b) | Dimensionless Wave Amplitude (C_1) 1. $C_1 = 0.04$ 2. $C_1 = 0.13$ 3. $C_1 = 0.25$ 4. $C_1 = 0.37$ 5. $C_1 = 0.49$ 6. $C_1 = 0.61$ 7. $C_1 = 0.67$ | (5.5b) |

Note: The two-phase friction multiplier ϕ_{TPF} and friction factor f_F are calculated using the Lockhart-Martinelli parameter x_{tt} which is given by Lockhart et al (1949), Martinelli et al (1948) and Guide and Data Book (1965).

The burn-out values taken from Thompson et al (1964) lie within the range chosen in the above table.

A comparison between Figures (5.2) to (5.5) and the relevant ones of Figures (4.4) to (4.7) shows that the shape of the corresponding curves are similar, nevertheless the numerical values are different. Waves calculated by applying the two-phase model instead of single-phase model resulted in shorter wave periods and shorter distances advanced by the triple-phase front at the end of the wave period. In this exercise, if the parameters are the same, the corresponding values of the wave periods, triple-phase front were nearly halved due to the application of two-phase wave model instead of single-phase model.

Figures (5.6a) and (5.6b) show the relation between F_{qa} , G_a , ΔH , Cl and the triple-phase front average speed. Figure (5.6a), which is for water, shows that the results are not affected drastically by introducing the two-phase approach to the previous single-phase one which was described in Chapter 4. Figure (5.6b) is for the corresponding simulating Freon-12 values. Application of the two-phase model showed (Figure 5.7) that a slight increase in the mass velocity resulted in a steep increase in the triple-phase front speed and then a further increase in the mass velocity results in a

decline in the rate of increase of the triple front speed. This decline becomes prominent when the mass velocity exceeds a certain value. The ^{same} results are always found for water and the simulating Freon-12. These results agree with Shires et al (1964) and Hewitt's (1966) findings that the mass velocity has a negligible effect on the triple-phase advance. However, this is true only at higher mass velocities. It should be mentioned here that increasing the mass velocity in the single-phase model results in linear increase in the average triple front speed (Figure 4.9). The average triple front speed changes linearly with the other three parameters, i.e. F_{qa} , ΔH and Cl for both the models introduced in Chapter 4 and the present model described in Chapter 5.

5.5.2 Simulation of the triple-phase front speed

The R.M.S. error of the simulation of the triple-phase front speed of water at pressure 1000 lb/in^2 (Thompson et al (1964), data runs 218.03, 352.03 and 679.03) by Freon-12 at pressure 155 lb/in^2 are found. The parameters considered are F_{qa} , G_a , Cl and ΔH . In each case one of these parameters is changed while the other three are kept constant. The dimensionless simulating groups are given by equation (4.25). It is shown in Chapter 4 that the diameter ratio has a significant effect on the simulation errors. Accordingly we

start the simulation calculations at different diameter ratios ($1.5 \geq \frac{D_{\text{Freon}}}{D_{\text{water}}} \geq 0.55$) for each of the parameters investigated (i.e. F_{qa} , G_a , Cl and ΔH) using the computer programme SIMG2, (see page 10).

Figures (5.11) and (5.12) show the percentage R.M.S. error and the standard deviation versus the diameter ratio $\frac{D_{\text{Freon}}}{D_{\text{water}}}$ for runs 679.03 and 218.03 respectively. In general, it can be seen from Figures (5.11) and (5.12) that the errors are lower than the errors applying the previous model; Figures (4.13) and (4.14). Concerning the effect of the diameter ratio, although the trend is the same, for both models, nevertheless the diameter ratios at which the minimum error occur differ from one model to the other. While the diameter ratio for minimum error in model I is about 0.68, in model II it is about 0.98.

Applying model II, the minimum percentage R.M.S. error at diameter ratio 0.98 for each of the tested parameters F_{qa} , G_a , ΔH and Cl are 0.88, 0.76, 28.1 and 0.15 respectively. Also, the minimum percentage R.M.S. error for another run are 1.81, 0.72, 18.51 and 0.006 respectively (Table 5.4). For $24 \leq \Delta H \leq 108$, the percentage R.M.S. error is about 28. Decreasing this range to $50 \leq \Delta H \leq 108$ resulted in a decrease

in the percentage R.M.S. error to about 7% (Table (5.2)).

Figures (5.11e) and (5.12e) show ΔH as a variable parameter for the range of $50 \leq \Delta H \leq 108$ versus the diameter ratio for the burn-out runs 679.03 and 218.03, Thompson et al (1964).

TABLE 5.2

Run No. 679.03

| Figure | Parameter under Investigation | Minimum % RMS Error | Minimum Standard Deviation | Diameter Ratio for minimum % RMS & St.Dev. |
|--------|-------------------------------|---------------------|----------------------------|--|
| 5.11a | F_{qa} | 0.81 | 0.49×10^{-2} | 0.95 |
| 5.11b | G'_a | 0.76 | 0.21×10^{-2} | 0.93 |
| 5.11c | Cl | 0.15 | 0.04×10^{-2} | 0.98 |
| 5.11d | ΔH | 28.1 | 1.71×10^{-2} | 0.95 |
| 5.11e | ΔH for small range | 7.3 | 1.05×10^{-2} | 1.00 |

Run No. 218.03

| Figure | Parameter under Investigation | Minimum % RMS Error | Minimum Standard Deviation | Diameter Ratio for minimum % RMS & St.Dev. |
|--------|-------------------------------|---------------------|----------------------------|--|
| 5.12a | F_{qa} | 1.81 | 0.16×10^{-2} | 0.98 |
| 5.12b | G'_a | 0.72 | 0.093×10^{-2} | 0.98 |
| 5.12c | Cl | 0.006 | 0.0008×10^{-2} | 0.99 |
| 5.12d | ΔH | 18.51 | 1.45×10^{-2} | 0.95 |
| 5.12e | ΔH for small range | 6.75 | 0.78×10^{-2} | 1.15 |

Comparing Figures (4.13), (4.14) and Figures (5.11) and (5.12), it is clear that in model II the percentage R.M.S. error is less than that for model I at the same diameter ratio.

From these results it can be concluded that the triple-phase front movement for water can be simulated by Freon-12 with a small percentage R.M.S. error at diameter ratio of about 0.98. It has to be emphasised that the effect of the diameter ratio is small in model II.

To complete the investigation, the dimensionless triple-front speed (SP) for water and the simulating Freon-12 is calculated for the dimensionless groups π_1 , ψ_{CHF} , π_5 and Cl at diameter ratio 0.98 (see equations (4.25)). The water burn-out data for run 679.03, Thompson et al (1964), is used (Table (4.1)). The results are shown in Figures (5.8a, b, c and d). The percentage R.M.S. error and the condition under which each of the parameters is tested are given in Table (5.3).

TABLE 5.3

| Figure | Dimensionless Group | Parameter under test in this group | Simulation % R.M.S. |
|--------|--|---|---------------------|
| 5.8a | $\pi_1 = \frac{F_{qa}}{G'_a \cdot H_{fg}}$ | Surface Heat Flux (F_{qa}) For Water: $0.171 \times 10^6 \leq F_{qa} \leq 0.699 \times 10^6$ For Freon-12: $0.933 \times 10^5 \leq F_{qa} \leq 0.383 \times 10^5$ | 1.38 |
| 5.8b | $\psi_{CHF} = \frac{G'_a \cdot D \cdot \gamma^{\frac{1}{2}} \cdot \mu_l^{n_1}}{\mu_l \cdot D \cdot \rho_l^{\frac{1}{2}}} \cdot \left(\frac{\rho_l}{\rho_v}\right)^{n_2}$ | Mass Velocity (G'_a) For Water: $0.52 \times 10^6 \leq G'_a \leq 0.252 \times 10^7$ For Freon-12: $0.333 \times 10^6 \leq G'_a \leq 0.161 \times 10^7$ | 1.44 |

TABLE 5.3 (continued)

| Figure | Dimensionless Group | Parameter under test in this group | Simulation % R.M.S. |
|--------|-----------------------------------|--|---------------------|
| 5.8c | $\pi_5 = \frac{\Delta H}{H_{fg}}$ | Subcooling ΔH For Water: $24.8 \leq \Delta H \leq 108.0$ For Freon-12: $2.12 \leq \Delta H \leq 8.6$ | 28.3 |
| 5.8d | C1 | Dimensionless Wave Amplitude (C1) For Water and Freon-12 $0.04 \leq C1 \leq 0.64$ | 0.305 |

Different runs from Thompson et al (1964, runs 218.03 and 352.02, Table (5.4), were also tested and the results showed that the percentage R.M.S. error is always small, Figures (5.9) and (5.10).

TABLE 5.4

| Run 218.03 | Run 352.03 |
|--|--|
| $F_{qa} = 464000.0 \text{ Btu/h.ft}^2$ | $F_{qa} = 516500.0 \text{ Btu/h.ft}^2$ |
| $G_a = 1400000.0 \text{ lb/hr.ft}^2$ | $G_a = 870000.0 \text{ lb/hr.ft}^2$ |
| $\Delta H = 68.1 \text{ Btu/lb}$ | $\Delta H = 78.6 \text{ Btu/lb}$ |
| $D = 0.22 \text{ in.}$ | $D = 0.368 \text{ in.}$ |
| $L = 68.0 \text{ in.}$ | $L = 79.0 \text{ in.}$ |

In conclusion, accurate simulation of the triple front movement can be achieved using model II.

5.6 SIMULATION OF TRIPLE-PHASE FRONT APPLYING THE DIMENSIONLESS GROUPS DERIVED IN CHAPTER 2

The dimensionless groups derived for the annular flow model in Chapter 2 are used in simulating the triple-phase front speed. These groups are:

$$\pi_1 = \frac{F_{qa}}{H_{fg} \cdot \rho_l \cdot W_i}, \quad \psi_{CHF} = \frac{K_l}{D \cdot C_{pl} \cdot \rho_v \cdot W_i} \cdot \left(\frac{\gamma^{\frac{1}{2}} \cdot \mu_l^{n_1}}{D \cdot \rho_l^{\frac{1}{2}}} \right) \cdot \left(\frac{\mu_l}{\mu_v} \right)^{n_2}$$

$$\pi_5 = \frac{\Delta H}{H_{fg}}, \quad \pi_6 = \frac{\rho_l}{\rho_v}, \quad \pi_7 = \frac{L}{D}$$

When testing the effect of the diameter ratio on the simulation percentage R.M.S. error for each of the four variable parameters (F_{qa} , G_a , ΔH , Cl) it is found that the minimum errors occur at a diameter ratio 0.98. Figure (5.13) shows the dimensionless triple-phase front versus the above dimensionless groups π_1 , ψ_{CHF} , π_5 and the dimensionless wave celerity Cl at diameter ratio 0.98 for water and the simulating Freon-12.

The results also demonstrated here that simulation of the movement of the triple-phase front in the case of water at 1000 lb/in² and conditions as described in the runs 679.03 and 218.03 can be simulated by Freon-12 with a minimal percentage error.

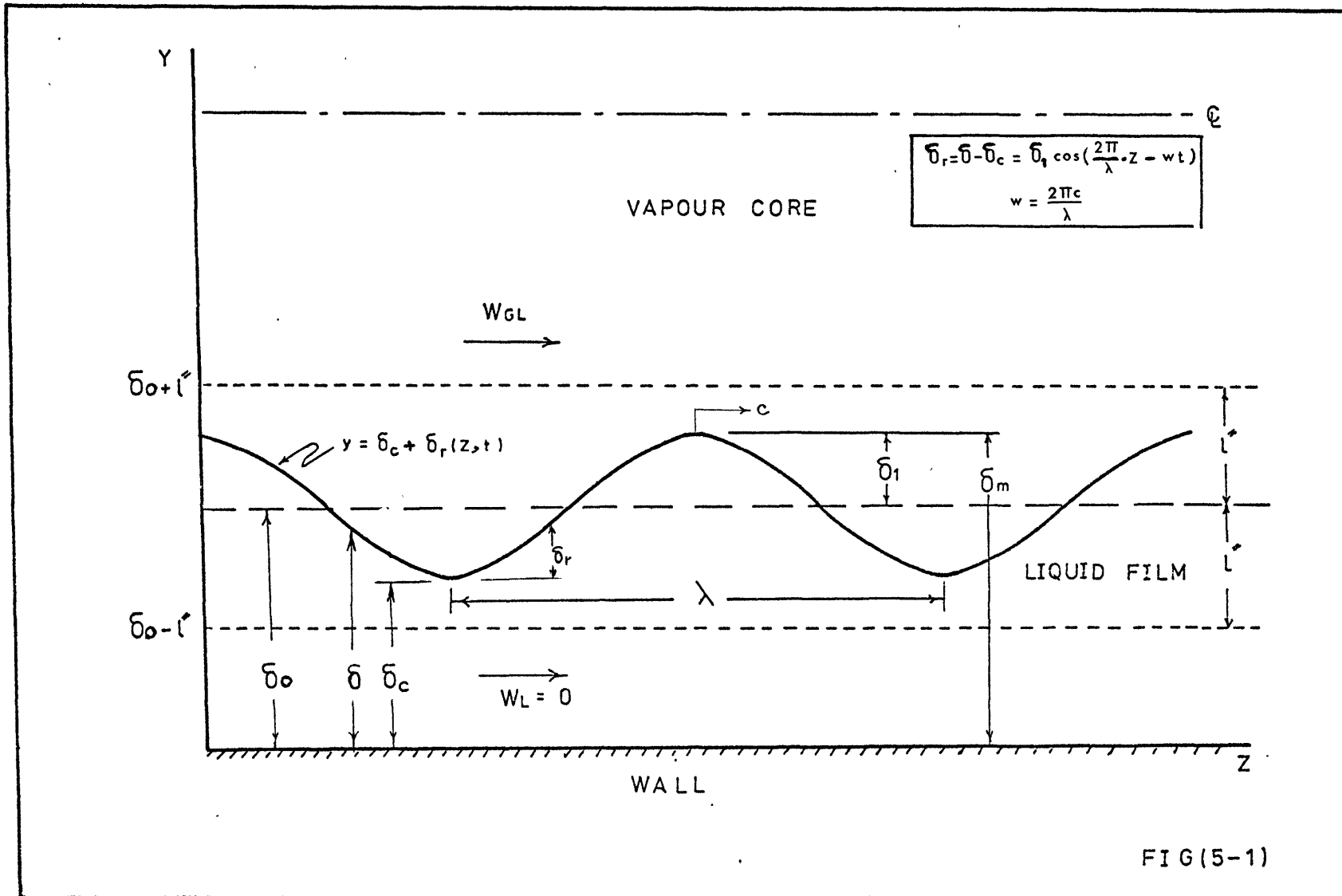


FIG (5-1)

Figure (5.2a): Interface triple-phase front position during two waves for different values of F_{qa} . Water at pressure = 1000 lb/in². Constant parameters: $G_a = 0.740 \times 10^6$ lb/h.ft²; $\Delta H = 72.8$ Btu/lb; $Cl = 0.4$. Contour line of: A) one wave period, B) two wave periods.

| | | | | |
|----|----------|---|---------------------|-----------------------|
| 1. | F_{qa} | = | 0.519×10^6 | Btu/h.ft ² |
| 2. | F_{qa} | = | 0.557×10^6 | Btu/h.ft ² |
| 3. | F_{qa} | = | 0.607×10^6 | Btu/h.ft ² |
| 4. | F_{qa} | = | 0.657×10^6 | Btu/h.ft ² |
| 5. | F_{qa} | = | 0.699×10^6 | Btu/h.ft ² |
| 6. | F_{qa} | = | 0.707×10^6 | Btu/h.ft ² |
| 7. | F_{qa} | = | 0.757×10^6 | Btu/h.ft ² |

Figure (5.2b): Interface triple front position during two waves for different values of G_a . Water at pressure = 1000 lb/in². Constant parameters: $F_{qa} = 0.6069 \times 10^6$ Btu/h.ft²; $\Delta H = 72.8$ Btu/lb; $Cl = 0.4$. Contour line of: A) one wave period, B) two wave periods.

| | | | | |
|----|-------|---|---------------------|----------------------|
| 1. | G_a | = | 0.574×10^6 | lb/h.ft ² |
| 2. | G_a | = | 0.605×10^6 | lb/h.ft ² |
| 3. | G_a | = | 0.628×10^6 | lb/h.ft ² |
| 4. | G_a | = | 0.646×10^6 | lb/h.ft ² |
| 5. | G_a | = | 0.688×10^6 | lb/h.ft ² |
| 6. | G_a | = | 0.730×10^6 | lb/h.ft ² |
| 7. | G_a | = | 0.771×10^6 | lb/h.ft ² |

INTERFACE TRIPLE FRONT POSITION DURING TWO WAVES

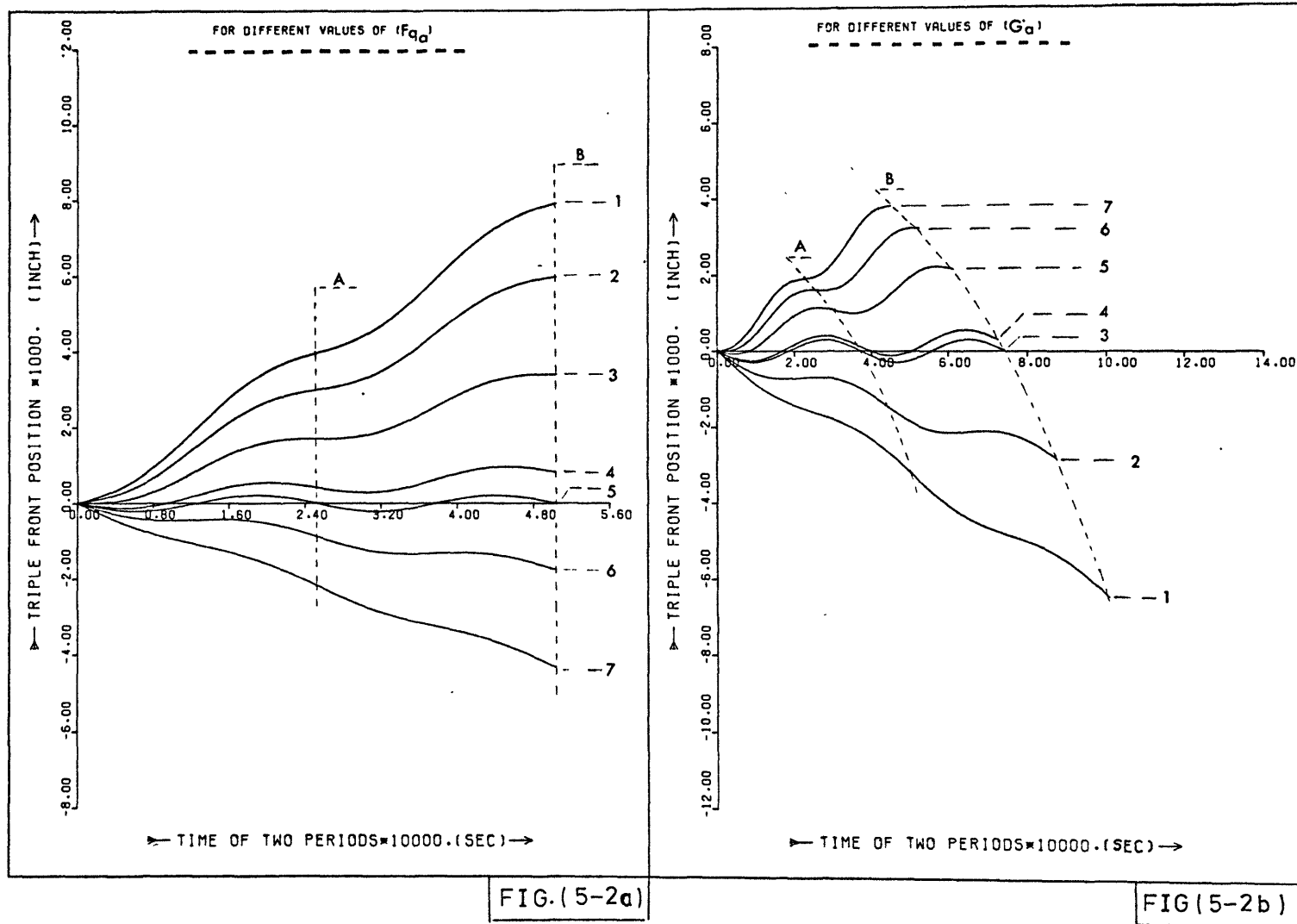


FIG. (5-2a)

FIG (5-2b)

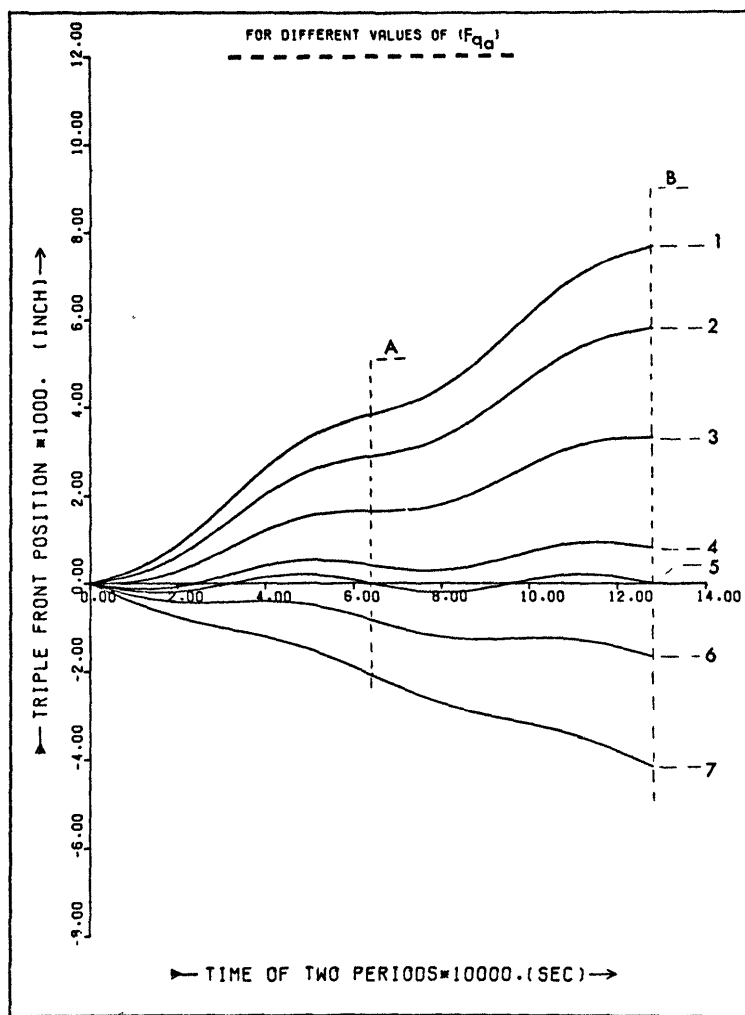
Figure (5.3a) Interface triple front position during two successive waves for different values of F_{qa} . Freon-12 at pressure = 155 lb/in². Constant parameters: $G'_a = 0.473 \times 10^6$ lb/h.ft²; $\Delta H = 6.21$ Btu/lb; $Cl = 0.4$. Contour line of: A) one wave period; B) two waves period.

| | | |
|----|------------------------------|-----------------------|
| 1. | $F_{qa} = 0.284 \times 10^5$ | Btu/h.ft ² |
| 2. | $F_{qa} = 0.304 \times 10^5$ | Btu/h.ft ² |
| 3. | $F_{qa} = 0.331 \times 10^5$ | Btu/h.ft ² |
| 4. | $F_{qa} = 0.359 \times 10^5$ | Btu/h.ft ² |
| 5. | $F_{qa} = 0.383 \times 10^5$ | Btu/h.ft ² |
| 6. | $F_{qa} = 0.386 \times 10^5$ | Btu/h.ft ² |
| 7. | $F_{qa} = 0.413 \times 10^5$ | Btu/h.ft ² |

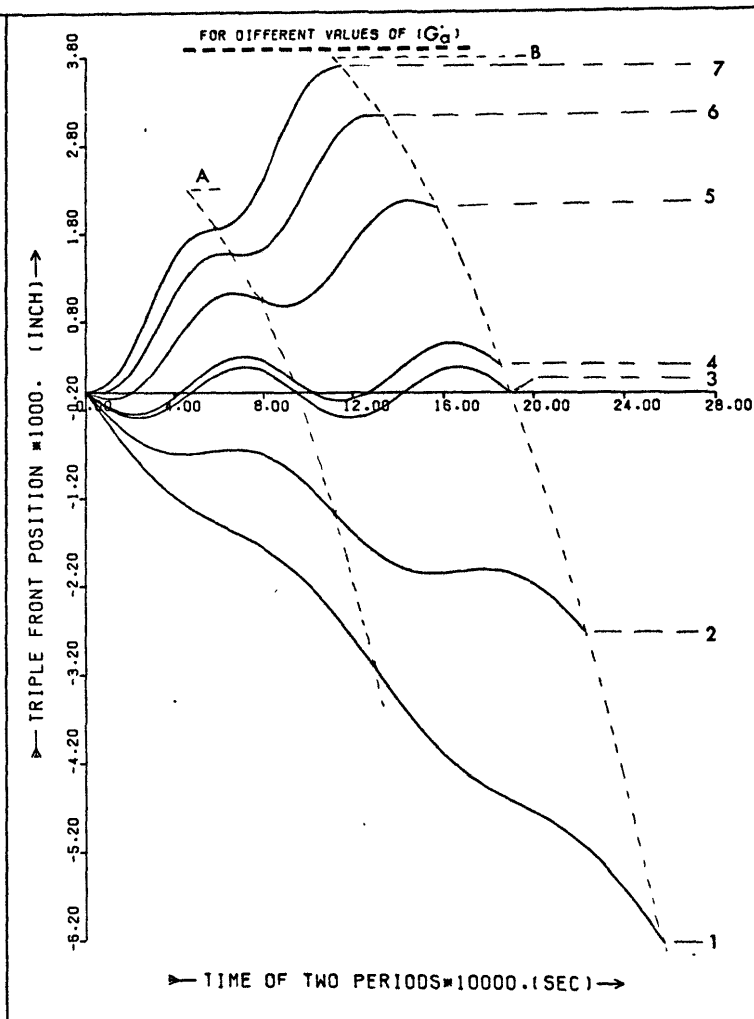
Figure (5.3b) Interface triple front position during two successive waves for different values of G'_a . Freon-12 at pressure = 155 lb/in². Constant parameters: $F_{qa} = 0.331 \times 10^5$ Btu/h.ft²; $\Delta H = 6.21$ Btu/lb; $Cl = 0.4$. Contour line of: A) one wave period; B) two waves period.

| | | |
|----|----------------------------|----------------------|
| 1. | $G'_a = 0.367 \times 10^6$ | lb/h.ft ² |
| 2. | $G'_a = 0.387 \times 10^6$ | lb/h.ft ² |
| 3. | $G'_a = 0.401 \times 10^6$ | lb/h.ft ² |
| 4. | $G'_a = 0.414 \times 10^6$ | lb/h.ft ² |
| 5. | $G'_a = 0.440 \times 10^6$ | lb/h.ft ² |
| 6. | $G'_a = 0.467 \times 10^6$ | lb/h.ft ² |
| 7. | $G'_a = 0.493 \times 10^6$ | lb/h.ft ² |

INTERFACE TRIPLE FRONT POSITION DURING TWO WAVES



FIG(5-3a)



FIG(5-3b)

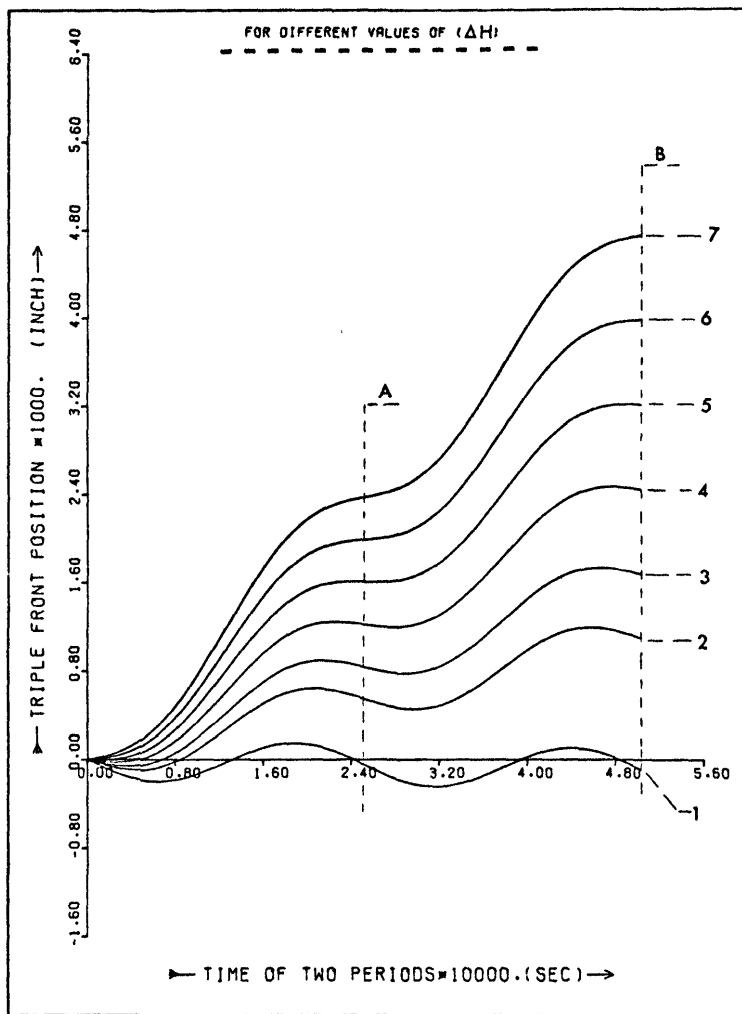
Figure (5.4a) Interface triple front position during two successive waves for different values of ΔH . Water at pressure = 1000 lb/in². Constant parameters: $F_{qa} = 0.6069 \times 10^6$ Btu/h.ft²; $G_a = 0.740 \times 10^6$ lb/h.ft²; $C1 = 0.4$. Contour line of: A) one wave period, B) two wave periods.

- | | | |
|----|--------------------|--------|
| 1. | $\Delta H = 0.0$ | Btu/lb |
| 2. | $\Delta H = 24.8$ | Btu/lb |
| 3. | $\Delta H = 36.8$ | Btu/lb |
| 4. | $\Delta H = 52.8$ | Btu/lb |
| 5. | $\Delta H = 68.8$ | Btu/lb |
| 6. | $\Delta H = 84.8$ | Btu/lb |
| 7. | $\Delta H = 100.8$ | Btu/lb |

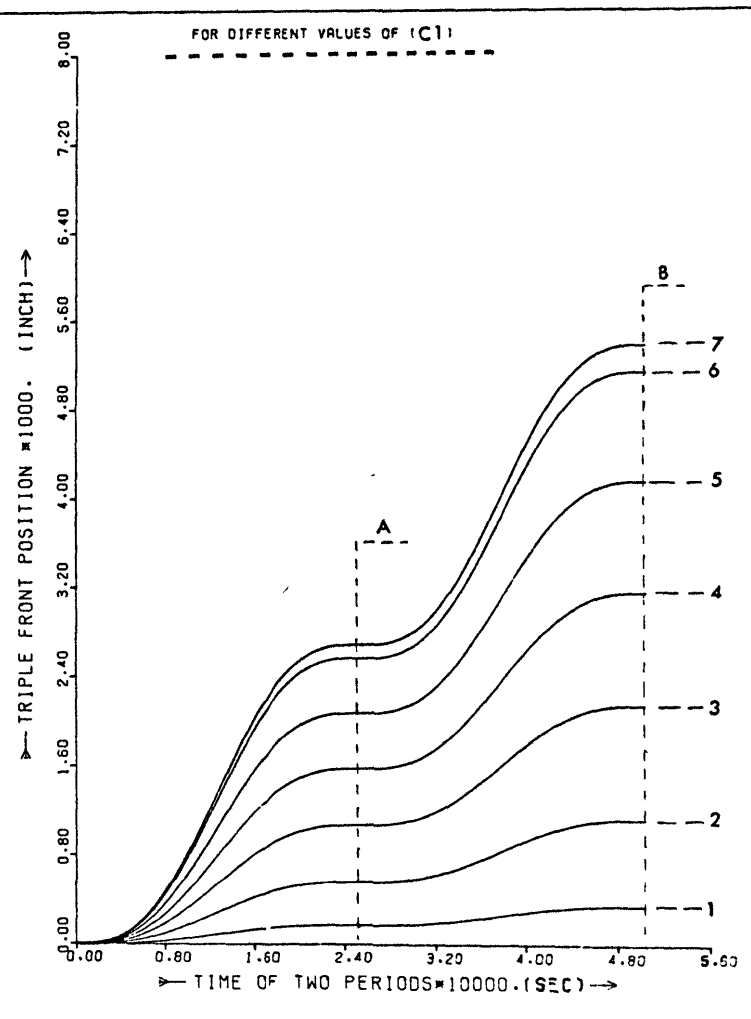
Figure (5.4b) Interface triple front position during two successive waves for different values of $C1$. Water at pressure 1000 lb/in². Constant parameters: $F_{qa} = 0.6069 \times 10^6$ Btu/h.ft²; $G_a = 0.740 \times 10^6$ lb/h.ft²; $\Delta H = 72.8$ Btu/lb. Contour line of: A) one wave period, B) two wave periods.

- | | |
|----|-------------|
| 1. | $C1 = 0.04$ |
| 2. | $C1 = 0.13$ |
| 3. | $C1 = 0.25$ |
| 4. | $C1 = 0.37$ |
| 5. | $C1 = 0.49$ |
| 6. | $C1 = 0.61$ |
| 7. | $C1 = 0.64$ |

INTERFACE TRIPLE FRONT POSITION DURING TWO WAVES



FIG(5-4a)



FIG(5-4b)

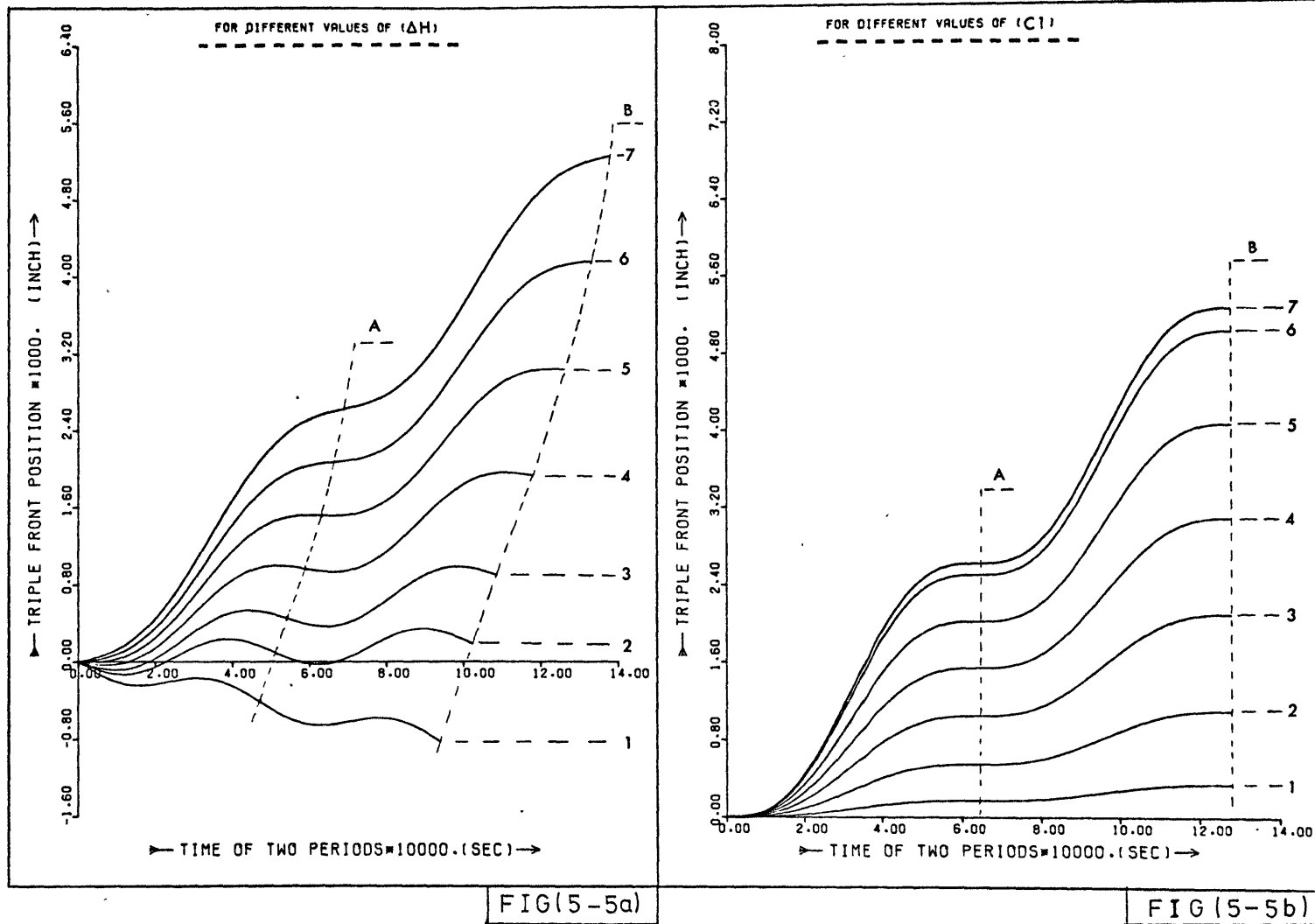
Figure(5.5a) Interface triple front position during two successive waves for different values of ΔH . Freon-12 at pressure = 155 lb/in². Constant parameters: $F_{ga} = 0.331 \times 10^5$ Btu/h.ft²; $G'_a = 0.473 \times 10^6$ lb/h.ft²; $C1 = 0.4$. Contour line of: A) one wave period; B) two waves period.

- | | | |
|----|-------------------|---------|
| 1. | $\Delta H = 0.0$ | Btu/lb. |
| 2. | $\Delta H = 2.12$ | Btu/lb. |
| 3. | $\Delta H = 3.14$ | Btu/lb. |
| 4. | $\Delta H = 4.50$ | Btu/lb. |
| 5. | $\Delta H = 5.87$ | Btu/lb. |
| 6. | $\Delta H = 7.24$ | Btu/lb. |
| 7. | $\Delta H = 8.60$ | Btu/lb. |

Figure(5.5b) Interface triple front position during two successive waves for different values of $C1$. Freon-12 at pressure = 155 lb/in². Constant parameters: $F_{ga} = 0.331 \times 10^5$ Btu/h.ft²; $G'_a = 0.473 \times 10^6$ lb/h.ft²; $\Delta H = 6.21$ Btu/lb. Contour line of: A) one wave period; B) two waves period.

- | | |
|----|-------------|
| 1. | $C1 = 0.04$ |
| 2. | $C1 = 0.13$ |
| 3. | $C1 = 0.25$ |
| 4. | $C1 = 0.37$ |
| 5. | $C1 = 0.49$ |
| 6. | $C1 = 0.61$ |
| 7. | $C1 = 0.64$ |

 INTERFACE TRIPLE FRONT POSITION DURING TWO WAVES



INTERFACE TRIPLE FRONT SPEED
VERSUS (QA,GA,C1,DELH)

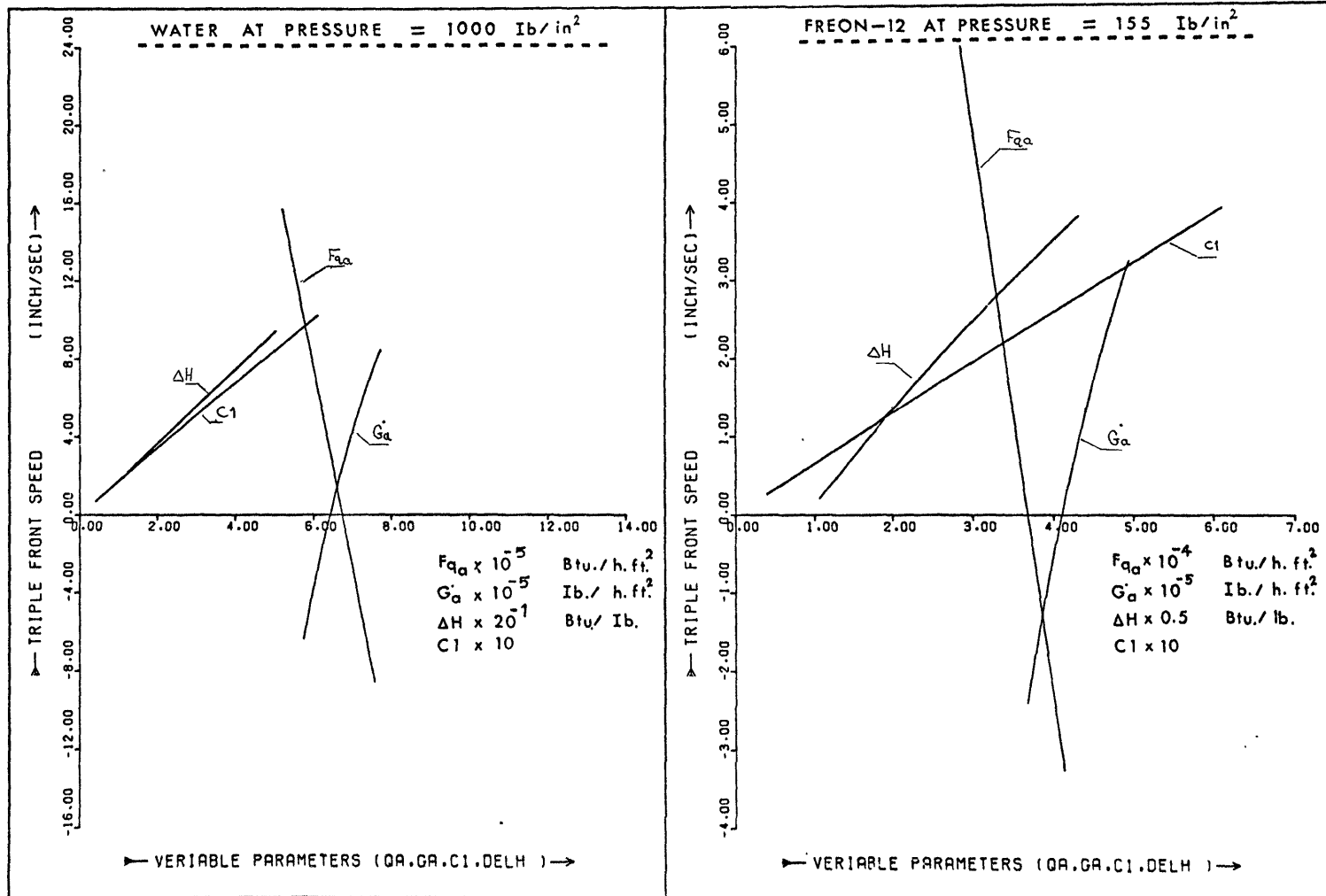


FIG (5-6a)

FIG(5-6b)

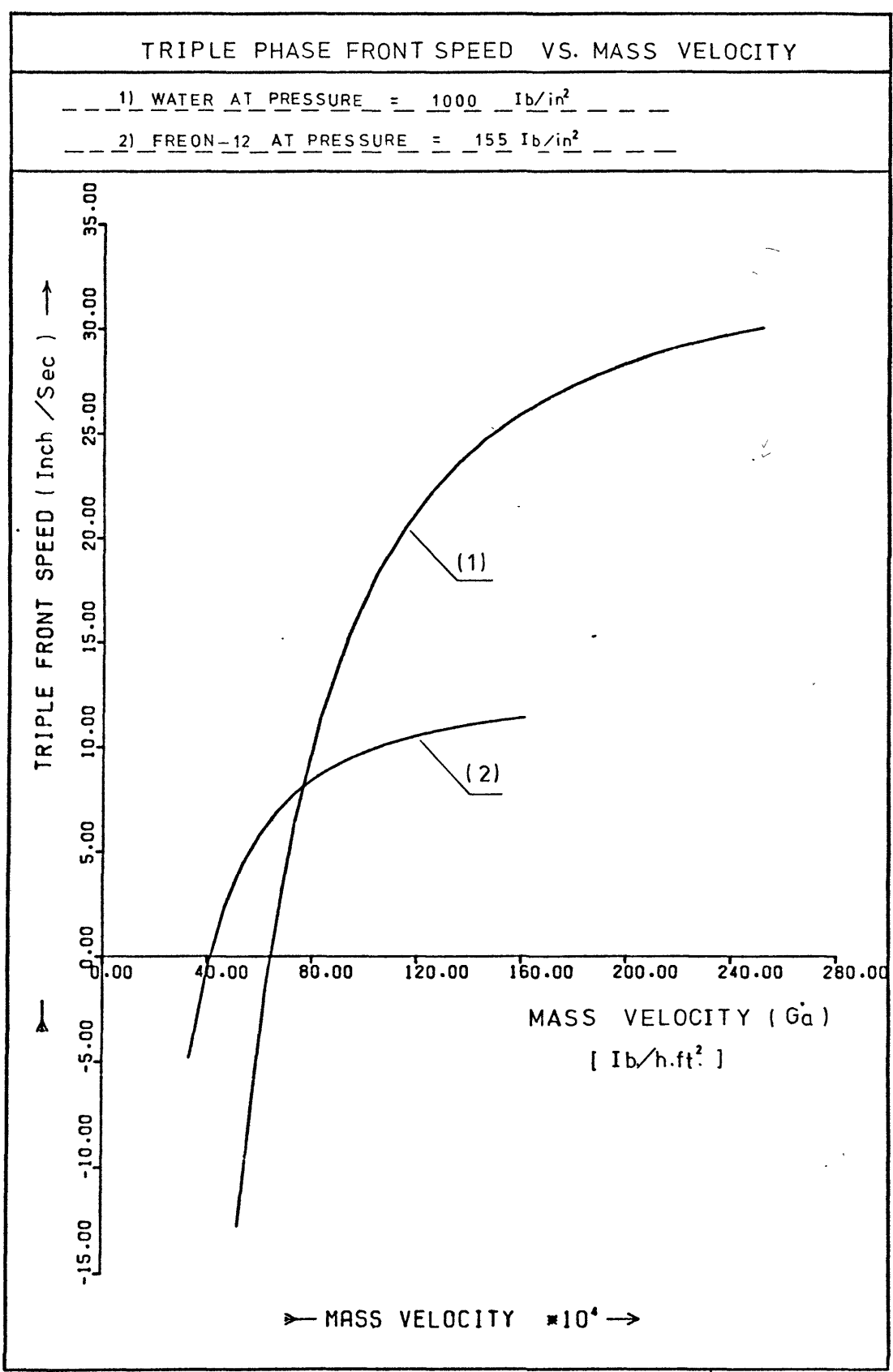
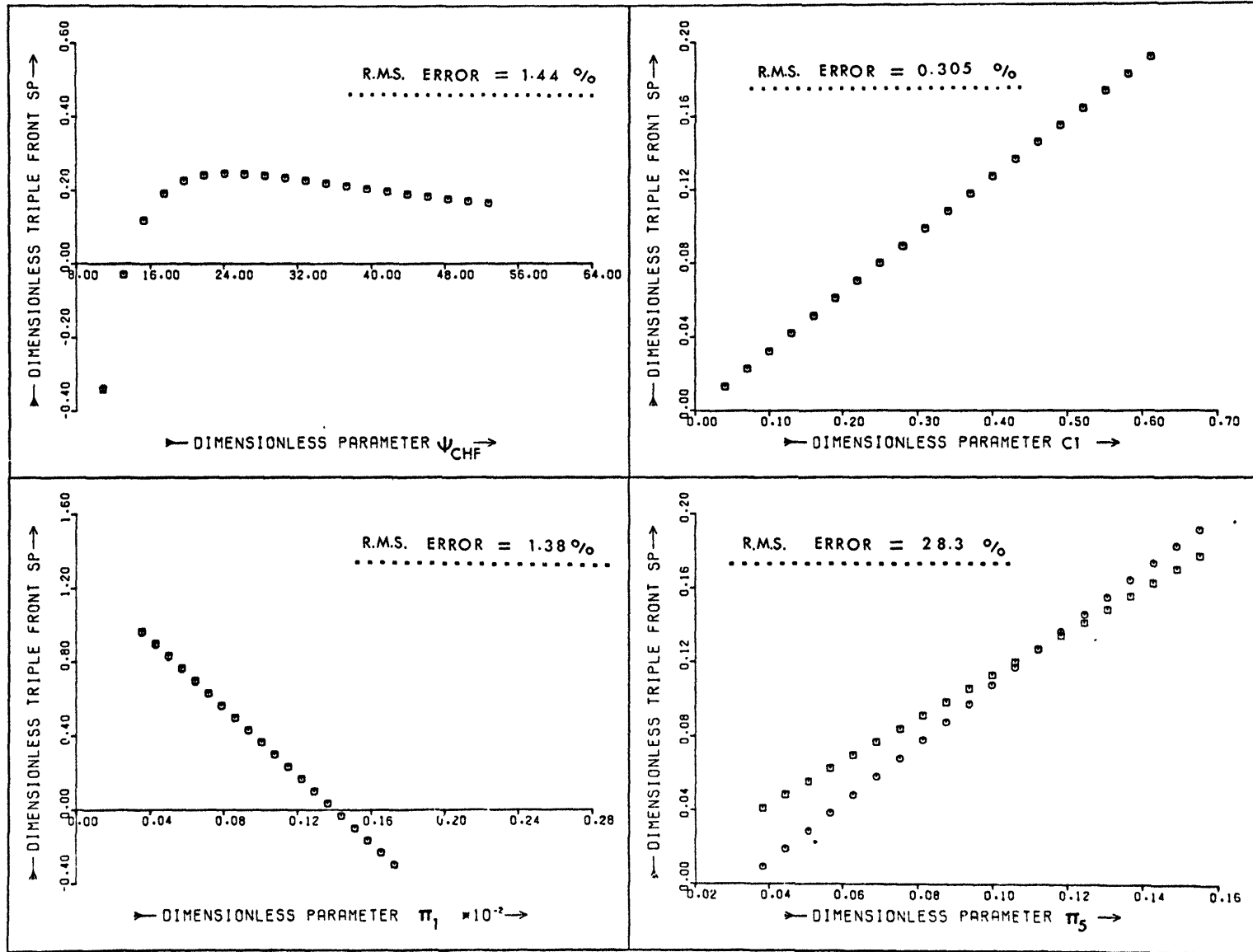


FIG (5-7)

DIMENSIONLESS PARAMETERS ($\pi_1, \psi_{CHF}, \pi_5, C_1$) VERSUS DIMENSIONLESS TRIPLE FRONT SPEED (SP)



DIMENSIONLESS PARAMETERS (π_1, ψ, π_5, C_i) VERSUS DIMENSIONLESS TRIPLE FRONT SPEED (SP)

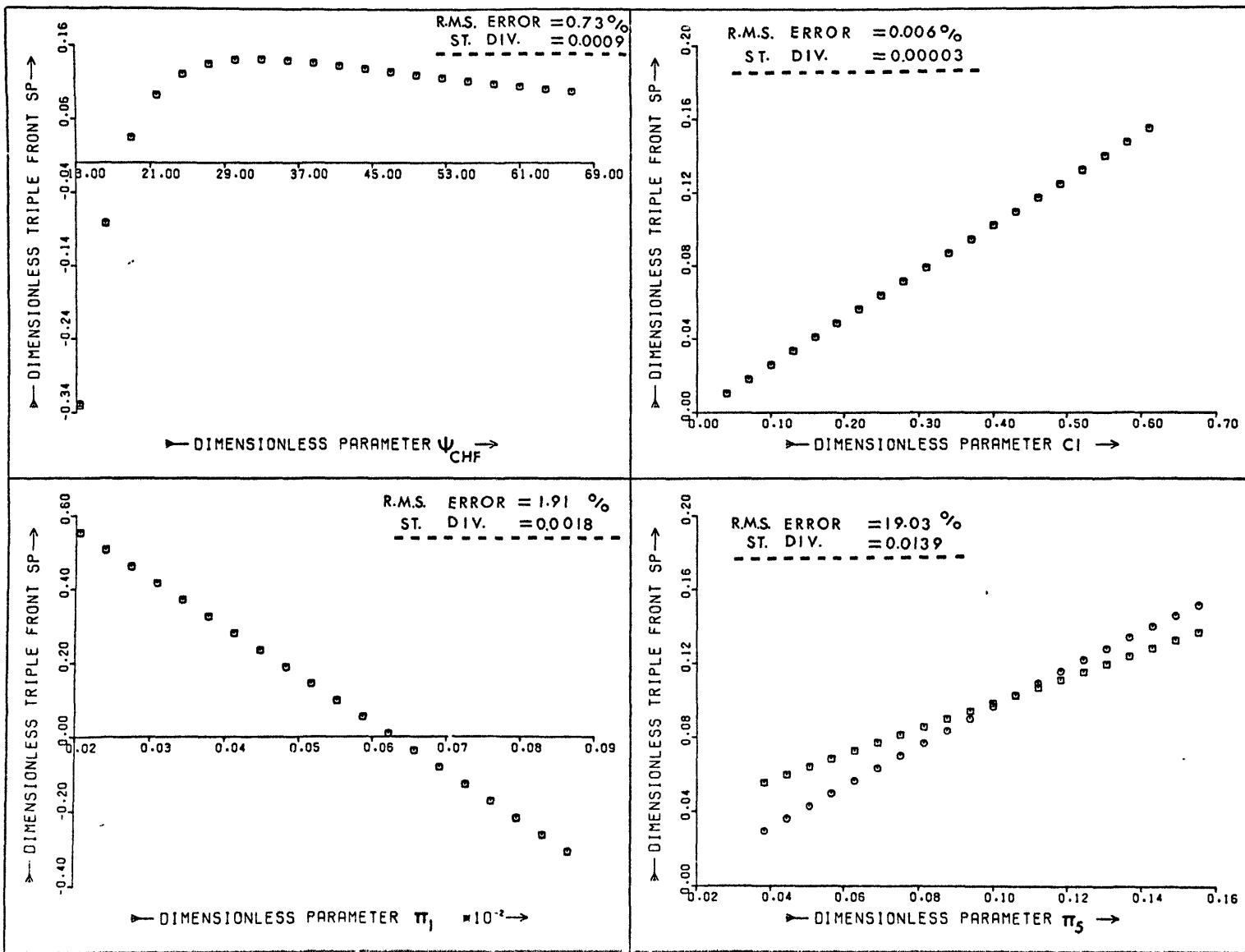
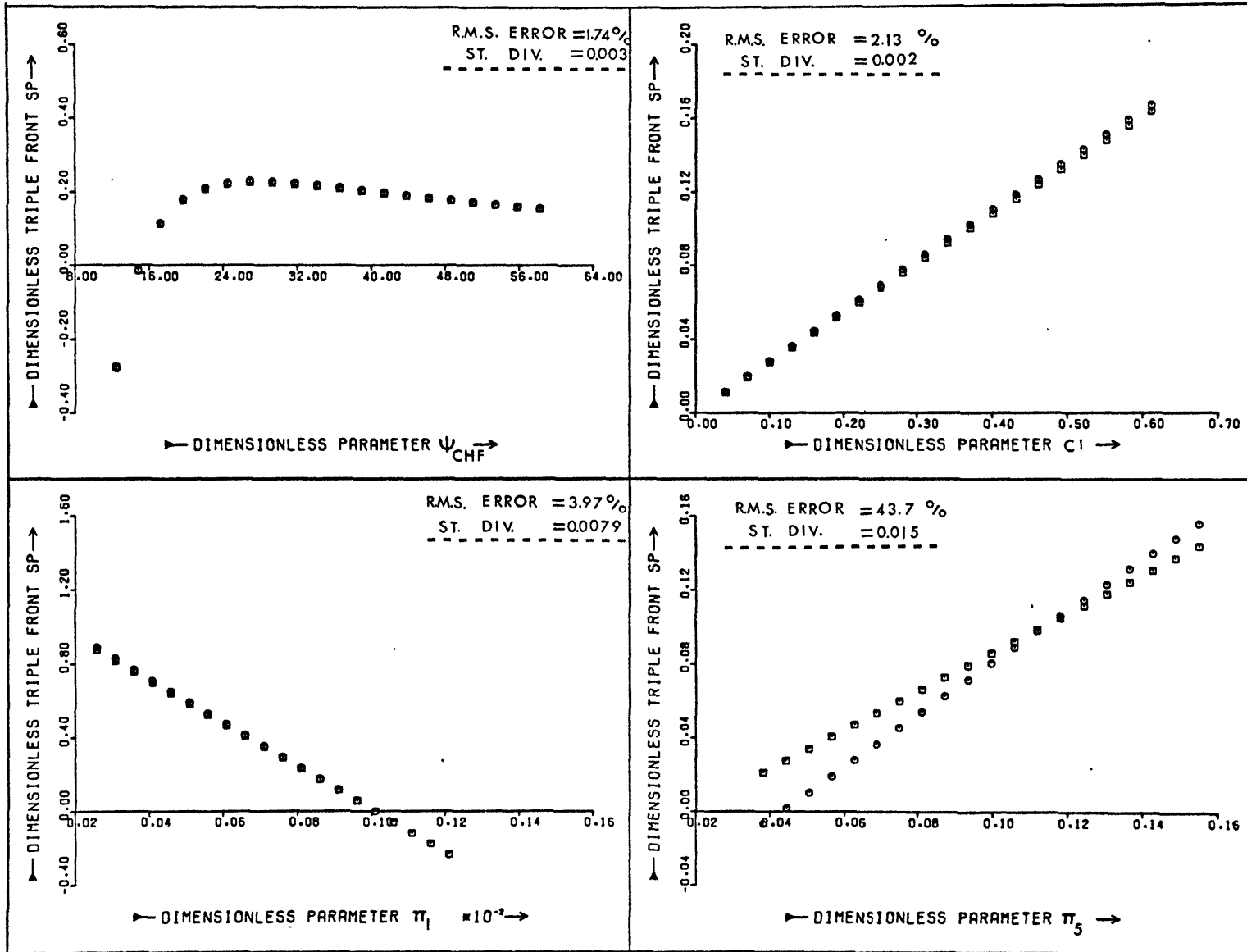
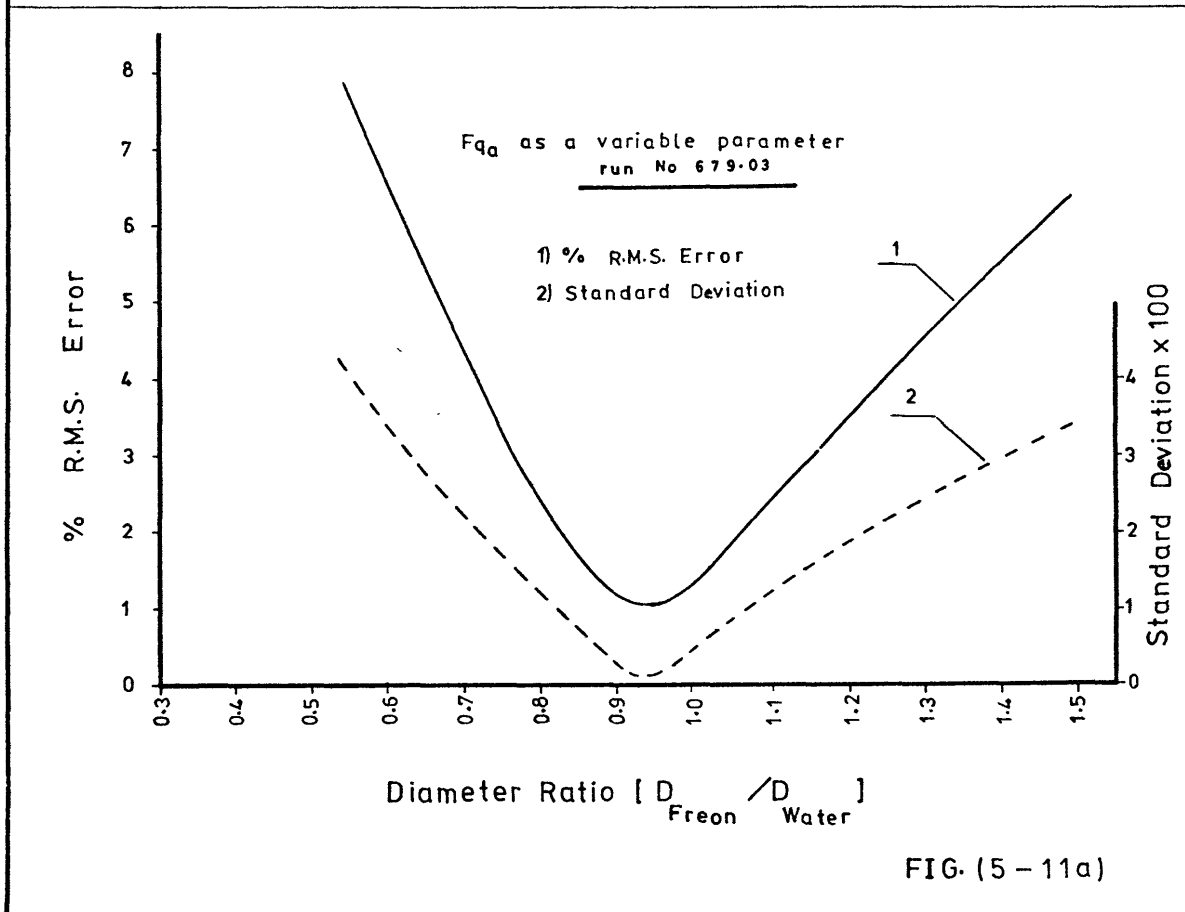
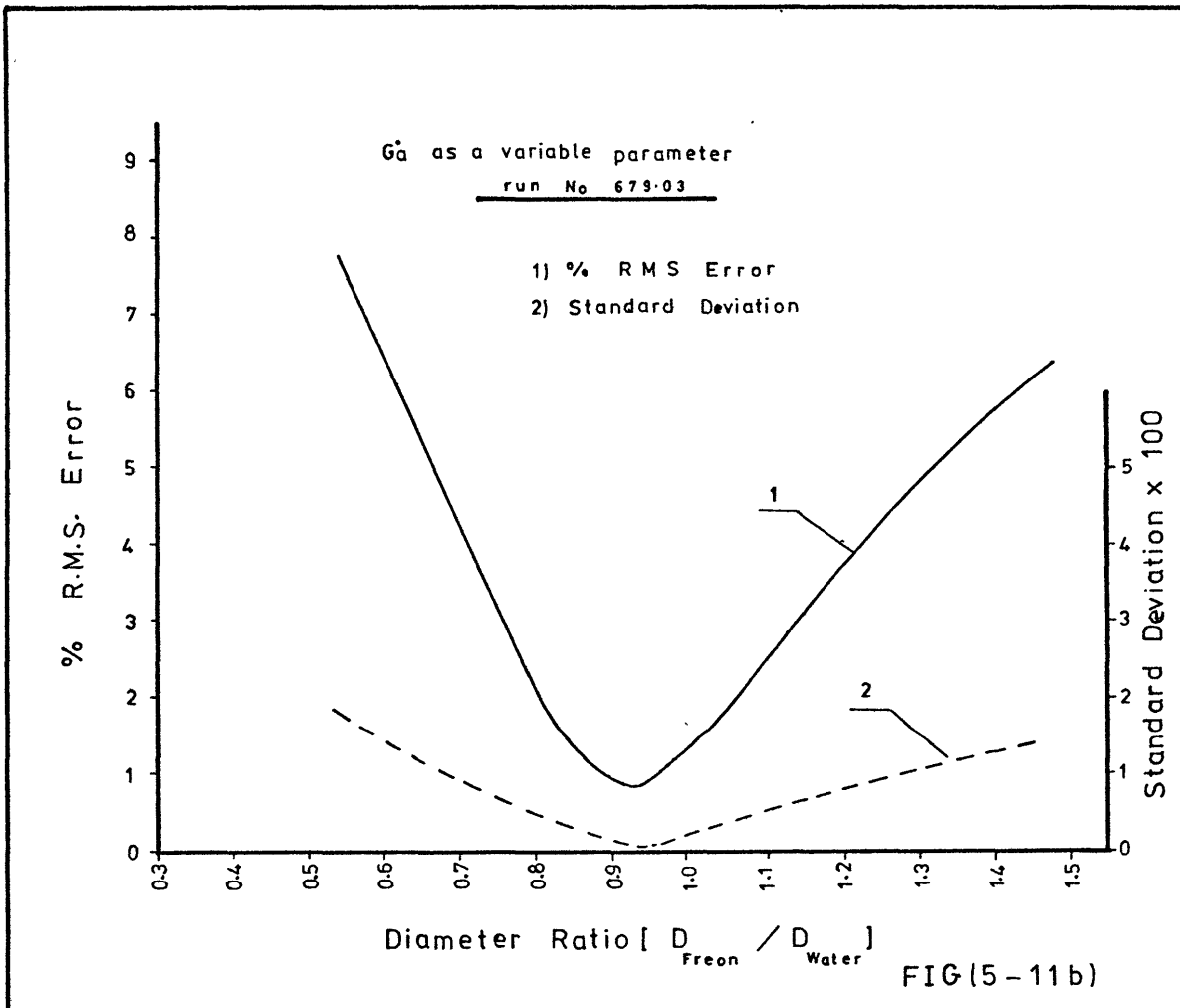


FIG (5-9)

DIMENSIONLESS PARAMETERS (π_1, ψ, π_5, C_1) VERSUS DIMENSIONLESS TRIPLE FRONT SPEED (SP)





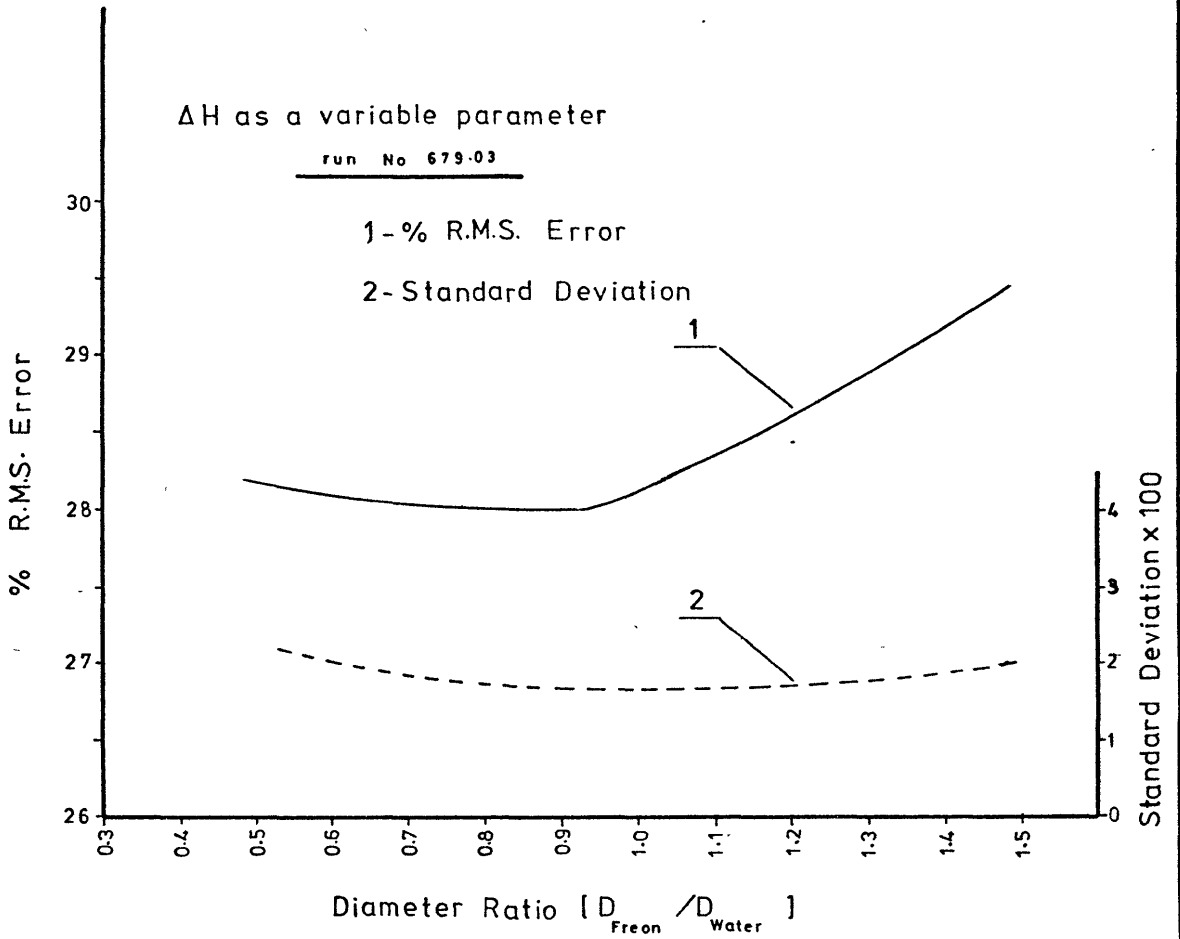


FIG (5-11d)

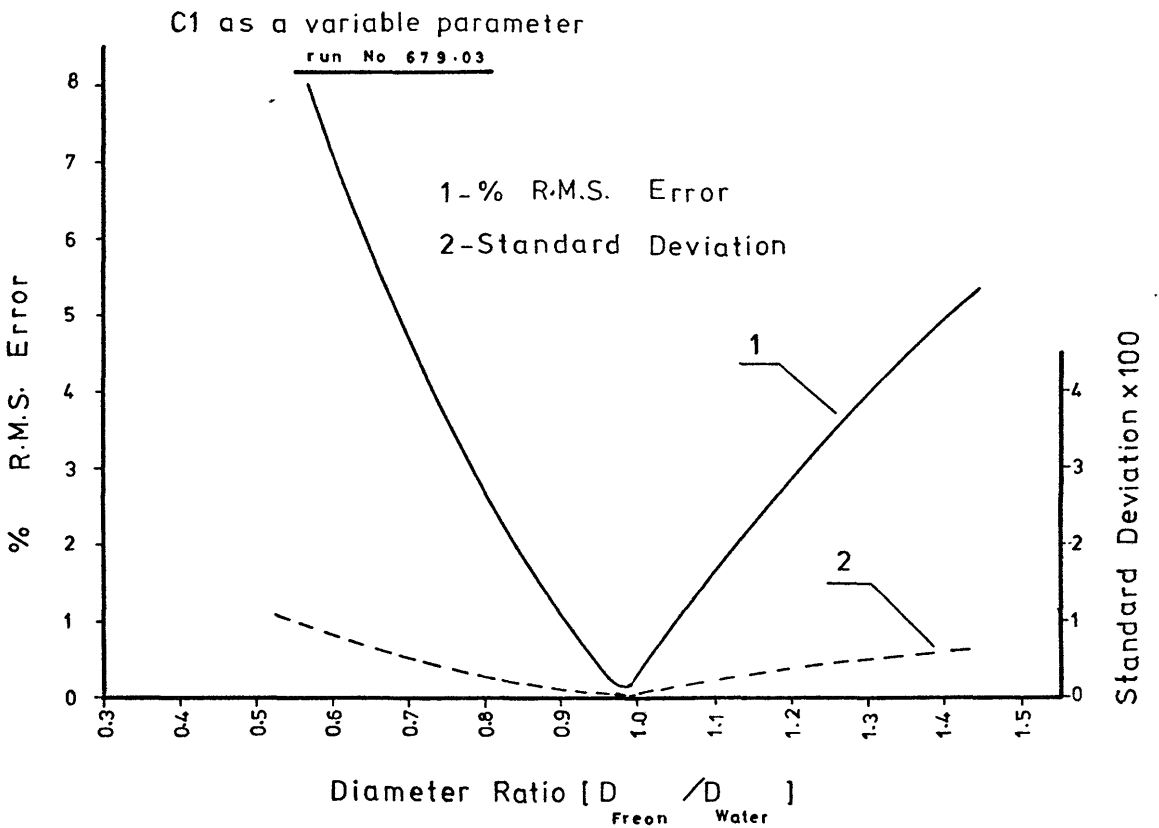
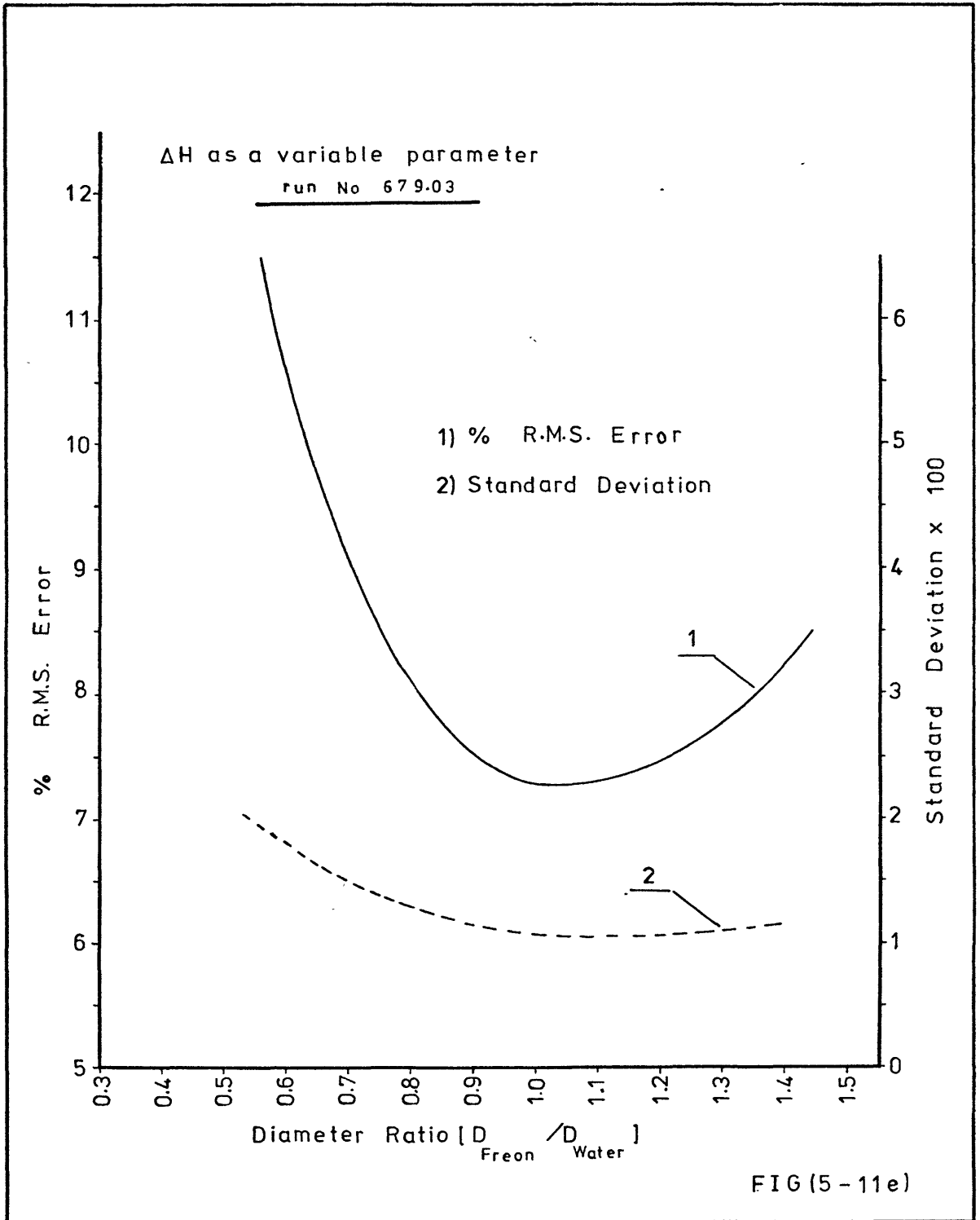


FIG. (5-11c)



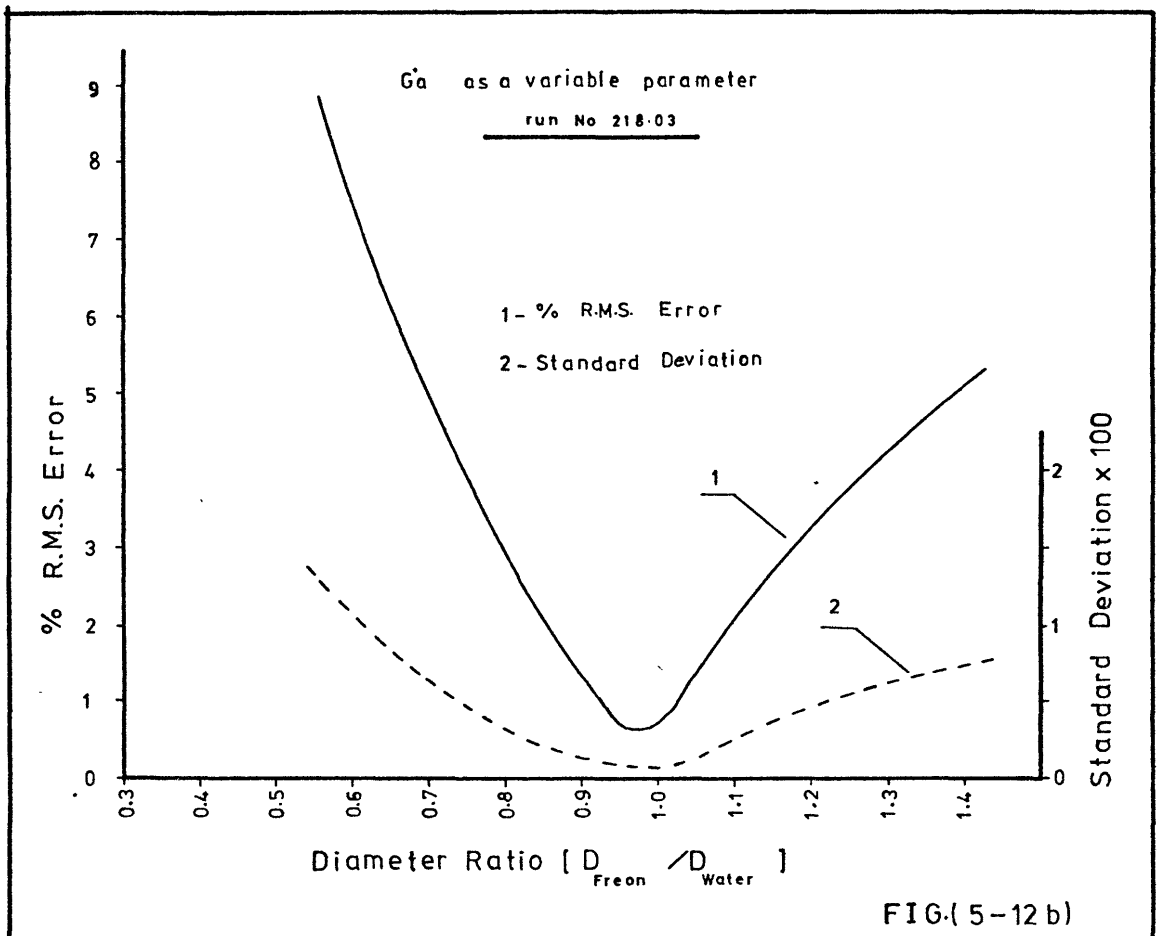


FIG.(5-12 b)

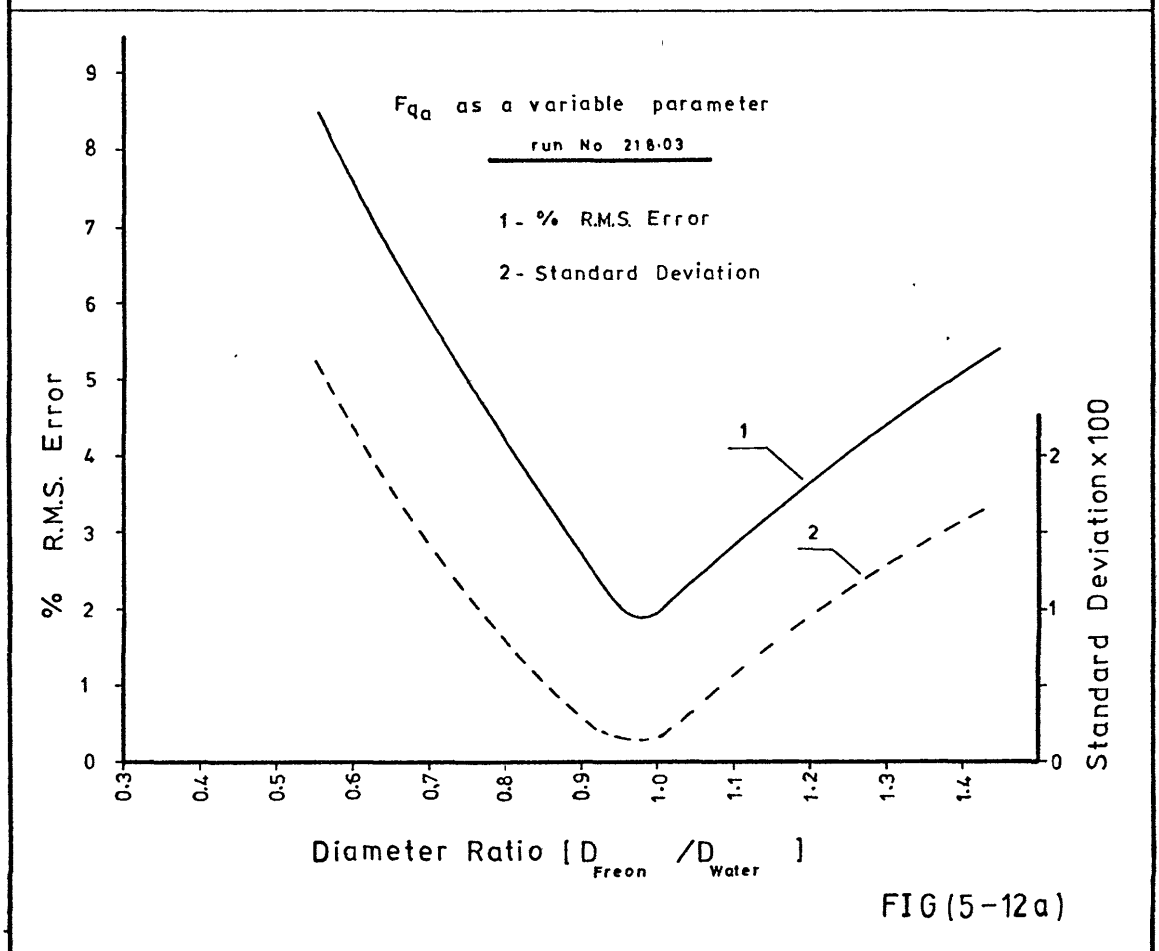
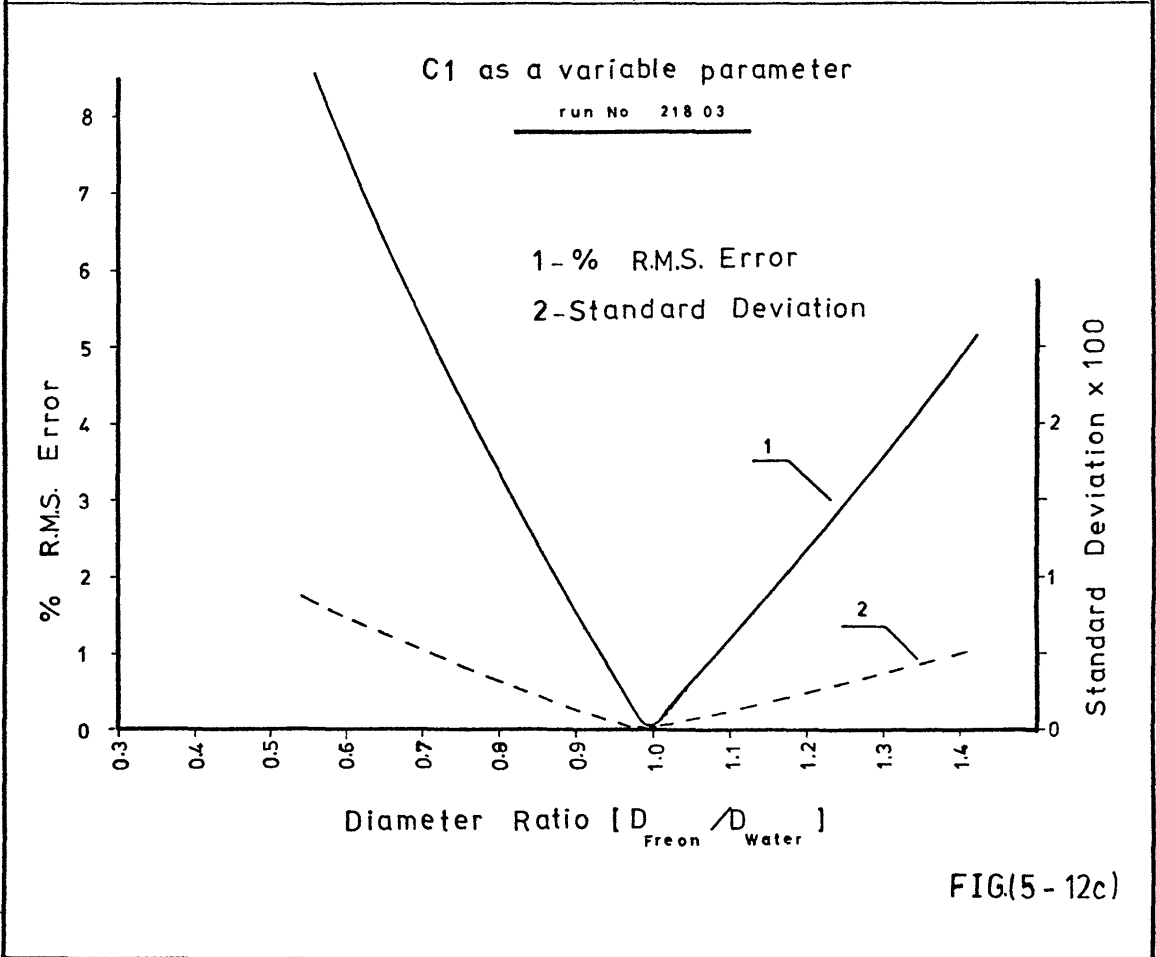
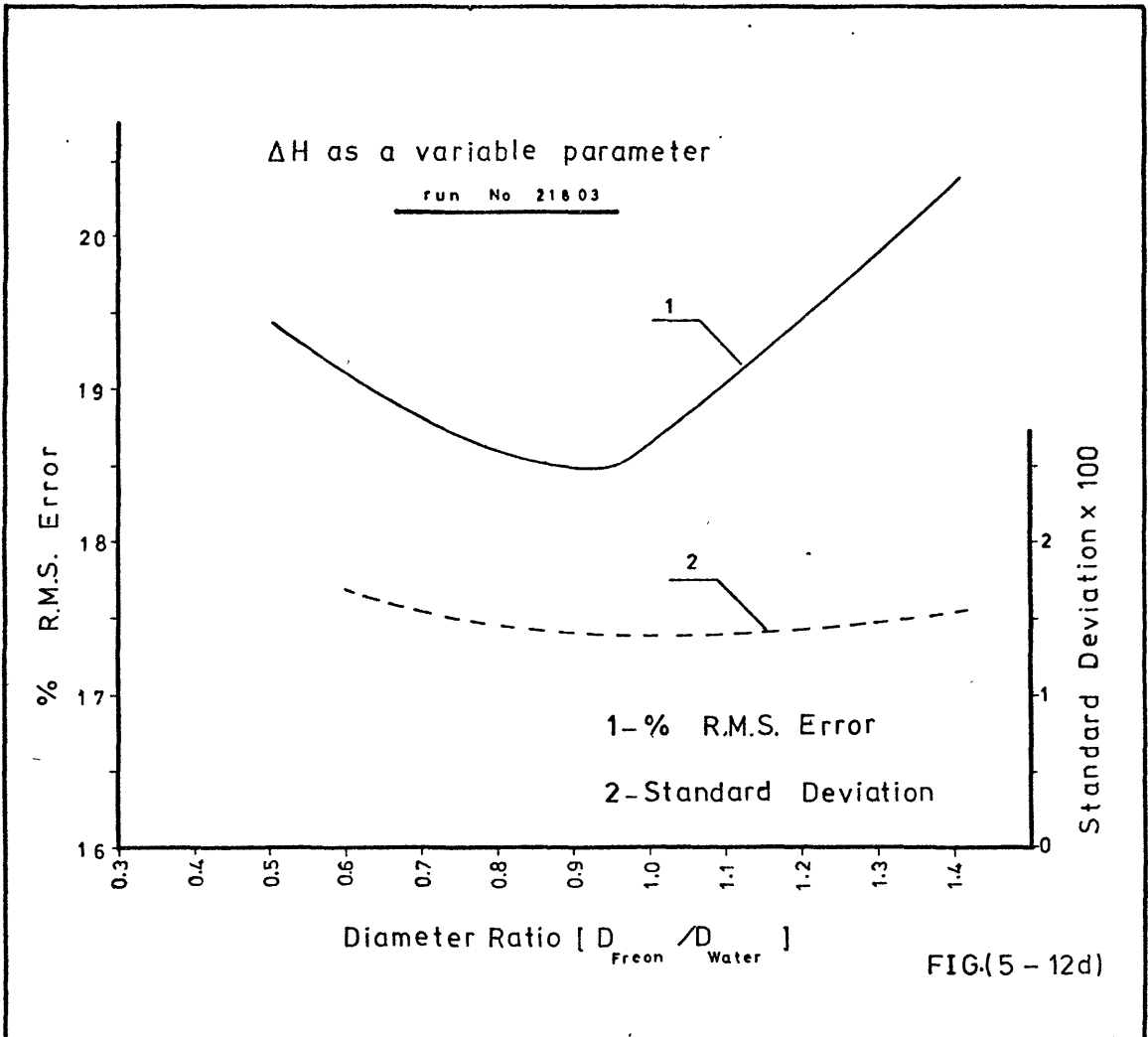
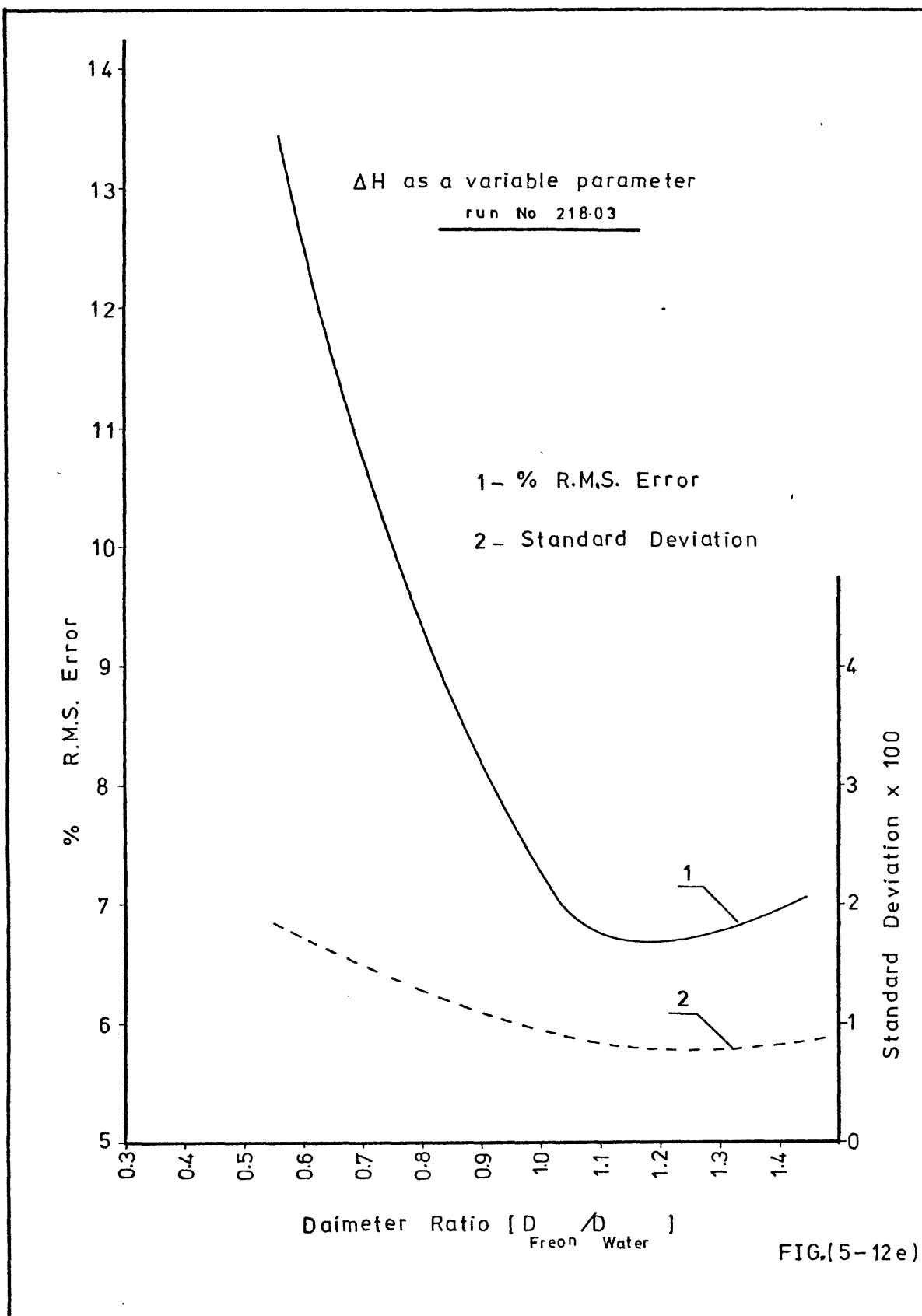
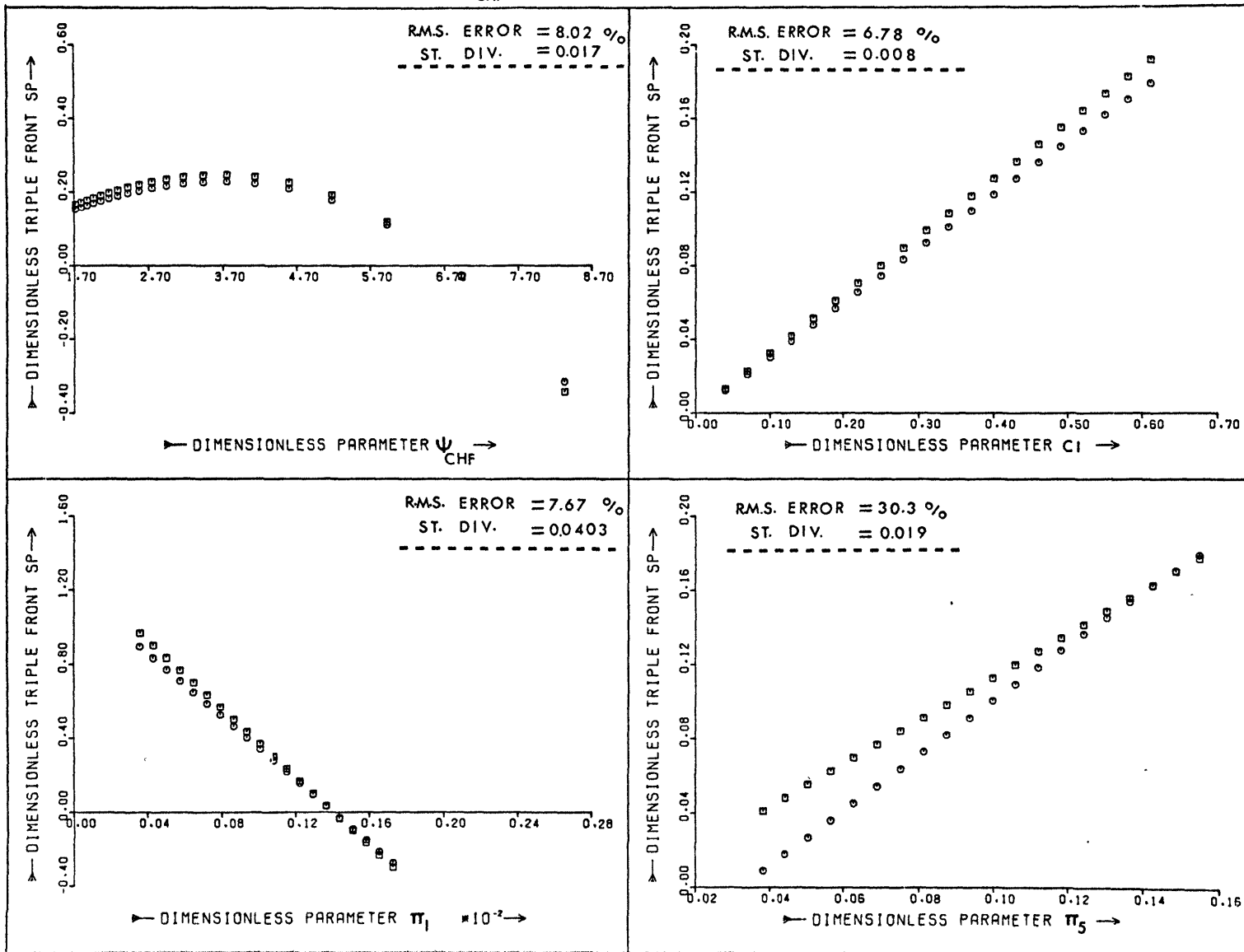


FIG (5-12a)





DIMENSIONLESS PARAMETERS (Ψ , C_1 , Π_1) VERSUS DIMENSIONLESS TRIPLE FRONT SPEED (SP)



CHAPTER 6

GENERAL CONCLUSIONS AND RECOMMENDATIONS

The present work is concerned with an investigation into methods of simulation of different burn-out and boiling phenomena in high pressure steam generators using Freon to simulate water. The conception of this simulation and modelling and a review of the relevant modelling techniques has been presented in Chapter 1. This showed that Barnett et al (1964) most consistent set is the one described by equation (1.1) by which errors in simulation were not likely to be reduced below +7%. To reduce this error Barnett suggested the inclusion of one of the following property groups: $(H_{fg} \cdot \gamma / \beta \cdot C_{pl})$, $(C_{pl} \cdot \sigma \gamma^{1/2} \cdot \rho_l^{1/2} / K_l)$ or $(\mu_l \cdot C_{pl} / K_l)$ to equation (1.1). This entails that the two property groups ρ_l / ρ_v and one of the above groups should be equal in the two systems. But this is not possible in Freon/water modelling.

It appears that the method used by Ahmad (1971) has proven to be promising in the development of the modelling procedure.

After reviewing previous work of other researchers on modelling in this field the author proposes in Chapter 2 a new extension of a technique previously reported by Ahmad

(1971) - the so-called "Distortion technique". As a demonstration, new correlations are produced by this technique from existing data and are shown to be an improvement on previous correlations based on the same data. It is noticed that applying Ahmad's dimensionless groups coupled with the present method of distortion achieves more favourable results (i.e. a R.M.S. error is in the order of 1%)^(that is insignificant with the error found practically) for simulation than applying Barnett's dimensionless groups (equations (2.1), (2.2) and (2.3)) which give an R.M.S. error of the order of 5% (i.e. Tables 2.3 and 2.4). Also, in Chapter 2 dimensionless groups developed from annular flow model are derived. The new distortion technique has been applied to these dimensionless groups in order to examine their accuracy in simulating burn-out in water by Freon. These groups showed a simulation R.M.S. error in the order of 20%. Including Barnett's (1964) group $(\gamma^{1/2} \cdot \mu_l / D \cdot \rho_l^{1/2})$ to the annular flow model groups reduced the R.M.S. error to nearly 3%. Thus Barnett's group proved to be a significant group in this model.

As a recommendation for future work in simulating boiling phenomena in a heated channel each boiling regime should be modelled separately. Hence, the influence of the dimensionless groups developed for each region can be carefully studied and analysed. This will determine the groups which

describe the various processes in each individual regime. These groups can then be shown alongside their respective regimes. Such a method of display can be used to determine the dimensionless groups which control the various mechanisms in the system as a whole.

It is also recommended that the developed groups should be used to simulate each individual regime in water by Freon. This will lead to more understanding of the factors that govern simulation. These groups can then be used to determine the length of each regime for water and Freon. By adding these lengths, the total length from subcooling up to burn-out of the heated tube for water can be predicted by Freon.

As an application of the previous recommendations, we have studied the annular flow regime. The compensating distortion technique is used for simulation and modelling of the rewetting of dry patches formed in motivated thin films flowing on heated surfaces. The interfacial surface waves on the film were considered and its effect on the motion of the triple-phase front was found. The characteristics of the surface waves of heated liquid film were studied in Chapter 3, while in Chapters 4 and 5 two mathematical models were developed to study the effect of interfacial waves on the

triple-phase front movement of a dry patch. The distortion technique was used to simulate the triple-phase front motion of water-steam by Freon. In Chapter 4, the percentage R.M.S. error at diameter ratio 0.68 varies from 0.05 to 7.5 (Table 4.3) depending on the parameter under consideration, e.g. F_{qa} , G_a , Cl or ΔH . The percentage R.M.S. error was found to be a function of the diameter ratio ($D_{\text{Freon}}/D_{\text{water}}$) and has a minimum value $\approx 4\%$ at diameter ratio equal to 0.68.

In Chapter 5, the values of wave length and celerity for two-phase flow model replaced the values of the single-phase ones in the model developed in Chapter 4. Moreover, the interface shear forces between the two-phases were considered. This resulted in a simulation percentage R.M.S. error less than those found using the method in Chapter 4. This is over a wide range of diameter ratio (i.e. $0.5 \leq D_{\text{Freon}}/D_{\text{water}} \leq 1.5$) (see Table 5.4). From these results it can be concluded^{theoretically} that the triple-phase front movement for water can be simulated by Freon-12 with a small percentage R.M.S. error.

A liquid-vapour Freon-113 closed loop has been designed (see Appendix 4), manufactured and constructed with the objective of providing additional validation of the simulation technique for burn-out and rewetting of a dry patch. It is recommended that this rig be used to investigate the

cooling of a hot rod and the interfacial waves characteristics of annular flow and to simulate the water data results given by previous researchers (e.g. Yamanouchi, 1968; Elliott et al, 1970 and 1971; Duffey et al, 1972 and 1973; Rogers et al, 1972; Piggott et al, 1973; Sun et al, 1974 and 1975; and Tien et al, 1975).

REFERENCES

ABI-ZADEH, D.

A Theoretical and Experimental Investigation of Thin Falling Films on Vertical Cylinders.

M.Sc. Thesis, Mech. Dept., Imperial College, University of London, 1972.

AHMAD, S.Y.

Fluid to Fluid Modelling of Critical Heat Flux: A Compensated Distortion Model.

Atomic Energy of Canada Ltd., AECL-3663, Clark River, Ontario, December 1971.

AHMAD, S.Y. and GROENEVELD, D.C.

Fluid Modelling of Critical Heat Flux in Uniformly Heated Annuli.

Atomic Energy of Canada Ltd., AECL-4070, January, 1972.

AHMAD, S.Y. and GROENEVELD, D.C.

Freon-12 C.H.F. Data for Uniformly Heated Tubes.

Atomic Energy of Canada Ltd., 1969.

AJAKAIYE, B.A.

An Investigation of the Change in Thickness of Liquid Films flowing down the Outside of a Vertical Cylinder.

M.Sc. Thesis, Mech. Dept., Imperial College, London, 1971.

ANDERSON, R. and PEJTERSEN, V.S.

A Critical Literature Study on Scaling Laws for Heat Transfer and Burn-Out in Two-Phase Flow with Special Reference to Boiling Water Reactors.

Danish Atomic Energy Commission Research Establishment, Risø Report No. 207, 1969.

BARNETT, P.G.

The Scaling of Forced Convection Boiling Heat Transfer.
U.K. Atomic Energy Authority, AEEW-R 134, 1963.

BARNETT, P.G.

An Experimental Investigation to determine the Scaling
Laws of Forced Convection Boiling Heat Transfer. Part 1:
The Preliminary Examination of Burnout Data for Water
and Arcton-12.

U.K. Atomic Energy Authority, AEEW-R 363, 1964.

BARNETT, P.G. and WOOD, R.W.

An Experimental Investigation to determine the Scaling Laws
of Forced Convection Boiling Heat Transfer. Part 2: An
Examination of Burnout Data for Water- Freon-12 and
Freon-21 in a Uniformly Heated Tube.

U.K. Atomic Energy Authority, AEEW-R 443, 1965.

BEHAR, M.

Burnout Scaling Laws Experimenta at High Pressures.
Symposium
Paper presented at Winfrith, U.K., June 1967.

BENJAMIN, T.B.

Wave Formation in Laminar Flow down an Inclined Plane.
J. Fluid Mech., Vol. 2, p. 554, 1957.

BERBENTE, C.P. and RUCKENSTEIN, E.

Hydrodynamics of Wave Flow.
A.I.Ch.E. J. , p. 772, September 1968.

BERBENTE, C.P. and RUCKENSTEIN, E.

Hydrodynamics of Wave Flow.
A.I.Ch.E. J. , p. 670, May 1971.

BIASI, L., CLERICI, G.C., GARRIBBA, S., SALA, R. and TOZZI, A.

Studies in Burnout, Part 3: A New Correlation for Round
Ducts and Uniform Heating and its Comparison with World Data.
Energia Nucleare, 14, No. 9, September 1967.

BINNIE, A.M.

The Stability of a Falling Sheet of Water.
Proc. R. Soc. London, A.326, p. 149, 1972.

BIRD, R.B., STEWART, W.E. and LIGHTFOOT, E.N.

Transport Phenomena.
Wiley, New York (1960).

BOURE, J.A.

A Method to Develop Similarity Laws for Two-phase Flows.
A.S.M.E. Paper No. 70-HT-25, 1971.

BUCKINGHAM, E.

On Physically Similar Systems - Illustrations of the Use
of Dimensional Equations.
Phys. Rev., Vol. IV, No. 4, p. 345, 1914.

COFFIELD, R.D.

A Subcooling D.N.B. Investigation of Freon-113 and its
Similarity to Subcooled Water D.N.B. Data.
Ph.D. Thesis in Mechanical Engineering Dept., University
of Pittsburgh, 1969.

COFFIELD, R.D. Jr., ROHRER, W.M. and TONG, L.S.

A Subcooled DNB Investigation of Freon-113 and its
Similarity to Subcooling Water DNB Data.
Nuclear Engineering and Design, No. 11, p. 143, 1969.

COLLIER, J.G.

Convective Boiling and Condensation.
McGraw-Hill Book Co. Ltd., (1972).

DAVIES, J.T.

The Importance of Surfaces in Chemical Engineering.
Trans. Inst. Chem. Engrs., Vol. 38, p. 289, 1960.

DAVIES, J.T., BELL, G. and LAW, P.J.S.

Spontaneous Emulsification Ripples on a Wetted Wall Column.
Research Project, Dept. Chem. Eng. Cambridge University, 1960.

DAVIES, J.T. and BRADLEY, P.J.

The Damping of Capillary Waves.
Research Project Dept. Chem. Eng. Cambridge University, 1960.

DEAN, R.A.

Effect of Vapour Injection on the Critical Heat Flux in a
Subcooled R-113 (Freon) Flow.
Ph.D. Thesis, University of Pittsburgh, 1970.

DIX, G.E.

Freon-Water Modelling of C.H.F. in Round Tubes.
A.S.M.E. Paper No. 70-HT-26, 1970.

DUCKLER, A.E.

Dynamics of Vertical Falling Liquid Films.
Chem. Eng. Progr. Vol. 55, No. 10, p. 62, 1959.

DUFFEY, R.B. and PORTHOUSE, D.T.C.

Experiments on the Cooling of High-Temperature Surfaces
by Water Jets and Drops.
Central Electricity Generating Board, RD/B/N2386, 1972.

DUFFEY, R.B. and PORTHOUSE, D.T.C.

The Physics of Rewetting in Water Reactor Emergency
Core Cooling.
Nuclear Engineering and Design, No. 25, p. 379, 1973.

EFFERDING, L.E., BISHOP, A.A. and TONG, L.S.

A Photographic Study of Nucleate Boiling and D.N.B. with
Freon-113 under Conditions of Flow and Pool Boiling on
Vertical Surfaces.
WCAP-2645, 1964.

EL-SHANAWANY, M.M.

The Flow of Heated Liquid Films with Special Reference to Dry-Out.

Ph.D. Thesis, University of London, 1974.

ELLIOTT, D.F. and ROSE, P.W.

The Quenching of a Heated Surface by a Film of Water in a Steam Environment at Pressure up to 53 Bar".

U.K. Atomic Energy Authority,
AEEW-M976, 1970.

ELLIOTT, D.F. and ROSE, P.W.

The Quenching of a Heated Zircaloy Surface by a Film of Water in a Steam Environment at Pressure up to 53 Bar".

U.K. Atomic Energy Authority,
AEEW-M1027, 1971.

FIRMAN, E.C., GARDNER, G.C. and CLAPP, R.M.

A Review of the Application of Boiling Heat Transfer Developments to Plant Problems.

The Inst. of Mechanical Engineers, Proc. Vol. 180,
Part 3C, 1965-66.

FRISK, D.P.

The Enhancement of Heat Transfer by Waves in Stratified Gas-Liquid Flow.

Clarkson College of Technology, (New York), Chem. Eng. Dept., June 1971.

FUJIE, H.

A Relation between Steam Quality and Void Fraction in Two-Phase Flow.

A.I.Ch.E. J. , p. 227, Vol. 10, No. 2, 1964.

GRIFFITH, P.

A Dimensional Analysis of the Departure from Nucleate Boiling Heat Flux in Forced Convection.

WAPD-TM-210, Westinghouse, Pittsburgh, 1959.

GROENEVELD, D.C.

Freon Dryout Correlations and their Applicability to Water.
Atomic Energy of Canada Ltd., Chalk River, Ontario,
September, 1969.

GROENEVELD, D.C.

Similarity of Water and Freon Dryout Data for Uniformly
Heated Tubes.

A.S.M.E. Paper No. 70-HT-27, 1970.

GUIDE AND DATA BOOK (ASHREA)

Chapter 6, p. 90 (1965).

HARTLEY, D.E. and MURGATROYD, W.

Criteria for the Break-up of Thin Liquid Layers Flowing
Isothermally over Solid Surface.

Int. J. Heat Mass Trans., Vol. 7, p. 1003, 1964.

HATTON, A.P. and WOOLLEY, N.H.

Laminar Combined Natural and Forced Convection in
Rectangular Field.

I. Mech. E. Symposium, 15th September, 1971.

HAUPTMANN, E.G., LEE, V. and MACADAM, D.W.

Two-Phase Fluid Modelling of the Critical Heat Flux.
Proc. 3rd Canadian Congress of Applied Mechanics,
p. 721, CACAM, Calgary, 1971.

HEWITT, G.F., BENNETT, A.W., KEARSEY, H.A. and KEEYS, R.K.F.

The Wetting of Hot Surfaces by Water in a Steam
Environment at High Pressure.

AERE-R 5146, 1966.

HEWITT, G.F. and TAYLOR, N.S.H.

Annular Two-Phase Flow.

Pergamon Press, p. 190, (1970).

HSU, Y.Y., SIMON, F.F. and LAD, J.F.

Destruction of a Thin Liquid Film flowing over a Heating Surface.

Chem. Eng. Progr. Symposium. Ser., 61, N. 57, p. 139, 1965.

JONES, L.O. and WHITAKER, L.S.

An Experimental Study of Falling Liquid Films.

A.I.Ch.E. J. , Vol. 12, p. 525, May 1966.

KAPITZA, P.L. and KAPITZA, S.P.

Waves Flowing in Thin Film of Viscous Liquids.

J. of Experimental Theoretical Physics, U.S.S.R., 18, 3, 1948.

KRANTZ, W.B. and SIMON, L.G.

Bimodal Wave Formation on Thin Liquid Films flowing down a Plane.

A.I.Ch.E.J., Vol. 17, No. 2, p. 494, 1971.

LANGHAAR, H.L.

Dimensional Analysis and Theory of Models.

John Wiley and Sons, New York (1967).

LEE, D.H. and OBERTELLI, J.D.

An Experimental Investigation of Forced Convection Burnout in High-Pressure Water. Part 1: Round Tubes with Uniform Flux Distribution.

U.K. Atomic Energy Authority,
AEEW-R213, 1963.

LEONG, C.Y.

An Investigation on the Characteristics of a Thin Liquid Film flowing freely down a Conical Surface.

M.Sc. Thesis, Mech. Eng. Dept., Imperial College, University of London, 1974.

LEVICH, V.G.

Motion and Diffusion in Thin Liquid Films.

Physico-Chemical Hydrodynamics, Prentice-Hall (1962).

LEVY, S.

Steam Slip-Theoretical Prediction from Momentum Model.
J. Heat Transfer (A.S.M.E. Trans.), p. 113, May 1960.

LOCKHART, R.W. and MARTINELLI, R.C.

Proposed Correlation of Data for Isothermal Two-Phase,
Two-Component Flow in Pipes.
Chem. Eng. Prog., Vol. 45, No. 1, 1949.

LUDVIKSSON, V. and LIGHTFOOT, E.N.

The Dynamics of Thin Liquid Films in the Presence of
Surface-Tension Gradients.
A.I.Ch.E. J. , Vol. 17, No. 5, p. 1166, September 1971.

MARIY, A.H., EL-SHIRBINI, A.A. and MURGATROYD, W.

The Effect of Waves on the Motion of the Triple-Phase
Front of a Dry Patch formed in a thin motivated Liquid Film.
Int. J. Heat Mass Transfer, No. 17, p. 1141, 1974.

MARTINELLI, R.C., NELSON, D.B. and SCHENECTADY, N.Y.

Prediction of Pressure Drop during Forced-Circulation
Boiling of Water.
Trans. A.S.M.E., p. 695, 1948.

MASSOT, C., IRANI, F. and LIGHTFOOT, E.N.

Modified Description of Wave Motion in a Falling Film.
A.I.Ch.E. Journal, Vol. 12, No. 3, p. 445, May 1966.

MATTSON, R.J.

A Photographic Study of Subcooled Flow Boiling and the
Boiling Crisis in Freon-113.
Ph.D. Thesis, University of Michigan, 1972.

MATTSON, R.J., HAMMITT, F.G. and TONG, L.S.

A Photographic Study of the Subcooled Flow Boiling
Crisis in Freon-113.
A.S.M.E. Paper No. 73-HT-39, 1974.

NARASIMHAN, T.V.

A Study of Surface Waves in Stratified Gas-Liquid Flow.
Clarkson College of Technology (N.Y.), Chem. Eng. Dept.,
June 1971.

NEWMAN, F.H. and SEARLE, V.M.L.

The General Principles of Matter.
4th Edition Arnold Press, London (1951).

NUSSELT, W.

The Surface Condensation of Steam.
Ver. Deut. Ingr. Z., Vol. 60, p. 541, 1916.

PAVRI, Y.N.

An Investigation of Thin Liquid Films flowing freely
down an Inclined Surface.
M.Sc. Thesis, Mech. Dept., Imperial College, University
of London, 1973.

PORTALSKI, S.

Eddy Formation in Film Flow down a Vertical Plate.
I & EC Fundamentals, Vol. 3, No. 1, February 1964.

PORTALSKI, S. and CLEGG, A.J.

An Experimental Study of Wave Inception on Falling Liquid
Films.
Chem. Eng. Science, Vol. 27, p. 1257, 1972.

PIGGOTT, B.D.G. and PORTHOUSE, D.T.C.

Water Reactor Emergency Core Cooling: The Effect of
Pressure, Subcooling and Surface Condition on the Rewetting
of Hot Surfaces.
Central Electricity Generating Board, RD/B/N2692, 1973.

REID, C.R. and SHERWOOD, T.K.

The Properties of Gasses and Liquids.
McGraw-Hill Book Company (1966).

ROGERS, A.E. and LEONARD, J.E.

An Analytical Model of the Transient Reactor Core Spray Cooling Process.

Chem Eng. Progr., Symposium Ser., No. 119, Vol. 67, 1972.

RUCKENSTEIN, E.

On the Break-Up of Thin Liquid Layers flowing along a Surface.

Int. J. Heat and Mass Transfer, No. 14, p. 165, 1971.

RUSHTON, E. and GRAHAM, A.D.

Linear Analysis of Liquid Film Flow.

A.I.Ch.E.J., p. 670, May 1971.

SCHLICHTING, H.

Boundary Layer Theory.

6th Edition, McGraw-Hill Book Company (1968).

SHAIR, F.H.

Dispersion in Laminar Flowing Liquid Films involving Heat Transfer and Interfacial Shear.

A.I.Ch.E.J., p. 920, Vol. 17, No. 4, 1971.

SHIRES, G.L., PICKERING, A.R. and BLAKER, P.T.

Film Cooling of Vertical Fuel Rods.

U.K. Atomic Energy Authority,

AEW-R 343, 1964.

SMITH, S.L.

Void Fraction in Two-Phase Flows: A Correlation based upon equal Velocity-Head Model.

Heat and Fluid Flow, No. 1, Vol. 1, 1971.

SOCIETE NATIONALE D'ETUDE ET DE CONSTRUCTION DE MOTEURS D'AVIATION

Influence of Centrifugal Twisted Tapes in Freon Burnout Flux.

Special Report No. 4, EURAEC-145, 1961.

STAINTHORP, F.P. and ALLEN, J.M.

The Development of Ripples on the Surface of a Liquid Film

flowing inside a Vertical Tube.

Trans. Inst. Chem. Eng. (London), Vol. 43, p. 85, 1965.

STANIFORTH, R. and STEVENS, G.F.

Experimental Studies of Burnout using Freon-12 at Low Pressure, with reference to Burnout in Water at High Pressure. Proc. Inst. Mech. Eng. (London), p. 180, PT 3C, 1965/66.

STAUB, F.W.

Two-Phase Fluid Modelling - the Critical Heat Flux. Nuclear Science and Engineering, 35, p. 190, 1969.

STEVENS, G.F. and KIRBY, G.J.

A Quantitative Comparison between Burnout Data for Water at 1000 psia and Freon-12 at 155 psia. Uniformly Heated Round Tubes, Vertical Upflow. U.K. Atomic Energy Authority, AEEW-R 327, 1964.

STEVENS, G.F., ELLIOTT, D.F. and WOOD, R.W.

An Experimental Investigation into Forced Convection Burnout in Freon, with reference to Burnout in Water. Uniformly Heated Round Tubes with Vertical Upflow. U.K. Atomic Energy Authority, Report AEEW-R 321, 1964.

STEVENS, G.F., ELLIOTT, D.F. and WOOD, R.W.

An Experimental Comparison between Forced Convection Burnout in Freon-12 Flowing Vertically upwards through Uniformly and non-Uniformly Heated Round Tubes. U.K. Atomic Energy Authority, AEEW-R 426, 1965.

STEVENS, G.F. and MACBETH, R.V.

The Use of Freon-12 to Model Forced Convection Burnout in Water: The Restriction on the Size of the Model. Paper No. 70-HT.20, A.S.M.E. Fluids and Heat Transfer Meeting, Detroit, Michigan, 1970.

SUN, K.H., DIX, G.E. and TIEN, C.L.

Cooling of a Very Hot Vertical Surface by Falling Liquid Film.
J. Heat Transfer, A.S.M.E., Vol. 96, Series C, No. 2, May 1974.

SUN, K.H., DIX, G.E. and TIEN, C.L.

Effect of Precursory Cooling of Falling-Film Rewetting.
A.S.M.E. Paper No. 74-WA/HT-52, 1975.

TAILBY, S.R. and PORTALSKY, S.

The Hydrodynamics of Liquid Films flowing on a Vertical
Surface.

Trans. Inst. Chem. Engrs., Vol. 40, p. 114, 1962.

TAYLOR, N.H.

The Motion and Frequency of Large Disturbance Waves in
Annular Two-Phase Flow of Air-Water Mixtures.

Chem. Eng. Sci., No. 18, p. 537, 1963.

THOMPSON, B. and MACBETH, R.V.

Boiling Water Heat Transfer Burnout in Uniformly Heated
Round Tubes. A Compilation of the World Data with
Accurate Correlations.

U.K. Atomic Energy Authority, AEEW-R 356, 1964.

THOMPSON, T.S. and MURGATROYD, W.

Stability and Breakdown of Liquid Films in Steam Flow
with Heat Transfer.

4th International Heat Transfer Conference, Versailles,
September 1970.

TIEN, C.L. and YAO, L.S.

Analysis of Conduction-Controlled Rewetting of a Vertical
Surface.

A.S.M.E., Paper No. 74-WA/HT-49, 1975.

TIPPETS, F.E.

Critical Heat Flux and Flow Pattern Characteristics of High Pressure Boiling Water in Forced Convection.

GEAP-3766, April 1962, Ph.D. Thesis, Stanford University.

TIPPETS, F.E.

Analysis of the Critical Heat-Flux Condition in High-Pressure Boiling Water Flows.

A.S.M.E. J. of Heat Transfer, February 1964.

TONG, L.S.

Boiling Heat Transfer and Two-Phase Flow.

John Wiley & Sons Inc., New York (1965).

TONG, L.S., MOTLEY, F.E. and CERMAK, J.O.

Scaling Law of Flow-Boiling Crisis.

4th Int. Heat Transfer Conf., Versailles, Paris, Vol. VI, p. B6.12, 1970.

TONG, L.S., EFFERDING, L.E. and BISHOP, A.A.

A Photographic Study of Subcooled Boiling Flow and D.N.B. of Freon-113 in a Vertical Channel.

A.S.M.E. Paper No. 66 WA/HT-39, 1966.

VOHR, J.H.

Flow Patterns of Two-Phase Flow - A Literature Survey.

TID-11514, 1960.

VOHR, J.H.

A Photographic Study of Boiling Flow.

NYO-9650, 1963.

WEDEKIND, G.L.

An Experimental Investigation into the Oscillatory Motion of the Mixture-Vapour Transition Point in Horizontal Evaporating Flow.

J. Heat Transfer (A.S.M.E. Trans.), p. 47, February 1971.

WEDEKIND, G.L. and STOECKER, W.F.

Theoretical Model for Predicting the Transient Response of the Mixture-Vapour Transition Point in a Horizontal Evaporating Flow.

J. Heat Transfer (A.S.M.E. Trans.), p. 165, February 1968.

YAMANOUCHI ATSUO

Effects of Core Spray Cooling at Stationary State after Loss of Coolant Accident.

J. Nuclear Science and Technology, No. 5, Vol. 9, p. 498, 1968.

YAMANOUCHI ATSUO

Effects of Core Spray Cooling in Transient State after Loss of Coolant Accident.

J. Nuclear Sci. and Technology, No. 5, Vol. 11, p. 547, 1968.

ZUBER, N. and STAUB, F.W.

Stability of Dry Patches forming in Liquid Films flowing over Heated Surfaces.

Int. J. Heat and Mass Transfer, Vol. 9, p. 897, 1966.

Mathematical Procedure in the Derivation
of Equations in Chapter 3

(a) The buoyancy term in equation (3.7 a) can be written as follows:

$$g\beta_s \frac{\delta_o}{W_o} (T-T_\infty) = g \frac{\beta_s \delta_o}{W_o} \{ (T-T_w) + (T_w-T_\infty) \}$$

Substituting for $(T-T_w)$ from equation (3.8) we get:

$$g\beta_s \frac{\delta_o}{W_o} (T-T_\infty) = g \frac{\beta_s \delta_o}{W_o} \left[F_{qa}^* \cdot T_{sat} \cdot \delta^* \left\{ \frac{1}{2} \left(\frac{Y^*}{\delta^*} \right)^3 - \frac{1}{8} \left(\frac{Y^*}{\delta^*} \right)^4 - \frac{Y^*}{\delta^*} \right\} + (T_w - T_\infty) \right]$$

$$\therefore g\beta_s \frac{\delta_o}{W_o} (T-T_\infty) = \frac{\beta_s \cdot F_{qa}^* \cdot \delta^* \cdot T_{sat}}{N_{Fr}^2} \left\{ \frac{1}{2} \left(\frac{Y^*}{\delta^*} \right)^3 - \frac{1}{8} \left(\frac{Y^*}{\delta^*} \right)^4 - \frac{Y^*}{\delta^*} \right\} + 16 \frac{Gr}{N_{Re}^2}$$

where $N_{Fr} = \frac{W_o}{\sqrt{g\delta_o}}$, $Gr = \frac{g\beta_s \delta_o^3 (T_w - T_\infty)}{v^2}$, $Re = \frac{W_o \delta_o}{v}$

$$N_{Re} = 4Re \text{ and } F_{qa}^{**} = F_{qa}^* \cdot \beta_s \cdot T_{sat}$$

$$\therefore g\beta_s \frac{\delta_o}{W_o} (T-T_\infty) = F_{qa}^{**} \cdot \frac{\delta^*}{N_{Fr}^2} \left\{ \frac{1}{2} \left(\frac{Y^*}{\delta^*} \right)^3 - \frac{1}{8} \left(\frac{Y^*}{\delta^*} \right)^4 - \frac{Y^*}{\delta^*} \right\} + 16 \frac{Gr}{N_{Re}^2}$$

(b) The following equations express the equality of the shear stresses and the equality of the normal stresses at the free surface, and were given by Berbente (1968) and Bird (1960):-

$$P_{zy} \cos 2\theta - \frac{1}{2}(P_{zz} - P_{yy}) \sin 2\theta = 0 \quad (I)$$

at $y = \delta$

$$P_{zz} \sin^2 \theta + P_{yy} \cos^2 \theta - P_{zy} \sin 2\theta + P_a + P_G = 0 \quad (II)$$

where

$$P_{zz} = -p + 2\mu \frac{\partial W}{\partial z}, \quad P_{yy} = -p + 2\mu \frac{\partial W}{\partial y}, \quad P_{zy} = \mu \left(\frac{\partial W}{\partial y} + \frac{\partial W}{\partial z} \right);$$

and P_G = the capillary pressure due to the curvature of the surface,

$$= -\sigma \frac{\partial^2 \delta}{\partial z^2} / \left\{ 1 + \left(\frac{\partial \delta}{\partial z} \right)^2 \right\}^{3/2};$$

$$\theta = \tan^{-1}(\partial \delta / \partial z);$$

P_a = ambient pressure.

By substituting the continuity equation (3.3) in equation (II), it becomes:

$$-P + P_a + P_G + 2\mu \frac{\partial W}{\partial z} (\sin^2 \theta - \cos^2 \theta) - \mu \left(\frac{\partial W}{\partial y} + \frac{\partial W}{\partial z} \right) \sin 2\theta = 0$$

where $-\cos 2\theta = \sin^2 \theta - \cos^2 \theta$.

$$\therefore -P + P_a + P_G - 2\mu \frac{\partial W}{\partial z} \cos 2\theta - \mu \left(\frac{\partial W}{\partial y} + \frac{\partial W}{\partial z} \right) \sin 2\theta = 0 \quad (III)$$

Similarly equation (I) can be reduced to:

$$\mu \left(\frac{\partial W_z}{\partial y} + \frac{\partial W_y}{\partial z} \right) \cos 2\theta - 2\mu \frac{\partial W_z}{\partial z} \sin 2\theta = 0$$

$$\therefore \mu \left(\frac{\partial W_z}{\partial y} + \frac{\partial W_y}{\partial z} \right) = 2\mu \frac{\partial W_z}{\partial z} \sin 2\theta / \cos 2\theta \quad (IV)$$

From (III) and (IV):

$$-P + P_a + P_\sigma - 2\mu \frac{\partial W_z}{\partial z} \cos 2\theta - 2\mu \frac{\partial W_z}{\partial z} \frac{\sin^2 2\theta}{\cos 2\theta} = 0$$

$$-P + P_a + P_\sigma - 2\mu \frac{\partial W_z}{\partial z} \left(\cos 2\theta + \frac{\sin^2 2\theta}{\cos 2\theta} \right) = 0$$

$$\therefore P - P_a = P_\sigma - \frac{2\mu}{\cos 2\theta} \frac{\partial W_z}{\partial z}$$

or $P - P_a = P_\sigma + (2\mu / \cos 2\theta) (\partial W_y / \partial y) \quad (V)$

P_a is the ambient pressure which may be taken as zero.

$$\text{Since } \tan \theta = \frac{\partial \delta}{\partial z}$$

$$\text{and } \cos 2\theta = \frac{1 - \tan^2 \theta}{1 + \tan^2 \theta} = \frac{1 - (\partial \delta / \partial z)^2}{1 + (\partial \delta / \partial z)^2}$$

equation (V) becomes:

$$P = P_\sigma + 2\mu \left[\frac{1 - (\partial \delta / \partial z)^2}{1 + (\partial \delta / \partial z)^2} \right] \frac{\partial W_y}{\partial y} \quad (VI)$$

Non-dimensionalising equation (VI) with the dimensionless terms in equation (3.5), substituting for the capillary pressure P_σ and $\cos 2\theta$, we get:

$$-\rho_l W_o^2 P^* - \frac{\sigma}{\left[1 + \frac{\delta_o^2}{\lambda^2} \left(\frac{\partial \delta^*}{\partial z^*} \right)^2 \right]^{3/2}} \cdot \frac{\delta_o}{\lambda^2} \cdot \frac{\partial^2 \delta^*}{\partial z^{*2}} + 2\mu.$$

$$\left[\frac{1 + (\delta_o^2 / \lambda^2) (\partial \delta^* / \partial z^*)^2}{1 - (\delta_o^2 / \lambda^2) (\partial \delta^* / \partial z^*)^2} \right] \frac{W_o \cdot \partial V}{\lambda \partial Y^*} = 0 \quad (VII)$$

where

$$P_{\sigma} = - \frac{\sigma}{\left[1 + \left(\frac{\partial \delta}{\partial z}\right)^2\right]^{3/2}} \cdot \frac{\partial^2 \delta}{\partial z^2}$$

$$= - \frac{\sigma}{\left[1 + \frac{\delta_o^2}{\lambda^2} \left(\frac{\partial \delta^*}{\partial z^*}\right)^2\right]^{3/2}} \cdot \frac{\delta_o}{\lambda^2} \cdot \frac{\partial^2 \delta^*}{\partial z^{*2}}$$

$$\cos 2\theta = \frac{1 - \tan^2 \theta}{1 + \tan^2 \theta} = \frac{1 - (\partial \delta / \partial z)^2}{1 + (\partial \delta / \partial z)^2}$$

$$= \frac{1 - (\delta_o^2 / \lambda^2) \cdot (\partial \delta^* / \partial z^*)^2}{1 + (\delta_o^2 / \lambda^2) \cdot (\partial \delta^* / \partial z^*)^2}$$

Substituting ξ (i.e. = δ_o / λ) and dividing by $\rho_{\ell} W_o^2$ in equation (VII) we have:

$$-P^* - \frac{\sigma}{\rho_{\ell} \cdot W_o^2 \delta_o} \cdot \xi^2 \cdot \frac{1}{\left[1 + \xi^2 \left(\frac{\partial \delta^*}{\partial z^*}\right)^2\right]^{3/2}} \cdot \frac{\partial^2 \delta^*}{\partial z^{*2}} + \frac{2\mu\xi}{\rho W_o \delta_o} \cdot \left[\frac{1 + \xi^2 (\partial \delta^* / \partial z^*)^2}{1 - \xi^2 (\partial \delta^* / \partial z^*)^2} \right] \cdot \frac{\partial v}{\partial y^*} = 0$$

$$\therefore -P^* - \frac{\xi^2}{N_{We}} \cdot \frac{1}{\left[1 + \xi^2 \left(\frac{\partial \delta^*}{\partial z^*}\right)^2\right]^{3/2}} \cdot \frac{\partial^2 \delta^*}{\partial z^{*2}} + \frac{8\xi}{N_{Re}} \left[\frac{1 + \xi^2 (\partial \delta^* / \partial z^*)^2}{1 - \xi^2 (\partial \delta^* / \partial z^*)^2} \right] \cdot \frac{\partial v}{\partial y^*} = 0$$

(VIII)

But $\left[1 + \xi^2 \left(\frac{\partial \delta^*}{\partial z^*}\right)^2\right]^{3/2} = 1 - \frac{3}{2} \xi^2 \left(\frac{\partial \delta^*}{\partial z^*}\right)^2 + \dots$

and

$$\frac{1 + \xi^2 (\partial \delta^* / \partial z^*)^2}{1 - \xi^2 (\partial \delta^* / \partial z^*)^2} = \frac{1 + \xi^2 (\partial \delta^* / \partial z^*)^2}{1 - \xi^2 (\partial \delta^* / \partial z^*)^2} \cdot \frac{1 + \xi^2 (\partial \delta^* / \partial z^*)^2}{1 + \xi^2 (\partial \delta^* / \partial z^*)^2}$$

$$= \frac{1 + 2\xi^2 (\partial \delta^* / \partial z^*)^2 + 4\xi^4 (\partial \delta^* / \partial z^*)^4}{1 + 4\xi^4 (\partial \delta^* / \partial z^*)^4}$$

Therefore equation (VII) reduces to:

$$-P^* - \frac{\xi^2}{N_{We}} \cdot \left[1 - \frac{3\xi^2}{25} \left(\frac{\partial \delta^*}{\partial Z^*} \right)^2 + \dots \right] \cdot \frac{\partial^2 \delta^*}{\partial Z^{*2}} + \frac{8\xi}{N_{Re}} \cdot \left[\frac{1 + 2\xi^2 \left(\frac{\partial \delta^*}{\partial Z^*} \right)^2 + 4\xi^4 \left(\frac{\partial \delta^*}{\partial Z^*} \right)^4}{1 + 4\xi^4 \left(\frac{\partial \delta^*}{\partial Z^*} \right)^4} \right] \cdot \frac{\partial V}{\partial Y^*} =$$

Neglecting the higher orders of ξ , i.e. (ξ^3, ξ^4, \dots etc.)

$$\therefore -P^* - \frac{\xi^2}{N_{We}} \cdot \frac{\partial^2 \delta^*}{\partial Z^{*2}} + \frac{8\xi}{N_{Re}} \cdot \frac{\partial V}{\partial Y^*} = 0 \quad (IX)$$

(c) The dimensionless film thickness δ^* is expressed in terms of the dimensionless free surface deformation function ϕ as follows:

$$\delta^* = \frac{\delta}{\delta_0} = 1 + \phi \quad (X)$$

The relationship between the two dependent variables δ^* and W_1^* is provided by a microscopic mass balance as shown by Rushton (1971) and Massot (1966) which may be written in dimensionless form as follows:

$$\frac{\partial \delta^*}{\partial T^*} = - \frac{\partial}{\partial Z^*} \int_0^{\delta^*} W^* dY^* = -\alpha \frac{\partial \delta^*}{\partial Z^*} = - \frac{\partial}{\partial Z^*} (W_1^* \cdot \delta^*) \quad (XI)$$

Substituting equation (X) into (XI) and integrating from $Z^* = 0$ to $Z^* = 1$, we get:

$$W_1^* = \frac{1 + \alpha \phi}{1 + \phi}$$

(d) The y component of velocity (V) is derived from equation (3.14) through the use of the equation of continuity (3.16) as follows:

Differentiating equation (3.14) w.r.t. Z^* we get,

$$\frac{\partial W^*}{\partial Z^*} = 3 \left[\frac{\partial W_1^*}{\partial Z^*} \left\{ \frac{Y^*}{\delta^*} - \frac{1}{2} \left(\frac{Y^*}{\delta^*} \right)^2 \right\} + W_1^* \left\{ - \frac{Y^*}{\delta^{*2}} \cdot \frac{\partial \delta^*}{\partial Z^*} + \frac{Y^{*2}}{\delta^{*3}} \cdot \frac{\partial \delta^*}{\partial Z^*} \right\} \right]$$

Substituting in the continuity equation (3.6) for $\frac{\partial W^*}{\partial Z^*}$ and integrating w.r.t. Y^* we have,

$$V = - \int \frac{\partial W^*}{\partial Z^*} dY^* = -3 \left[\frac{\partial W_1^*}{\partial Z^*} \left\{ \frac{Y^{*2}}{2\delta^*} - \frac{Y^{*3}}{6\delta^{*2}} \right\} - W_1^* \frac{\partial \delta^*}{\partial Z^*} \left\{ \frac{Y^{*2}}{2\delta^{*2}} + \frac{Y^{*3}}{3\delta^{*3}} \right\} \right] + k$$

$$\text{at } Y^* = 0 \quad V = 0 \quad \therefore k = 0$$

$$\therefore V = -3 \frac{\partial W_1^*}{\partial Z^*} \left\{ \frac{Y^{*2}}{2\delta^*} - \frac{Y^{*3}}{6\delta^{*2}} \right\} + 3W_1^* \frac{\partial \delta^*}{\partial Z^*} \left\{ \frac{Y^{*2}}{2\delta^{*2}} - \frac{Y^{*3}}{3\delta^{*3}} \right\}$$

(e) The pressure distribution equation (3.17) is evaluated as follows:

Neglecting the terms with higher order of ξ (i.e. ξ^2 and ξ^3), equation (3.7 b) reduces to:

$$\frac{v}{\delta_o W_o} \cdot \xi \frac{\partial^2 V}{\partial Y^{*2}} - \frac{\partial P^*}{\partial Y^*} = 0$$

But $N_{Re} = \frac{4\delta_o W_o}{v}$. Therefore the above equation becomes:

$$\frac{4}{N_{Re}} \cdot \xi \cdot \frac{\partial^2 V}{\partial Y^{*2}} - \frac{\partial P^*}{\partial Y^*} = 0 \quad (XII)$$

Integrating equation (XII) w.r.t. Y^* we get:

$$P^* = \frac{4\xi}{N_{Re}} \cdot \frac{\partial V}{\partial Y^*} + K \quad (XIII)$$

and by differentiating equation (3.16) w.r.t. Y^* we get:

$$\frac{\partial V}{\partial Y^*} = -3 \frac{\partial W_1^*}{\partial Z^*} \left\{ \frac{Y^*}{\delta^*} - \frac{Y^{*2}}{2\delta^{*2}} \right\} + 3W_1^* \cdot \frac{\partial \delta^*}{\partial Z^*} \left\{ \frac{Y^*}{\delta^{*2}} - \frac{Y^{*2}}{\delta^{*3}} \right\} \quad (XIV)$$

At $Y^* = \delta^*$ equation (XIV) reduces to:

$$\frac{\partial V}{\partial Y^*} = -\frac{3}{2} \frac{\partial W_1^*}{\partial Z^*} \quad (XV)$$

From equations (XIII) and (XV):

$$P^* = \frac{4\xi}{N_{Re}} \left(-\frac{3}{2} \frac{\partial W_1^*}{\partial Z^*} \right) + K \quad \text{at } Y^* = \delta^* \quad (XVI)$$

Also, from equation (XV) and boundary condition (3), equation (3.12) we have:

$$-P^* + \frac{8}{N_{Re}} \xi \left(-\frac{3}{2} \frac{\partial W_1^*}{\partial Z^*} \right) - \left(\frac{\xi^2}{N_{We}} \right) \cdot \frac{\partial^2 \delta^*}{\partial Z^{*2}} = 0 \text{ at } Y^* = \delta^* \quad (\text{XVII})$$

From equations (XVI) and (XVII) we get:

$$K = \frac{4}{N_{Re}} \xi \left(-\frac{3}{2} \cdot \frac{\partial W_1^*}{\partial Z^*} \right) - \frac{\xi^2}{N_{We}} \cdot \frac{\partial^2 \delta^*}{\partial Z^{*2}} = -\frac{6\xi}{N_{Re}} \cdot \frac{\partial W_1^*}{\partial Z^*} - \frac{\xi^2}{N_{We}} \cdot \frac{\partial^2 \delta^*}{\partial Z^{*2}} \quad (\text{XVIII})$$

Substituting equation (XVIII) in equation (XIII) we get:

$$P^* = \frac{4\xi}{N_{Re}} \cdot \frac{\partial V}{\partial Y^*} - \frac{6\xi}{N_{Re}} \cdot \frac{\partial W_1^*}{\partial Z^*} - \frac{\xi^2}{N_{We}} \cdot \frac{\partial^2 \delta^*}{\partial Z^{*2}}$$

(f)

The integration of $-\alpha \xi \int_0^{\delta^*} \frac{\partial W^*}{\partial Z^*} \cdot dY^*$

Differentiating equation (3.14) w.r.t. Z^* we get:

$$\frac{\partial W^*}{\partial Z^*} = 3 \frac{\partial W_1^*}{\partial Z^*} \left\{ \frac{Y^*}{\delta^*} - \frac{Y^{*2}}{2\delta^{*2}} \right\} + 3W_1^* \left\{ -\frac{Y^*}{\delta^{*2}} \cdot \frac{\partial \delta^*}{\partial Z^*} + \frac{Y^{*2}}{\delta^{*3}} \cdot \frac{\partial \delta^*}{\partial Z^*} \right\}$$

Integrating from $Y^* = 0$ to $Y^* = \delta^*$:

$$\begin{aligned} \int_0^{\delta^*} \frac{\partial W^*}{\partial Z^*} dY^* &= \left[3 \frac{\partial W_1^*}{\partial Z^*} \left\{ \frac{Y^{*2}}{2\delta^*} - \frac{Y^{*3}}{6\delta^{*2}} \right\} + 3W_1^* \left\{ -\frac{Y^{*2}}{2\delta^{*2}} \cdot \frac{\partial \delta^*}{\partial Z^*} + \frac{Y^{*3}}{3\delta^{*3}} \cdot \frac{\partial \delta^*}{\partial Z^*} \right\} \right]_0^{\delta^*} \\ &= 3 \frac{\partial W_1^*}{\partial Z^*} \cdot \delta^* \left\{ \frac{1}{2} - \frac{1}{6} \right\} + 3W_1^* \frac{\partial \delta^*}{\partial Z^*} \left\{ \frac{1}{3} - \frac{1}{2} \right\} \\ &= \delta^* \frac{\partial W_1^*}{\partial Z^*} - \frac{1}{2} W_1^* \frac{\partial \delta^*}{\partial Z^*} \end{aligned}$$

Multiply by $-\alpha \xi$:

$$\therefore -\alpha \xi \int_0^{\delta^*} \frac{\partial W^*}{\partial Z^*} dY^* = \frac{1}{2} \alpha \xi W_1^* \frac{\partial \delta^*}{\partial Z^*} - \alpha \xi \delta^* \frac{\partial W_1^*}{\partial Z^*}$$

The integration of $\xi \int_0^{\delta^*} W^* \frac{\partial W^*}{\partial Z^*} dY^*$

Differentiating equation (3.14) w.r.t. Z^* :

$$\frac{\partial W^*}{\partial Z^*} = 3 \frac{\partial W_1^*}{\partial Z^*} \left\{ \frac{Y^*}{\delta^*} - \frac{Y^{*2}}{2\delta^{*2}} \right\} + 3W_1^* \left\{ -\frac{Y^*}{\delta^{*2}} \cdot \frac{\partial \delta^*}{\partial Z^*} + \frac{Y^{*2}}{\delta^{*3}} \cdot \frac{\partial \delta^*}{\partial Z^*} \right\}$$

and multiplying by equation (3.14), i.e. $W^* = 3W_1^* \left\{ \frac{Y^*}{\delta^*} - \frac{1}{2} \left(\frac{Y^*}{\delta^*} \right)^2 \right\}$:

$$\begin{aligned}
 \therefore W^* \frac{\partial W^*}{\partial Z^*} &= 3W_1^* \left\{ \frac{Y^*}{\delta^*} - \frac{1}{2} \left(\frac{Y^*}{\delta^*} \right)^2 \right\} \cdot \left[3 \cdot \frac{\partial W_1}{\partial Z^*} \left\{ \frac{Y^*}{\delta^*} - \frac{Y^{*2}}{2\delta^{*2}} \right\} + 3W_1^* \left\{ - \frac{Y^*}{\delta^{*2}} \cdot \frac{\partial \delta^*}{\partial Z^*} + \right. \right. \\
 &\quad \left. \left. + \frac{Y^{*2}}{\delta^{*3}} \cdot \frac{\partial \delta^*}{\partial Z^*} \right\} \right] \\
 &= 9W_1^* \frac{\partial W_1}{\partial Z^*} \left\{ \frac{Y^{*2}}{\delta^{*2}} - \frac{1}{2} \frac{Y^{*3}}{\delta^{*3}} - \frac{1}{2} \frac{Y^{*3}}{\delta^{*3}} + \frac{Y^{*4}}{4\delta^{*4}} \right\} + 9W_1^* \left\{ - \left(\frac{Y^{*2}}{\delta^{*3}} \right) \frac{\partial \delta^*}{\partial Z^*} \right. \\
 &\quad \left. + \left(\frac{Y^{*3}}{\delta^{*4}} \right) \frac{\partial \delta^*}{\partial Z^*} + \frac{Y^{*3}}{2\delta^{*4}} \cdot \frac{\partial \delta^*}{\partial Z^*} - \frac{Y^{*4}}{2\delta^{*5}} \cdot \frac{\partial \delta^*}{\partial Z^*} \right\}
 \end{aligned}$$

Integrating from $Y^* = 0$ to $Y^* = \delta^*$:

$$\begin{aligned}
 \int_0^{\delta^*} W^* \frac{\partial W^*}{\partial Z^*} dY^* &= \left[9W_1^* \frac{\partial W_1}{\partial Z^*} \left\{ \frac{Y^{*3}}{3\delta^{*2}} - \frac{Y^{*4}}{8\delta^{*3}} - \frac{Y^{*4}}{8\delta^{*3}} + \frac{Y^{*5}}{20\delta^{*4}} \right\} \right. \\
 &\quad \left. + 9W_1^* \left\{ - \frac{Y^{*3}}{3\delta^{*3}} \cdot \frac{\partial \delta^*}{\partial Z^*} + \frac{Y^{*4}}{4\delta^{*4}} \cdot \frac{\partial \delta^*}{\partial Z^*} + \frac{Y^{*4}}{8\delta^{*4}} \cdot \frac{\partial \delta^*}{\partial Z^*} \right. \right. \\
 &\quad \left. \left. - \frac{Y^{*5}}{10\delta^{*5}} \cdot \frac{\partial \delta^*}{\partial Z^*} \right\} \right]_0^{\delta^*} \\
 &= 9W_1^* \delta^* \frac{\partial W_1}{\partial Z^*} \left\{ \frac{16}{120} \right\} + 9W_1^* \frac{\partial \delta^*}{\partial Z^*} \left\{ - \frac{7}{120} \right\} \\
 &= \frac{144}{120} \cdot W_1^* \cdot \delta^* \frac{\partial W_1}{\partial Z^*} - \frac{63}{120} W_1^* \frac{\partial \delta^*}{\partial Z^*}
 \end{aligned}$$

Multiplying by ξ :

$$\therefore \xi \int_0^{\delta^*} W^* \frac{\partial W^*}{\partial Z^*} dY^* = \frac{144}{120} \xi W_1^* \delta^* \frac{\partial W_1}{\partial Z^*} - \frac{63}{120} \xi W_1^* \frac{\partial \delta^*}{\partial Z^*}$$

Integration of $\xi \int_0^{\delta^*} v \frac{\partial W^*}{\partial Y^*} dY^*$

Differentiate equation (3.14) w.r.t. Y^* :

$$\frac{\partial W^*}{\partial Y^*} = 3W_1^* \left\{ \frac{1}{\delta^*} - \frac{Y^*}{\delta^{*2}} \right\}$$

Multiplying by equation (3.16):

$$\begin{aligned} v \frac{\partial W^*}{\partial Y^*} &= 3W_1^* \left\{ \frac{1}{\delta^*} - \frac{Y^*}{\delta^{*2}} \right\} \cdot \left[3 \cdot \frac{\partial W_1^*}{\partial Z^*} \left\{ \frac{Y^{*3}}{6\delta^{*2}} - \frac{Y^{*2}}{2\delta^*} \right\} + 3W_1^* \left\{ \frac{Y^{*2}}{2\delta^{*2}} \cdot \frac{\partial \delta^*}{\partial Z^*} \right. \right. \\ &\quad \left. \left. - \frac{Y^{*3}}{3\delta^{*3}} \cdot \frac{\partial \delta^*}{\partial Z^*} \right\} \right] \\ &= 9W_1^* \frac{\partial W_1^*}{\partial Z^*} \left\{ \frac{Y^{*3}}{6\delta^{*3}} - \frac{Y^{*2}}{2\delta^{*2}} - \frac{Y^{*4}}{6\delta^{*4}} + \frac{Y^{*3}}{2\delta^{*3}} \right\} + 9W_1^{*2} \left\{ \frac{Y^{*2}}{2\delta^{*3}} \cdot \frac{\partial \delta^*}{\partial Z^*} \right. \\ &\quad \left. - \frac{Y^{*3}}{3\delta^{*4}} \cdot \frac{\partial \delta^*}{\partial Z^*} - \frac{Y^{*3}}{2\delta^{*4}} \cdot \frac{\partial \delta^*}{\partial Z^*} + \frac{Y^{*4}}{3\delta^{*5}} \cdot \frac{\partial \delta^*}{\partial Z^*} \right\} \end{aligned}$$

Integrating from $Y^* = 0$ to $Y^* = \delta^*$:

$$\int_0^{\delta^*} v \frac{\partial W^*}{\partial Y^*} dY^* = 9W_1^* \delta^* \frac{\partial W_1^*}{\partial Z^*} \left\{ \frac{1}{24} - \frac{1}{6} - \frac{1}{30} + \frac{1}{8} \right\} + 9W_1^{*2} \frac{\partial \delta^*}{\partial Z^*} \left\{ \frac{1}{6} - \frac{1}{12} - \frac{1}{8} + \frac{1}{15} \right\}$$

Multiplying by ξ :

$$\therefore \xi \int_0^{\delta^*} v \frac{\partial W^*}{\partial Y^*} dY^* = \frac{27}{120} \xi W_1^{*2} \frac{\partial \delta^*}{\partial Z^*} - \frac{36}{120} \xi W_1^* \delta^* \frac{\partial W_1^*}{\partial Z^*}$$

Integration of $\frac{4\xi^2}{N_{Re}} \int_0^{\delta^*} \frac{\partial^2 W^*}{\partial Z^{*2}} dY^*$

Differentiate equation (3.14) twice w.r.t. Z^* in order to obtain the second derivative:

$$\frac{\partial^2 W^*}{\partial Z^{*2}} = 3 \left[\frac{\partial^2 W_1^*}{\partial Z^{*2}} \left\{ \frac{Y^*}{\delta^*} - \frac{Y^{*2}}{2\delta^{*2}} \right\} + 2 \frac{\partial W_1^*}{\partial Z^*} \left\{ -\frac{Y^*}{\delta^{*2}} \cdot \frac{\partial \delta^*}{\partial Z^*} + \frac{Y^{*2}}{\delta^{*3}} \cdot \frac{\partial \delta^*}{\partial Z^*} \right\} \right. \\ \left. + W_1^* \left\{ \frac{2Y^*}{\delta^{*3}} \cdot \left(\frac{\partial \delta^*}{\partial Z^*} \right)^2 - \frac{Y^*}{\delta^{*2}} \frac{\partial^2 \delta^*}{\partial Z^{*2}} - \frac{3Y^{*2}}{\delta^{*4}} \left(\frac{\partial \delta^*}{\partial Z^*} \right)^2 + \frac{Y^{*2}}{\delta^{*3}} \frac{\partial^2 \delta^*}{\partial Z^{*2}} \right\} \right]$$

Integrating from $Y^* = 0$ to $Y^* = \delta^*$:

$$\int_0^{\delta^*} \frac{\partial^2 W^*}{\partial Z^{*2}} dY^* = \delta^* \frac{\partial^2 W_1^*}{\partial Z^{*2}} - \frac{\partial W_1^*}{\partial Z^*} \cdot \frac{\partial \delta^*}{\partial Z^*} - \frac{1}{2} W_1^* \frac{\partial^2 \delta^*}{\partial Z^{*2}}$$

Multiplying by $\frac{4\xi^2}{N_{Re}}$:

$$\therefore \frac{4\xi^2}{N_{Re}} \int_0^{\delta^*} \frac{\partial^2 W^*}{\partial Z^{*2}} dY^* = \frac{4\xi^2}{N_{Re}} \delta^* \frac{\partial^2 W_1^*}{\partial Z^{*2}} - \frac{4\xi^2}{N_{Re}} \cdot \frac{\partial W_1^*}{\partial Z^*} \cdot \frac{\partial \delta^*}{\partial Z^*} - \frac{2\xi^2}{N_{Re}} W_1^* \frac{\partial^2 \delta^*}{\partial Z^{*2}}$$

Integration of $\frac{4}{N_{Re}} \int_0^{\delta^*} \frac{\partial^2 W^*}{\partial Y^{*2}} dY^*$

Differentiate equation (3.14) twice w.r.t. Y^* in order to obtain the second derivative:

$$\frac{\partial W^*}{\partial Y^*} = 3W_1^* \left\{ \frac{1}{\delta^*} - \frac{Y^*}{\delta^{*2}} \right\}$$

$$\frac{\partial^2 W^*}{\partial Y^{*2}} = -\frac{3W_1^*}{\delta^{*2}}$$

Integrate from $Y^* = 0$ to $Y^* = \delta^*$ and multiply by $\frac{4}{N_{Re}}$:

$$\therefore \frac{4}{N_{Re}} \int_0^{\delta^*} \frac{\partial^2 W^*}{\partial Y^{*2}} dY^* = -\frac{12}{N_{Re}} \cdot \frac{W_1^*}{\delta^*}$$

Integration of $16 \int_0^{\delta^*} \frac{Gr}{N_{Re}^2} dY^*$

$$16 \int_0^{\delta^*} \frac{Gr}{N_{Re}^2} dY^* = 16 \left(\frac{\delta^*}{N_{Re}^2} \cdot Gr \right)$$

Integration of $-\xi \int_0^{\delta^*} \frac{\partial P^*}{\partial Z^*} dY^*$: Differentiating equation (3.16) with respect to Z^* :

$$\begin{aligned} \frac{\partial V}{\partial Z^*} = & -3 \left[\frac{\partial^2 W_1^*}{\partial Z^{*2}} \left\{ \frac{Y^{*2}}{2\delta^*} - \frac{Y^{*3}}{6\delta^{*2}} \right\} + \frac{\partial W_1^*}{\partial Z^*} \left\{ -\frac{Y^{*2}}{2\delta^{*2}} \cdot \frac{\partial \delta^*}{\partial Z^*} + \frac{Y^{*3}}{3\delta^{*3}} \cdot \frac{\partial \delta^*}{\partial Z^*} \right\} \right] \\ & + 3 \left[\frac{\partial W_1^*}{\partial Z^*} \left\{ \frac{Y^{*2}}{2\delta^{*2}} \cdot \frac{\partial \delta^*}{\partial Z^*} - \frac{Y^{*3}}{3\delta^{*3}} \cdot \frac{\partial \delta^*}{\partial Z^*} \right\} + W_1^* \left\{ -\frac{Y^{*2}}{\delta^{*3}} \left(\frac{\partial \delta^*}{\partial Z^*} \right)^2 + \frac{Y^{*2}}{2\delta^{*2}} \cdot \frac{\partial^2 \delta^*}{\partial Z^{*2}} \right. \right. \\ & \left. \left. + \frac{Y^{*3}}{\delta^{*4}} \left(\frac{\partial \delta^*}{\partial Z^*} \right)^2 - \frac{Y^{*3}}{3\delta^{*3}} \cdot \frac{\partial^2 \delta^*}{\partial Z^{*2}} \right\} \right] \quad \text{at } Y^* = \delta^*. \\ \frac{\partial V}{\partial Z^*} = & -\delta^* \frac{\partial^2 W_1^*}{\partial Z^{*2}} + \frac{\partial W_1^*}{\partial Z^*} \cdot \frac{\partial \delta^*}{\partial Z^*} + \frac{1}{2} W_1^* \frac{\partial^2 \delta^*}{\partial Z^{*2}} \quad \text{(XIX)} \end{aligned}$$

Differentiate equation (3.17) w.r.t. Z^* :

$$\frac{\partial P^*}{\partial Z^*} = \frac{4\xi}{N_{Re}} \cdot \frac{\partial^2 V}{\partial Y^* \partial Z^*} - \frac{6\xi}{N_{Re}} \cdot \frac{\partial^2 W_1^*}{\partial Z^{*2}} - \frac{\xi^2}{N_{We}} \cdot \frac{\partial^3 \delta^*}{\partial Z^{*3}}$$

then integrate from $Y^* = 0$ to $Y^* = \delta^*$:

$$\int_0^{\delta^*} \frac{\partial P^*}{\partial Z^*} dY^* = \frac{4\xi}{N_{Re}} \cdot \frac{\partial V}{\partial Z^*} \Big|_{Y^*=\delta^*} - \frac{6\xi}{N_{Re}} \cdot \frac{\partial^2 W_1^*}{\partial Z^{*2}} \delta^* - \frac{\xi^2}{N_{We}} \cdot \frac{\partial^3 \delta^*}{\partial Z^{*3}} \cdot \delta^*$$

Substituting for $\frac{\partial V}{\partial Z^*} \Big|_{Y^*=\delta^*}$ equation (XIX):

$$\begin{aligned} \int_0^{\delta^*} \frac{\partial P^*}{\partial Z^*} dY^* = & -\frac{4\xi}{N_{Re}} \delta^* \frac{\partial^2 W_1^*}{\partial Z^{*2}} + \frac{4\xi}{N_{Re}} \frac{\partial W_1^*}{\partial Z^*} \cdot \frac{\partial \delta^*}{\partial Z^*} + \frac{2\xi}{N_{Re}} W_1^* \frac{\partial^2 \delta^*}{\partial Z^{*2}} \\ & - \frac{6\xi \delta^*}{N_{Re}} \cdot \frac{\partial^2 W_1^*}{\partial Z^{*2}} - \frac{\xi^2 \delta^*}{N_{We}} \cdot \frac{\partial^3 \delta^*}{\partial Z^{*3}} \end{aligned}$$

Multiply by $-\xi$:

$$-\xi \int_0^{\delta^*} \frac{\partial P^*}{\partial Z^*} dY^* = \frac{4\xi^2}{N_{Re}} \delta^* \frac{\partial^2 W_1^*}{\partial Z^{*2}} - \frac{4\xi^2}{N_{Re}} \frac{\partial W_1^*}{\partial Z^*} \frac{\partial \delta^*}{\partial Z^*} - \frac{2\xi^2}{N_{Re}} W_1^* \frac{\partial^2 \delta^*}{\partial Z^{*2}} + \frac{6\delta^* \xi^2}{N_{Re}} \frac{\partial^2 W_1^*}{\partial Z^{*2}} + \frac{\delta^* \xi^3}{N_{We}} \frac{\partial^3 \delta^*}{\partial Z^{*3}}$$

Integration of $F_{qa}^{**} \frac{\delta^*}{N_{Fr}^2} \int_0^{\delta^*} \left\{ \frac{1}{2} \left(\frac{Y^*}{\delta^*} \right)^3 - \frac{1}{8} \left(\frac{Y^*}{\delta^*} \right)^4 - \frac{Y^*}{\delta^*} \right\} dY^*$

$$F_{qa}^{**} \frac{\delta^*}{N_{Fr}^2} \int_0^{\delta^*} \left\{ \frac{1}{2} \left(\frac{Y^*}{\delta^*} \right)^3 - \frac{1}{8} \left(\frac{Y^*}{\delta^*} \right)^4 - \frac{Y^*}{\delta^*} \right\} dY^*$$

$$= \frac{F_{qa}^{**}}{N_{Fr}^2} \left[\delta^* \left\{ \frac{1}{8} \delta^* - \frac{\delta^*}{40} - \frac{\delta^*}{2} \right\} \right]$$

$$= - \frac{4}{10} \frac{F_{qa}^{**} \delta^{*2}}{N_{Fr}^2}$$

APPENDIX 2

Periodic Solution for the Wavy Film Flow

The periodic solution adopted in Chapter 3, which describes the wavy film flow, is given by:

$$\phi = C_1 \sin n(z - ct) \quad (XX)$$

From (3.5) we have:

$$Z^* = \frac{z}{\lambda}, \quad T^* = \frac{tW_0\xi}{\delta_0}, \quad n = \frac{N_w}{\delta_0}, \quad \text{and} \quad \alpha = \frac{C}{W_0} \quad (XXI)$$

From (XX) and (XXI) we have:

$$\phi = C_1 \sin \frac{N_w}{\xi} (Z^* - \alpha T^*)$$

The first, second and third derivatives of ϕ are obtained by differentiating the preceding equation with respect to Z^* :

$$\phi' = C_1 \cdot \frac{N_w}{\xi} \cos \frac{N_w}{\xi} (Z^* - \alpha T^*)$$

$$\phi'' = -C_1 \cdot \left(\frac{N_w}{\xi}\right)^2 \sin \frac{N_w}{\xi} (Z^* - \alpha T^*)$$

$$\phi''' = -C_1 \cdot \left(\frac{N_w}{\xi}\right)^3 \cos \frac{N_w}{\xi} (Z^* - \alpha T^*)$$

(b) In order to evaluate the dimensionless wave celerity

(α) from:

$$N_{We} = \frac{6 \left[3 - \alpha + \frac{1}{30} \frac{N_{Re}}{N_{Fr}^2} \bar{\phi} \right]}{(7\alpha - 9) \left(\alpha^2 - \frac{12}{5}\alpha + \frac{6}{5} \right)}$$

Put:

$$Z1 = \alpha^2 - \frac{12}{5}\alpha + \frac{6}{5}$$

$$Z2 = 7\alpha - 9$$

$$Z3 = 3 - \alpha + \left(\frac{N_{Re}}{30 \cdot N_{Fr}^2} \right) \bar{\phi}$$

$$Z4 = 2\alpha - \frac{12}{5} \quad (\text{i.e. first derivative of } Z1)$$

$$FUNK = (N_{We} \cdot Z2 \cdot Z1) - (6 \cdot Z3)$$

$$\frac{d}{d\alpha} FUNK = DFUNK = N_{We} (Z2 \cdot Z4) + (Z1 \cdot 7) + 6$$

By using Newton's method of iteration as in Appendix (3.a), the dimensionless celerity is calculated.

APPENDIX 3

Newton's Method of Iteration

(a) Newton's method of iteration is used in solving equation (4.24) for δ_c :

$$\text{i.e. } \frac{\rho_l}{15} \left[\frac{g \Delta \rho}{\rho_l v_l} \right] \delta_c^4 = \frac{\sigma(1 - \cos \theta)}{\delta_c} + \frac{d\sigma}{dT} \cdot \frac{F_{qa}}{K_l} \cos \theta + \rho_v \left[\frac{F_{qa}}{\rho_v (H_v - H_l)} \right]^2 \frac{\Delta \rho}{\rho_l} \cos^2 \theta$$

Put:

$$\text{TERM1} = \frac{\sigma(1 - \cos \theta)}{\delta_c} + \frac{d\sigma}{dT} \cdot \frac{F_{qa}}{K_l} \cos \theta$$

$$\text{TERM2} = \rho_v \left[\frac{F_{qa}}{\rho_v (H_v - H_l)} \right]^2 \frac{\Delta \rho}{\rho_l} \cos^2 \theta$$

$$\text{TERM3} = \frac{\rho_l}{15} \left[\frac{g \cdot \Delta \rho}{\rho_l v_l} \right] \cdot \delta_c^4$$

$$\text{FUNK1} = \frac{\sigma(1 - \cos \theta)}{\delta_c} + \frac{d\sigma}{dT} \cdot \frac{F_{qa}}{K_l} \cos \theta + \rho_v \left[\frac{F_{qa}}{\rho_v (H_v - H_l)} \right]^2 \cdot \frac{\Delta \rho}{\rho_l} \cos^2 \theta - \frac{\rho_l}{15} \left[\frac{g \cdot \Delta \rho}{\rho_l v_l} \right] \cdot \delta_c^4$$

$$\frac{d}{d\delta_c}(\text{FUNK1}) = \text{DFUNK2} = \frac{-\sigma(1 - \cos \theta)}{\delta_c^2} - \frac{\rho_l}{15} \left[\frac{g \cdot \Delta \rho}{\rho_l v_l} \right] \cdot \left[4\delta_c^3 \right]$$

$$\text{TERM4} = \frac{-\sigma(1 - \cos \theta)}{\delta_c^2}$$

$$\text{TERM5} = - \frac{\rho_l}{15} \left[\frac{g \cdot \Delta \rho}{\rho_l v_l} \right] \cdot \left[4\delta_c^3 \right]$$

$$\text{FUNK1} = \text{TERM1} + \text{TERM2} + \text{TERM3}$$

$$\text{DFUNK2} = \text{TERM4} + \text{TERM5}$$

Method of solution:-

Assume initial value for δ_c , then calculate FUNK1 and DFUNK2. Calculate $(\delta_c)_1$ new from:

$$(\delta_c)_1 = \delta_c - \frac{\text{FUNK1}}{\text{DFUNK2}}$$

If the value of FUNK1 is greater than a specified error, repeat the calculation with the new δ_c until FUNK1 is less than or equal to a specified error.

APPENDIX 4

Description of the Experimental Facilities

A4.1 Introduction

This appendix describes an experimental facility designed and constructed by the author in which a continuous steady supply of Freon vapour and Freon liquid be supplied independently to a working section. The idea is to make available a tool in which specific single and two-phase heat transfer phenomena can be investigated using Freon as the working medium and then to apply the author's simulation technique in order to compare the results with available water-steam results. Hence, after gaining confidence in the simulating results, it would be possible to design and construct different working sections to simulate and predict other two-phase boiling phenomena directly without the necessity of having water-steam results.

The design, manufacture, erection and commissioning of the two-loop test facility was not an easy task and it took the author more than two years to build the rig. We have chosen as its first application a test section to investigate the behaviour of a motivated falling thin liquid film on a vertical heated rod as explained in Section A4.4. The test section as designed by the author can be used for other single

and two-phase heat and mass transfer investigations, e.g. interfacial wave characteristics.

4.1.1 The idea of using refrigerants as a simulating substance:

Fluids used for simulation, such as the refrigerant family, are selected for their low latent heats of vapourisation compared with water, hence reduced power requirements for boiling. Also, the critical pressures and temperatures are much lower than water; therefore the simulating pressure and temperature is only a fraction of the corresponding water pressure and temperature (Table A4.1). The required experimental facilities are therefore simpler and much less expensive. The lower heat fluxes and temperatures reduce the chances of physical burnout. Also, instrumentation is less complex and experimental testing is safer. Transparent test sections can be used which enables visualisation of different boiling phenomena.

Of the commercially available refrigerants, Freons (e.g. Freon-12, Freon-11, Freon-21, Freon-22, Freon-113, etc.) have low toxicity, non-corrosive properties, and low cost. It has been established that the density ratio (ρ_l / ρ_v) is one of the important parameters in simulation (Stevens and Macbeth,

1971). With this knowledge in mind and the fact that both Freon-12 and Freon-113 resemble water in their pressure-density ratio characteristics, it becomes evident that the selection of these two types of Freons would give the best simulation when compared with the rest of the Freon family. The boiling point of Freon-113 at normal ambient conditions is 117.6°F, which is higher than the ambient temperature. Therefore it could be stored at normal pressure and temperature. This favours Freon-113 compared with Freon-12, because the latter has a lower saturation temperature than the ambient one. In addition, Bankoff (1971) argues that Freon-113 is a better simulant for sodium film breakup studies.

Freon-113 has been used by many investigators, e.g. Dean (1970), Tong et al (1966), Mattson (1972), Mattson et al (1974), Coffield et al (1969), Tong et al (1970) and Efferding (1964), and there was no mention in their reports of any hazards due to its use. The Imperial Chemical Industry report TS/C/2038/2 states that Freon-113 is non-toxic, non-flammable and safe to use. Freon-113 is manufactured in the United Kingdom in large quantities for different uses; therefore it is available.

TABLE A4.1

| ρ_l / ρ_v | <u>Freon-113 pressure (lb/in²)</u> | <u>Corresponding water pressure (lb/in²)</u> |
|-------------------|---|---|
| 41.1 | 71 | 570 |
| 20.6 | 137 | 1000 |
| 11.8 | 190 | 1500 |
| 7.2 | 300 | 2000 |

A4.2 General Description of the Test Facility

The test facility consists mainly of two fluid loops which supply the test section independently with continuous flow of Freon-113 liquid and Freon-113 vapour at a maximum rate of 0.1 lb/sec and 0.16 lb/sec respectively (Figs. A4.1a, A4.1b and A4.1c). The vapour leaves the test section to the condenser via the flow meter FM(4) and the condensate is accumulated in the holding tank, while the liquid leaving the test section goes directly to the holding tank via the flow meter FM(3). A circulating pump is positioned at a lower level beneath the holding tank and is used to supply liquid Freon to the heating tank from the holding tank. As it was difficult to obtain a pump which suited our requirements of pressure discharge characteristics, an orifice meter is fitted at the discharge side of the pump where a portion of the discharged Freon is returned to the holding tank while the rest is directed towards the heating tank. The heating tank is fitted

with two electric immersion heaters (2 x 7.5 kW). Vapour Freon is withdrawn from the top of the heating tank to be supplied via flow meter FM(2) to the test section. Heated Freon liquid at saturation temperature is discharged from the bottom of the tank to the test section via flow meter FM(1).

Temperature (T) and Pressure (P) Measuring Stations

- T₁ and P₁ Liquid Freon at test section inlet,
- T₂ and P₂ Vapour Freon at test section inlet,
- T₃ and P₃ Liquid Freon at test section exit,
- T₄ and P₄ Vapour Freon at test section outlet,
- T₅ and P₅ Liquid Freon at outlet of condenser,
- T₆ and P₆ Liquid Freon at exit of pump,
- T_{7,8} and P_{7,8} Condenser cooling water at inlet,
- T₉ and P₉ Heating tank temperature and pressure,
- P₁₀ Holding tank pressure, and
- T₁₁ and P₁₁ Liquid Freon at pump inlet.

A4.3 Components, Control and Safety Devices in the Rig

A4.3.1 Heating tank:

Design specifications (Fig. A4.2):

- Inner diameter = 2.5 ft.
- Length between tangent lines = 4.0 ft.
- Vessel capacity = 24.0 ft.³

| | | | |
|-----------------------------|---|-----------------|--------------------|
| Maximum working pressure | = | 100.0 | lb/in ² |
| Maximum working temperature | = | 250.0 | °F |
| Design pressure | = | 130.0 | lb/in ² |
| Design temperature | = | 275.0 | °F |
| Hydraulic test pressure | = | 180.0 | lb/in ² |
| Shell thickness | = | 5/16 | in. |
| Material | = | Mild Steel | |
| Flanges | = | BS.10 Table E | |
| Insulation | = | 1" mineral wool | |

The liquid level in the heating tank is indicated by means of a reflex sight-glass gauge which is connected to flanges K₁ and K₂ (Fig. A4.2). Valves are fitted to allow for the isolation and removal of the sight-glass without depressurising the vessel. The valves are equipped with a safety ball which instantly shuts off the flow of the Freon in the event of a glass breakage.

An automatic control level gauge system is incorporated to the tank and connected to flange (F), Fig. (A4.2), to indicate the liquid level and to give an alarm signal if the level in the tank reaches one foot above the tank centre line or six inches below it. This device is a safeguard against either liquid flooding or starvation.

A spring safety valve is fitted to flange (D), Fig. (A4.2), and is set to open at 130 lb/in². Heat is supplied

to the fluid inside the tank by means of two immersion heaters which are inserted in the tank through flanges J_1 and J_2 , Fig. (A4.2). Each heater is rated at 440 V, 7.5 kW and consists of six elements 0.5 diameter by 97 inches long connected in parallel.

The pressure in the heating tank is kept constant at a set value by means of a pneumatic indicating controller (I), Fig. (A4.1a), connected to flange (G), Fig. (A4.2). The pneumatic controller produced 3 to 15 lb/in² gauge output signal which is proportional to the pressure sensed in the heating tank. The output pressure signal is then transformed to an electric signal by means of a transscope Pneumo-electric transducer which converts the 3-15 lb/in² gauge pressure signal to 1-5 mA D.C. electric signal. This electrical signal is then applied to a thyristor unit which in turn controls the electrical power supply to the heaters.

A4.3.2 Condenser

The vapour Freon leaving the test section is condensed by a five branch co-axial double-pipe condenser (Fig. A4.3). The diameter of the outer tubes of the first four branches is 1.5 inch IPS while the inner tube diameter is 1.0 IPS. The

fifth branch has an outer tube diameter of 1.0 IPS and an inner tube diameter of $\frac{1}{2}$ " IPS. The condenser is designed to the following specifications:

| | | | |
|---------------------------|---|-------------|----------------------|
| Rated Freon vapour flow | = | 864.0 | lb/hr. |
| Rated cooling water flow | = | 4700 | lb/hr. |
| Freon working pressure | = | 70 | lb/in ² . |
| Freon working temperature | = | 222 | °F |
| Subcooling temperature | = | 30 | °F |
| Condenser cooling load | = | 53,000 | BTU/hr. |
| Hydraulic test pressure | = | 150 | lb/in ² . |
| Tube material | = | Mild steel. | |

The Freon flows through the inner pipes while the cooling water passes through the annular space between the two co-axial pipes in a counter flow direction. Thermocouples and pressure gauges are used to measure the water and Freon temperature and pressure at inlet to the condenser and at the outlet, Fig. (A4.1). The condenser's pressure is controlled by regulating the mass flow rate of the cooling water.

A4.3.3 Holding tank

The holding tank is made of mild steel with plate ends 12 inches. N.B. Sch. 20 tubular body, with all flanged connections manufactured according to B.S.T.E. (BS. 1500).

Holding tank design specifications:

| | | | |
|-------------------------|---|------|--------------------|
| Length between plates | = | 30 | in. |
| Working pressure | = | 70 | lb/in ² |
| Working temperature | = | 222 | °F |
| Design pressure | = | 110 | lb/in ² |
| Design temperature | = | 255 | °F |
| Hydraulic test pressure | = | 165 | lb/in ² |
| Tank capacity | = | 1.96 | ft ³ |

The level in the holding tank is measured by means of a reflex sight-glass gauge which is connected to flanges J₁ and J₂, Fig. (A4.4). An automatic control level gauge system is connected to flange (I), Fig. (A4.4). This control gauge indicates the liquid level in the tank. Also, the control starts the pump if the liquid is 4.5 inches above the tank centre line. The pump is switched off when the liquid level reaches 4.5 inches below the tank centre line. The pressure in the holding tank is maintained at a set value by means of a pneumatic indicating controller (3), Fig. (A4.1a), which is connected to flange (A), Fig. (A4.1a). The pneumatic controller produces 3 to 15 lb/in² gauge output signal proportional to the pressure sensed in the holding tank. The output pressure signal is then transferred to a Hi-flow Diaphragm valve which accordingly controls the flow rate of the cooling water to the condenser. A spring safety valve (flange B, Fig. A4.4) is set to relieve the pressure at 110 lb/in².

A4.3.3 Circulating pump

A canned-glandless centrifugal pump is used to pump liquid Freon from the holding tank to the heating tank. The pump and motor are integral, and the stator windings are sealed by a corrosion-resistant non-magnetic can. The rotor shaft is carried on P.T.F.E. tape bearings.

Pump Specifications:

| | | | |
|---------------------|---|-----------------------------|--------------------------|
| Capacity | = | 10 | g.p.m. |
| Differential head | = | 123 | ft. |
| Suction head | = | 4 | ft. |
| Pumping temperature | = | 199 | °F |
| Design pressure | = | 300 | lb/in ² gauge |
| Test pressure | = | 450 | lb/in ² gauge |
| Impeller diameter | = | 6.25 | in. |
| Motor | = | 3 phase | |
| Voltage | = | 220-380/420 | V |
| Cycles | = | 50 | |
| Speed | = | 2880 | r.p.m. |
| Full load | = | 5.9 | amps |
| Other features | = | Stator water cooled jacket. | |

A4.4 The test section

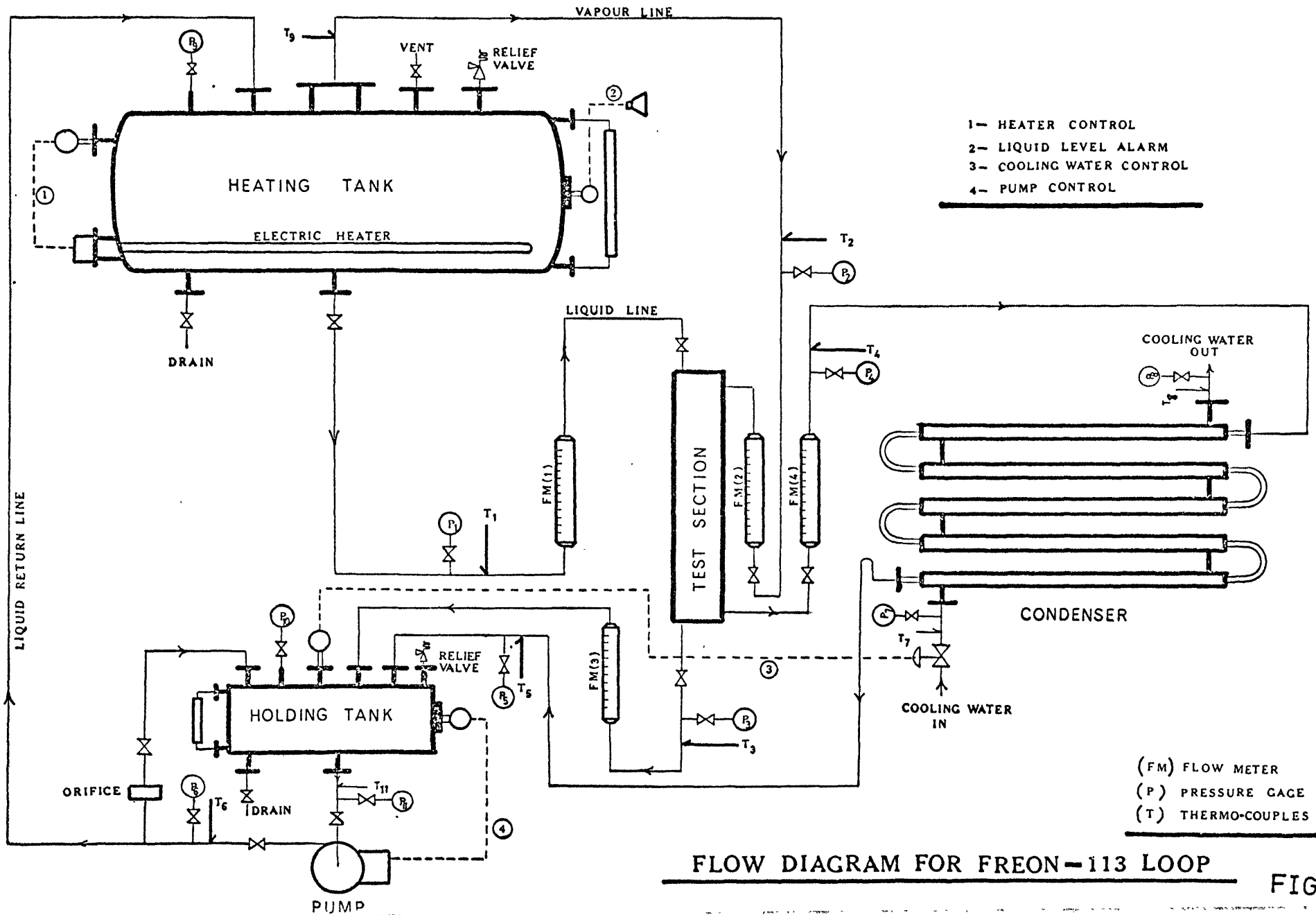
The test section consists mainly of a glass tube (1" inside diameter - maximum working pressure and temperature 100 lb/in² and 200°C respectively) which contains a coaxial heating rod (Figs. A5.5a and A5.5b). The inlet supply head of the testing section is designed to supply the heating rod with a uniform enveloping thin liquid film which is discharged through a slit (3) (Fig. A4.5a). The flow of the motivating vapour passes through a porous disc (2) to the annular space between the glass tube and the heating rod. Other details of the supply head are shown in Fig. A4.5a. The lower end of the glass tube is connected to an arrangement by which vapour and liquid Freon leaves the test section separately (Fig. A4.5a). The glass tube has side openings through which probes can be applied so as to measure the characteristics of the fluid on the surface of the heating rod. Fig. A4.6 is a schematic diagram of the probes and the mechanism which is designed for the probe traverse and transmission of signals.

The heating rod (Figs. A4.7a and A4.7b) consists of two co-axial tubes. The stainless steel tube (0.5" O.D.) accommodates a 4.5 kW heater tape. The tube is filled with magnesia powder which surrounds the heater tape. The magnesia powder is a good heat-conducting material and gives favourable

heat distribution per unit area. Twelve thermocouples are then placed on the outside surface of the inner tube at levels spaced by 4 inches between consecutive apices. The thermocouples are kept apart by means of stainless steel wires. All this structure is inserted in a 1 1/16" O.D. stainless steel tube and the assembly is swaged down to 5/8" (Figs. A4.7a and A4.7b). The heated part is 40 inches and there is 13 inches of cold end on both sides. The top thermocouple and the one before the last in the heated section are connected to a high speed recorder to measure the rewetting speed. The last thermocouple from the bottom in the heated region is connected to a thyristor which regulates the power supply to obtain a continuous pre-set temperature. The rest of the thermocouples in the heated section are connected to a trip relay system, which will cut off the power supply to the heater if any of the thermocouples measured a temperature higher than 800°F. This is carried out as a safety precaution against physical burn-out. The two thermocouples in the cold sections are used to measure the temperature so as to give an indication of the temperature at the "O" rings seals in the test section.

Figure A4.8 is a wiring diagram of the control and operating electric circuits.

Figure A4.9 shows the characteristics of the pneumatic controller after calibration.

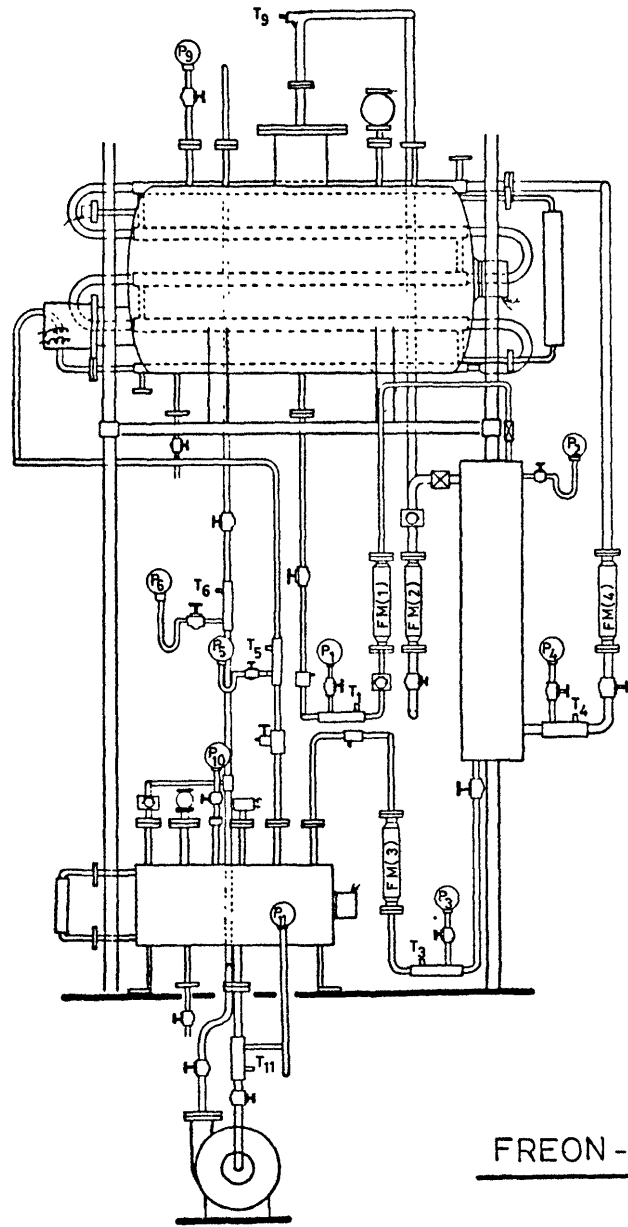


- 1- HEATER CONTROL
- 2- LIQUID LEVEL ALARM
- 3- COOLING WATER CONTROL
- 4- PUMP CONTROL

(FM) FLOW METER
(P) PRESSURE GAGE
(T) THERMO-COUPLES

FLOW DIAGRAM FOR FREON-113 LOOP

FIG.(A4.1a)



FREON-113 RIG

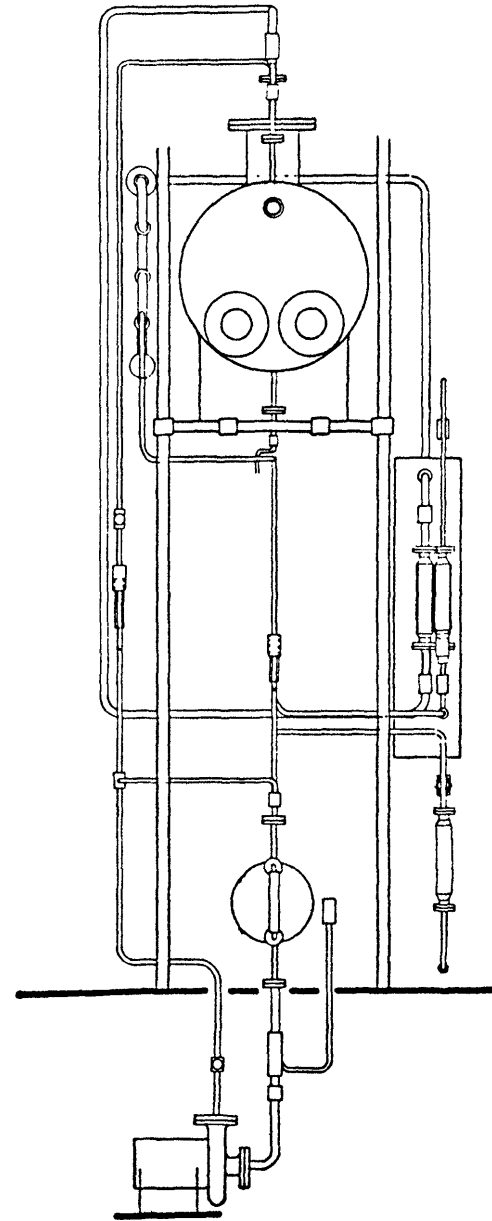
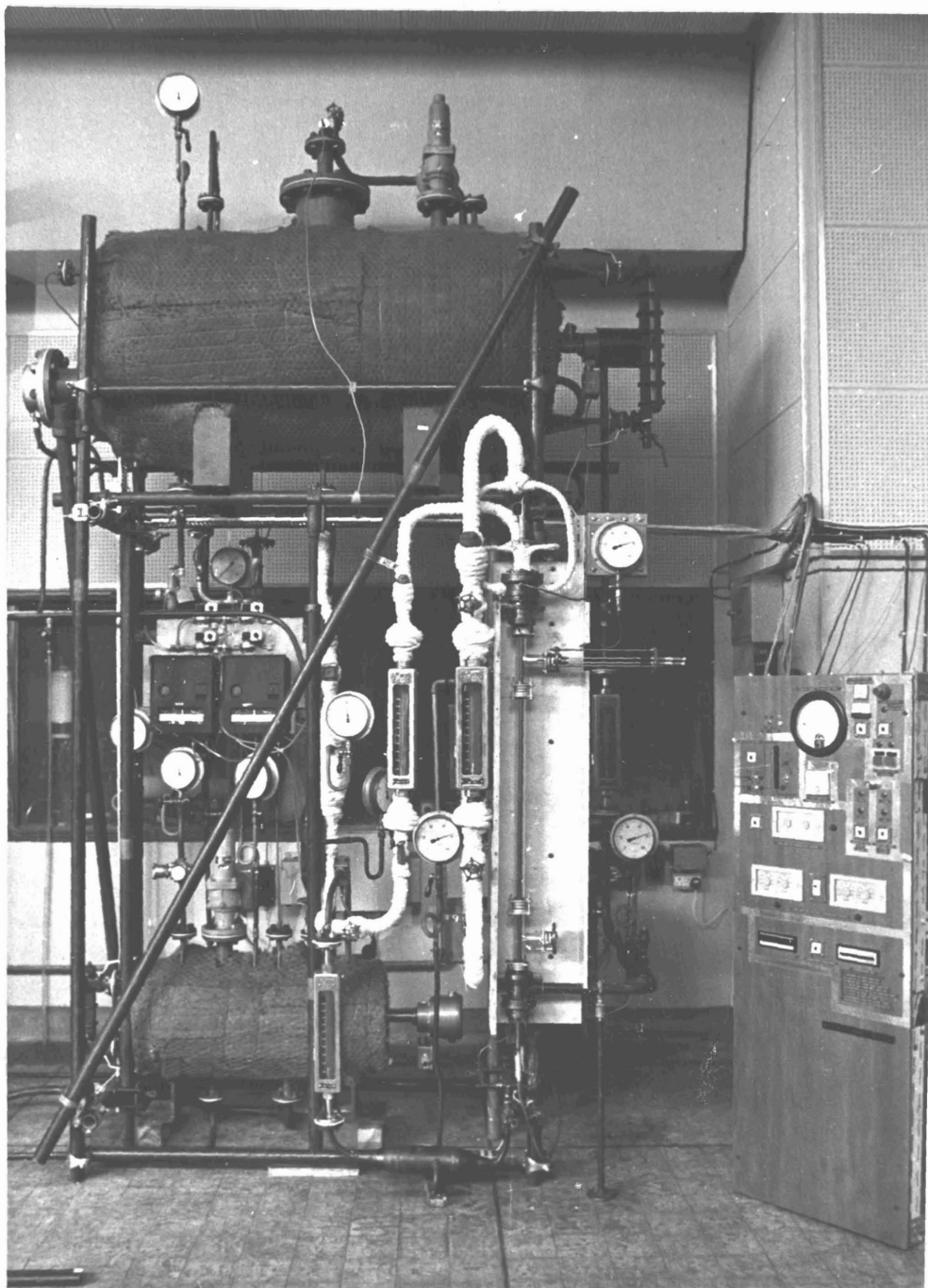


FIG.(A 4.1b)

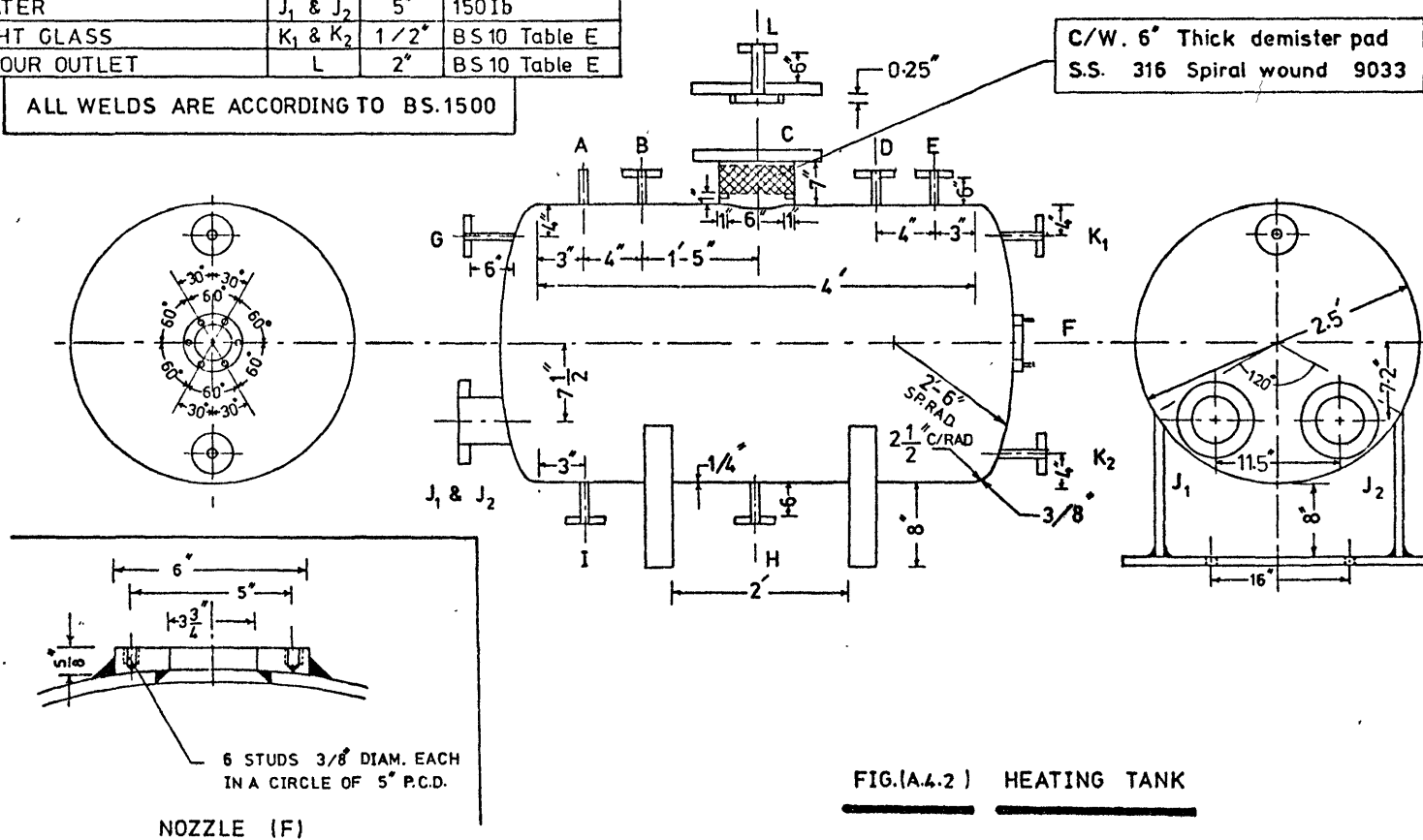


FREON 113 RIG

FIG(A 4.1c)

| NOZZLE DUTY | MARK | SIZE | RATE |
|--------------------|---------------------------------|--------|--------------|
| PRESSURE GAUGE | A | 3/8" | B S P |
| RETURN LIQUID LINE | B | 1/2" | BS10 Table E |
| VAPOUR OUTLET | C | 8" | BS10 Table E |
| RELIEF VALVE | D | 2" | BSTF |
| VENT | E | 1/2" | BS10 Table E |
| LEVEL INDICATOR | F | 3 3/4" | See Drawing |
| HEATER CONTROL | G | 1/2" | BS10 Table E |
| LIQUID OUTLET | H | 1/2" | BS10 Table E |
| DRAIN | I | 1/2" | BS10 Table E |
| HEATER | J ₁ & J ₂ | 5" | 150Ib |
| SIGHT GLASS | K ₁ & K ₂ | 1/2" | BS10 Table E |
| VAPOUR OUTLET | L | 2" | BS10 Table E |

ALL WELDS ARE ACCORDING TO BS.1500



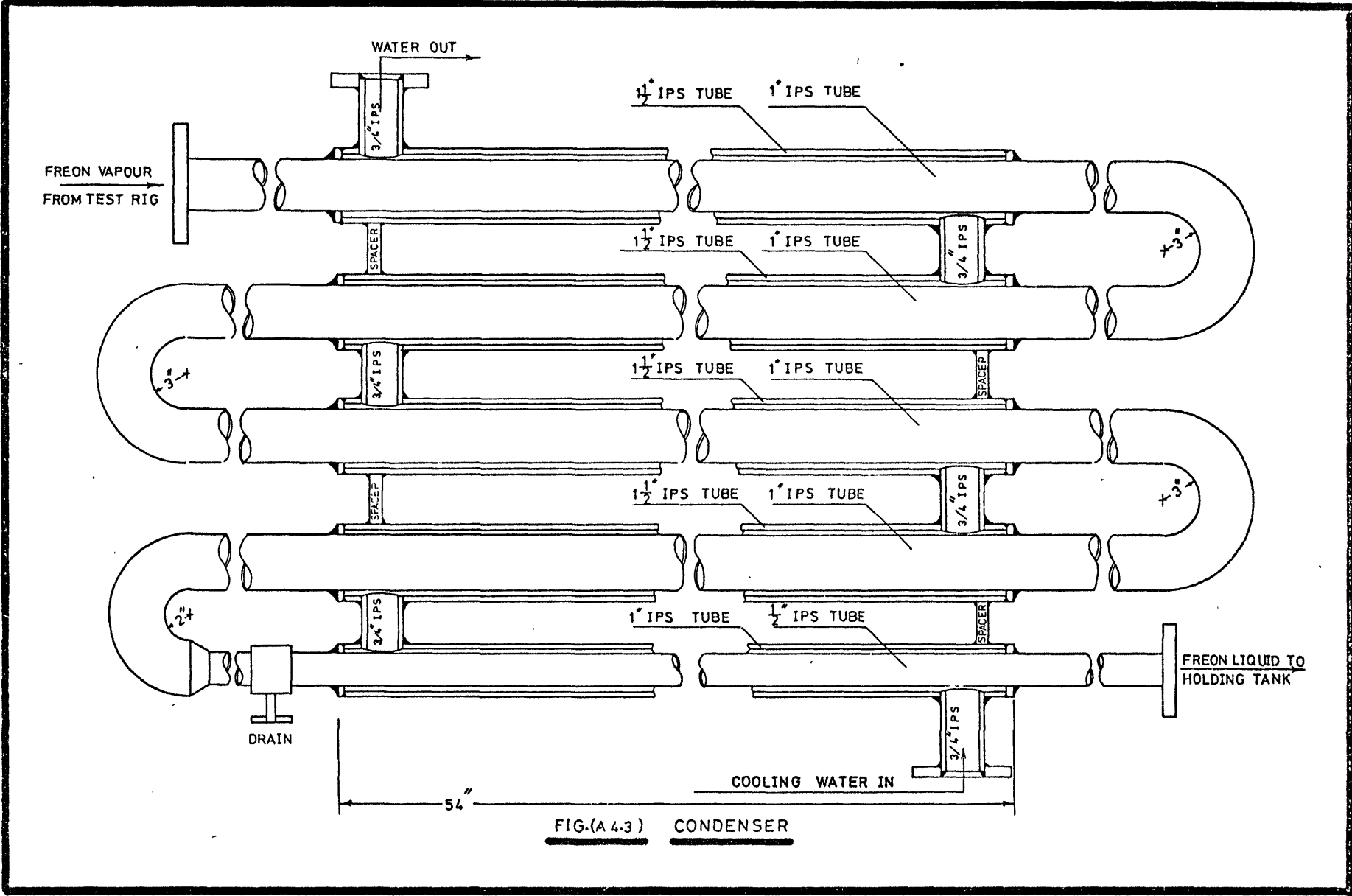
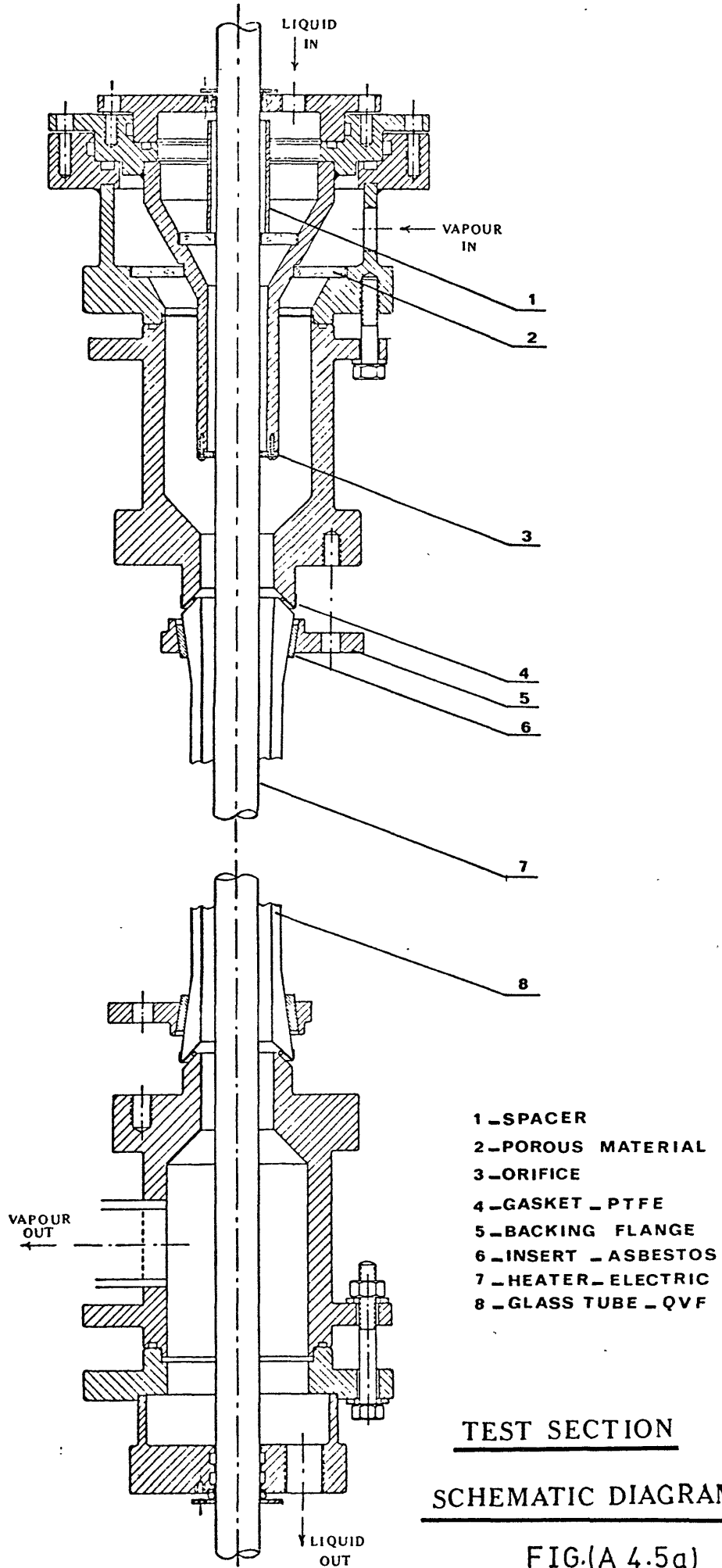
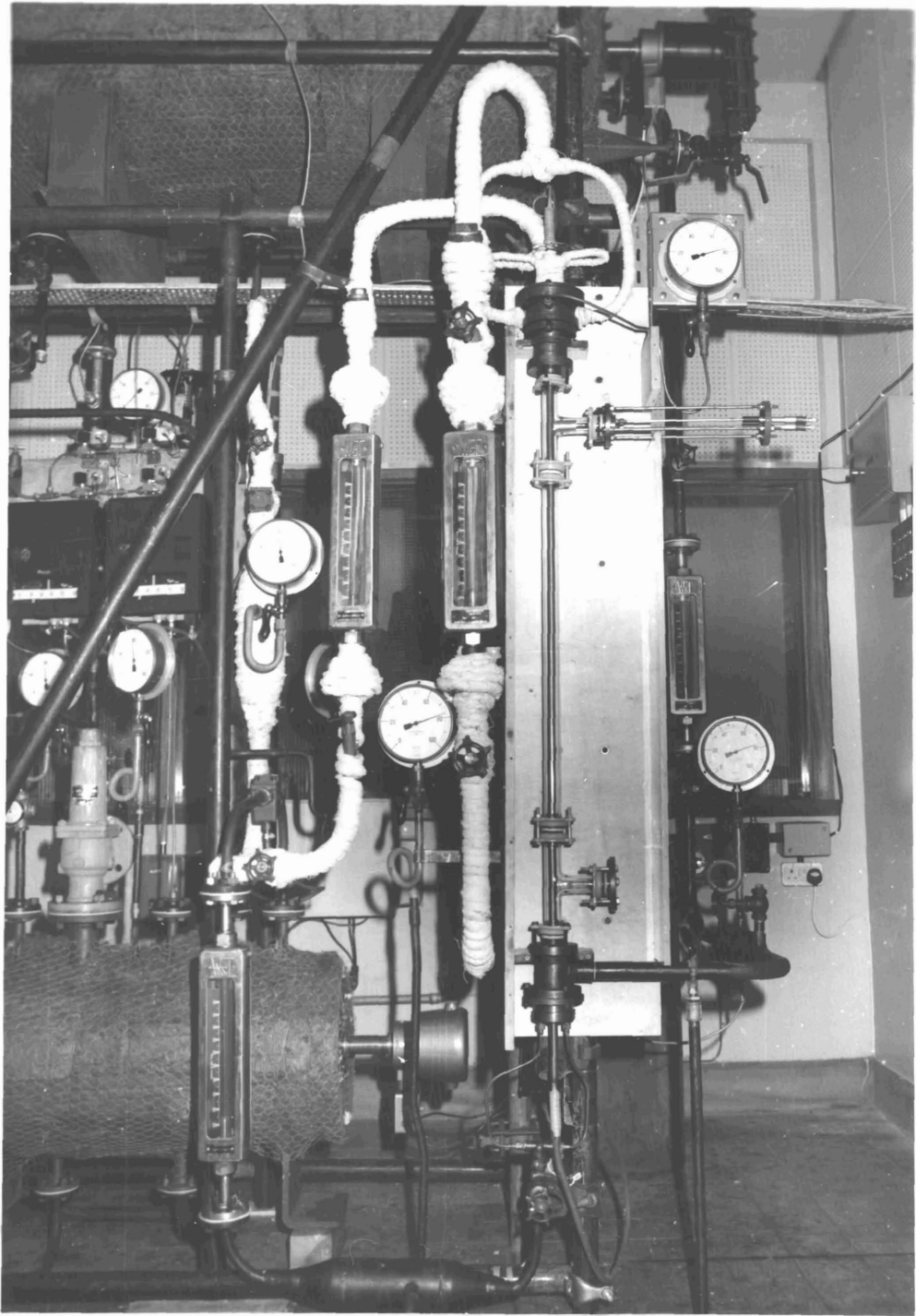


FIG.(A 4.3) CONDENSER





TEST SECTION

FIG(A4.5b)

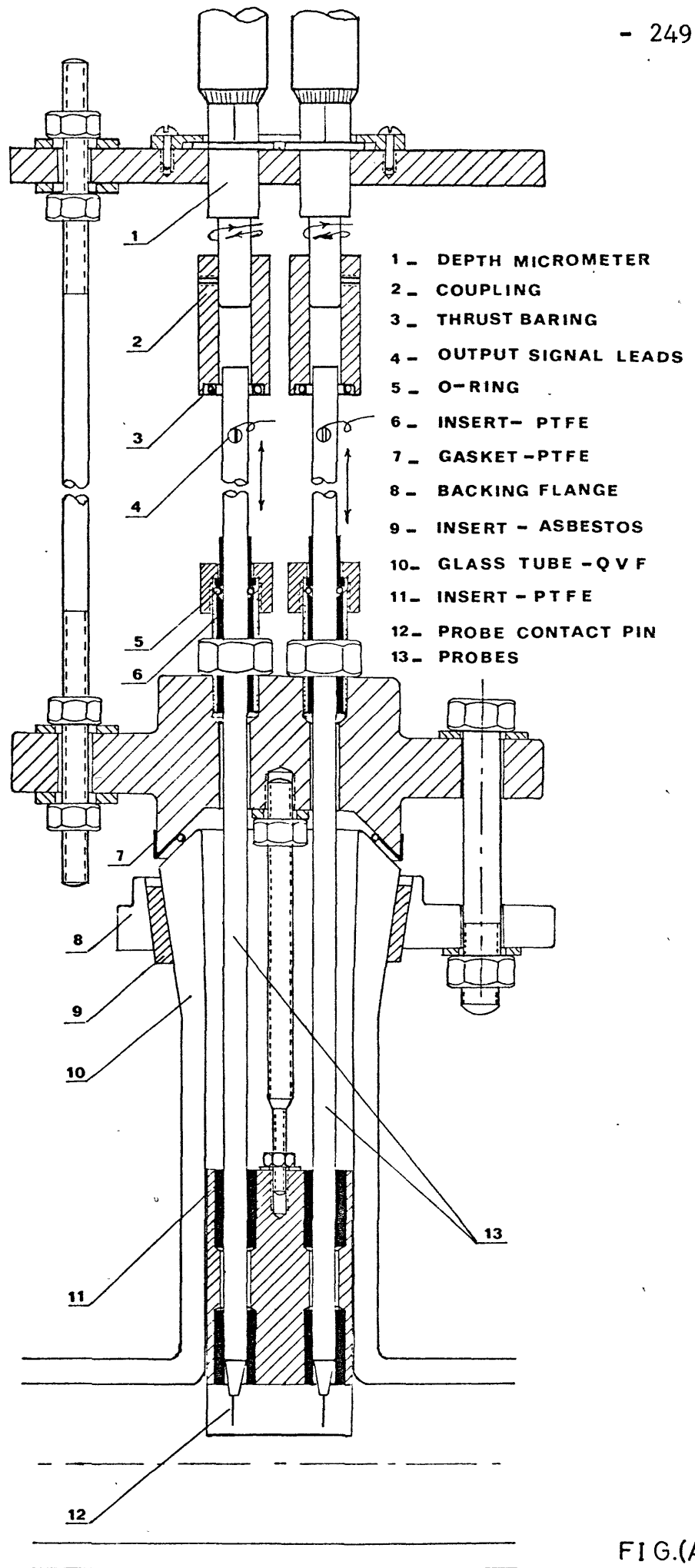
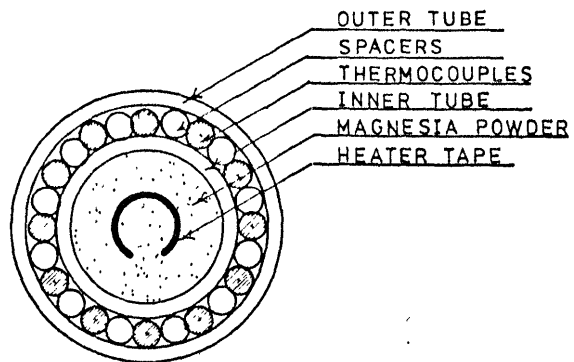
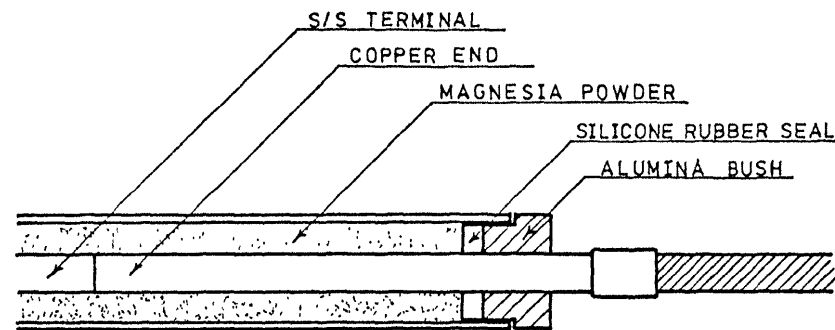


FIG.(A.4.6)

SCHEMATIC DIAGRAM OF PROBES AND RELATED INSTALLATION



CROSS SECTION
(A-A)



TOP AND BOTTOM ENDS

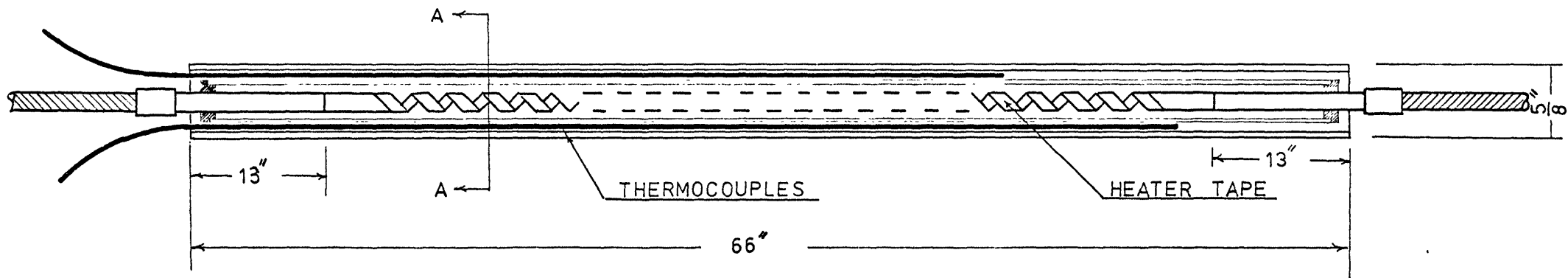
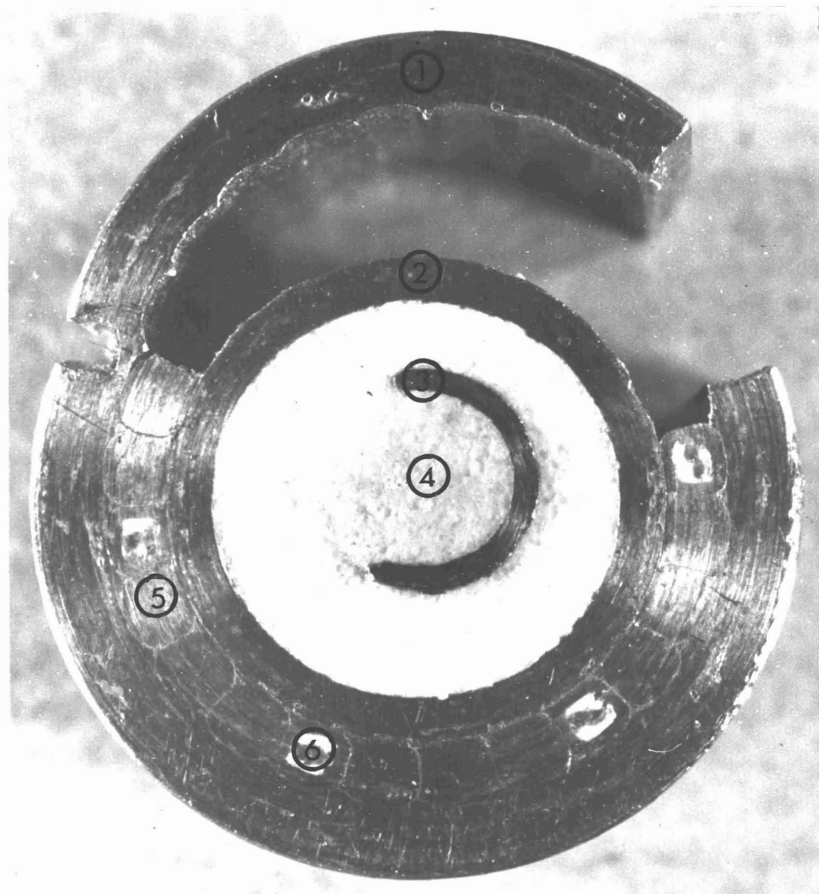


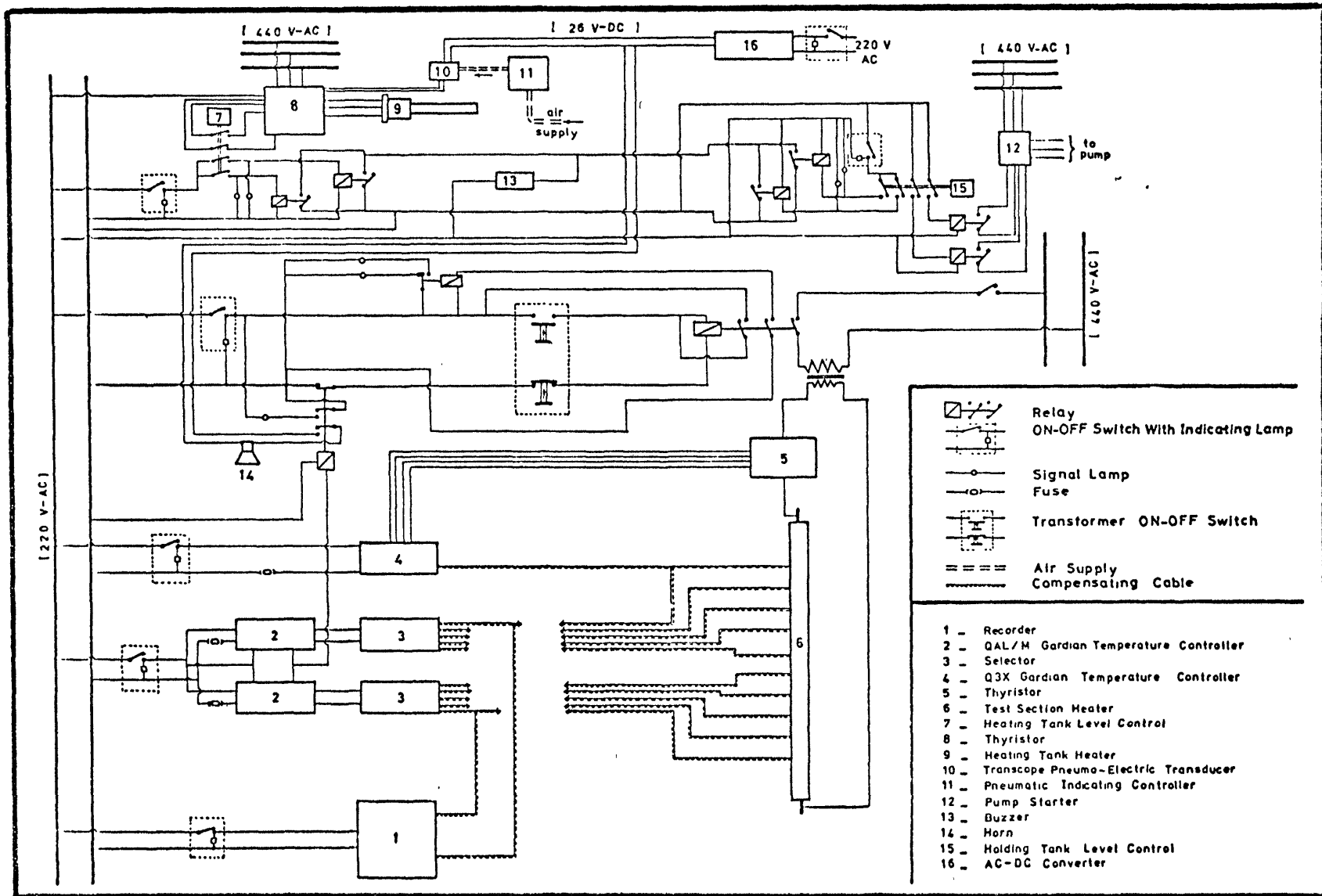
FIG (A4.7a) HEATER AND THERMOCOUPLE ASSEMBLY



- 1 - Outer Stainless Steel Tube.
- 2 - Inner " " " .
- 3 - Heater Tape.
- 4 - Magnesia Powder .
- 5 - Stainless Steel Wire.
- 6 - Thermocouple .

CROSS SECTION IN HEATER ROD

FIG. (A 4.7b)



FIG(A 4.8)

